UNIVERSITÉ DE STRASBOURG

ÉCOLE DOCTORALE DES SCIENCES DE LA VIE ET DE LA SANTÉ

ED414 – UNIVERSITÉ DE STRASBOURG

CNRS UPR3572, I2CT / Immunologie, Immunologie et Chimie Thérapeutique
Institut de Biologie Moléculaire et Cellulaire (IBMC)

THÈSE présentée par :

Wacym BOUFENGHOUR

soutenue le : 22/06/2023

pour obtenir le grade de : **Docteur de l'université de Strasbourg**

Discipline/ Spécialité : Biologie/Immunologie

Development of in vivo and in vitro models of acne inversa

THÈSE dirigée par :
  Dr. FLACHER Vincent   HDR, CNRS UPR3572

RAPPORTEURS :
  Pr. BURSZTEJN Anne-Claire   PR PUPH, CHRU NANCY, Université Lorraine
  Pr. GRUBER Florian   PR PUPH, Medical University of Vienna, Autriche

EXAMINATEUR :
  Pr. SOULAS-SPRAUEL Pauline   PR PUPH, INSERM U1109

Table of content

INTRODUCTION

1. The skin

In this general introduction, I will provide an overview on the skin, its structure, and functions as a physical and immune barrier, setting the stage for a detailed description of HS pathophysiology.

1.1. Development and structure

The skin is among the largest organs of the body, with a mean surface area of 2 square meters and a thickness of 0.5mm (eyelids) to 4mm (plantar feet region) in humans. The skin is made of three distinct superposed layers, from the outside to the inside: the epidermis, the dermis, and the hypodermis **(Figure 1A)**.

1.1.1 Skin development

Epidermis development in mammals is a process that begins three weeks after fertilization, during gastrulation, where the embryo organizes itself in three layers: the ectoderm, mesoderm, and endoderm. The skin develops from a fusion of the ectoderm, which gives the epidermis, and the mesoderm, giving the dermis and hypodermis. As a surface constantly exposed to the environment, the epidermis has undergone many adaptive changes through evolution. Ancestral vertebrates, aquatic and fishlike, were buffeted by water, which kept the living surfaces moist. Aquatic amphibians developed a thin, oily skin densely covered with mucous glands; terrestrial forms acquired a thicker, horny, pigmented skin[1]. Mammals adopted a dry, elastic skin, often covered with hair.

1.2 Epidermis

The epidermis is a keratinized, squamous stratified epithelium, mainly made from keratinocytes, yet also holds other cells with equally important functions. The epidermis is made of five different layers, from bottom to top: stratum basale, stratum spinosum, stratum granulosum, stratum lucidium, stratum corneum[2] **(Figure 1B)**. The epidermis is under constant renewal. This trait is necessary for its function of protection as the skin shields the organism from its harmful environment.

1.2.1 Stratum basale

Stratum basale, or basal layer, is a monolayer of proliferating stem cells allowing epidermis renewal and the production of the basal membrane on which they rest and anchor. These undifferentiated cells undergo regular asymmetrical mitotic divisions to renew both the upper epidermis layers and their own pool of cells. In human adults, the epidermal renewal time is estimated between 40 and 56 days. This rate is much lower in younger individuals, where it can reach as low as 14 days in babies. In mice, the epidermal turnover lasts around 10 days. However, epidermal renewal is a carefully orchestrated cycle, the duration of which fluctuates in relation to different signals.

The differentiation potential of basal stem cells varies with their localization in the layer. Stem cells situated on top of the rete ridges are the most undifferentiated, their divisions pushing sideways previously generated cells. These transit-amplifying stem cells

divide frequently for a few cycles, until they reach the bottom of the ridges, initiating their terminal differentiation process. The expression of β1 integrin is directly correlated with this differentiation state, since the corresponding signaling pathway is necessary to maintain stemness.

(A)

(B)
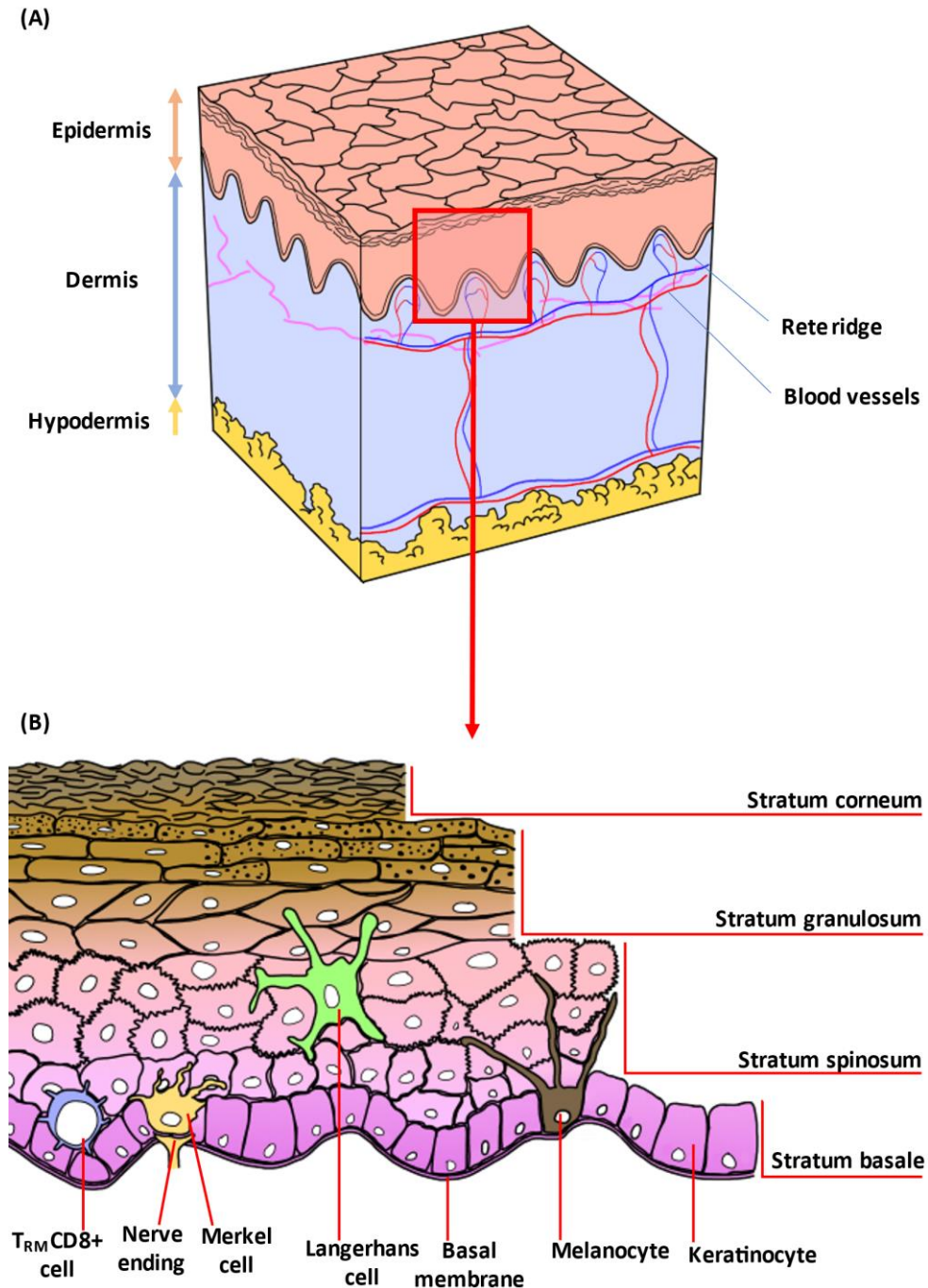
Figure 1. Anatomy of the human skin and microanatomy of the human epidermis.

(A) Overall structure of the human skin. (B) Epidermal structure and cellular composition. Basal keratinocytes divide asymmetrically. One daughter cell moves to the upper layers, where melanocytes transfer them melanin pigments. Keratinocytes end up as a cornified layer near the surface. Langerhans cells are immune cells monitoring the environment. Resident memory CD8+ T_{RM} cells can be found near the basal membrane. Merkel cells in the basal layer transmit pressure signals from the surface.

Basal membrane

The function of proliferating keratinocytes also includes the production, on their basal side, of the particular extracellular matrix on which they set: the basal membrane, or **dermal-epidermal junction**. A similar structure exists under every epithelium and serves not only to anchor the tissue but also as a guide for its reconstruction during wound healing.

Structurally, the DEJ is composed of laminin and collagen fiber proteins polymerized into a dense, continuous yet nanoporous net. The basal keratinocytes latch onto the DEJ using structures called hemi-desmosomes, which work as protein-based adapters between the cytoskeleton of keratin fibers and the transmembrane integrin proteins bound to the underlying extracellular net **(Figure 2)**. In addition, the dermal collagen network covalently binds to components of the DEJ. This arrangement allows a tight junctional cohesion between the basal layer and the dermis below. Moreover, the porous nature of the basal membrane allows the passage of water, oxygen, nutrients, and small messaging molecules into the epidermis, ensuring energetic supply and intercellular communication.

The DEJ fosters a second role as a signaling platform by capturing growth factors and messaging molecules, a function notably allowed by proteoglycans. Proteoglycans are core proteins heavily decorated with glycosaminoglycan chains, which can either bind or release growth factors present in the medium, thus influencing the fate of surrounding cell. In the epidermal basal membrane, this role is filled by perlecan proteins, which increase adherence of stem cells through the expression of Keratin 15 and integrin β1[3].

Melanocytes

Another crucial component of the basal layer is the melanocyte, which produces melanin, protecting the body from the ultraviolet rays and giving skin and/or its appendages (hair, feather, scales) their pigmentation. In humans, melanocytes reside between stem cells of the basal layer, they are usually smaller than basal stem cells but present extensive cytoplasmic dendrites extending upwards into the granular layer. There are around 1500 melanocytes per mm² of skin, a 1:10 ratio with the basal layer stem cells. While one might believe skin pigmentation to be related to melanocyte density, it is in fact related to melanocyte activity[4,5]. The leading role of melanocytes is the production of melanin, or melanogenesis, a pigment protein family from which eumelanin is the most abundant member in humans. Melanogenesis occurs in the melanosomes, highly specialized organelles of the melanocytes with an acidic interior. It starts with the amino acid tyrosine, which is transformed into dopaquinone by a melanocyte specific enzyme: the tyrosinase[6]. Once eumelanin is matured, it is packaged inside melanosomes. They travel upwards through the melanocyte cytoplasmic extensions, until they are released and taken up by keratinocytes of the granular layer[7].

1.2.2 Stratum spinosum

In the *Stratum spinosum,* keratinocytes adopt a polyhedral shape and develop spiny projections from intracellular keratin filaments, thus the name of prickly (spiny) layer. At this stage, keratinocytes are often called prickle cells. They are highly interconnected through

desmosomes, a specialized structure linking cells together through hydrophobic, homophilic cadherins **(Figure 2)**. The intracellular part of the desmosome is connected to the cytoskeleton through the same keratin filaments that produce the spiny projections. The overall layer is shaped as a dense net of strongly adherent cells, which span over several layers. It is in this region that most Langerhans cells are present. Prickle cells, like basal stem cells, are the most susceptible to UVB-induced DNA damage coming from extensive sun exposure, most notably in fair skin individuals[8]. This vulnerability to UVB can be attributed to the absence of melanin protection, which is not found in this layer but rather in the stratum granulosum.

1.2.3 Stratum granulosum and stratum lucidum

Stratum granulosum, or granular layer, is where keratinocytes find themselves in contact with the melanocyte extensions and capture the melanin vesicles into their cytoplasm. While the keratinocytes kept a polyhedral shape in the previous layer, granular keratinocytes adopt a flattened rectangular shape[9] and maintain cell-to-cell tight junctions initiated in the *stratum spinosum*. At this stage, keratinocytes initiate the process of cornification, or terminal differentiation, by undergoing two major changes. First, they induce the maturation of keratohyalin granules, which are dense, protein-rich vesicles that contain keratin, profilaggrin, loricin and trichohyalin. Profilaggrin, loricin and trichohyalin are bridging proteins, they bind keratin fibers together and with the lipid membrane of keratinocytes, forming a sturdy and continuous mesh all around our body. The second major event undergone by granular keratinocytes is the gradual removal of their organelles. Mitochondria, the cellular powerhouses, are subject to a progressive dismantling process[10].

Keratins

In vertebrates like humans and mice, keratins give the outer layer of the skin its rigid, robust structure, protecting them physically from the outside environment. Keratins belong to a wide family of near-ubiquitous fibrous proteins, at the basis of most skin appendages in Animalia, from horse hooves to fish scales. There are more than 54 functional keratin genes in the human genome, each produced differentially during development and adult life depending on the epithelia. In the mammalian epidermis, keratins 14 and 5 are characteristic of the basal layers, while keratin 10 and keratin 1 are induced upon differentiation in the upper layers.

Functionally, keratin proteins can be divided into two main groups: hard and soft keratins. Hard keratins are found in skin appendages: nails, hair, claws. True to their name, hard keratins' main function is to provide a strong yet flexible cement for highly differentiated tissue. Soft keratins are found in softer tissues, mostly the epidermis, but also in glands and in Hassall's corpuscles of the thymus. Soft keratins' main function is to provide a scaffold for intracellular organization, and as such are an important part of the cytoskeleton.

1.2.4 Stratum corneum

The final and outermost layer of the epidermis, the corny layer is the physical barrier in direct contact with the exterior. Composed entirely of cornified keratinocytes, appearing as very flattened sacks of lipid, keratin, and melanin. The keratinocytes in this layer completely

lack any organelle or nucleus, only remains in their cytoplasm the melanin and mature keratin linked in a thick and strong network, tightened by desmosome junctions between them. As new keratinocytes move upwards from the underneath layers, they push the dead cells upwards, causing them to break apart and fall over. This process is known as desquamation must be tightly regulated. In the ichthyosis vulgaris disease, profilaggrin protein is defective, provoking a continuous and excessive desquamation.

Cell-cell connectivity

As tissues are made from the careful spatial organization of cells, the ways they connect and remain cohesive is paramount to tissue structure and function. In epithelia particularly, tight junctions and desmosomes are particularly important to create mechanical stability, watertightness and enable tissue-wide communication.

Desmosomes were discovered in 1864 by Bizzozero. Extensive electron microscopy studies allowed to describe a structure divided into three parallel and symmetric zones **(Figure 2)**. First, from the outside-in, transmembrane proteins of the cadherin family interact with extracellular heads of desmoglein (DSG) and desmocollin (DSC), which form solid bounds as homo or heterodimers. DSG and DSC intracellular tails bind to plakoglobin (PG) and plakophilins (PKP), both members of the Armadillo family of proteins. PG and PKP finally link DSG and DSC to desmoplakins, anchoring the cell-cell junction complex to the intermediary filaments network. In the skin, these intermediary filaments are made from keratins. Cadherin proteins require calcium to bind effectively: the shape of their extracellular domain depends on calcium and requires high concentrations to rigidify and produce a mature desmosome. This process is referred to as hyperadhesion and is mostly observed in mature keratinocytes of the higher layers, whereas basal keratinocytes are mitotically active and require some liberty to self-renew.

Desmosome protein variants are differentially expressed across keratinocyte layers. As keratinocytes move towards the surface the levels of DSG1 and DSC1 increase, but DSG2 and DSC2 are downregulated. In the cornified layer, a unique desmosome complex is found: the corneodesmosome, containing a unique cadherin, the corneodesmosin, the cleavage of which controls desquamation.
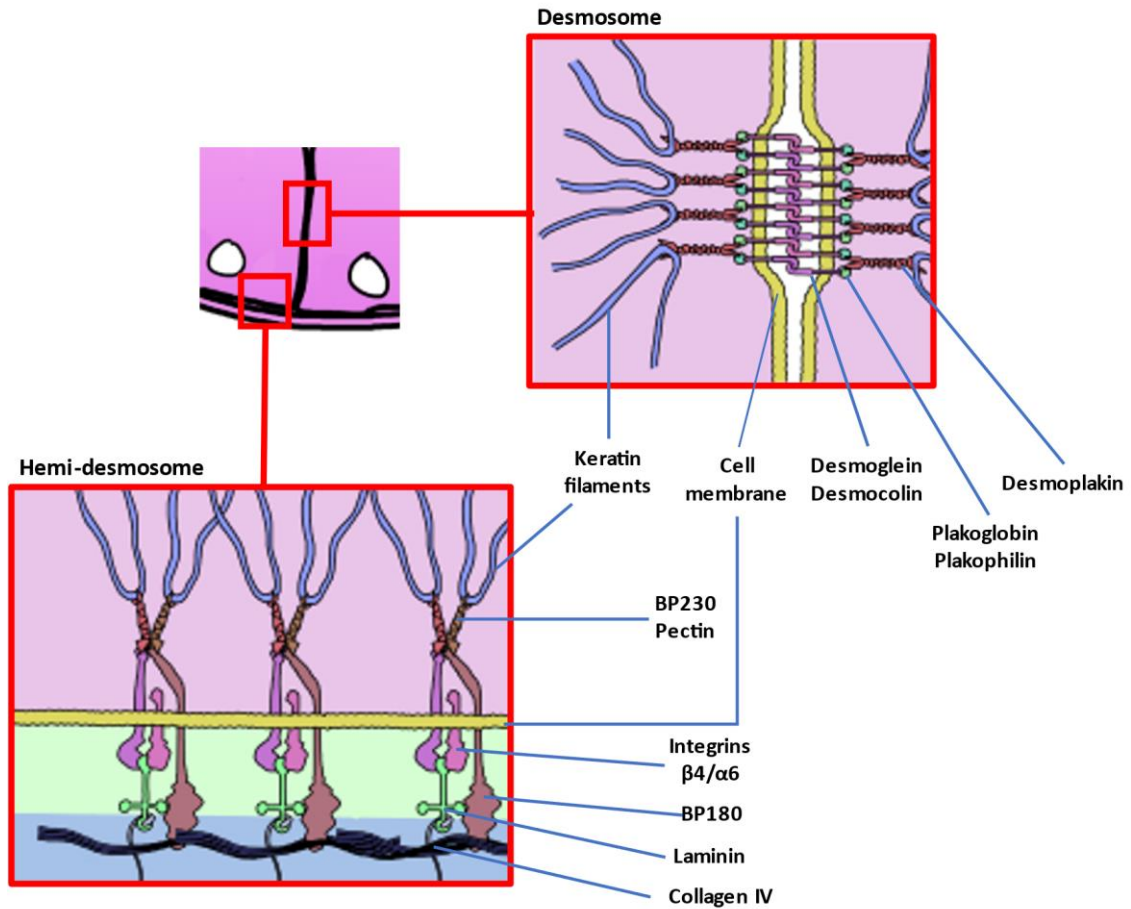
Figure 2. Structure of desmosomal and hemidesmosomal junctions.

Keratinocytes of the epidermis are joined together via solid Velcro-like areas, desmosomes, linking both their cytoskeletons. Transmembrane proteins of the cadherins family bind together in the presence of calcium, their intracellular part linked to a protein complex of intermediary adapter proteins, allowing solid with the keratin filaments of the cytoskeleton.

Linking with the basal membrane involves a similar process: instead of cadherins, integrins play the role of linker with the extracellular laminin. The link is further reinforced by bp180, a collagen binding transmembrane protein.

1.2.3 Microbiota

The microbiota is the entire population of micro-organisms, bacteria, archaea, fungi, and viruses, residing on the skin and within most exterior cavities like the digestive or respiratory tracts. This represents more cells than those composing the body itself: for an estimated 30 trillion animal cells[11,12], classical estimates show the human body harbor ten times more prokaryotic cells, although a more recent estimation places the ratio closer to 1:1[12]. These microorganisms form a large micro-ecosystem in symbiosis with their mammalian hosts, and constantly monitored by the immune system[13]. They provide vital nutrients[14], aid in pathogen defense[15–17], and communicate directly with the nervous system through the gut-brain axis[18].

The first elements of human epidermal microbiota are obtained at birth: newborns acquire the flora of their mother's vagina via natural delivery or their mother's skin via Caesarian section. Some studies suggest that the delivery method has long term consequences on health due to this variance in microbiota composition, including autism, diabetes and immunity[19]. New strains are then introduced via the environment in which the newborns grow and develop, making their microbiota distinct from their mother's.

The skin microbiota functions similarly to a protection layer by occupying the ecological niche of the skin[20,21], preventing potential pathogens to grow and infect the body. Furthermore, the microbiota has other important roles in shaping the immune repertoire and response. As any functional part of the body, the microbiota can fail, in a process called dysbiosis, an imbalance between the different micro-organisms living on the body. Disruption of the microbiota balance is mostly the consequence of environmental factors, although genetic background can set the stage for long-term immunosurveillance failure.

Skin microbiota studies used metagenome sequencing to know its species composition. Bacterial species show heterogeneous repartition in relation to the skin region considered:

- *Propionibacterium sp.* are found in lipophilic environments, i.e. the sebaceous gland. They are anaerobic, gram-positive rod-shaped bacteria capable of producing propionic acid during their metabolization of fatty acids. Beyond its well-known odor, propionic acid is bacteriostatic[20], acts as an immune messenger[22,23] and promotes tissue repair[24]. This genus can also have deleterious effects: *Propionibacterium acnes* is the main drive behind acne vulgaris by obstructing the follicle canal, inducing, and feeding the inflammation.
- The *Staphylococcus* genus is also found in abundance on the mammalian skin: they are aerobic, Gram-positive cocci found in clusters on the surface of the moist areas of the epidermis. *Staphylococcus epidermis* is the most common specie found on human skin, it produces lipoteichoic acid capable of inhibiting the inflammatory response of keratinocytes[25]. *Staphylococcus aureus* is infrequently found in the skin microbiota and more associated with nosocomial infections. It infects the skin by competing with the local microbiota and may enter the body through any potential breach of the epidermis.

- *Corynebacterium* genus are also rod-shaped gram-positive aerobic bacteria present in moist areas. *Corynebacterium jeikeium* is the most common representative in human microbiota.

1.2.4 Dermis

Below the robust and cell-packed protective layer of the epidermis is found an elastic connective tissue with low cell density, the dermis. The dermis is the thickest layer of the skin, with an average thickness of 2-4mm. Beyond support, the dermis provides nutrition, thermoregulation, sensory inputs and is an important base of operations for the immune system. The dermis is made up mostly of fibrous collagens and an extracellular matrix secreted by mesenchymal cells, the fibroblasts. These cells have numerous functions, including tissue maintenance, inflammation and wound healing[26–28]. Like keratins for the epidermis, collagens represent the largest protein family in the dermis. Collagens are helical proteins conferring a robust, yet flexible structure to the dermis. There are 28 different collagen proteins in humans. The dermis is composed of collagen I and III, at a ratio of around 5:1, but this distribution can highly vary with age and environmental factors.

The dermis can be divided in two layers of distinct structure and functions:

The papillary dermis, the most superficial layer, is composed of loose collagen fibers, a dense vascular network and most of sensory nervous fibers and corpuscles. The papillary fibroblasts are more numerous, smaller, spindle shaped and proliferate faster than reticular fibroblasts[29]. They participate in angiogenesis and interact with the basal layer of the epidermis. A high density of blood vessels in this layer, organized as an anastomotic, subepidermal plexus, provides the avascular epidermis with the nutrients through diffusion. These vessels are also essential for communication with the rest of the body and the entry of immune cells. To exit the skin, immune cells enter the blunt ends of lymphatic capillaries that drain the area directly under the basal membrane. Lymph vessels then congregate further down until reaching the deeper, thicker subcutaneous collecting vessels, which lead immune cells and extracellular fluid into skin-draining lymph nodes.

The reticular dermis is the deepest and thickest layer. Its fibroblasts are larger, stellate and quiescent[29], their main function is the production of fibrous proteins. Deeper into the reticular dermis we find another vascular plexus, directly feeding from the regional artery, acting as an intermediary crossroad for the subepidermal plexus further up.

Sensory interface

The skin has a crucial role in conveying touch and pain, allowing mammals to sense their environment and detect any harmful danger. A wide array of nervous sensors and fibers decorate the three layers of the skin in variable density: hands, lips and genitals are more sensible and have more resolution than other regions, a concept cleverly imaged in the homunculus of Penfield.

Skin touch receptors include several elements. Merkel cells, embedded in the basal layer of the epidermis are responsible for sensing edgy or pointy type of pressure. Meissner

corpuscles, responding to light pressure, are found in the papillary dermis. Ruffini endings respond to stretching. Pacinian corpuscles deeper below in the reticular dermis respond to vibrations[30,31]. The hair follicle has a dedicated mechanoreceptor, further detailed in **Chapter 2.3**. Beyond these specialized mechanoreceptors, the most common skin sensors are free nerve endings, also called nociceptors, extending all the way up to the *stratum granulosum*. Nociception is the ability to sense deleterious stimuli as pain or itch, a vital ability to react to the environment and avoid bodily harm, it is carried by free nerve endings A and C fibers. These nerve clusters are sensitive to pain, temperature, and light pressure. They are unmyelinated, providing a slower nervous impulse.

2. The pilosebaceous unit, an organ within an organ

The hair is a characteristic feature of mammals, defining their appearance and serving various important functions from protection to social interactions. It grows from the hair follicle, a fantastic mini organ embedded in the whole skin depth, from the epidermis to the deepest layer of the dermis. The hair follicle is never alone and is always flanked with sebaceous glands, producing sebum that lubricates the skin and the hair. In this chapter, we will learn how hair follicles are sculpted, what makes them grow and fall, and their contribution to our physiology.

2.1 Evolutionary overview and morphogenesis

2.1.1 Evolution

Early stages of mammary, sweat glands and hair follicle are morphologically similar: localized thickening of the ectoderm into a placode, budding into the mesenchyme and development of a lumen. All have in common the crosstalk between different cells of the ectoderm with the underlying mesenchyme.

During evolution, *Sauropsidae* have developed glandular skin to keep their skin moist through secretions, as they lacked scales or any hardened protective layer above their thin skin, and this has evolved into typical amphibian skin. Hair development could have been an adaptation to aid delivery of glandular secretions to eggs. In fact, members of the *Monotremata* clade (platypus and echidnas) completely lack mammary glands and their younglings feed after birth by sucking on milk-impregnated specialized hairs. Marsupials do have nipples; however, they are conjointly developed with hair follicles. Only placental animals like humans and mice have hairless nipples.

2.1.2 Hair follicle development

The organogenesis of the hair follicle in humans start happening at the 10th week of gestation, corresponding to E10.5 in mice. In both cases, it is a complex crosstalk between the fetal epidermis and the dermis below, which we will separate in three distinct stages, each with a unique morphological and molecular profile:

Wnt signaling pathway

Within an undifferentiated epidermis, the initiating event in hair follicle differentiation is the release of multiple molecular messengers, the most of important of which being the Wnt family of proteins. Wnt signaling pathway is a ubiquitous cell signaling system implicated in multiple important embryogenesis events across the *Mammalia* animal class, like epithelial-mesenchymal transition. In fact, the Wnt pathway is extremely conserved and plays a role in development of insects: mutations in genes encoding the Wnt receptor Frizzled or the signaling hub Disheveled, result in improper orientation of body and wing hairs in *Drosophila melanogaster*.
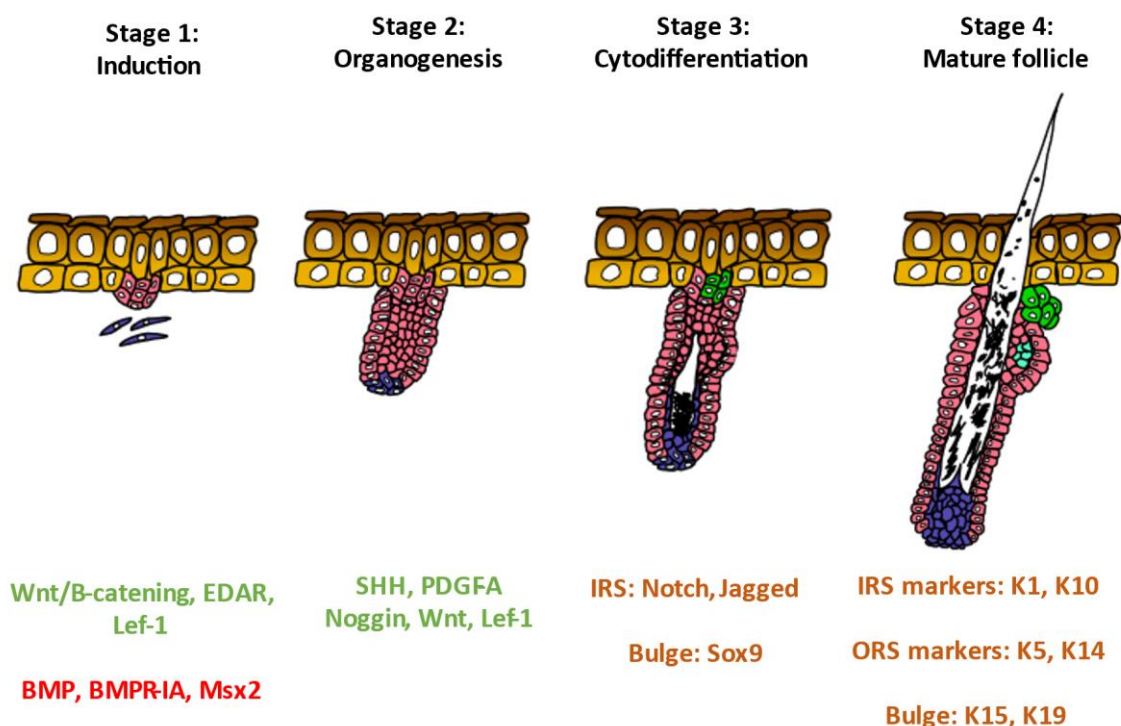
Figure 3. Four stages of hair follicle development in mice and humans: First, Wnt/B-catenin and EdaR pathways commit keratinocytes and fibroblasts into a placode. Second, Shh promotes dermal papilla and keratinocyte rapid proliferation. Lastly, differentiated tissues and the shaft appear as the hair follicle fully matures.

Three Wnt pathways have been evidenced so far: the canonical, noncanonical and calcium pathways. All three share a common inducing event, when a Wnt signaling protein ligand binds to the transmembrane receptor Frizzled. Frizzled receptors are G-protein coupled receptors (GPCR), a family of cell surface receptors that can, when activated by their ligand, activate an associated "G-protein" by linking it a GTP molecule. The activated G-protein is then able to contact its downstream targets, starting the intracellular transduction of the message. These targets are often proteins activated by phosphorylation, the addition of a phosphate

group on one of their amino acids. In essence, GPCRs are molecular levers, translating external inputs into intracellular actions through the gears of the signaling chain.

Next, Frizzled activation triggers the release of the Disheveled phosphoprotein, which initiates the canonical pathway: Disheveled induces the accumulation of beta-catenin proteins in to the cytoplasm, and is eventually translocated into the nucleus, where it associates with the TCF/LEF family proteins. In the absence of beta-catenin, these proteins act as transcriptional repressors, binding to their target genes with the help of Groucho proteins family of co-repressors. TCF/LEF associate with nuclear beta-catenin, triggering transcription of the target genes. This dual function is called a bimodal transcription factor.
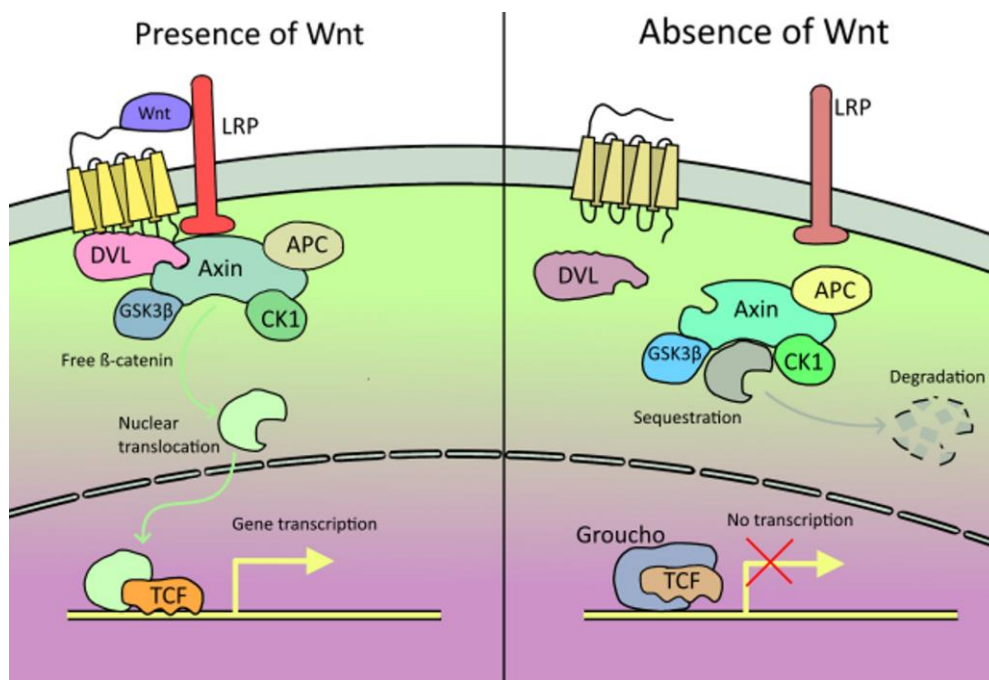
Figure 4. Overview of the Wnt/β-catenin signaling pathway. Wnt is necessary to release β-catenin from the an ubiquitin-ligase complex made out of Axin, APC, GSK3β and CK1. Wnt binds its receptor and recruits Dvl, complexing Axin and freeing β-catenin. Translocation to the nucleus allow β-catenin to drive transcription of its target genes.

During hair follicle morphogenesis, the paracrine secretion of Wnt proteins by both the epidermis and the dermis creates a gradient between areas with low and high Wnt concentrations. Molecular gradients are a necessary and vital concept in development, as no biological mechanism is binary, but is the result of nuanced inputs: An activation threshold is necessary to be reached to definitively start differentiation Wnt concentrations that are high enough induces the aggregation of the responding basal keratinocytes, which assemble into a regularly interspaced structure called the hair placode. This placode will form the core of the future hair follicle. Together, Wnt/β-catenin and Noggin/Lef-1 are also responsible for inhibiting the expression of the critical cell–cell adhesion molecule E-cadherin[32], resulting in the epithelial-mesenchymal transition necessary for shaping the future hair follicle.

The ectodysplasin ligands are a family of two trimeric transmembrane proteins, Eda A1 and Eda A2, composed of a short intracellular domain, a single transmembrane section and a larger extracellular portion containing a collagen domain and a TNF-ligand motif domain. Eda A1 and A2 are very specific to their receptors, Edar and Xedar respectively, a specificity conveyed by a difference in only two amino-acids alone in the TNF motif domain[33].

Eda A1/A2 ligands are released from the cell membrane via enzymatic cleavage by a furine-like protein, allowing them to bind their cognate receptors and induce intracellular signaling. Edar, the receptor involved in follicle induction, recruits EDAR proteins, activating NF-kB, which translocates into the nucleus and activates its target genes.

In East Asian populations, EDARV370A variant produces thicker, straight hairs and increased number of sweat glands[34]. The introduction of this mutation in mice produces the same type of phenotype[35] implying a conserved evolutionary mechanism.

Stage 2, Organogenesis

Epithelial cells recruited previously into the placode signal back to the underlying dermal cells and future fibroblasts to proliferate, ultimately condensating and giving rise to the future dermal papilla. This dermal condensate will become the signaling and organizational center of the shaping future follicle, mainly via the production of **Sonic Hedgehog (SHH)**. SHH is a soluble small glycoprotein involved in epithelial proliferation and patterning, by contacting its receptor at the surface of the placode cells. Its signal is carried downstream by **Smoothened (Smo)** and **Gli** transcription factors. By rapidly proliferating, placode epithelial cells push downwards, following the SHH gradient from the dermal condensate, deeply penetrating the dermis. This new structure is called the hair germ. After this intense growth period, the epithelial cells start surrounding the dermal papilla, encapsulating the dermal condensate which starts differentiating.

Stage 3, Cytodifferentiation

At this stage, the future hair follicle structures are formed through differentiation of the epithelial layers. The inner keratinocytes give rise to the inner root sheath, which starts giving rise to the future hair shaft through terminal differentiation of the most inner cells. The outer keratinocytes will give rise to the outer root sheath, it's layering encapsulating the inner root sheath. This actively differentiating structure, resembling an onion through its many layers, is called the bulbous peg and is not yet a fully-fledged hair follicle. In this context, Notch is an important actor in fate decision for each subset of follicular keratinocyte. Notch are transmembrane receptors binding various ligands, inducing their cleaving by surface metalloproteases and γ-secretase, culminating to the release of **Notch Intracellular Domain (NICD).**
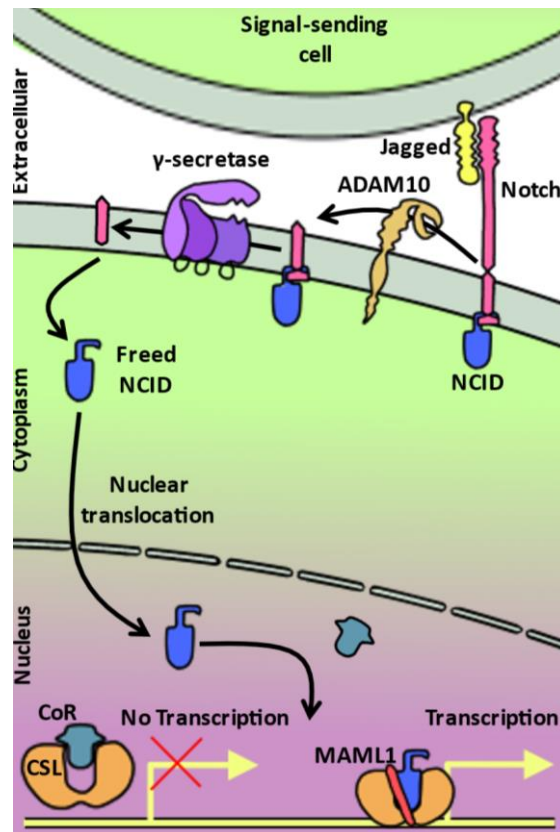
Figure 5. Overview of the Notch pathway, featuring the role of the γ-secretase. Notch requires two proteolytic cleavages to release NCID and activate its target genes: the first enzyme to act is a membrane-bound metalloprotease of the ADAM family, the second is the γ-secretase.

2.2 Structure and cycle of the mature hair follicle

The fully developed hair follicle can be summarized as an invagination of the epidermis into the dermis, at the bottom of which a highly specialized keratinized structure, the hair, develops. The epidermis, dermis and hair all meet at the dermal papilla, an area of intense exchange where blood vessels and nerves are also present.

2.2.1 The hair

The hair is a hyperspecialized multilayered structure composed of 95% keratin, the same family of proteins found in skin appendages or the epidermis. While in the epidermis we see mainly soft keratin, the main components of mammalian hair are cysteine-rich type I and type II keratins[36], also known as hard-keratins or ''hair keratins.'' The hair structure can be divided in three distinct parts[37]:

The cuticle

It is the outermost layer of the hair, made from overlapping scale-like cells, like roof tiles, 60 micrometers long and 6 micrometers wide[38]. Its main function is to protect the hair from the environment, be it natural attacks or the more recent artificial ones (cosmetics, pollution).

Hair cuticle cells are organized in three successive layers[39]: the most superficial A-layer, exocuticle and endocuticle. These layers differ by their cysteine residues which play a role in protein crosslinking. During the cuticle cell differentiation, fatty acids are incorporated and covalently linked to the cuticle surface via thioester bonds, including stearic, palmitic, and anteiso-18-methyleicosanoic acids, the latter constituting up to 70% of the covalently bound fatty acids. They ensure the highly hydrophobic nature of the cuticle and add additional protection. These seemingly fusioned cuticle cells create a lipo-protein membrane referred to as the epicuticle.

The cortex

The main component of the hair, composed of long, parallel keratin chains oriented along the length of the hair. In a similar fashion to muscular or nervous organization, the hair can be divided in macrofibrils, made from microfibrils, made from protofibrils. The hair cortex also contains melanin, which is produced by the melanocytes present in the bulb of the follicle. In the same mechanism as in the epidermis, these melanocytes transfer melanin-rich vesicles into the keratinocytes that are bound to differentiate into hair cells. Thus, melanin (or lack thereof) is what gives hair its color.

The medulla

The innermost and central layer, it is a hollow shaft filled with an amorphous and greasy substance, similar to sebum, and a few medullary cells remaining from the dehydration process during hair maturation.

2.2.2 The follicle

The follicle is a multilayered epidermal structure producing the terminal hair, deep seated inside the dermis with which it communicates. For ease of understanding, we will first describe the hair follicle in its most developed form, then the differences in relation to the cycle stages.

At the core of the follicle is the matrix, containing keratinocytes that are still capable of rapid mitosis, they generate all the differentiated cells that will eventually give rise to the three hair layers. The matrix is surrounded by the root sheath, an extension of the epidermis closely adhering to the hair. It is made of two layers: the inner and outer root sheaths. The inner root sheath (IRS) is itself subdivided into three layers: the cuticle (akin to the hair's cuticle and in contact with the root), the Huxley's layer and the Henle's layer (like the prickly layer of the epidermis). The inner root sheath is the terminally differentiated part, with cornified cells on the cuticle layer and flat, keratin-filled cells in the outer layers. In contrast, the outer root sheath (ORS), which corresponds to the epidermis basal layer, features non-cornified cubic cells capable of dividing and renewing the hair follicle. In vitro, ORS cells extracted from a human follicle can be expanded and used to produce a fully differentiated epidermis[40].

The follicle itself can be divided in four main segments:

Infundibulum

The infundibulum is the upper segment of the hair follicle, from the epidermis to the sebaceous duct. Keratinocytes in this region appear very similar to those in the interfollicular areas, displaying typical epithelial hallmarks such as EpCAM. Yet, they also express specific markers, i.e. CD200, which is present in all regions of the follicle.

Isthmus

The isthmus follows the infundibulum, it is a short region defined between the opening of the sebaceous gland above and the bulge below. It contains stem cells dedicated to sebaceous gland renewal, expressing Lgr6 and Lrig1[41].

Bulge

The bulge, marked by the insertion point of the arrector pili muscle, contains the keratinocyte stem cell reservoir, necessary for hair follicle cycle and self-renewal[42]. These stem cells express the transcription factor Sox9 during embryogenesis and adulthood.

Variable region/Bulb

The variable region, or bulbar region, from the bulge to the dermal papilla. Resulting from the proliferation of stem cells in the anagen phase of the hair follicle cycle (see below), this part is absent when the follicle is resting (telogen).

The hair follicle is associated with two other structures: a sebaceous gland and the arrector pili muscle.

Sebaceous gland

The sebaceous gland is an exocrine, multilobed gland found either associated with hair follicles or independently in sites devoid of hair. It is usually located between the epidermis and the follicle bulge. The gland is composed of sebocytes, specialized cells that produces sebum, connected to a hollow duct that either opens into the hair follicle infundibulum or directly on the outside. It is a holocrine gland, meaning its content is produced in the cytoplasm and released via plasma membrane rupture, killing the sebocyte. Another example of such exocrine secretion mechanism is meibomian glands found on the eyelid, producing the meibum that moisturize the eye. The sebum is an oily substance with multiple functions: beyond keeping the skin moisturized and lubricated, it has a role in commensal flora population control[43,44] and vitamin production and delivery to the skin[45]. Sebum is made from varying lipids ranging from cholesterol, triglycerides and wax esters[46]. This composition is key to its function, as dysregulations of sebum quality is a cofounding factor of regular acne.
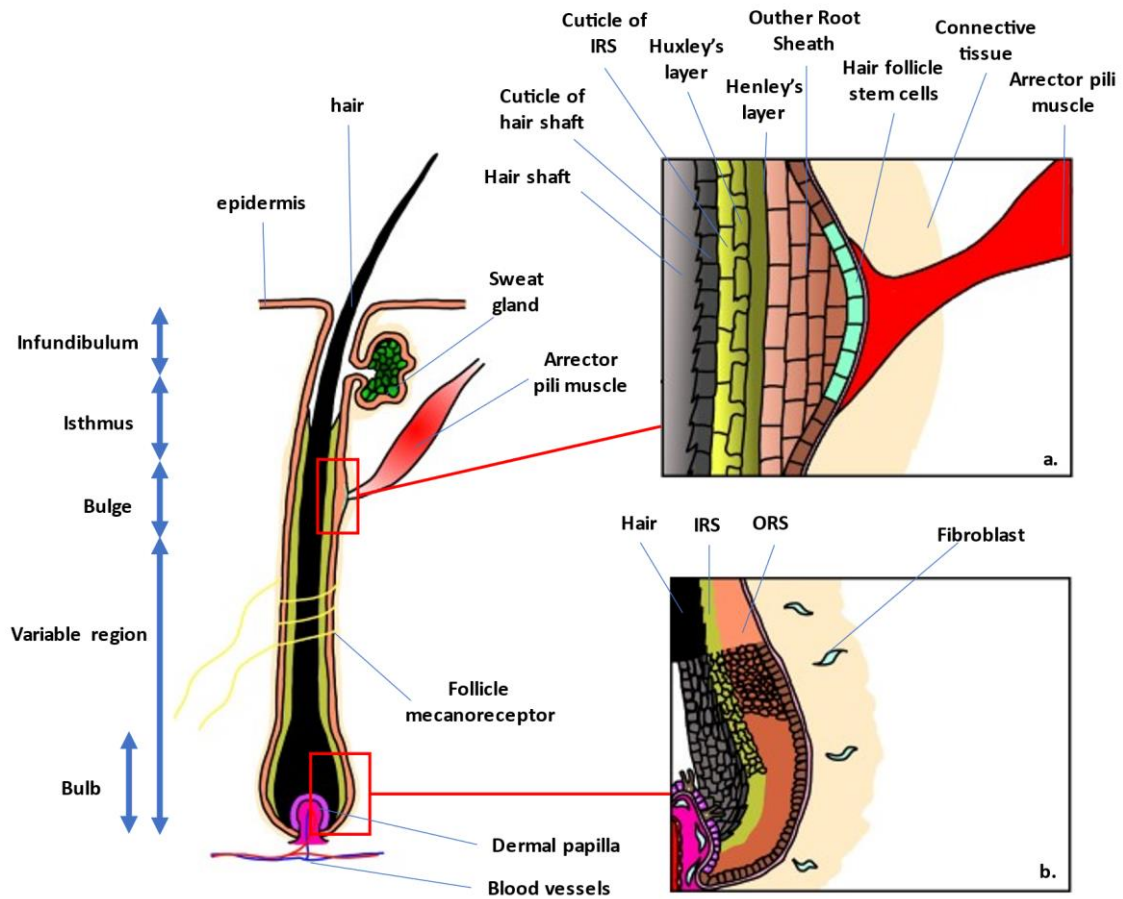
Figure 6. Adult hair follicle anatomy

a. Microanatomy of the bulge: from left to right, the concentric layers wrap around the hair shaft. Hair follicle stem cells involved in the hair cycle concentrate at the junction with the arrector pilli muscle. b. Microanatomy of the bulb.

2.3 Follicular cycle

Hair follicle cycle goes through three main phases, during which the proliferation of matrix keratinocytes varies. The duration of each phase can vary with different species and hair follicle, as it is controlled by hormonal and environmental factors.

2.3.1 Anagen

The anagen, termed from the prefix ana-, meaning "up", and the suffix -gen meaning "producer of something", is the phase of hair growth and elongation. The stem cells in the bulge proliferate rapidly, producing a new variable region and giving rise to hair matrix keratinocytes.

In mice, anagen starts 4 weeks after birth and displays as a body-wide synchronized growth wave from the anterior to posterior of the body. While the first two hair growth waves are synchronized, the following cycles are asynchronous in the adult mouse, with spontaneous cycling in patches observed all along the fur.

2.3.2 Catagen

From the prefix cata-, meaning "down", is a phase of involution following the rapid anagen. This phase starts when the hair stops growing and starts regressing, where it slowly detaches from the dermal papilla and thus its blood supply. It remains a shorter and transitional phase of the cycle, ultimately leading to the longer telogen phase.

2.3.3 Telogen

After a short period of recession, the hair follicle enters the telogen, where biological activity hits its lowest point, and the hair falls off. While the hair follicle seems quiescent, the telogen phase is also a preparatory period for the upcoming cycle. The dermal papilla cells physically contact the bulge cells, inducing their proliferation. In mice, the first telogen is barely noticeable, happening in a matter of a day or two, before leaving place to the second anagen and a new cycle.
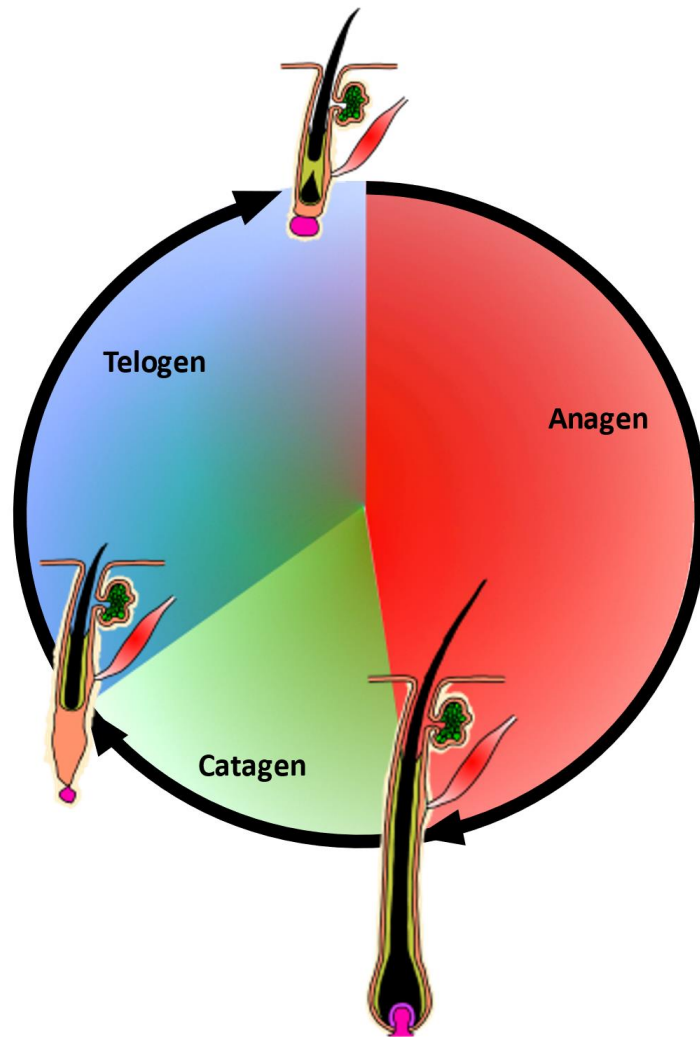
Figure 7. Three stages of hair follicle cycle in mice and humans
First, Wnt/B-catenin and EdaR pathways commit keratinocytes and fibroblastes into a placode. Second, Shh promotes dermal papilla and keratinocyte rapid proliferation. Last, differentiated tissues and the shaft appear as the hair follicle fully matures.

2.4 Microbiota

The hair follicle microbiota is quite similar to the skin's with some key differences, partially due to the specific environment created by the follicular shaft: less oxygen, favoring anaerobic species, less light and thus less UV damage, moister and less acidic[47]. This relatively favorable environment allows symbiotic micro-organisms to easily develop and persist, introducing the idea of hair follicles being reservoirs for skin recolonization by the commensal flora after a dysbiosis or disinfection event[47]. The anatomic regions of the hair follicle have different flora distribution, with species favoring the upper, middle or lower areas[48].

One of the main differences with interfollicular skin's microbiota is the dominance of *Burkholderia* Gram-negative species. The hair follicle microbiota also harbors two hyperspecialized commensal species of mites, *Demodex folliculorum* and *Demodex brevis*. While *D. folliculorum* prefers to live in the middle to upper part of the follicle, *D. brevis* favors the sebaceous glands' lumen. They are thin, worm-shaped mites with four pairs of stubby legs for limited locomotion, mainly feeding on sebaceous secretions. *Demodex* mites reproduce at night at the top of the hair follicle and deposit their eggs in the sebaceous gland. Their life cycle is around 14 days, with 6 days in adulthood, *Demodex* are thus short-lived mites and reproduce at a high rate unbeknownst to their hosts. Demodex mites are a potential actor in the immune response through the production of cytokines[49].

2.5 Functions

Hairs have been a vital organ in the history of animals and warm-blooded mammals. Their primary function is to isolate the body from the outside, trapping the heat generated by metabolism, translating as a net save in energy consumption to maintain body temperature constant. One extreme adaptation of temperature isolation is found in arctic mammals like white bears, who evolved thicker hairs with a shaft filled with air. The air acting as excellent isolation from the cold outside temperature. Moreover, hair along with pigmented skin also acts as protection against the ultraviolet bearing sunrays.

Hairs also serves an important defense mechanism: fur-bearing animals can contract their arrector muscles to straighten their hairs, appearing larger to predators or competitors. The quills of porcupines, which are highly specialized, modified hairs, are an extreme and famous example of this behavior. If it comes to a physical confrontation, hairs act as a cushion dampening the force from received hits. To note, one ambitious study hypotheses than beards in humans can significantly reduce fist-delivered trauma to the face.[50]

Through their association with sebaceous glands, the hair canal also acts as the delivery system of the sebum at the surface of the skin. Sebum is important for lubrification, where it prevents irritation especially in the regions where skin flaps rub together, like the axillae, groin, the area under the breasts or the buttocks. The high concentration of lipids found in the sebum contributes to the impermeability of the skin, especially in humans where hairs are thinner than in most mammals, by creating a thin wax-like barrier on top of it.

Beyond defense, the hair can serve as an important sensory organ, as it is directly connected to the skin nervous system through the mechanoreceptor fiber. In most

mammals, except humans, hairs act as an important touch organ, as their skin is covered by them.

3. Skin immunity, a delicate balance

3.1 The actors of skin immunology

While the skin acts as a natural, physical barrier between us and the tiresomely hostile exterior environment, it also hosts a unique and very active immune system dispersed in each of its three layers. The skin immune system has a wide spectrum of tasks ranging from homeostasis, surveillance, microbiota control, defense against invasions and wound healing. The diverse population of immune cells residing and intervening in the skin reflects this complex and vital mission. The skin adopts a defense in depth, with the epidermis layer constituting its frontline with three types of cells safeguarding us from the exterior aggressors:

3.1.1 Macrophages

To ensure a permanent monitoring of tissues and especially epithelia, in contact with the exterior, resident leukocytes called macrophages occupy a niche in-between the extracellular matrix. As their name suggests ("macro" from the Greek *markos* meaning "large" and "phage" from *phagein*, meaning "to eat"), macrophages primary and first discovered function is phagocytosis. Elie Metchnikoff was the first in 1883 to reveal and explore phagocytosis, for which he was awarded with the Nobel Prize of medicine in 1908. Elie Metchnikoff started establishing his "theory of phagocytosis" by puncturing starfish larvae with rose thorns, then observing the fast migration and accumulation of mesodermal cells near the injury site. Phagocytosis is at the core of immune defense in all pluricellular organisms and most likely the most primitive cellular defensive mechanism in existence. Phagocytosis happens in a series of typical steps, the first one being contact with the target, which can range from bacteria to apoptotic cells or large particles like ink droplets, enabling tattooing. Phagocytosis is triggered by an array of different receptors at the surface of the immune cell, the most common being Fc and opsonin receptors.

Fc receptors are a family of transmembrane proteins able to recognize the constant segment of antibodies, conferring the ability to intake immune complexes in the medium, and initiate a signaling cascade. There is a vast array of Fc receptors, each with a specific antibody isotype recognition, but the widest family remain the FcγR able to bind IgG antibodies. The extracellular segment is made by two or sometimes three Ig-like domains able to bind to constant antibody segment, the intracellular part is ITAM domains, except for FcγRIIb which has a ITIM domain instead and FcγRIIIb which has no intracellular domain and acts as a decoy receptor. After the target has been identified via surface receptors, the phagocyte starts reshaping its membrane to engulf it.

Relatively recent findings have shed light on the ontogeny of macrophages. Dermal macrophages come from either yolk sac or fetal liver monocyte precursors and are maintained post-birth by the division of these precursors. Beyond phagocytosis, macrophages are a key factor in cytokine production, inflammation control, wound healing, and tissue maintenance.

3.1.2 Polymorphonuclear neutrophils

Neutrophils were first observed by Max Schultze in 1865 while describing blood leukocytes. Paul Ehrlich coined the name "neutrophils" by staining blood cells with neutral dyes and noticing the strong coloration obtained on "cells with polymorphous nuclei". Recently, neutrophils have been more and more referred to as "polymorphonuclear neutrophils" as to distinguish them further from other neutral dye-colored cells.

Neutrophils are myeloid cells, the most common leukocyte type in the blood. They originate from the common granulocyte-monocyte progenitor in the bone marrow, which gives rise to a pool of mature, mobilizable neutrophils reserve kept within the bone marrow via the expression of SDF-1 chemokines by local stromal cells, interacting with highly expressed CXCR4 receptor on neutrophils surface. When called upon for service, mature neutrophils exit the bone marrow transcellularly through the sinusoidal endothelium cells instead of diapedesis. This unique egress allows to finely control the levels of neutrophils in the blood via the endothelium pores. Neutrophils mainly follow the gradient of chemokines locally released by macrophages and epithelial cells[51–53] from immunologically active areas, including CXCL8, TNFα and C5a complement subunit. The foot soldiers of the immune system, neutrophils are among the earliest recruited cells on an inflammation site.

Leukocytes and neutrophils enter tissues from the bloodstream through the process of diapedesis. To mount an efficient immune response, this recruitment follows four main steps. First, locally secreted proinflammatory mediators trigger the expression of adherence proteins at the luminal surface of endothelial cells, notably E-selectin, enabling neutrophils to weakly attach on the endothelium while following the chemokine gradient in a process named rolling. Similar to other leukocytes, they attach to E-selectin mainly via PSGL-1, The increase in chemokine concentration induces in turn a higher expression of adherence molecules at the surface of neutrophils, at which point they adhere enough to stop rolling and start the process of extravasation out of the vessel. Neutrophils experience a sudden reshaping, from a rolling, spherical cell they flatten and start crawling on the endothelium searching for a point of entry. There are two ways a neutrophil can exit the endothelium: the classic paracellular exit, which is used by all leukocytes: the extravasating cell finds itself squeezing in between two endothelial cells, piercing through adherence junctions and the basal membrane until reaching the tissue. In a more unique mechanism, neutrophils have been shown to also pass *through* endothelial cells, this is the transcellular way.

Once in the tissue, neutrophils move very quickly: in migration assays in vitro, they are the most motile of leukocytes, reaching around 20 µm/min, 4 times faster than lymphocytes. Neutrophils possess two additional features with a pivotal role for their participation in immune defense: multiple cytotoxic granules and a polylobed, specialized nucleus. Upon contact with a pathogen, neutrophils primary response is phagocytosis in a similar fashion to macrophages, the second one is degranulation. Neutrophil cytoplasmic granules are vesicles filled with proteases and various enzymes destined to destroy pathogens either via secretion

or fusion with the phagosome, and digest tissues to increase immune cells motility[53–55], they come in three main types:

1. Primary or azurophil granules contain the important myeloperoxidase (MPO) and three proteinases (cathepsin G, neutrophil elastase (NE), proteinase 3). The primary granules are also coated with bactericidal/permeability-increase proteins, allowing to pierce bacterial wall and facilitate the antimicrobial action of the secreted content. MPO is a transmembrane protein, highly concentrated in primary granules (~100 mg/mL) and has a direct role in killing pathogens by oxidizing chloride ions with hydrogen peroxide. Azurophil granules content is inactive in resting neutrophils by being restricted in an "azurosome" complex, upon activation the production of reactive oxygen species (ROS), most notably H_2O_2 through NE activation, dissociates the complex, releasing the active proteases.

2. Secondary or specific granules contain lactoferrin, **Matrix MetalloProteinase 9 (MMP9, also known as gelatinase B)**, transcobalamin II and a high quantity of lysozyme. Lactoferrin binds iron and copper, necessary oligo-elements for bacterial growth[56]. Lysozymes are highly conserved antimicrobial peptides found in many secretions like tears, maternal milk, or saliva. They act as both an opsonin and a muramidase, a lytic enzymatic activity aimed towards peptidoglycan and therefore a prime weapon against Gram positive bacterial cell wall. Secreted lysozyme peptides bind bacteria cell wall, covering their target, neutralizing it, and facilitating phagocytosis by the surrounding immune cells.

3. Tertiary or gelatinase granules containing MMP9 but no lactoferrin, are very close to secondary granules. MMP9 is a metalloprotease involved in enzymatic digestion of the extracellular matrix composing the basement membrane and mesenchymal tissues. MMP9 primary function is to facilitate leukocyte migration and movement into and inside inflamed tissues, but is also involved in cytokines regulation, for example by cleaving CXCL8, increasing its chemotactic properties[57].

In addition to these specialized granules, standard secretory vesicles are also part of the neutrophil's arsenal, they contain antimicrobial peptides, the most common being **LL37, also called cathelicidin.**

While neutrophils are very short-lived cells and do not proliferate, they keep a characteristic, polylobed nucleus. This unique shape increases agility and speed when transmigrating through vessels. In another display of exceptionalism, neutrophils can turn their nucleus into a devastating weapon against a wide range of pathogenic bacteria, forming neutrophil extracellular traps in a process called **NETosis**. In the eukaryotic nucleus, DNA is tightly packed in a complex called chromatin by specific proteins: histones. Histones usually stay within the nucleus under all circumstances, but in the unique case of NETosis, chromatin is released into the extracellular compartment, providing an unexpected role in host defense. NETosis is a complex process triggered by the accumulation of ROS within the cytoplasm, started by the activation and release of NE from the azurosome membrane via oxidation by the MPO, which then translocated into the nucleus. Inside the nucleus, MPO and NE uncouple histones from the DNA, decondensing the chromatin which will form the webbed scaffolding

of the NET. Furthermore, MPO produce ROS like chlorinated polyamines which crosslink NET-associated proteins, forming a more stable and stronger antimicrobial web. The increased space taken by the increasingly decondensed chromatin consequently swells the nucleus and ends in nuclear membrane breakdown, where the chromatin is now in full contact of the cytoplasm content and granules. The chromatin now mixed with various antimicrobial components overwhelms the cytoplasm and ruptures it, violently releasing the NET. This unique "kamikaze" capability shows the extreme differentiation neutrophils undergone to fulfill their task. An alternative NET releasing mechanism, called "vital NETosis", allows a faster release of NET by neutrophils via nuclear vesicles mixing with primary granules, instead of the above-mentioned "classical" NETosis system, which involves total membrane rupture and cell death.

During NETosis, histone subunits undergo reduction of their arginine residues into citrulline by PAD4 enzyme activity, activated by an increase of ROS, in a process called citrullination and allowing further chromatin decondensation. This composition of NETs may initiate autoimmune diseases, where antibodies directed against chromatin or citrullinated residues are often found in the affected tissues[52]. Thus, NETosis is an effective weapon against pathogens, but the release of nuclear proteins can be a double-edged sword.

3.1.3 Dendritic cells

Similarly to other organs, **dendritic cells (DCs)** are found in the dermis and epidermis. They present a star-like shape with extensive pseudopodia used to probe their environment and intake antigens. Skin DCs are hematopoietic, myeloid cells migrating from the bone marrow to various tissues where they reside and differentiate into different subsets. Naive DCs are perfectly capable of entering the skin via the expression of CD62L on their surface. This makes DCs a heterogeneous population, with different specific functions: human cDC1 subset, is oriented towards ILC activation and MHC I antigen presentation to CD8+ T cells, thus driving an early effector response and the adaptative cytotoxic response against viruses. cDC2 subset express MHC II and is further capable of activating CD4+ T cells, initiating and orientating T helper differentiation, ultimately shaping the local adaptative response. In this context DCs appear as a functional bridge between the early warning function of the innate immune system and the powerful counterstrike of the adaptative one.

Their antigen presentation role goes hand in hand with their ability to produce different cytokines in context of the detected threat, these cytokines will shape the future adaptative response and recruit further myeloid cells in the skin in the early stages of the infection. cDC1 produce IFNγ, TNFα and IL-12, strong pro-inflammatory cytokines able to activate innate defenses from nearby keratinocytes, fibroblasts, and macrophages. Furthermore, cDC1 drive the entry of myeloid cells in the skin by producing CXCL9 and 10 chemokines. cDC2 subset produces TNFα, but also IL-8 and IL-1, the former inducing the extravasation of blood circulating neutrophils in the dermis. In contrast to their role in

inflammation, cDC2 also produce IL-23 and IL-10, two immunomodulating cytokines able to recruit and activate Tregs, promoting resolution after a successful response.

To accomplish their function, DCs show two distinct functional phenotypes:

- Immature DCs, acting as sentinels in the epidermis or dermis: dendrites constantly probe the surroundings to intake and process antigens. This sampling behavior allows to quickly react in case of a foreign microorganism or substance entering the skin. In this state, the DCs are expressing low levels of MHC-II at their surface, secrete little cytokines and use less energy by downregulating glycolysis[58].
- Once a danger signal activates DCs, i.e., through TLR recognition, they switch to a more active, or "mature", phenotype. They adopt a more motile behavior, commit to antigen presentation, and increase the expression of MHC surface proteins and co-stimulatory molecules on their surface. DCs initiate a migrating movement from their resident tissue to the nearest draining lymph node, where it can activate naive antigen-specific T cells. This migration is made possible by the upregulation of CCR7, a receptor for chemokines CCL19 and CCL21, which brings them first towards lymphatic vessels, then, once in lymph nodes, to areas rich in CCR7+ naive T cells.

While this description holds true of conventional DCs, another subset exists in the name of **plasmacytoid DC (pDC)**. They do not reside in the skin but can enter it via the initial release of CXCL9/10/111, to which pDCs respond via the expression of CXCR3 at their surface. pDC role is found in the anti-viral response, with the massive production of interleukins once activated.

It is currently debated if pDCs are in fact DCs, or more a subset of ILCs, as they are not involved in the activation of an adaptive response by lacking the high expression of MHC surface proteins in an activated state.

3.1.4 Langerhans cells

Langerhans cells, discovered in 1868 by Paul Langerhans, were first mistaken as epidermal nerve endings due to their prolonged dendrites, but later studies established them as part of the immune system. Langerhans cell are easily identified through their unique type of racket-shaped vesicles in their cytoplasm, called Birbeck granules or bodies. Although they have been associated with DC function[59] the classification of Langerhans cells as macrophages has been debated lately[60]. These arguments are primarily derived from an ontogenic perspective. Indeed, Langerhans cells possess a peculiar origin, stemming from fetal liver monocytes, and they renew from local progenitors. Nevertheless, they do migrate towards lymph nodes, qualifying them as DCs.

3.1.5 T cells

T lymphocytes are a group of lymphoid immune cells produced in the bone marrow and matured in the thymus. They are part of the adaptative immune system and can strongly react to precise threats in the form of specific antigen recognition. This specificity is carried out by their unique **T Cell Receptor (TCR)** expressed at their surface and capable of recognizing antigens presented by MHC molecules. CD4+ T cells recognize MHC-II presented antigens, while CD8+ recognize MHC-I ones. To generate the necessary array of TCRs able to respond to any potential threat, T cells undergo a unique recombination of their genome, where they rearrange the TCR gene semi-randomly. This process is undergone in the thymus, where T cells go through two selections ensuring the quality of their generated TCR: The first selection is called positive selection and checks the ability of the TCR to bind to MHC complexes. The following and last exam, the negative selection, ensures the T cell does not react to presented self-antigens. Failing T cells can undergo a second row of tests, but ultimately commit apoptosis if they fail a second time. This mechanism ensures no T cell reacts to host antigens, preventing autoimmunity. As autoimmune diseases still exist, it is safe to assume the thymic function has room for improvement. When reaching adulthood, the human thymus starts a slow and gradual process of involution until becoming vestigial, but without losing its primary function of T cell education. The reason behind this process is currently unknown.

In mice, a particular population of T cells reside in the epidermis: **dendritic epidermal T cells (DETCs).** DETCs are produced in the thymus and already home in the skin *in utero*, representing the largest immune cell population found in mice skin. DETC expresses the γδ T-cell receptor, giving them the ability to activate without MHC presentation: Indeed, the γδ receptors are tailored toward phosphoantigens recognition, either in peptide, lipid, or sugar forms. These antigens are found in many microorganisms, pathogens or metabolically altered host cells, allowing DETC to react quickly to multiple threats and produce an early immune response if needed. Beyond these defensive activities, and in line with the ambivalent function of the immune system, DETC also carry an important role of wound healing: Being positioning in the epidermis, they are at the forefront of the re-epithelialization effort, and produce various cytokines driving inflammation down and promoting tissue repair. They produce TGFβ, an immunomodulator, and keratinocyte growth factors (KGF-1 and KGF-2) which induces keratinocytes proliferation and reoccupation of the space left empty after injury.

In humans, both αβ and γδ T cells are present within the epidermis and the skin, although the role of the γδ T cells is not as clear as for resident αβ T cells, called **resident memory T cells (T$_{RM}$).** CD8+ T$_{RM}$ are preferentially found in the epidermis, while CD4+ T$_{RM}$ are seen in the dermis. They both act as early warning, as they can be quickly reactivated by antigens they met previously. CCR10 and CXCR6, recognizing CCL27 and CXCL16 respectively, are required for T$_{RM}$ to remain in the skinC. CCL27 is uniquely produced by keratinocytes when submitted to pro-inflammatory cytokines like TNFα or IFNγ[61]. CXCL16 is a bizarre molecule, poorly resembling other chemokines. It is expressed at the surface of keratinocytes, where it remains membrane-bound until its cleavage via metalloproteinases. The soluble form of

CXCL16 then travels to the bloodstream where it creates an attracting gradient for CXCR6+ lymphocytes[62].

Skin-homing requires the expression of several chemokine receptors: CXCR3, CCR10 and CCR4. To enter the dermis, human T and B lymphocytes uniquely express a variant of PSGL-1 carrying a post-translational modification called the **cutaneous lymphocyte antigen (CLA)**. It is unclear how the CLA exactly helps addressing lymphocytes specifically to the skin, especially considering its absence in mice, a specie still harboring skin resident and recirculating lymphocytes.

Thelpers

Activated and differentiated CD4+ T cells are called helper T cells and responsible for overseeing the immune response via the production of various cytokines and the activation of key adaptative actors like B lymphocytes.

Naive T cells are regrouped in the lymph nodes where they await activation via migrating dendritic cells carrying their cognate antigens. Dendritic cells following the lymphatic stream end up in contact of T cells and produce antigen-carrying MHC II and I molecules at their surface. The antigen-MHC complex is recognized by the TCR and its accessory molecule CD4 for MHC II or CD8 for MHC I complexes, this cross-linking initiates the T cell activation process. The reciprocal expression and linking of costimulatory surface proteins and the dendritic cells produced cytokines will influence the CD4+ T helper cells differentiation. We can describe 4 main differentiation outcomes:

Th1 subtype. Activated CD4+ differentiate in Th1 via the production of IFNγ and IL-12 by DCs, and themselves produce IFNγ and TNFα. They have an important role in intracellular pathogen response, where their IFNγ stimulates anti-viral defenses in nearby cells and overclock macrophages, boosting their phagocytosis and ROS production.

Th2 differentiation is induced by IL-4, which isn't produced by DCs but basophils and ILCs. Th2 are associated with the immune response against extracellular pathogens and helminth parasites, however Th2 cells are way more involved in tissue repair. Th2 produce IL-4, IL-5, IL-10, and IL-13 that effect several immune cells: IL-4 is a pleiotropic cytokine that activates mast cells in anti-parasitic responses, IL-5 fills the same role but on eosinophils. IL-4, like IL-13, also work on macrophage, potentializing them to promote tissue repair and reduce inflammation. Finally, IL-4 induces B cells to class-switch to IgE, antibodies specialized in anti-parasitic response. IL-10 is an important immunomodulator and activator of Treg. Th2 response can be elicited by epithelial-produced cytokines: Il-25, IL-33 and TSLP. Th2 and Th1 interactions are mostly inhibitory, as IL-10 and IL-4 drives Th1 differentiation and function down, while IFNγ does the same on Th2.

Th17 cells produce a variety of cytokines and are mostly known for producing IL-17A, IL-17F and IL-22. They are also involved in defense against extracellular pathogens like Th2, but contrary to them have a strong pro-inflammatory effect. Th17 are best known for being regulatory specialist at barrier sites: intestinal, respiratory and the skin epithelia, all harbor

Th17 in steady-state. In the skin, Il-22 is an important cytokine, as it can induce enhanced anti-microbial defense by the production of defensins and antimicrobial peptides. Il-22 also induces cell proliferation, enhancing the barrier function of epithelia. In a positive feedback loop, keratinocytes respond to Il-17 by producing CCL20 chemokine, recognized by CCR6 at the surface of the Th17. CCL20 role is to further attract Th17 in the skin and retain them *in situ* to carry out their function. Due to their enhanced plastic properties, some Th17 cells can retain Th17 surface markers and produce IFNγ instead of Il-17, these effectors are often dubbed Th17/Th1 cells and are found in both mice and humans.

Treg are a subset defined by its ability to reduce the activity of immune competent cells. Some Tregs are naturally present in the body, called natural Tregs, while other are induced by antigen presentation. Tregs produce IL-10 and TGF-β, two anti-inflammatory cytokines able to limit the immune response, preventing excessive tissue damage and maintain homeostasis. Tregs have an important relationship with Th17 in the skin,

3.1.6 Innate Lymphoid Cells

Lymphoid cells responding to innate signals, without antigen specificity, are a raising area of research in both steady state and pathology. ILCs do not express standard T or B cell markers, but instead display CD132, CD25, CD90 and CD127 at their surface. Their survival and development are dependent on Il-7 and Notch signaling. There are currently 3 functional groups of ILCs mirroring the functional groups of Thelpers:

ILC1, express the nuclear factor t-bet and produce class II interferons and TNFα. Typically associated with inflammatory bowel diseases. **ILC2**, dependent on GATA3 and produce IL-4, 5 and 13, they also express CCR6, the receptor of CCL20, a cytokine produces in the upper part of the hair follicle. **ILC3**, they express RORγt and produce Il-17 and 22. In between these rigid definitions, ILCs possess significant plasticity, with reported ILC1 turning into ILC2 under the action of IL4 and reverted to ILC1s via IL-1b and IL-12.

ILCs are heterogeneously distributed in the skin, with ILC3 focused on the epidermis while ILC2 are enriched in the subcutis. epidermal ILC3s express the CLA marker and are involved in microbiota tolerance. ILC3 also express IL-33R, making them responsive to specific keratinocyte signaling.

3.1.7 B cells

B lymphocytes are a vital component of the adaptive immune response, as they can produce the highly effective antibodies proteins and serve as a memory pool to better fight against repeated encounters with pathogens. Mammals possess different types of B cell populations:

Conventional B-2 cells, the most common type of B cells, can react to presented antigens and produce specifics antibodies in response. B-2 cells emerge from bone marrow

progenitors and relocate into primary and secondary lymphoid organs like the spleen or lymph nodes. Innate-like B-1 cells do not originate from the bone marrow but fetal yolk sack progenitors *in utero* and reside in pleural tissues where they constitutively secrete polyreactive antibodies. This means B-1 cells can develop long before the adaptive immune response provided by B-2 cells is operational, providing a low-affinity defense against potential infections in the early stages of life. B-1 secreted antibodies are mostly aimed towards non-protein antigens, like gluconic and lipidic residues.

B cells express at their surface the B cell receptor (BCR), consisting in a membrane-bound antibody adjoined by transmembrane proteins allowing intracellular signal transduction when the receptor binds its cognate antigen. Antibodies are highly specialized and efficient molecules able to link their cognate antigen, obstructing the movement and function of bound pathogens. Antibodies come in various variants, called classes: D, M, G, E and A, each with varying functions in antigen binding, complement activation or eliciting phagocytosis. Each B cell has a unique BCR, which is the fruit of the random assembly of three predetermined sequences found in different variants in our genome. Through a DNA recombination mechanism like the one found in T cells', one individual can produce as much as 3.5×10^{10} unique BCRs and corresponding antibodies. In avians this process is done in a dedicated organ, called the bursa of Fabricius, giving B cells their name. Following selection, naive B cells exit the stroma and navigate through the bloodstream into secondary lymphoid organs. There, B cells are organized in segregated structures called follicles, making up the mobilizable pool of potential responders in case of an intrusion.

The B cell activation process begins with activated DCs entering the lymph node and contacting the naive T cells residing there, priming them against a specific antigen via their antigen-bearing MHC. Activated Thelper cells can now co-stimulate **naive B cells** present in the follicles of the lymphoid organs, this migration from the T to B zone requires expression of the CXCL13 chemokine to attract a specific subset of T cell: **T follicular helper cells (Tfh)**. At the same time, B cells that captured the same antigen through the lymphatic stream via their BCRs can migrate to the edge of the follicle, towards the Tfh cells. The meeting of T and B cell at the frontier between T and B zone allows physical contact and co-stimulation of primed B cells and activated T helper CD4+ cells via a family of surface proteins. BCR activation requires the help of accessory molecules, mainly CD19 and CD20, both surface markers of B cells. B cell activation ultimate purpose is the production of secreted antibodies, which necessitate a final differentiation as **plasma cells.** Plasma cells appear as giant antibody factories, with an overly developed Golgi apparatus, and lose the expression of CD19, while expressing CD138 or syndecan-1 at their surface. To enhance their ability to fight pathogens, B cells undergo class switching in the lymph node follicles. Class switching is an irreversible process, as the DNA itself is excised to switch the antibody class from M to G, E or A. Class switching is context dependent, as it specializes the produced antibody: E class antibodies are tailored against pathogens, able to activate eosinophils and basophil degranulation; IgA are better suited for action in the barrier areas like the intestine or the skin. After resolution, surviving B cells

become memory B cells and express the CD27 at their surface, they can either be **unswitched** or **switched memory B cells** depending on their previous history.

B cells in the skin

B lymphocytes are usually not associated with the homeostatic skin immune system and more believed to act as distant agents producing antibodies that diffuse from the blood into the tissues. B cells are only found in very low percentage upon digestion of the dermis in healthy mice and humans. Despite this, recent studies have found evidence of B cell recirculation from healthy skin: analysis of skin-draining lymphatic fluid shows the presence of B cells in sheep and humans. Moreover, local production of antibodies is also demonstrated in healthy and diseased skin, with resident plasma cells producing IgA, IgG and IgM isotypes. IgA is found natively in sweat and sebum, in line with the presence of antibody-secreting cells near the eccrine glands, while IgM can be found in the skin. In addition, B cells can exit from the bloodstream, as they express adhesion molecules to bind endothelium-expressed selectins and initiate diapedesis. Akin to T cells, CLA expression has been described in bloodborne B cell populations, notably on memory switched (CD27+ IgM-) B cells. B cells are receptive to skin-homing chemokines, with high expression of CCR6 and CXCR3. CCR6 is the receptor of CCL20 which is expressed at low levels by the cutaneous endothelium and upregulated upon skin inflammation, while CXCR3 binds CXCL9,10 and 11.

Beyond homeostasis, cutaneous B cells were found in various chronic inflammatory diseases. B-2 cells have been observed in the skin of patients with pemphigus vulgaris, where blistering of skin and mucosa occurs because of antibodies produced against cell-cell adhesion proteins at the surface of keratinocytes. In systemic sclerosis, where 95% of patients display autoantibodies in the skin, prominent B cell infiltrates are found in patients' dermis.

pathogens

commensals

MemT CD8+

Langerhans cell

Macrophage (resting)

Dendritic Cell (surveillance)

Thelper

Degranulation

NETosis

Phagocytosis

Neutralisation

Monocyte

DC migration

Ab production

Neutrophils

Thelpers

Leucocytes recruitment

Vasodilatation
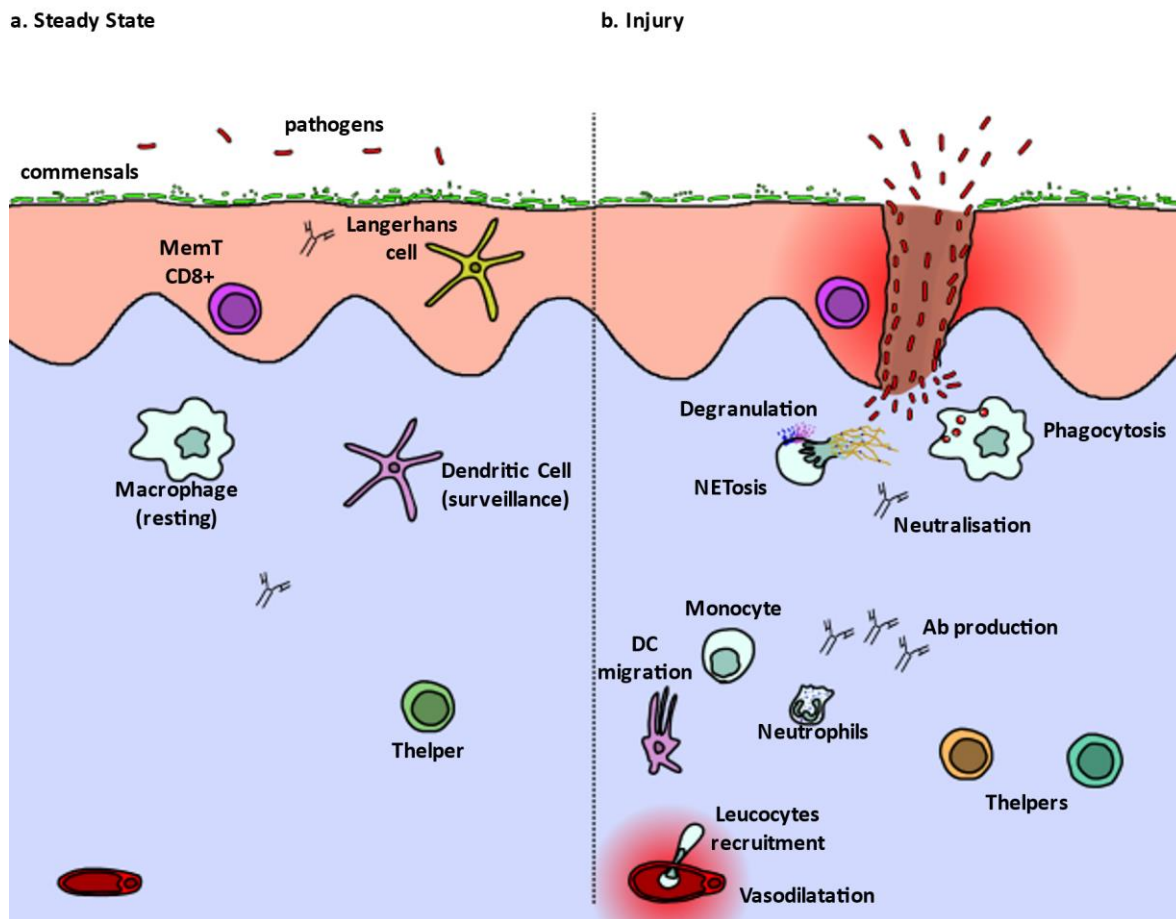
Figure 8. The skin immune system in steady state (a) and during a immune response (b).
Macrophage and dendritic cells oversee the tissues while antibodies transverse to the outside and regulate microbiota proliferation on the skin surface. As the skin is wounded, the barrier breaks and pathogens infiltrates, prompting the recruitment of neutrophils and lymphocytes in the dermis to contain and stop the infection.

3.2 The immune response

3.2.1 Pathogen Recognition Receptors

The immune system has a requirement to detect, identify and defend against threats. These threats can be of very different nature: mechanical, bacterium, virus, fungi, or toxins. The skin is especially exposed to most dangers and constitute a prime area for entry for pathogens. A typical threat would first be picked up by an array of sensory receptors expressed on the surface and inside macrophages and DCs residing in the tissue: the pathogen recognition receptors, able to recognize a wide variety of threats.

3.2.1a Toll-like receptors and C-type lectin receptors

The most widely expressed PRRs are the TLRs, a wide family of transmembrane receptors expressed at the surface of all immune cells as well as stromal cells, including keratinocytes. Their primary function is to detect molecules that are not naturally found in mammalian bodies, or pathogen-associated molecular patterns. Pathogens might evolve faster and bolster a variability, but some of their vital functions still require specific highly

conserved components. PRRs have evolved to recognize these conserved molecules to detect and allow the destruction of pathogens.

The first toll gene was discovered in 1985 by Christiane Nüsslein-Volhard and her team, working on fruit fly development. Her reaction to the underdeveloped toll-muted fruit fly, "Das ist ja toll!", gave its name to the gene. Later, Hoffmann's team discovered the immune properties of toll in anti-fungal infection in 1996. Toll-like proteins were discovered in humans around 1994, to this day 13 mammalian TLRs have been discovered. All TLRs share a similar structure: in their functional form all are dimers of a singular receptor with an N-terminal ectodomain organized in a long concave helix made of leucin-rich repeat motifs able to specifically bind to its cognate ligand; a transmembrane segment; a C-terminal endodomain.

Each TLR receptor is tasked with recognizing a certain type of PAMP, allowing to build a vast network of sensors effectively covering the spectrum of potential PAMPs. TLRs can be divided in two categories: surface and intracellular receptors, reflecting the PAMP they are meant to recognize. Surface TLRs will be activated by antigens on the surface of pathogens, like the lipids or sugars of their cell wall and membrane that shed into the extracellular medium. They include TLR1, 2, 4, 5, 6, and 10. TLRs in cell compartments are dedicated to recognizing the genetic material specific of pathogens, like DNA, double stranded RNA or CpG rich DNA. They include TLR3, 7, 8, and 9. When a TLR is activated, the intracellular portion will trigger a signaling cascade within the cell. There are two types of signaling cascade triggered by TLRs. Both pathways end up activating NF-κB, a transcription factor that then translocate in the nucleus and activate multiple proinflammatory genes, inducing the early release of IL-6, TNFα and proIL-1β.

C-type lectin receptors are found either at the surface of DCs and macrophages or secreted in the medium like SP-A/D or MBP proteins. When binding carbohydrate ligands from pathogens, they trigger intracellular signaling which may synergize with that of TLRs. Consequently, one pathogen can trigger different PRRs of different families leading to signaling pathway synergic activation. CLRs are structured in three domains: an extracellular recognition domain made from one or multiple carbohydrate recognition domains (CRDs), a transmembrane domain and an intracellular signaling domain i.e., ITAM or ITIM motifs. CRDs contain sugar-binding sites, the affinity of which relies on the presence of calcium.

CLRs are especially important for antigen capture response, as they allow internalization, degradation, and subsequent surface presentation in MHC molecules. Many markers defining functionally different subsets of DCs or macrophages, such as CD209/DC-SIGN (dermal DCs) or CD207/Langerin (epidermal LCs), are CLRs.

3.2.1b NOD-like receptors, RIG-I-like receptors and the inflammasomes

The nucleotide oligomerization domain (Nod)-like receptors, second family of PRRs widely expressed in epithelial and immune cells, they differ from TLRs as being cytosolic sensors. A NOD receptor is a multidomain protein made up of an effector region, a central NOD domain and a self-inhibitory C-terminal domain made of LRRs. In the steady state, NLRs are inactivated by the weak linking of LRRs with the NOD domain, which can recognize various

bacterial specific PAMPs. When LRRs preferentially binds to their ligand, they release the NOD domain which now enact dimerization with other activated NLRs. The effector domain can be a CARD caspase recruiting domain or PYD pyrin domain, both homophilic domains active in apoptosis. Ultimately, NLR activation recruits pro-caspase 1, which self-activate through proteolytic activity and contribute to the activation of pro-IL1β and pro-IL18, both inflammatory cytokines, and starting the process of pyrolysis. Caspase-1 is active as a tetrameric heterodimer and is part of the caspase family, a group of cysteine proteases implicated in immune response and apoptosis.

RLRs are quite similar to NLRs: they are cytoplasmic receptors able to bind viral RNA via a helical domain, producing conformational changes exposing the CARD domains. CARD domains can then recruit caspase-1, whose activation takes place in a kolovrat-shaped macromolecular complex born from the assembly of multiple NLR/RLR and associated proteins, called the inflammasome. The assembly of the inflammasome is either triggered by cytosolic PRRs or the accumulation of ROS, and acts as a macromolecular caspase hub. The centralization of all the caspase activity allows rapid cleavage of pre-IL-1β and its quick release outside, alerting nearby cells and the immune system of an infection. One of the most studied and versatile being the NLRP3 inflammasome, capable of recognizing multiple like bacterial MDP, RNA, LPS, ATP, polyI:C, an analog of dsRNA or other chemical compounds.

3.2.2 Complement system

The blood of animals contains enzymes and proteins able to bind to, opsonise and lyse bacteria, they are an innate and powerful last line of defense sanctuarizing the circulatory system and can diffuse into inflamed tissues. First discovered by observing the bactericidal properties of blood, Paul Ehrlich coined the term "complement" as they were believed to be accessory to the function of antibodies. While the complement has established roles in metabolism and cell regulation, it's function as an effector of innate immunity is its most studied function. The complement in humans is made of 50 proteins, with C1 to C9 being the classical constituents, and various receptors and regulators. Complement proteins are either produced by the liver or other cells like keratinocytes, fibroblasts or cutaneous immune cells, the proteins enter the bloodstream as inactive precursors and are gradually activated by cascading proteolysis. The initial event is classically the presence of immune-complexes, antibody constant chain can recruit forming the C1 complex, formed of hexameric C1q, C1r and C1s proteins. C1q hexameric nature is important, as it gates complement activation behind the close of proximity of immunoglobulins as only found in immune complexes. Immunoglobulins vary in their avidity to the C1 complex, IgM, IgG and IgA are competent in complement activation, with varying strength: IgM pentamers gives them a natural advantage to bind and activate C1, with IgG1 and IgG3 being the strongest inducers in the IgG family. Bound to antibodies, C1 complexes start lysing free floating C2 and C4 proteins, giving C2b and C4b subunits which jointly binds together and latch onto the microbial surface, forming a complex called the C3 convertase. Each C3 convertase cleaves C3 into C3a, a chemokine, and C3b, an opsonin. After enough C3b has accumulated, it can bind to the C3 convertase, upgrading it to a C5 convertase, having a similar proteolytic role for C5, giving the

chemoattracting C5a and C5b. C5b is an opsonin able to start the process of complement-driven lysis, by recruiting the protein C6 through C9 of the membrane attack complex, which are able to embed in the bacterial membrane and perforate it.

Immune cells harbor complement receptors at their surface, allow them to react to complement activation: this is first done by the release of C3a and C5a, both acting as chemokines on mast cells, neutrophils and macrophages. Before inducing lysis, complement opsonins are recognizing by phagocytic cells.

3.2.3 Immune privilege

Various locations in the human body are considered under a immune privilege, meaning they are restricted areas for the immune system. This is typically the case of the brain, which is protected by its own patrol force of microglial cells while entry is severely controlled via the blood brain barrier. Other areas of the body benefit from this unique status, like the placenta, testicles, liver, cornea, and the hair follicle. Immune privilege is variably enforced on a per tissue basis, thus immune privilege is not a black and white situation and different tissues have different privileges. The general mechanisms involved in restricted immune system's freedom are either directed at physically preventing entry of immune cells or preventing their activation.

To prevent entry, some tissues simply lack physical access by absence of lymphatic vessels or blood vessels, rendering access more difficult. Extracellular matrices can be reinforced to act as physical barriers, as seen in brain blood vessels, or biological barriers, by expressing death receptors ligands like FasL or PDL1, inducing the death of activated immune cell nearby.

Immune cell activation is limited in privileged tissues by reducing MHC proteins expression on cell surface These mechanisms essentially function as firewalls to keep a potential inflammation out of sensitive tissues, which possess important functions and low regenerative potential. In the unique case of placental immunity, immune privilege prevents destruction of the precious fetus who is technically a foreign object in the mother's body.

However, by sheltering self-antigens from the immune system constant surveillance, an unforeseen consequence is auto-immune reaction in case of an encounter. This is better illustrated in the case of immune cell entry in testicle tissue after an injury, which can cause partial or complete sterility via destruction of the seminiferous tubules and infertility.

The hair follicle has been identified as a site of immune privilege, notably the proximal part of the follicle, that knows the most changes throughout its cycle. The expression of MHC I is quasi-absent in the proximal hair layers,

4. Hidradenitis suppurativa, unknown yet visible

4.1 Definition and History of HS

4.1.1 Generalities

Hidradenitis suppurativa (HS), also called acne inversa or, in France, maladie de Verneuil (Verneuil's disease), is a chronic inflammatory skin disease affecting the pilosebaceous unit of the groin, breasts, buttocks, pubis or abdomen of patients. The disease usually happens in surges of inflammatory boil-like nodules and abscesses, evolving into deep, interconnected, purulent sinuses and scars after years of affliction.

Symptoms of HS, ranging from inflamed nodules to deep seated tracts all along the inflamed skin area, which produce significant pain and handicap for patients. Patients often describes the associated pain as sharp or throbbing, such pain correlates with the disease stage.

Tendrils (keratinized) and other lesions (cysts) initially sterile are colonized by entering microbiota opportunists, triggering an inflammatory response and initial tissue destruction. Further loss of barrier function allows entry of unchecked micro-organisms in the dermis, to which the immune system answers in full effect.

At late disease stages, the dermis has been deeply invaded by the growing keratinized tunnels, producing deep fistulas and scars. Destroyed follicles are now leaving room for crypt-like caves of continuous and interconnected subcutaneous tracts collecting purulent fluids out on the skin surface.

4.1.2 History

Hidradenitis suppurativa was first discovered in 1839 by French surgeon Frederick Velpeau, describing a "tuber shaped phlegmon". He observed such events on the axillary, mammary and perianal regions, areas prone to friction, rich in sebaceous follicles and often poorly cleaned in patients. Velpeau noticed that the process "usually ends in suppuration; healing is exceptional". He postulated this inflammation stems from the sebaceous follicles.

The disease was thus shortly known as Velpeau's Disease until 1854, when Aristide Verneuil, another French surgeon, independently described a similar affliction on patients affected by skin, sudoral tumors. In an autopsy, Verneuil depicted lesions as "a great number of little eschars scattered under the buttock area, with cavities linked by thin channels across the dermis, indicative of sudoral glands necrosis".

4.1.3 Populations and prevalence

The geographical distribution and prevalence of HS is highly heterogeneous: While most papers quote a tacitly accepted worldwide prevalence rate of 1%, no recent study support this number. Some mention a Danish estimate of HS morbidity, finding a prevalence of 4%. However, the most recent and comprehensive study on HS demographics and distribution gives a 0.3% prevalence worldwide, with deep geographic differences. The biggest prevalence is found in Europe (0.8%), while the rest of the world shows roughly a 0.2% HS rate. This heterogeneity in HS cases is illustrated by two national studies: A first study focused on Australian cases concluded that 0.67% of the population is affected, whereas a similar

study in China found a prevalence of 0.03%, with males four times more often affected than females[63].

4.1.4 Environmental factors

Hidradenitis suppurativa has been associated to multiple environmental factors, with smoking and obesity representing the two most clearly linked with the disease.

Smoking

In a German cohort study of HS, 55% of HS patients were smokers, as compared to an average rate of 22% for this country. An American study showed that smokers had 10-fold increase in prevalence as compared to the general population. The effect of nicotine on hidradenitis suppurativa etiology is not yet understood, one possible explanation could come from the aryl hydrocarbon receptor (AHR). AHR is a cytoplasmic transcription factor mediating the effects of numerous ligands, the most common and studied being dioxin, but also tobacco smoke and microbiota-derived indole metabolites. AHR plays a critical role in cutaneous inflammatory responses by activating the release of IL-22, produced by Th17 cells, a cytokine with a role in skin homeostasis and inflammatory responses. AHR is also highly expressed in the folliculosebaceous unit in humans. Constitutive AHR activation can affect epidermis proliferation and immune function.[64]

Obesity

Obesity, defined as having a body mass index over 25, is considered as a state of inflammation, a condition closely related to HS etiology. More than 80% of HS patients are overweight or obese[65]. Fat is a known factor in inflammatory diseases, as adipocytes can produce pro-inflammatory cytokines, adipokines, driving immune cell activity up. In the context of HS, where a chronic inflammation is observed, it is relevant to consider the role of adipocytes and nutrition on the disease onset. It is likely obesity isn't the trigger, as some HS patients do not present it, but significantly exacerbate its onset by increasing basal inflammation and skin rubbing. Furthermore, one dietary treatment banning yeast-based products produced positive outcomes on HS lesions[66].

Microbiota & Hygiene

In HS, microbiota has been shown to be a significant factor in the induction of the disease. Lesional skin displays an increased number of antimicrobial peptides.

Very few studies have been exploring the microbiota in HS, despite it being a skin disease, where microbiota vital role has been established and well understood.

Coagulase-negative *Staphylococci*, *Streptococci* and *Staphylococcus aureus* were found in most HS lesions on superficial and deep level cultures. [67]A great systematic review of microbiota samplings in HS lesions show anaerobic Gram negative rods are the predominant colonizers of HS lesions, with a majority of *Porphyromonas, Prevotella*, and *Bacteroides*[68]. Different profiles in relation to Hurley stage: 50% lesions stage I, *Staphylococcus lugdunensis* is found, more rarely *Propionibacterium acnes*. 90% of stage II and III lesions show *Prevotella* and *Prophyromonas, Strepotococcus milleri*[69].
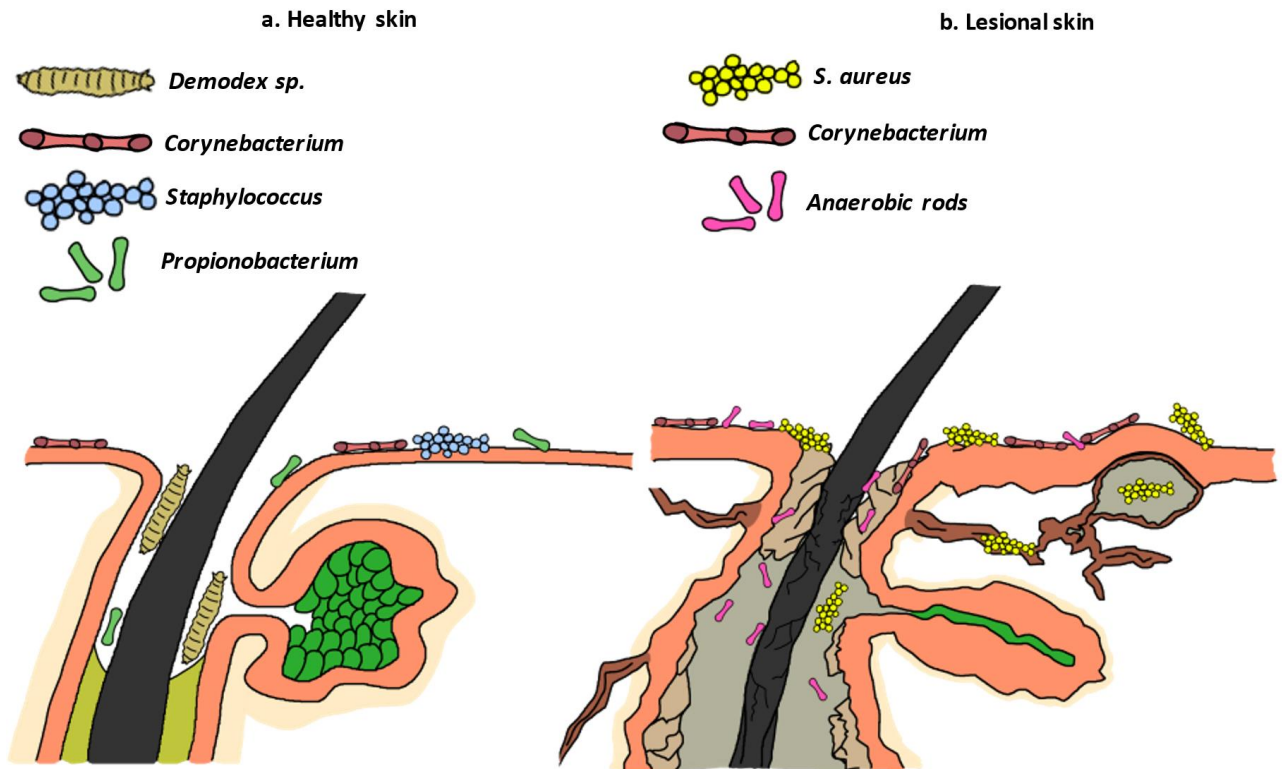
Figure 9. Hidradenitis suppurativa patients present important skin dysbiosis.
Distinguishing features of HS lesions are their colonization by opportunistic Staph aureus strains, from the hair shaft to the invading tendrils. Various anaerobic bacteria further invade the follicle, taking advantage of the abandoned niches from dying commensals. The fate of Demodex sp. is unknown in HS.

4.1.5 Diagnosis

Scoring methods

Hidradenitis suppurativa severity is assessed by a variety of classification systems. The first method and still the most widespread today, is the classification of Hurley he created in 1989. Using local skin lesions of a patient, Hurley separates them in 3 distinct stages:

1. Hurley Stage I: Singular or few abscesses, without scarring tissue or subcutaneous extensions.

2. Hurley Stage II: Recurring abscesses, scarring tissue and fistulas are observed. Some healthy tissue remains in-between lesions.

3. Hurley Stage III: Recurring abscesses without any remaining healthy tissue, scarring tissue interlinked via subcutaneous keratinized ducts.

Hurley's classification offers a good benchmark for HS progression and helping with decision making in the medical consult. However, it lacks the ability to judge the disease progression from multiple lesion sites, as it was initially created for axillary lesions. It is also unfit to assess the extent of the inflammation, and its rigidity reduces its ability to judge treatment response. The system can however be refined, as recently proposed by Horvath et al., where each stage is subdivided in relation to the observed symptoms and lesions.[70]

In a tentative to allow treatment response monitoring, a second system was put in place: the Sartorius score, declined in a few variants. The method consists of counting the number of affected regions, the number of lesions and the distance between two lesions. In some Sartorius variants, regions and lesions are weighted to emphasize their severity in the disease progression. However, this score was never validated by medical professionals, and other proven alternative scoring methods arrived, forcing the gradual abandonment of the Sartorius score by some countries.

One example of an improved system is the Hidradenitis Suppurativa Clinical Response (HiSCR) score, tailored towards treatment response. The HiSCR is defined by a decrease of ≥ 50% in the number of inflammatory lesions (nodules, abscesses, fistulas) without increased number of abscesses and fistulas. Although well indicated for clinical studies, this score fails to address disease severity.

A recently proposed assessment method is the International Hidradenitis Suppurativa Severity Score System or IHS4[71]. IHS4 is based on an experts' panel opinion about existing classification methods, ultimately producing its own scoring methodology. IHS4 looks like the Sartorius score, as it uses the number and type of lesions and the number of affected areas to appreciate the disease progress. IHS4 score is easier to perform in daily clinical practice and achieves a greater degree of accuracy in relation to Hurley's scale.

Diagnosis delay

Hidradenitis suppurativa patients suffer from a high diagnosis delay, with a worldwide average of 7.2 years between the apparition of symptoms and the first confirmed diagnosis by a doctor. This astonishing lag is the consequence of many factors. Patients themselves are

often unbothered or refusing to seek help for a series of symptoms that they underestimate. Physicians can be mistaken as the disease is often confused with other skin diseases of a similar appearance (eczema and vitiligo). Access to healthcare can also delay the diagnosis in some countries. These aggravating factors are not unique to HS, but the evolution of the disease, its impact on the patient life and the few treatments available significantly worsen the outcome of a late diagnosis.

4.1.6 Treatment

Antibiotics

One of the first prescribed treatments for an HS diagnosis is antibiotics. In France, a questionnaire addressed to physicians revealed the widespread use of antibiotics on all stages of HS, with only 20% of them not prescribing antibiotics[72]. Most antibiotics used are tetracyclines and a combination of ceftriaxone and metronidazole for severe cases. Tetracyclines are large spectrum bacteriostatic inhibitors able to passively diffuse through membranes. They act by obstructing the 30S ribosomal subunit and stop protein synthesis, preventing motion and growth, paralyzing bacteria completely rather than outright killing them. However, this mechanism also affects mammalian cells to some extent, which makes the prolonged and intense usage of tetracyclines toxic. Several attempts were made to develop a standardized antibiotics course to treat HS. In France, the "tritherapy" from Necker-Pasteur by Aude Nassif et al., combining rifampicin, moxifloxacine and metronidazole yielded 57% of complete remission, varying with Hurley stages (100% at stage I, 87% at stage II, 17% at stage III)[69]. In the UK, a ten-week combined course of rifampicin and clindamycin was tested on a small cohort of 14 patients. 8 patients attainted remission, while 4 did not show delayed disease progression[73]. However, the length of the antibiotic exposure slightly exceeded the usually recommended maximum of three months of continuous treatment[72].

Biologics

Considering the auto-inflammatory nature of the disease, one of the first administered treatments for hidradenitis suppurativa are anti-TNF-α. As seen in Chapter 5, TNF-α is an ubiquitous pro-inflammatory cytokine, which multiple studies now found elevated in HS serum.

Hormonal blockades

Spironolactone is a steroid analog of androgen hormones, blocking the hormone receptor for aldosterone, testosterone and dihydroxytestosterone and reduces the level of male hormones. Alternative finasteride, a 5a-reductase inhibitor, or DHT blocker, has also being trialed.[74] Such medication is often prescribed to reduce hirsutism in women or early puberty in men, again suggesting a direct link between sex hormones balance and HS.

Chemo and radiotherapies

An unconventional case report freshly published in Thailand describes the use of radiotherapy in a chronic hidradenitis suppurativa patient. 3 months after treatment, the affected skin did not relapse[75]

Type	Name	Mechanism
Antibiotics	Tetracyclines	Wide spectrum bacteriostatics
	Rifampycin + clindamycin	Wide spectrum bacteriostatics
	Rifampycin + moxifloxacin + metronidazole	Wide spectrum bacteriostatics
Hormonal therapies	Spironolactone, finasteride	Androgens specific competitors
	Contraceptive pill	Higher estrogen levels
Biologics	Adalimumab, Infliximab	Anti-TNF-α antibody
	Anakinra	Recombinant IL-1R antagonist
	Ustekinumab	Anti-IL12/23 Antibody
Others	Radiotherapy	Halts epithelial proliferation

Table 2. Available treatments for hidradenitis suppurativa patients.

4.2 Etiology of hidradenitis suppurativa

4.2.1 Generalities

The current understanding of HS physiopathology is highly dynamic and subject to change. While the disease is usually assessed and described using the Hurley stages, it is better understood through the actual physiological reactions underneath the skin. We will separate the disease progression in three stages, not only to mimic Hurley's classification but also because it fits with the pathological mechanisms identified so far.

4.2.2 Genetic background

40% of HS cases have familial antecedents, underlying a genetic component to the disease[76]. Hidradenitis suppurativa is often associated with other skin or auto-inflammatory diseases: Crohn's disease, an inflammatory bowel disease, is often developed secondarily to HS.

Γ-secretase

γ-secretase is a multidomain protease widely distributed in mammal tissues. Among its four domains, two are most important for its function: Nicastrin, a glycoprotein implicated in the complex stability and structure, and Presenilin, the catalytic subunit. γ-secretase cleaves a variety of substrates, the most famous ones being APP and Notch.

Multiple studies on HS genetic background point at a family of genes related to the Gamma (γ)-secretase complex. It is unclear how exactly gamma-secretase is implicated in HS onset. While it has an important role in Notch signaling, a pathway relevant to hair follicle development, HS patients bolster seemingly normal hair follicles until the disease starts.

Genetic studies on HS patients discovered a number of mutations on the γ-secretase itself, most of them focused on the extracellular segment of the nicastrin subunit.[77] Most mutations either produce a truncated protein or prevent its splicing, both likely to activate the unfolded protein response pathway and ultimately the destruction of the mutated protein.

While we know so far of γ-secretase mutations in , a study shows they represent a marginal portion of the patient population, relativizing the importance of the protein in the disease physiopathology.[78]

Sex hormones and AHR

Hidradenitis suppurativa develops early in life, often soon after puberty, hinting at a hormonal component in the disease evolution. In one case, HS flared up after a boost in ovarian androgens, and similarly during menses, with low estrogens levels.[79,80]

4.2.3 Initiating events

Follicular epidermis dysfunction

Lesional skin epidermis appears thicker with irregular rete ridges, suggesting profound structural defects[81]. This mainly affects the outer root sheath, appearing hyperplasic with material build up in the nearby lumen, observed as cornified debris and keratin rod-like remnants. This suggests an accumulation of lysing keratinocytes in the infundibular area, and improper debris clearance by the immune system. While active phagocytosis is registered in the affected areas, bigger keratin debris often cannot be disposed of, producing large multinucleated bodies from the fusing macrophages around them[82]. Furthermore, lesional skin displays a thinner basal membrane, allowing more immune cell infiltration and potentially breaching the immune privilege of hair follicles[83].

Microbiota perturbation

Skin microbiota of HS lesions differ significantly from healthy skin, where it features an abnormal balance of commensals and opportunistic pathogens. The abundance of anaerobic bacteria in lesions correlates with disease severity.[84] Bacteria are found widespread in various HS lesions, including the, prefiguring their eventual entry to the dermis.

4.2.4 Immune system overreaction

The description of the immune system role in HS has been mostly descriptive, as it appeared as a consequence of the initial cause more than an trigger of the disease[83,85]. However there are signs of a sustained and damaging inflammation associated with HS lesions[86–89]. Resident skin T cells and macrophages[82] are first implicated in the inflammatory process. Macrophage activation and the release of pro-inflammatory cytokines and chemokines allow to recruit and stimulate other immune cells.

Neutrophils are the first to enter the dermis in HS [82,90], their contribution to the disease has been observed in various aspects. HS lesions also show the presence of NETs[88], most likely triggered by the invading microbiota from micro ruptured tunnels or unknown sterile activators. While NETs are a potent bacterial control tool, they can also induce the production of autoantibodies. Hidradenitis suppurativa patients possesses elevated titers of autoantibodies directed against NET compounds: dsDNA, citrullinated proteins, histones H2A and H4 and LL37[91]. These antibodies are mostly of the IgG isotype, although IgA was also reported. Antibodies imp, we must now dive into the adaptative aspect of HS inflammation.

Adaptative immunity

As fundamental actors of autoimmunity, B lymphocytes and antibodies were oddly absent from HS physiopathology, likely due to the misconception that B cells are largely uninvolved in skin autoimmunity. First solid evidence of B cell implications in Hidradenitis suppurativa

came in a 2012 study by Van der Zee et al.[82] which depicted CD79a+ B cells and CD138+ plasma cells infiltrating chronic HS lesions. More recently, the work of Byrd et al. allowed to better understand the function of B cells in HS, as they demonstrated the presence of antibodies directed against citrullinated proteins[88]. These antigens come directly from NETs produced by infiltrating neutrophils, which react to dermis invasion by the abnormal follicular epithelium and/or by the associated microbiota. More studies came to confirm the presence of antibody-secreting cells in HS lesions[92] and peripheral blood[93]. More recently, Carmona-Rivera et al. cemented the notion of autoantibodies directed at self-nuclear antigens in HS lesions.[91] As to how B lymphocytes manage to find and enter HS lesional skin, Witte-Händel et al. showed an increase of pro-inflammatory messengers, including CXCL13, which has a chemoattracting effect on CXCR5-expressing B cells.[94]

We have yet to understand how B cells are activated and prompted to produce antibodies against autoantigens. We know Th17 cells and related cytokines IL-17A and IL-22 are heavily featured in HS lesional skin and blood, as quantified, for instance, by an elevated Th17/Treg ratio[89,95]. Th17 cells can act as potent helper cells for B cell activation, proliferation, and antibody secretion. IL-17A and IL-22, cytokines produced by Th17 cells, can induce class switching to different IgG subtypes *in vitro*[96].

One of HS hallmarks is an overproduction of defensins and an activation of the complement within the dermis[97,98], both pathways being supported by Th17 cells[99]. A Th17 orientation also stimulates granulopoiesis and recruitment of granulocytes in the tissue via IL-17. CXCL8, found abundantly in HS lesions and responsible for neutrophil infiltration, can be cleaved by NE enzyme to activate Th17 production of IL-17, creating a self-destructive positive feedback loop[100].

It may thus be important to consider the dysregulated Th17/Treg balance in HS as a tipping point in the disease progression. Indeed, in one study, more than 80% of patients showing Th17/Treg imbalance were at Hurley stage II or III[95]. As to why this T cell ratio is abnormal in HS patients, it is best to keep in mind that this ratio is also affected by a myriad of environmental factors and conditions: smoking, obesity, or inflammatory bowel diseases, which are all associated with HS, promote Th17 and inflammation systemically. Furthermore, effective anti-TNF therapy against HS symptoms lead the Th17/Treg ratio to shift in favor of regulation[95]. All this of course presupposes the imbalance is present beforehand, instead of being a consequence of the local inflammation. Unfortunately, no solid literature so far addresses the Th17/Treg ratio in patients per Hurley stage.

Integrated physiopathological model

Here, I will attempt to propose a general integrated hypothesis of lymphocytes role in HS. Overall, our knowledge of how B cells affect HS progression remains young and opaque, deserving of further clarifications to better understand its mechanisms and uncover potential diagnostic tools. It is unclear whether HS should be primarily linked to epithelial dysfunction, microbiota, or immune activity. The apparition of swelling and dermis invasion prior to

inflammation, unresolved disease progression despite anti-inflammatory treatment, both these findings suggest to us epithelial dysfunction is the first step of the disease. Regardless, the combination of these three factors further fuels this vicious cycle, where it inevitably spirals out of control and leads to follicular swelling and tissue damage, eventually leading to a ruptured follicle. Both T and B cells may enter the skin via the expression of the CLA on their surface, following the gradient of chemokines, including CXCL13, produced by the inflamed tissue. B cells may be an important yet late actor in HS inflammation. In the dermis, B cells differentiate into plasma cells, under the influence of the strong pro-inflammatory local environment of macrophages, granulocytes and Th17 cells. The dwindling numbers of Treg further sending the inflammation in an out-of-control spiral.

4.3 Research models for Hidradenitis suppurativa

Hidradenitis suppurativa is a uniquely human disease and almost no equivalent condition has been observed in animals. Worth noting is a case report published in 1969 for "canine HS"[101]. Yet, while the affected areas, lesions and symptoms seem close to the human HS, this was not due to a follicular disease, but to a sweat gland infection by *S. aureus*. It is therefore not suitable to study human HS pathophysiology. Patient samples remain the lone reliable material to conduct in-depth studies on its physiopathology. However, patient samples remain limited: low prevalence in the population, diagnosis delay, disease onset, specialist training and most importantly consenting patients are all restricting factors in further understanding HS . Thus, only a select number of institutes bolster the privilege of patient sample studies. There lies the benefit of laboratory models, be it *in vitro* or *in vivo,* as they open the door for widespread research means and potential. As a review of human-based models was previously published by we and collaborators[102] , this chapter will focus on animal models.

4.3.1 HS patient skin xenograft

In 2020 Quartey et al. introduced a potential hidradenitis suppurativa model using xenograft of healthy foreskin or HS patient lesional skin onto a NSG-SGM3 immunocompromised mice, lacking mature lymphocytes and producing human SCF, GM-CSF and IL-3[103]. They reported successful graft, with persistent pigmentation in the healthy tissue for two weeks. As opposed to healthy skin, grafted HS tissue was inflamed and lost pigmentation, which could be due to the presence of ROS that affect melanocyte function. Overall, very little in the way of the disease physiopathology was observed, however the concept merits discussion. Xenograft mice models have been widely utilized in the study of skin diseases, with successful models existing for psoriasis and alopecia areata.

While such models allow to study the disease in vivo, they still rely on patient samples, keeping the issue of availability unsolved for research teams without patient access. Furthermore, xenografts require immunocompromised mice, precluding direct studies on the

immune aspects of HS. The authors acknowledge this limitation and propose to repopulate immunodeficient mice with human immune cells, ideally also isolated from patients.

Thus, an HS xenograft model seems more relevant in studying the epidermal events related to disease progression or initiation, where more information could be gathered on how hair follicle epithelial layers grow uncontrollably into the characteristic tendril-like lesions.

4.3.2 Nicastrin knock out in basal keratinocytes

In the same year, Yang et al. published an "HS-like" mice model using a conditional knock-out of the NCSTN gene, encoding Nicastrin, in Keratin 5-expressing cells[104]. A crucial element for basal membrane contact, keratin 5 is both expressed in the basal layer of the epidermis, the ORS and the bulge[105]. Altered ɣ-secretase function in these cells will affect several pathways, most notably Notch, and previous studies showed the importance of Notch pathway in hair follicle development and maintenance[106–109]. The authors intend to delete Nicastrin expression in the whole epidermis as well as in superficial follicular layers. The authors monitored the skin, finding Notch protein decrease in the targeted NCSTN KO. Hair loss and hyperkeratosis was prevalent on homozygous knock outs, showing a relation between Nicastrin loss and basal keratinocyte homeostasis in the hair follicle. Inflammatory markers were observed in the KO skin, with IL-36a, a strong infiltration of macrophages and a Th17 response marked by RORɣt positive cells and some IL-17a. was observed. These suggests the outcome of the conditional deletion is more than on hair follicle structure, hair follicle destruction producing an inflammatory response.

This model is based on the finding of ɣ-secretase mutation in some AI-affected families[110–112], assuming ɣ-secretase has a direct role in the disease development. However, only a minority of HS patients display such mutations[78]. Mutations in the patients are not always total deletions and the level of tissue destruction observed is extreme, as it affects the entire skin, and isn't representative of the disease environment or progression.

Regardless, the model does produce an inflammatory response compatible with currently acknowledge HS hallmarks: pro-inflammatory cytokines and a Th17 response. The authors did not find a strong neutrophil infiltrate in the skin, one of HS tell-tale signs. It is also unclear if the inflammation happens early or is an understandable consequence to the massive tissue structural failure, while HS inflammation triggers relatively early in the disease progression.

In the end, the skin-wide approach and its consequences are understandable compromises for an *in vivo* model, especially with mice bolstering way more hair follicles than humans. The authors approach could be refined by choosing a more follicular relevant promoter like Sox9, CD200 or Keratin19.

4.3.3 Inflammation under a high-fat diet

In 2021, Nakamizo et al. have shown the effect of a high fat diet in mice on skin irritation[113]. In this model, hair follicles were plugged by dead keratinocytes when intaking a high amount of fat for eight weeks, a typically observed phenomenon in histology of lesional skin. This plugging was not accompanied by immune cell infiltration without further stimulation via a daily topical application of PMA to the ears for four days. Reminiscent of a hallmark of HS , PMA irritation produced neutrophil infiltration in the skin for 24 hours in mice with high fat diet, which was absent in control mice. The choice of a high fat diet is quite relevant, as hidradenitis suppurativa is strongly correlated to obesity. Yet, the exact pathways by which one influence the other remain so far unknown. In this paper, Nakamizo et al. prove a potential trigger and sustaining factor of HS lies in the poor diet of patients.

While this model succeeds in producing plugged, swollen follicles and immune infiltration, it fails to produce the characteristic tendril-like growth of HS. Furthermore, the high fat diet alone is not able to induce inflammation. This is in line with the multifactorial etiology of HS : obesity itself does not contribute alone to the physiopathology and clearly requires triggering events of unknown nature, as not every HS patient is obese. This is also where the model stops being relevant, as it cannot explain HS in patients without history of overweightness or obesity. Overall, a high fat diet could be a promising addition to any other potential mice model.

4.3.4 Folliculitis by Notch deficiency

Mice were engineered for a targeted deletion of ADAM10, a metalloprotease responsible for cleaving Notch, in the hair follicle [114]. As ADAM10 is necessary for NCID release, its absence disrupts Notch signaling. This resulted in a pro-inflammatory transcriptomic profile in the affected hair follicle cells, producing more CCL2, CCL20 and IL1α/β and expressing MHC class II on the keratinocytes' surface. 35 days after birth, the skin microbiota of *Adam10*-deleted mice were deeply changed, with the disappearance of some species (*Bacteroidetes*, *Bacteroidales*), these empty niches became occupied by Corynebacterium, which soon made-up the largest proportion of the mice's skin commensal flora. This dysbiosis further exacerbated the initial folliculitis, ultimately leading to complete hair follicle destruction.

While this does not represent a direct model of Hidradenitis suppurativa, as it lacks the hallmark tissue invasion and subsequent lesions, it remains interesting for multiple reasons. First, a dysfunction of Notch signaling is in line with known mutations in HS patients, as γ-secretase is also important in Notch signaling. While this covers a minority of patients, the induced dysbiosis is a well-studied aspect of HS and present in most patients. In both this model and HS patients, defensins function is altered. In their model, the authors correct the dysbiosis via antibiotics and reverse the slow epithelial destruction. In a similar fashion, antibiotherapy was shown to be relatively effective in HS patients. Interestingly, the mice immune systems try to counter the dysbiosis via a Th2 response. While Th2 response was not shown to be involved in HS, where a Th17 response seem predominant, it remains an understudied area of the disease and could be uncovered later. The folliculitis in the mice is

triggered by poly(I:C) injection, mimicking a type 1 interferon response to a viral infection. In HS, the disease is not related to a pathogenic trigger, but other inflammatory triggers could be tested on the *Adam10* mice model.
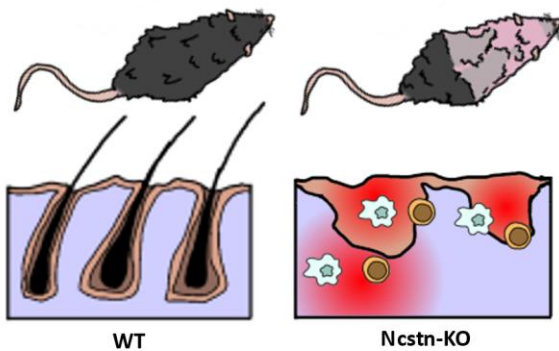
HS patient skin xenograft

foreskin

HS patient skin
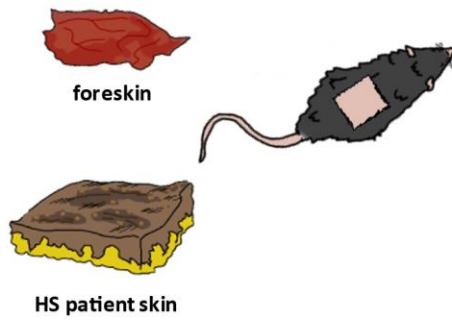
+ Use total human skin

− Still requires human samples
− No immune system

**Inflammation under a high-fat diet**

Regular diet   High-fat diet
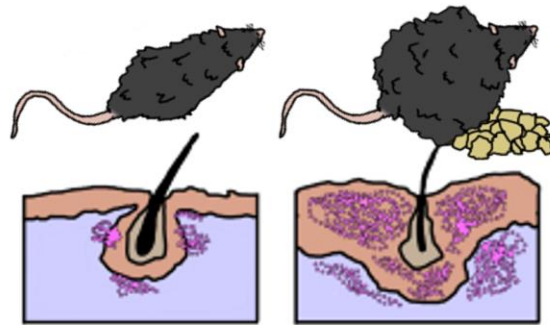
+ Neutrophilic response
+ Hyperkeratosis
+ Relevant environemental factor model

− Inflammation is PMA induced

Nicastrin KO in basal keratinocytes

WT   Ncstn-KO

+ γ -secretase deficency
+ TNFa and Th17 response

− Few patients have γ–secretase mutations
− Not all mutations are knock -out type
− No typical lesions and neutrophilic response

Folliculitis via Notch deficiency

WT   Adam10-KO
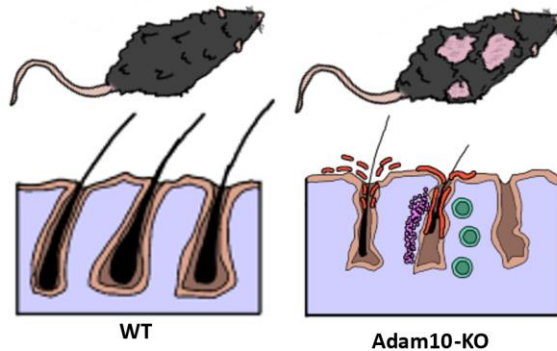
+ Notch deficency in the follicle
+ Dysbiosis model, treatable
+ Immune response with myeloid infiltrate

− Poly(I:C) induced
− Unclear myeloid infiltrate nature

Figure 10. Potential research models for Hidradenitis suppurativa and their main characteristics.

While not directly related to HS, these mice models present interesting characteristics for future research. Each model is graphically represented with its pros and cons underlined below.

RESULTS

Foreword

Through this introduction I have shown hidradenitis suppurativa is yet to be fully understood and treatable, causing significant damage to the affected individuals and representing an economic burden worldwide.

To expand our knowledge of the disease and foster innovation to the therapeutic arsenal et our disposal, this thesis was integrated into a greater, pan-European, effort: **B**iomolecular **A**nalysis for **T**ailored **M**edicine in **A**cne i**n**versa, or **BATMAN**.

BATMAN regroups several clinical and research teams across seven different countries, with the common objective of applying their expertise in tackling HS.

My objectives in this endeavor were the production of *in vitro* and *in vivo* models of HS, potentially relieving the deficiency in the available toolbox against the disease; and the analysis of patient blood lymphocytes populations to uncover markers of the disease progression. As such, our work was divided in three axes:

1. Human skin reconstruction on an already proven model of 3D culture used in our team.

We wanted to produce a reconstructed human skin from patient skin cells, be it keratinocytes, fibroblasts and seeding blood derived immune cells inside. Selected patients have known mutations that potentially affect keratinocyte homeostasis (γ-secretase) or skin barrier function (desmoplakin).

Scientific question: Will mutated keratinocytes-derived epidermis behave differently compared to a healthy human epidermis ?

One of HS hallmarks is an unchecked growth of keratinocytes, ultimately leading to epidermal invasion into the dermis. Mutated epidermis may show defects in growth, with overgrowth and altered structure. Desmoplakin mutated keratinocytes might show defect in reconstructed skin waterproofing.

We expect the human reconstructed skin model using patient cells to produce an altered epidermis, hyper, maybe growing into the dermis below. If immune cells are seeded inside these models, they could develop a pro-inflammatory phenotype in contact to the mutated epidermis.

2. Establishment of an *in vivo* model on either genetically engineered mice or via external stimulation.

Our goal here was to reproduce one or multiple HS hallmarks *in vivo*, using already available mice models of inducible and conditional Atg5 knock-out.

Scientific question: Can an autophagy deficiency in Sox9 derived hair follicle cells lead to like HS upon repeated induced stress?

Autophagy and γ-secretase function have been demonstrated *in vitro*, and a portion of HS patients display γ-secretase mutations disrupting its normal functions. We thought one of the ways γ-secretase could affect keratinocyte function is via autophagy, where it plays an

important regulatory role. Autophagy is also relevant to immune cell clearance. By inducing an Atg5 deletion in the hair follicle and resetting its cycle, we expected the autophagy deficiency, aided by depilation, to produce defective hair follicles.

3. Recovery, storage, and cytometric analysis of patient PBMC.

We wanted to establish a link between HS and blood-born lymphocyte populations, to uncover the role of the adaptative immune system in HS, confirm a suspected correlation between blood lymphocytes populations and disease severity, and facilitate future diagnosis of the disease. This study also allowed the of a bank of patients recruited from BATMAN, that can be further studied, and exploited in further experiments.

Scientific question: Do HS patients B and T lymphocytes subpopulations differ in proportions or in their cytokine profile to healthy controls?

Hypothesis: HS being an auto-inflammatory disease, we supposed T and B blood lymphocytes would reflect this condition by displaying more activated and differentiated T and B cells than healthy blood. While the literature shows most HS differences can be found in the skin, and few in the blood, we expected to find activated skin-homing T cells, with an increase in the Th17 subtype.

Gamma (γ)-secretase inhibition in vivo alters autophagy flux in specific regions of the hair follicle

Wacym Boufenghour[1], Michele Boniotto[2], Cécile Nait-Medour[2], Vincent Flacher[1*]

1 Laboratory CNRS UPR3572 Immunology, Immunopathology and Therapeutic Chemistry (I2CT) / Institut du Médicament de Strasbourg, Strasbourg, France.

2 University Paris Est Créteil, INSERM, 94010, IMRB- Équipe Leboyer, Créteil, France.

* Correspondence: v.flacher@ibmc-cnrs.unistra.fr

Summary

Hidradenitis suppurativa (HS) is an auto-inflammatory disease affecting the pilosebaceous unit in moist skin-fold areas (groin, armpits, under the breasts, buttocks, and scrotum), concerning around 0.2% of the world population so far. The causative events of pilosebaceous inflammation remain elusive, and no *in vivo* model allows yet to study the initiation and the progression of the disease. Several familial cases of HS have been linked with γ-secretase mutations. CRISPR/Cas9-mediated genetic editing allowed to replicate patient-derived nonsense mutations of NCSTN and PSENEN genes, encoding γ-secretase subunits, in the HaCat epithelial cell line *in vitro*. Both alterations of the ɣ-secretase led to an impairment of the autophagic flux. This prompted us to investigate whether and how hair follicles might be altered by these pathways *in vivo*. We performed systemic inhibition of the γ-secretase in C57BL/6 mice right after a depilation allowed to restart a synchronized hair follicle cycle. As a outcome, we could observe delayed follicle growth, hair depigmentation and impaired autophagy. This led us to hypothesize autophagy to be involved in hair follicle cycle growth and inflammatory regulation. Thus, *Sox9cre^{ERT2}*, *Atg5^{flox}* and *Atg5^{+/-}* mouse strains were combined to generate selective ablation of ATG5, a key element of the autophagy machinery, from the hair follicle. Consequently, a slight impairment of autophagy flux in cells of the upper follicular regions could be detected. However, our preliminary results did not depict obvious alterations of hair growth, pigmentation, or depilation-induced inflammation. Therefore, although γ-secretase inhibition had potent effects on both hair follicle cycle and autophagy, we are yet unable to unequivocally demonstrate that autophagy impairment alone could lead to significant defects in hair growth and immune monitoring of the follicular renewal.

Foreword

Hidradenitis suppurativa (HS) is a disease of the hair follicle defined by abscesses, deep-seated lesions and scarring on the skin surface. Discovered in the last century by French surgeons, first wrongly considered as an apocrine disease[79], several hypotheses have emerged to explain this perplexing condition. The disease often starts at puberty[115], where the body undergoes important hormonal changes including in the skin and hair follicles. Dysbiosis is often revealed in HS patients[84] and antibiotherapies have a demonstrated efficacy in relieving inflammation in HS patients[72]. Obesity and smoking are overrepresented in the patient

cohorts[116]. These facts suggest that HS is a multifactorial disease, where the combination of genetic, physiological, and environmental factors create the perfect storm in the hair follicles, with a now well-documented progression. In early stages of HS involve uncontrolled, tumor-like growth of the follicular epithelial layers[85,117], inducing an obstruction of the follicular canal and dermal invasion by keratinized tendrils sprouting from the follicle. Obstructed follicles swell from the accumulating epithelial debris and unchecked microbiota. The immune system predictably reacts, mobilizing professional phagocytes to try and contain the dysregulated epithelial tissues and commensals[89,90]. Ultimately, follicular rupture occurs into the dermis, producing a full immune response with a massive recruitment of neutrophils, T and B cells[88,91,92]. This phase may be considered as the physiological origin of the observed flare events in HS patients, where pain, inflammation and lesions reach their peak. Over time, these inflammatory flares irreversibly damage the follicle and the neighboring skin tissue. This results in deep-seated scars and keratinized ducts, with overwhelming consequences on the patient's quality of life. Therapies using anti-TNF-α and antibiotics succeed only in some patients, while the most extreme cases must resort to ablation of the affected skin region(s).

In 1992, Yoshinori Ohsumi and his colleagues at the University of Tokyo discovered that autophagy also occurs in yeast[118]. Using a light microscope, they noticed that a few hours after starving yeasts of nutrients, the vacuole was filled with vesicles containing cytoplasm components. The vesicles responsible for autophagy are called autophagosomes and spurts following a series of stereotypical steps[119] **(Figure XX)**. Autophagy is a vital process for cell homeostasis[120], metabolic processes[121], and apoptotic cell clearance[122]. Interestingly, autophagy is also relevant to hair follicle maintenance: stimulation of autophagy can increase hair growth[123], autophagy defects can lead to hair follicle cycle disruption[124]. Furthermore, defects in autophagy lead to important skin barrier dysfunction[6,7], improper neutrophil clearance, and increased inflammation[125,126].

The γ-secretase is a protein complex is assembled from four individual subunits, Nicastrin, Presenilin-1, APH-1 and PEN-2, respectively encoded by NCSTN, PSEN1, APH1A and PSENEN genes. The γ-secretase is in the transmembrane space of multiple cell types, where it is responsible for cleaving membrane-bound proteins to release their intracellular domains[127]. Thus, the γ-secretase can regulate a variety of essential physiological signaling pathways, most notably in Notch-regulated cell lineages like the hair follicle. In this context, γ-secretase seem to intervene in two points: hair follicle organogenesis, where Notch1 is required for placode patterning[128]; and hair follicle maintenance, where it drives cell fate decision during hair follicle stem cells asymmetrical division[106]. Notch role in stem cell maintenance is established and found in other cell types[129,130]. Independent whole exon sequencing of HS patients from across the globe uncovered several γ-secretase mutations, most notably on NCSTN and PSEN1[111,131–133].
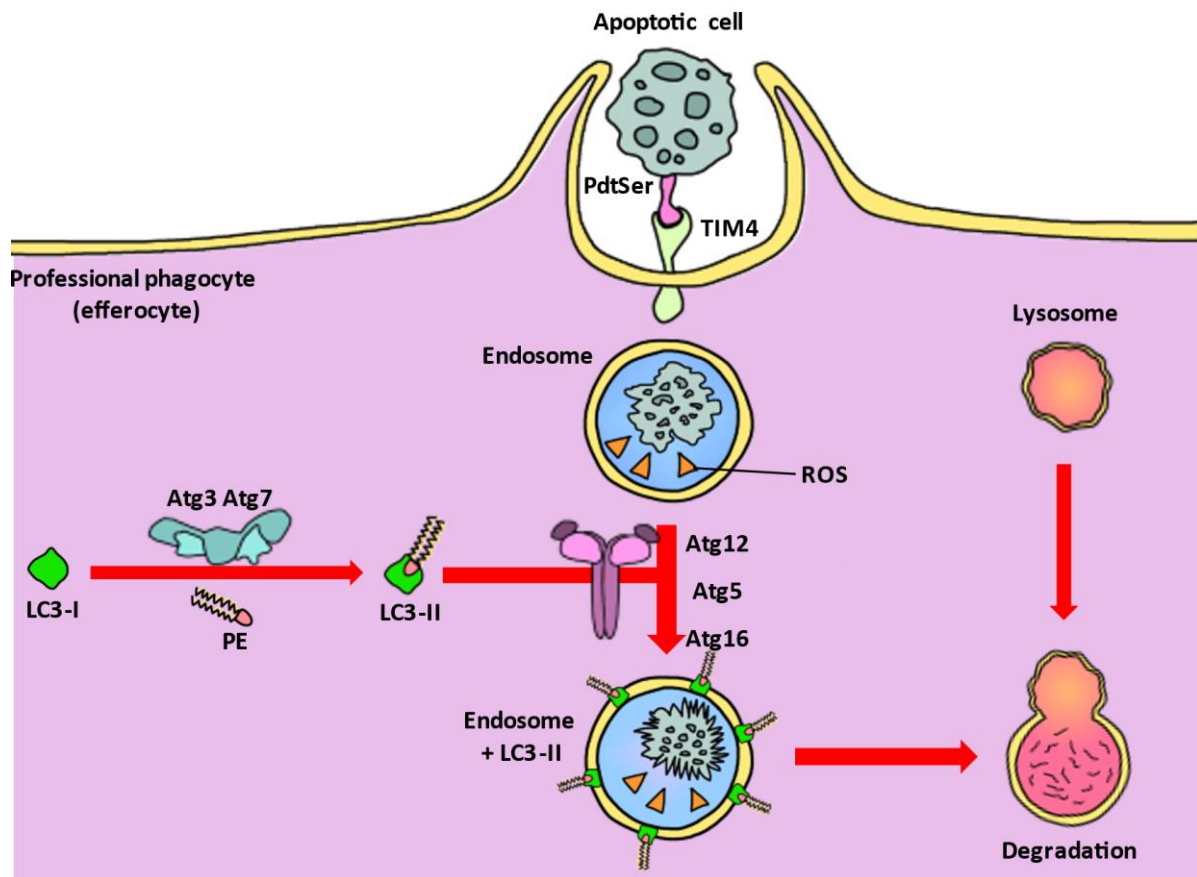
Figure 11. Autophagy pathway involved in apoptotic clearance (efferocytosis).
"Eat-me" molecules at the surface of dying cells trigger their phagocytosis by professional efferocytes.
Through the pathway of autophagy, LC3-I molecules are phosphoethanolaminylated by the Atg3/7/8
complex. LC3-II is now embedded in the endosome membrane via the Atg5/12/16 complex, allowing
its fusion with the lysosome and complete degradation of the apoptotic cell.

Here, we report an intriguing autophagy impairment in vitro resulting from PSENEN and NCSTN nonsense mutations observed in HS patients. Based on this, we developed two in vivo mouse models: one consisting in a systemic inhibition of γ-secretase, the other using hair follicle-specific genetic deletion of the key autophagy gene *Atg5*. We performed preliminary investigations of these models, attempting to highlight potential phenotypic alterations of the hair follicle that could be relevant to HS pathophysiology.

Material & Methods

LC3-RFP-GFP assay

Cells were infected with a lentivirus containing LC3-RFP-GFP, autophagy was then induced via starvation with HBSS. Cells were grown in iBIDI (Nanterre, France) 8-well microplates at 50,000 cells per well. The next day, the cells were deprived of nutrients and amino acids substituting the culture medium with Hanks' Balanced Salt solution (HBSS - Thermofischer Scientific) and treated or not with Bafilomycin A1 (200nM) to inhibit it.

Mice

Mice were bred and maintained on a C57BL/6J background at the animal facility of the Institut de Biologie Moléculaire et Cellulaire. Atg5$^{flox/+}$ and Sox9-cre^{ERT2} were obtained from collaborators and Atg5$^{+/-}$ mice were generated by Dr. Frédéric Gros[134]. [Atg5$^{+/-}$; Sox9-cre^{ERT2}] were obtained from a first cross between Sox9-cre^{ERT2} and Atg5$^{+/-}$, then bred to Atg5$^{flox/flox}$ to obtain [Atg5$^{flox/-}$; Sox9-cre^{ERT2}] and littermates [Atg5$^{flox/+}$; Sox-cre^{ERT2}] and [Atg5$^{flox/+}$]. Atg5$^{flox/flox}$ were obtained by breeding Atg5$^{flox/+}$ together until obtaining sufficient pool of Atg5$^{flox/flox}$ to generate [Atg5$^{flox/flox}$; Sox9-cre^{ERT2}] from a second cross with Sox9-cre^{ERT2} to obtain [Atg5$^{flox/flox}$; Sox9-cre^{ERT2}] and littermate [Atg5$^{flox/flox}$]. Mice were genotyped for their Atg5 allele and the Sox9-cre^{ERT2} transgene as previously described[134,135]. All mice were bred and maintained in accordance with guidelines of the local institutional Animal Care and Use Committee (CREMEAS).

Γ-secretase inhibition assay

The γ-secretase inhibitor LY-411,575 was purchased from Sigma-Aldrich and kept on dry ice at a concentration of 25mg/mL. Upon reception the LY-411,575 was diluted to 5mg/mL in DMSO and stored in 150μL aliquots at -20°C. For two weeks, mice were daily administrated with LY-411,575 diluted to 0.75mg/mL in cooking oil, calculated to deliver around 0.025 g/kg to each treated mouse. On the third day of treatment, mice were anesthetized, their back shaved and depilated with wax strips as to reset the hair follicle cycle.

Skin collection and digestion

Following mice sacrifice, back skin was shaved, harvested, and floated on cold PBS for 5 minutes. Skin was then laid upside down on a dry surface and the subcutis was carefully scrapped with a scalpel and discarded. Remaining skin (epidermis and dermis) was finely minced with scissors in a dry petri dish. Minced skin was placed into a 1.5mL Eppendorf with 1mL of digestion mix. Digestion mix consists of RPMI 30μL/mL Liberase 30μL/mL DNAse, tubes were placed at 37°C under 1000 rpm agitation (Thermomix). After 60min, 100mL of trypsin-EDTA 0.25% was added to each tube and digestion continues for 10 minutes. Tubes were collected, content was filtered through a cell strainer (100μL) and centrifuged (500g, 5min), supernatant discarded.

Autophagy inhibition

Collected pelleted cells from skin digestion were resuspended in complete RPMI at 20M/mL and 100μL were seeded in a sterile flatbottomed 96-well plate. Chloroquine and bafilomycin were diluted to 1/500 and 1/5000 respectively in complete RPMI and 100μL was added in each corresponding well **(see Figure XX)**, amounting to a final dilution of 1/1000 and 1/10000 respectively. For the uninhibited condition, 100μL of RPMI were added. Cells were kept overnight (16 hours) in a cell incubator at 37°C 5% CO2. The next morning cells were resuspended by up-and-down pipetting, seeding in a V-bottom 96-well plate, and pelleted via centrifugation (500g 5min).

LC3 assay and flow cytometry

Pelleted cells were washed with PBS one time and then stained with FVD450 at 1/1000 dilution in PBS for 15min. Surface staining was performed in SE (PBS 2% SVF) with anti-CD45,

anti-CD200 and anti-Sca1 antibodies to gate hair follicle subpopulations for 15min. Cells were washed with SE and measurements of autophagy fluxes were carried out using the Guava Autophagy LC3 Antibody-based Detection Kit (Luminex). Epidermal cells isolated through skin digestion were cultured 16h at 37°C with or without the autophagy inhibitor provided with the kit (60 µM hydroxychloroquine). After labelling by FVD450, cells were stained for CD45, EpCAM, Sca1, and CD200. Cells were permeabilized with 0.05% saponin (Merck Millipore) to wash out the cytosolic LC3-I, then membrane-associated LC3 (LC3-II) was preferentially stained with anti-LC3 FITC (clone 4E12). Flow cytometry analysis allowed to calculate autophagy fluxes, dividing the LC3-FITC mean fluorescence intensities of treated cells by that of untreated cells.

Depilation assay

8 weeks after birth mice were anesthetized, an area of their back was shaved and depilated with wax bands.

Induction of cutaneous inflammation

For each mouse, one ear was injected intradermally with 25µL of 100µg/mL alum hydroxide (Roche) or 25µL of poly(I:C) (Invivogen), and the contralateral ear was left untreated. 4h later, whole skin was digested, and cell suspensions were monitored by flow cytometry using the antibodies in **Table 3.**

Antibodies and reagents for flow cytometry

Antibody staining for flow cytometry were performed in SE buffer (Fetal Calf Serum 2%, EDTA 2.5mM). All antibodies are listed below in **Table 3**. Collected cells are pelleted in a 96 U-wells plate via centrifugation (1500g, 2mins) and resuspended in SE, centrifuged, and resuspended again, this time with the staining solution. Incubation is done 20 mins at 4°C, after which the cells are again washed in SE. If necessary, another staining with secondary antibodies is performed in the same way as the first. After staining is finished, cells are resuspended in 300µL of SE and the entire volume transferred into microwells, one for each condition.

Antibody	Supplier	Dilution (antibody:total)	Clone
FITC- Ly6G	Biolegend	1 :100	1A8
PE-Gr1	Becton-Dickinson	1 :100	RB6-8C5
PerCP-Cy5.5-CD11b	Biolegend	1 :300	M1/70
APC-CD3α	Biolegend	1 :300	145-2C11
AF700-IA/IE	Biolegend	1 :700	M5/114.15.2
APC-Cy7-CD45	Biolegend	1 :500	30F11

Table 3. Antibodies used for flow cytometry.

Results
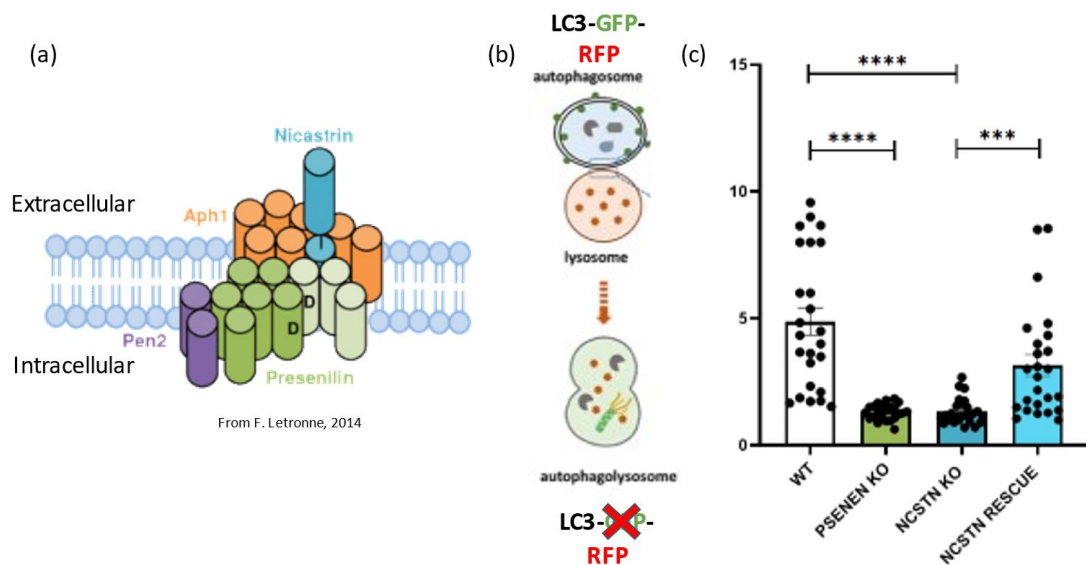
Figure 12. Knock-out of γ-secretase subunits silence autophagy.

*(a) γ-secretase general structure[136]. D, catalytic aspartate residues of Presenilin. (b) Experimental protocol for the study of autophagolysosome formation: HaCat cell transfected to express LC3-GFP-RFP fusion protein loses the GFP fluorescence when a fusion with the acidic lysosome occurs. (c) Quantification of the fluorescence ratio RFP/GFP-RFP. HaCat cells were genetically engineered by CRISPR/Cas9 to reproduce or rescue PSENEN and NCSTN mutations found in HS patients. Efficiency of autophagy was compared by the LC3-GFP-RFP assay in the resulting cell.*

γ-secretase subunit knock-outs impair autophagy *in vitro*

The expression of each subunit of the γ-secretase **(Figure 12a)** is essential to its function. We identified in Milano a HS family with a PSENEN mutation, replacing Arg39 with a stop codon. Later, a novel mutation of NCSTN[137] was found in an HS patient from Paris who also presented with Dowling–Degos disease, a syndrome that affects skin pigmentation. The mutation replaces Arg583 of PSENEN with a stop codon. Therefore, both mutations result in a lack of protein expression.

HaCaT line is a spontaneously transformed, immortal keratinocyte cell line isolated from adult human skin. Highly proliferative, HaCaT cells can be induced to differentiate by introducing calcium in the culture medium. They are a good model to study the outcome of such mutations *in vitro*. First, NCSTN KO and PSENEN KO HaCaT cell lines were engineered via CRISPR/Cas9, and NCSTN KO underwent another cycle of engineering to restore protein expression. Protein expression or lack thereof was confirmed via Western Blot (Nait-Meddour C, Boniotto M et al., manuscript in preparation). Next, cells were transfected to stably express the recombinant protein LC3-GFP-RFP and analyzed by immunofluorescence microscopy. Colocalization of GFP and RFP highlights autophagosomes, whereas, upon fusion with low pH lysosomes, GFP signal is lost, resulting in RFP+ autophagolysosomes **(Figure 12b)**. Comparing GFP-RFP and RFP signal intensities allows to determine whether autophagy is active in the cells analyzed. A high RFP/GFP-RFP ratio was observed in wild-type HaCaT cells, depicting the

normal levels of autophagy of proliferative HaCaT cells **(Figure 12c)**. However, HaCaT bearing nonsense mutations of PSENEN or NCSTN had a strongly reduced ratio, showing that a lack of functional γ-secretase inhibits the autophagy machinery and/or lysosomal fusion. Restoration of NCSTN expression was able to potently increase RFP/GFP-RFP ratios back to the levels observed in wild-type HaCaT cells. Altogether, we observed an apparent autophagy deficiency that was caused by single mutations affecting γ-secretase subunits.
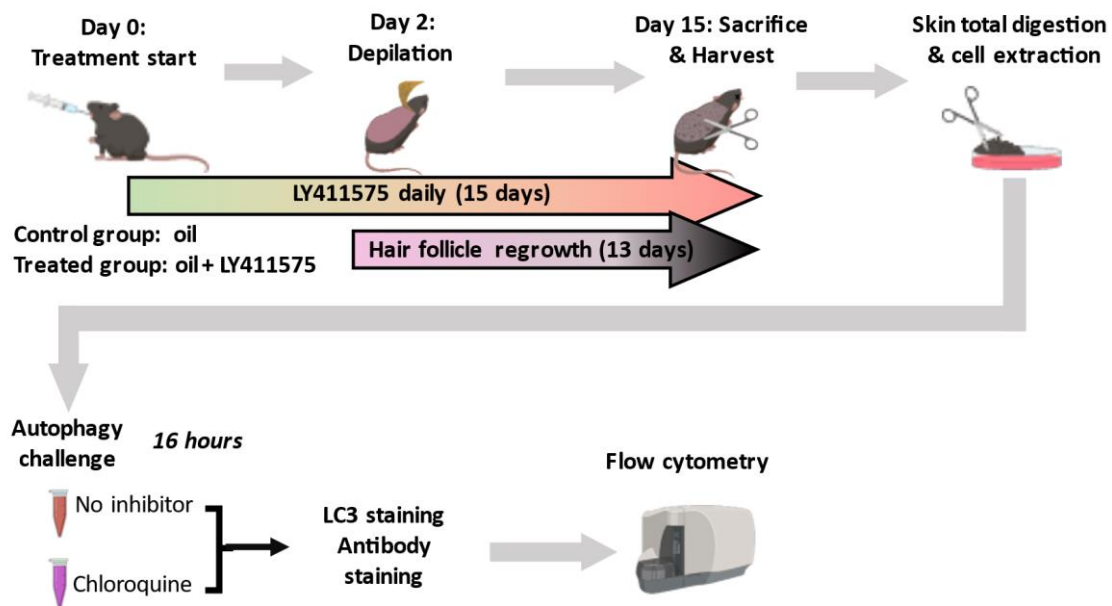
Figure 13. Experimental plan in the inhibition of γ-secretase.
Mice are treated once per day with LY411575 inhibitor for 15 days. On the second day, mice are depilated. On the fifteenth day, mice are sacrificed, the back skin is shaved and harvested. Extracted cells are then subjected to autophagy inhibitors (hydroxychloroquine, bafilomycin) for 16 hours, stained and analyzed through flow cytometry.

γ-secretase inhibition impacts autophagy specifically in the hair follicle

In the light of these *in vitro* results, we sought to investigate the relation between γ-secretase and the autophagy pathway *in vivo.* Thus, we depilated C57BL/6 adult mice to resynchronize the hair follicle cycle on the back skin, then systemically administered the γ-secretase inhibitor LY-411,575 for 14 days **(Figure 13)**. At this time point, the depilation-induced anagen is expected to be completed and the fur fully restored.

Figure 14. γ-secretase inhibition delays hair growth and alters melaninization.
Mice were administered orally with olive oil with or without g-secretase inhibitor LY-411,575 daily for 14 days post depilation. Left: two mice treated with oil+LY-411,575. Right: two control mice treated with oil alone. Image representative of 3 experiments.

Treated mice displayed shorter hair and loss of melaninization on the depilated portion of their back **(Figure 14)**. To investigate autophagy in hair follicle cells, we collected back skin, separated the epidermis, including hair follicles, by enzymatic digestion with Dispase and generated an epidermal cell suspension by further digestion with trypsin. We expected γ-secretase inhibition to impact autophagy similarly to how NCSTN and PSENEN mutations did. Among EpCAM+ epithelial cells, combinations of markers Sca1 and CD200, allowed to distinguish four cell subsets **(Figure 15a)**, corresponding to three follicular regions (CD200+ Sca1+ infundibulum, CD200+ Sca1- bulge, CD200- Sca1- variable region) and the interfollicular area (CD200- Sca1+).

Next, autophagy flux was assessed by comparing membrane-associated LC3 staining in cells untreated or treated with chloroquine, which blocks lysosomal acidification and halts degradation of the autophagosomes. If autophagy is active, this leads to an increase of the membrane-bound form of LC3 (LC3-II) that corresponds to the accumulation of autophagosomes **(Figure 15b)**. LC3 fluorescence ratios appeared similar in all the untreated follicular subsets **(Figure 15c)**. Treatment with LY-411,575 produced visible changes in the ratios, with a significant decrease observed in the infundibulum and the variable regions. On the other hand, the bulge region saw a 2-fold increase of its ratio. Interestingly, the interfollicular epithelial cells saw no visible change in their autophagy flux, suggesting that γ-secretase inhibition preferentially affects autophagy in the hair follicle rather than in the rest of the epidermis.
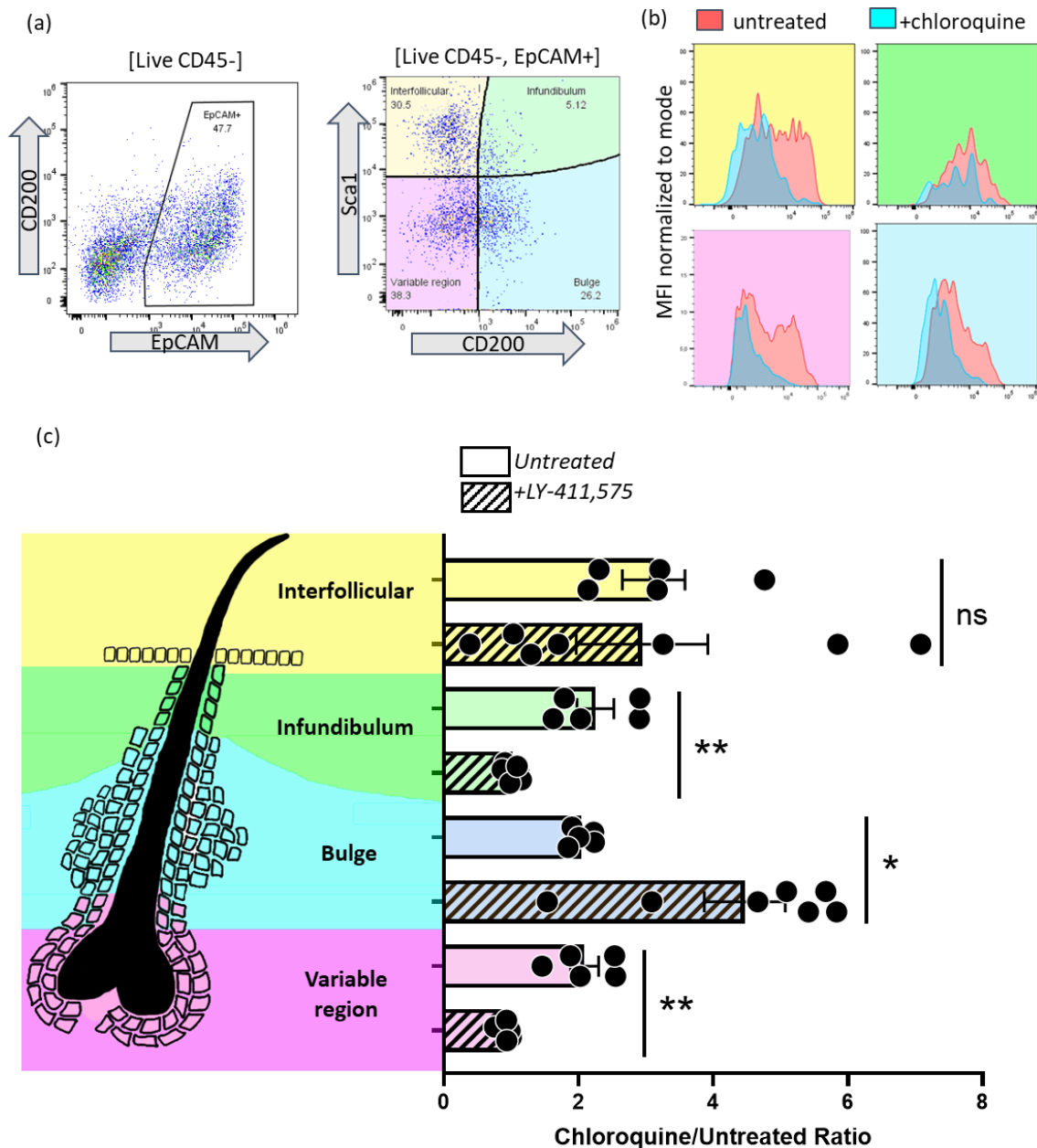
Figure 15. γ-secretase inhibition disrupts autophagic flux in follicular subsets.
*First panel is a drawing of the experimental protocol. **(a)** Identification strategy of hair follicle subsets. **(b)** LC3 detection in untreated (blue) and chloroquine treated cells (red) after 16 hours for four hair follicle subsets. **(c)** The diagram represents a hair follicle divided into four follicular regions. On the right, choloroquine-treated/untreated ratios were measured of the subsets in cell suspensions obtained from hair follicles. Unpaired t tests were used. Ns, nonsignificant; * p<0.05; ** p<0,01.*

Targeted autophagy deletion in the hair follicle

Autophagy is important to efferocytosis, which may be ensured, at least in part, by the hair follicle cells themselves to deal with apoptosis in the variable region during catagen[138]. Moreover, we have observed that the absence of γ-secretase subunits leads to deficient autophagy the upper parts of the hair follicle. Thus, we set out to design a genetic ablation model that would eliminate autophagy in cells expressing the transcription factor Sox9.

Indeed, SOX9 is present in a subset of stem cells mainly contributing to building the upper part of the follicle[139,140], as verified by Dr. Flacher et al. with the help of breeding with $tdTomato^{floxSTOPflox}$ (unpublished observations). Thus, we bred $Atg5^{flox/flox}$, $Atg5^{+/-}$ and $Sox9^{creERT2}$ strain to obtain the inducible model [$Sox9^{creERT2}$; $Atg5^{flox/-}$]. In these mice, upon tamoxifen treatment, $Sox9$ targeting is expected to produce a selective CRE-mediated recombination of the remaining floxed $Atg5$ allele in hair follicle stem cells and in regions that are above the bulge. Since hair follicle stem cells require SOX9 during anagen, mice were treated with tamoxifen at three weeks of age, corresponding to the onset of their first synchronized hair growth, to generate a stem cell-derived progeny with autophagy deletion. As opposed to the γ-secretase inhibition, we could not observe any visible alteration of the fur in these animals.

We noticed both a lower yield and a lower proportion of mice with a $Sox9^{creERT2/+}$ $Atg5^{flox/-}$ genotype, as compared to other in-house crossings that involved either the $Sox9^{creERT2}$ or the $Atg5flox/-$ strains **(Table 4)**. Interestingly, another breeding based on $Sox9^{creERT2}$ mice suffered from a lower proportion of KO as well, but its viability was not affected. Lower viability was noticed in the [$Cd207^{cre}$; $Atg5^{flox/-}$] crossing.

Breeding strategy	[$Sox9^{creERT2}$; $Atg5^{flox/-}$]	[$Cd207^{cre}$; $Atg5^{flox/-}$]	[$Sox9^{creERT2}$; $tdTomato^{flox}$]
Breeding pairs	$Sox9^{creERT2/+}$ $Atg5^{flox/flox}$ X $Atg5^{+/-}$	$Cd207^{cre/+}$ $Atg5^{flox/flox}$ X $Atg5^{+/-}$	$Sox9^{creERT2/+}$ X $tdTomato^{floxSTOPflox}$
Viability at weaning	**61%**	76%	86%
[Genotypes] Proportion	WT [Cre- f/+] 33%	WT [Cre- f/+] 29%	WT [Cre- f/+] 27%
	KO [Cre+ f/-] 17%	**KO [Cre+ f/-] 25%**	**KO [Cre+ f/+] 10%**
	LM [Cre- f/-] 30%	LM [Cre- f/+] 14%	LM [Cre- f/+] 52%
	LM [Cre+ f/+] 20%	LM [Cre+ f/+] 32%	LM [Cre+ f/+] 12%

Table 4. [$Sox9^{creERT2}$; $Atg5^{flox/-}$] crossing gives less knock-out mice than expected.
*Relative proportions of the four expected genotypes from three in-house crossings. Viability was measured as a percentage of mice reaching adulthood out of total birth counts. Data was collected from the survey of 2 years of crossings.*

These findings and the urgent need for consistent mouse production pushed us to introduce in parallel an alternative [$Sox9^{creERT2}$; $Atg5^{flox/flox}$] breeding. Therefore, the following experiments were performed on mice from either [$Sox9^{creERT2}$; $Atg5^{flox/-}$] and [$Sox9^{creERT2}$; $Atg5^{flox/flox}$] breeding strategies, as indicated. For clarity, the genotypes will be thereafter shortened to acronyms **(Table 5)**. These parallel breedings seemed to confirm that mainly affect "KO" animals with expected complete deletion of $Atg5$ alleles under control of the $Sox9$ promoter ($Sox9^{creERT2/+}$ $Atg5^{flox/-}$ and $Sox9^{creERT2/+}$ $Atg5^{flox/flox}$). The limited number of available animals imposed strong constraints on experimental planning and data interpretation.

Breeding strategy	Acronym	WT/LM/KO	Sox9	Atg5
[Sox9^{creERT2} ; Atg5$^{flox/-}$]	Atg5$^{WT/WT}$	WT	+ / +	flox / +
[Sox9^{creERT2} ; Atg5$^{flox/-}$]	Atg5$^{WT/Δ}$	LM	creERT2 / +	flox / +
[Sox9^{creERT2} ; Atg5$^{flox/-}$]	Atg5$^{WT/-}$	LM	+ / +	flox / -
[Sox9^{creERT2} ; Atg5$^{flox/-}$]	Atg5$^{Δ/-}$	KO	creERT2 / +	flox / -
[Sox9^{creERT2} ; Atg5$^{flox/flox}$]	Atg5$^{WT/WT}$	WT	+ / +	flox / flox
[Sox9^{creERT2} ; Atg5$^{flox/flox}$]	Atg5$^{Δ/Δ}$	KO	creERT2 / +	flox / flox

Table 5. Nomenclature of the different breeding strategies.

Despite these issues, we evaluated the efficiency of the targeted *Atg5* deletion on the autophagy flux by LC3 staining, as described above. As compared to *Atg5$^{WT/WT}$* control mice, the most important, yet nonsignificant decrease in autophagy was observed for infundibulum cells of *Atg5$^{Δ/Δ}$* mice **(Figure 16)**.
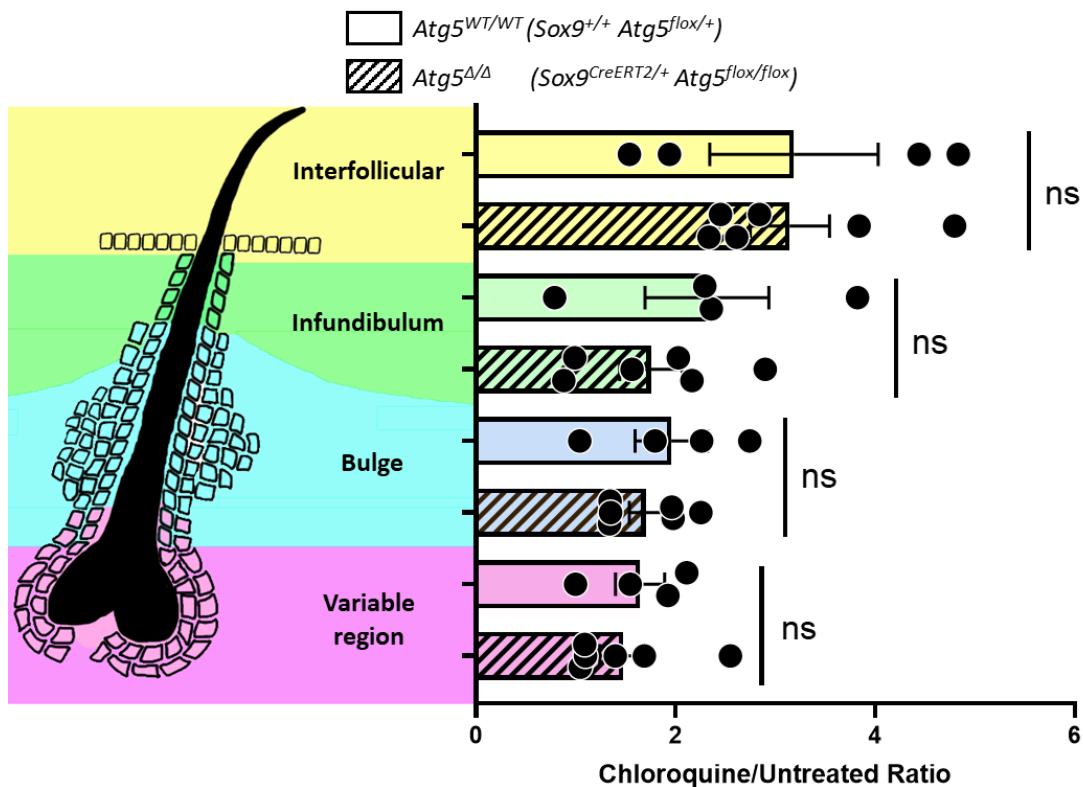
Figure 16. Autophagy flux in hair follicle cell subsets upon targeted Atg5 deletion.
The diagram represents a hair follicle divided into four follicular regions. On the right, choloroquine-treated/untreated ratios were measured of the subsets in cell suspensions obtained from hair follicles. Mann-Whitney tests were used for each comparison. Ns, nonsignificant.

Skin inflammation in HS is dominated by an entry of neutrophils into the dermis and around the hair follicle, which may be initiated by follicular fragility and possibly impaired hair follicle efferocytosis. To study whether a strong neutrophilic response may occur near an autophagy-deficient follicle, we wanted to quantify neutrophils in the skin of *[Sox9^CreERT2 Atg5^flox/-]* mice. We first sought to find the optimal time to detect a significant infiltrate upon skin inflammation. Poly(I:C) was injected intradermally into ears of C57BL/6 mice. Standard antibody panel and gating strategy for flow cytometry were also established during these tests, allowing us to identify three distinct myeloid (CD45$^+$ CD11b$^+$ CD3$^-$) populations: monocytes (Ly6G$^-$ Gr1$^+$), neutrophils (Ly6G$^+$ Gr1$^+$) and other myeloid cells (Ly6G$^-$ Gr1$^-$) **(Figure 17a)**. Poly(I:C) was most effective 4 hours after injection in ear skin, with total resolution of the infiltrate 12h (not shown) and 24h after treatment **(Figure 17b)**.
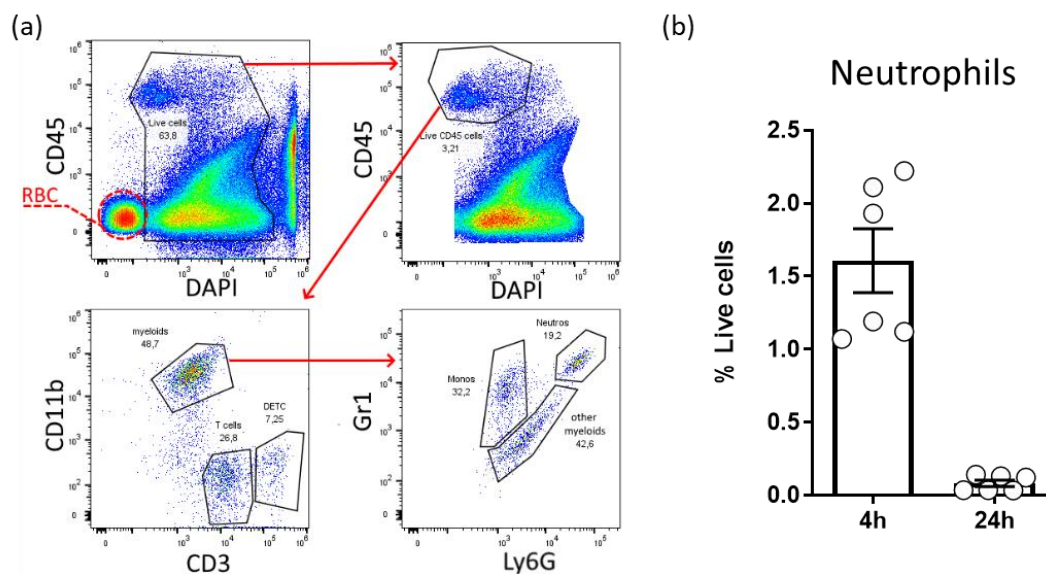
Figure 17. Poly(I:C) induces a short-lived neutrophilic infiltrate in the skin.

*Ears were digested 4h or 24h after poly(I:C) injection. **(a)** Flow cytometry gating strategy. **(b)** Proportion of CD11b+ CD3- Gr1+ Ly6G+ neutrophils out of total live ear cells. RBC, red blood cells.*

Evaluation of immune infiltration upon autophagy deletion in the hair follicle

We applied the poly(I:C) treatment to *Atg5^Δ/-*, *Atg5^WT/Δ* and *Atg5^WT/WT* mice, under the assumption that it may induce an exacerbated immune infiltrate upon hair follicle-targeted autophagy impairment. However, we could only notice a slight, nonsignificant increase in infiltrating neutrophils between treated and untreated *Atg5^Δ/-* mice, but not for the other genotypes **(Figure 18)**.
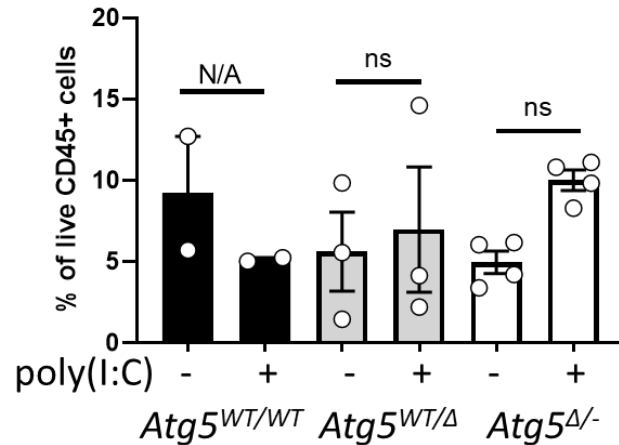
Figure 18. Poly(I:C) injection in Sox9 Atg5 mice.
Ears were digested 4h after poly(I:C) injection and the proportion of CD11b+ CD3- Gr1+ Ly6G+ neutrophils out of total CD45+ ear cells was calculated.

Next, we turned to a potentially more physiological inducer of inflammation: repeated depilation or shaving, which were reported as aggravating factors for chronic inflammation in HS. To replicate this situation, we set on to depilate $Atg5^{\Delta/-}$, $Atg5^{WT/\Delta}$ and $Atg5^{WT/WT}$ mice. We first assessed the lack of delayed hair regrowth or impaired pigmentation in this mouse model **(Figure 19)**.
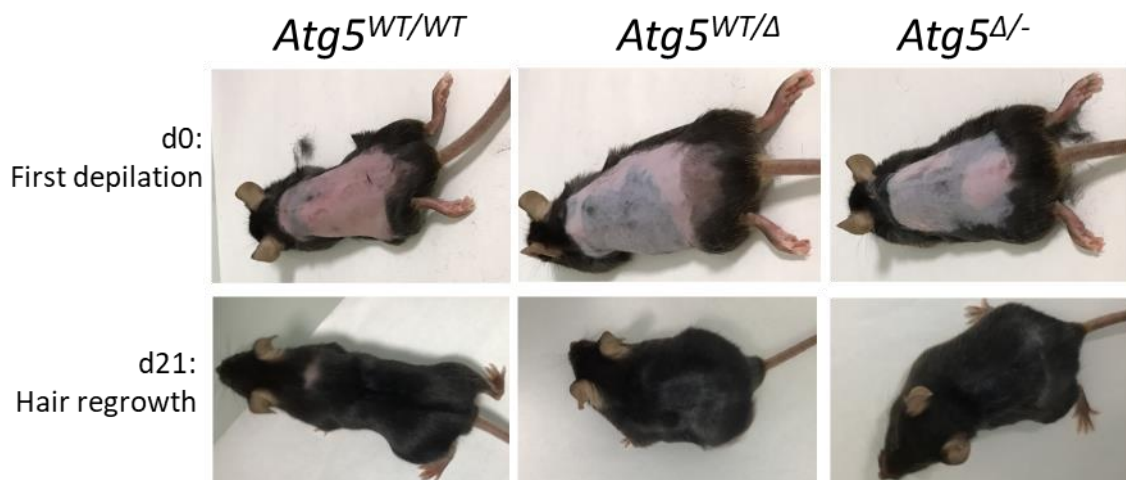
Figure 19. After depilation, hair growth does not differ between $Atg5^{\Delta/-}$ and $Atg5^{WT/WT}$ mice.
Mice were pictured every three days to follow hair follicle regrowth in all genotypes. Here are displayed the first and last pictures from the first depilation to the end of the hair cycle. Normal, darker patches of early anagen are noticeable on the mice at day 0.

We then performed a second depilation and quantified the resulting inflammation by digesting the back skin. Large CD45+ immune infiltrates were detected around hair follicles within hours post-depilation in both $Atg5^{\Delta/\Delta}$ and $Atg5^{WT/WT}$ **(Figure 20a)**. Flow cytometry allowed to measure the extent of infiltrates. Upon close inspection of the data, we realized that the interindividual variability for this assay was much more important in females than in

males. Consequently, depilation-induced immune infiltrates only showed a tendency to increase neutrophils and monocytes in $Atg5^{\Delta/\Delta}$ males, but this could not be observed in $Atg5^{\Delta/\Delta}$ females **(Figure 20b)**. Intriguingly, this tendency was not visible when the experiment was repeated in mice from the *[Sox9^{CreERT2} Atg5^{flox/flox}]* breeding **(Figure 20c)**.
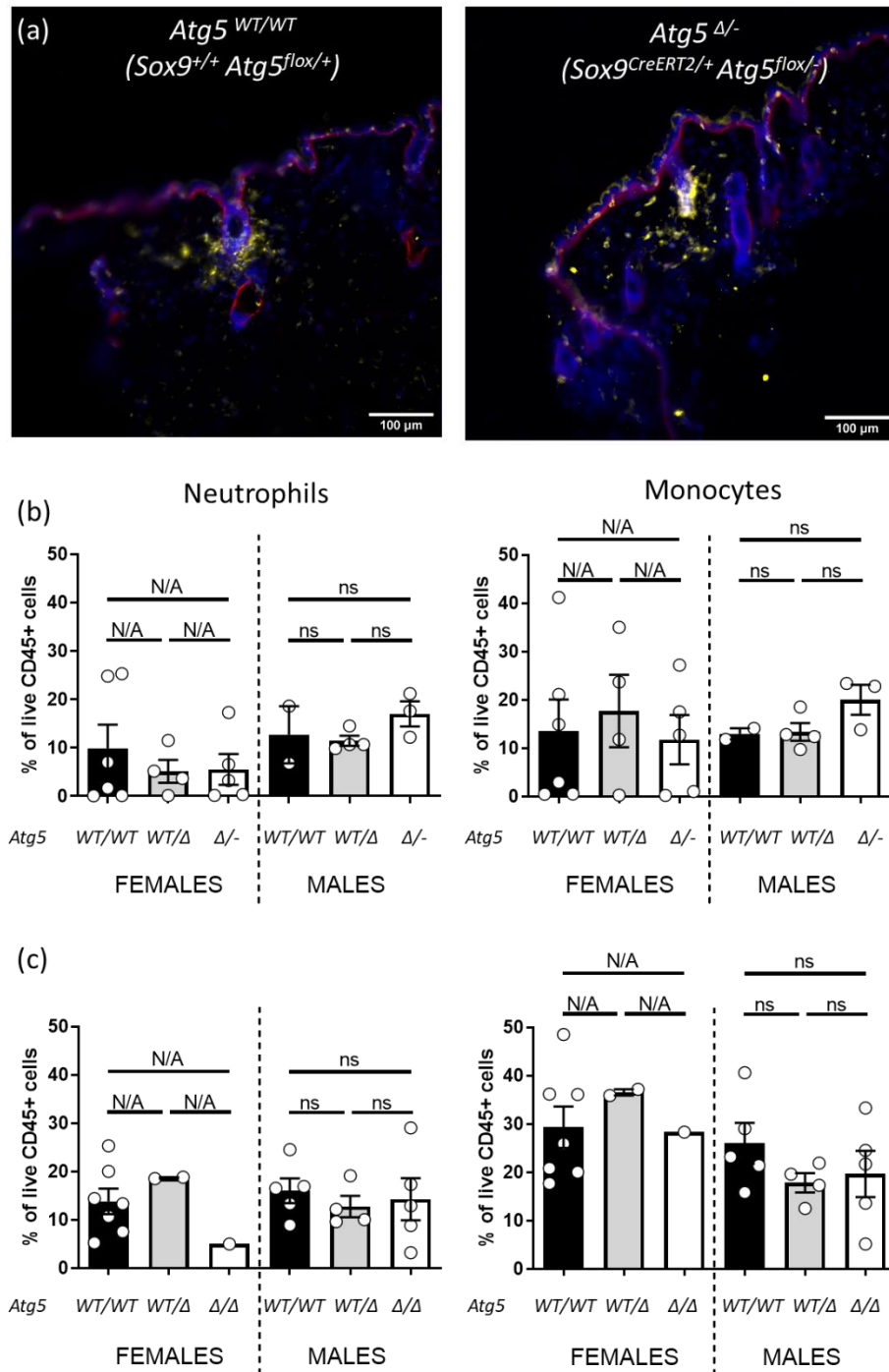
Figure 20. Depilation-induced inflammation may be increased in mice with deleted autophagy in hair follicles.

Back skin was collected 6h after the second depilation. (a) Immunofluorescence microscopy on cryosections of the skin for Atg5^{\Delta/\Delta} and Atg5^{WT/WT} mice. Blue = DNA, Red = α6 integrin/CD49f, Yellow = CD45. (c,d) Quantification of the infiltrating neutrophils and monocytes after back skin digestion in

*mice from either **(b)** [Sox9^CreERT2; Atg5^flox/-] or **(c)** [Sox9^CreERT2; Atg5^flox/flox] breeding strategies, as indicated.*

Discussion

By following the litters that were produced from the *[Sox9^CreERT2; Atg5^flox/-]* breeding strategy, we were struck by the unexpected Mendelian ratio for "KO" genotype *Sox9^CreERT2/+; Atg5^flox/-*. We introduced the *[Sox9^CreERT2; Atg5^flox/flox]* breeding to optimize the outcome of poorly efficient breeding. Despite this mitigation, both strategies resulted in small litters and an elevated mortality of pups. Consequently, we were unable to run reliable statistical comparisons due to a small number of samples. The reason behind this lack of sufficient numbers of viable litters remains unclear. The fact that similar effects were observed in [Sox9^CreERT2 tdTomato^floxSTOPflox] breeding, in which only one Atg5 allele is floxed, raises the possibility that the mere expression of CreER^T2 may be particularly detrimental to SOX9+ stem cells. Such observations are reminiscent of similar reports of intestinal stem cell impairment following targeted expression of CreER^T2 and tamoxifen treatment, because of their higher sensitivity to the consequences of DNA damage[141]. Of note, Sox9 is not exclusively expressed by stem cells of the hair follicle, but also in those of other organs, i.e. pancreas or the intestine[142]. Therefore, although CreER^T2 should not be active in the absence of tamoxifen treatment, leaky activation of the recombinase is possible and may interfere with essential pathways of development and renewal in different organs.

We were unable to satisfyingly solve the breeding issue and had to perform experiments with a small number of mice for each genotype, which made interpretation of results rather difficult. Targeted deletion of *Atg5* in the hair follicle did not result in gross impairments similar to those observed upon γ-secretase inhibition. However, flow cytometry assays for LC3 that we performed in *Atg5^Δ/Δ* vs. *Atg5^WT/WT* mice did not confirm a clear abrogation of autophagy in the hair follicle, which questions whether the expected deletion occurred. We have not verified whether both floxed *Atg5* alleles were recombined. This could be done by sorting the different subsets followed by RT-qPCR or genomic DNA PCR. Alternatively, the *Atg5^Δ/-* model relies only on the recombination of a single allele, which may result in a more efficient deletion. This is why we initially chose the *[Sox9^CreERT2; Atg5^flox/-]* breeding strategy that leads to this genotype.

As compared to poly(I:C), depilation provokes a clear, yet less pronounced immune infiltration. The immune cell types recruited in either condition were not analyzed in more details. It would be interesting to determine whether the presence of myeloid but also B cells, T cells and their functional subsets depends on the proinflammatory stimulus applied to the skin. Although we have very limited data to support this yet, we can speculate that a greater recombination efficiency may account for larger depilation-induced infiltrates in experiments performed with mice from the *[Sox9^CreERT2; Atg5^flox/-]* breeding. The greater variability in females regarding depilation-induced immune infiltration may be explained by the reproductive cycle, which is known to influence the hair cycle through hormonal regulation. Therefore, it may be more consistent to seek for differences in male mice.

Human 3D skin models of hidradenitis suppurativa in vitro

Introduction

One important objective of my thesis is the production of novel 3D human HS models. Several possibilities exist, which we describe and discuss in a review of the literature[102] published with partners of our European consortium focused on HS (BATMAN, Biomolecular Analyses for Tailored therapies of Acne inversa).

Here, we employed a 3D culture strategy that was introduced to the team a few years ago to build dermal equivalents or full-thickness (dermis+epidermis) skin models[143–145]. In this method, the cellular components of interest (fibroblasts, monocyte-derived DCs and keratinocytes) are sequentially seeded into chitosan/collagen sponges. As a result, we expect to obtain a multilayered epidermis covering the sponges, which represent a dermal equivalent harboring fibroblasts and DCs.

Our collaborator Michele Boniotto at the Institut Henri-Mondor (Créteil) has demonstrated that mutation of the γ-secretase subunit modify the secretory profile of keratinocytes grown in 2D[146]. Therefore, an immunocompetent skin model would be a great asset to determine the environmental clues associated with mutated keratinocytes grown in 3D and to study how they exert an influence on DCs and, subsequently, T-cell driven immune responses.

Material and methods

Preparation of the tissue-engineered 3D skin model

Collagen sponges were prepared as previously described[147] and seeded with 800,000 human fibroblasts in DMEM supplemented with 10% fetal calf serum (FCS) and 50mg/mL ascorbic acid for 7 days. Then, 400,000 fibroblasts were seeded on the opposite side of the sponge. After 7 days, sponges were flipped upside down and 1 million of epithelial cells (human keratinocytes, HaCaT or ORS) were seeded on top of sponge (opposite side to neurons) under immersion in the culture medium. Samples were cultured 7 days in DMEM-F12 with 5% Hyclone serum supplemented with 20 ng/mL BDNF (Feldan), 10ng/mL GDNF, 10ng/mL NGF, 50mg/mL ascorbic acid, 0.2µg/mL hydrocortisone, 2.5µg/mL insulin, 10ng/mL human epidermal growth factor and 10^{-10} M cholera toxin. Then, sponges were lifted at the air–liquid interface to promote differentiation for 17 days in the same medium but without EGF.

Immunofluorescence

Matrices were fixed with 4% PFA or 20% sucrose overnight at 4°C. Slides were permeabilized via cold acetone for 10 mins, then washed twice with PBS (Fisher Scientific), then incubated in immunofluorescence staining buffer, containing PBS, 0.3% triton X-100 (Biorad, Mississauga, Canada) and 5% horse serum, for 20 min at room temperature. Cells were stained overnight at 4°C with primary antibodies diluted in immunofluorescence staining buffer and were washed with PBS for 5min then incubated for 1h at room temperature with secondary antibodies in immunofluorescence staining buffer and finally were washed with

PBS before adding DAPI for 10min, washing again and mounting the coverslips on the slides with fluoromount-G. Coverslips were sealed with the slide via the application of a thin layer of nail polish all around.

Primary cells extraction

Human skin cells (keratinocytes, fibroblasts) are extracted from surgical wastes provided by the St Anne clinic. The donors, adults, sign a written consent before the operation in accordance with the current ethical rules, and the process is fully anonymized. The collection of the sample is carried out immediately at the end of the surgical procedure, it is then transported in ice and brought in for extraction, less than 2 hours after the operation, within our laboratory. The skin is thoroughly washed with ethanol, PBS, Dakin, and PBS again.

A dermatome knife is used to remove a 1mm thickness of the skin, thus comprising the epidermis and the upper part of the reticular dermis. These pieces are then placed in a Petri dish, cut into thin strips, bathed in a 0.5% trypsin solution (VWR), and incubated for 2 hours at 37°C, 5% CO_2. The epidermis is stirred in the incubator with a solution of 35mL RPMI, 10mL fetal calf serum (FCS; Corning), 5mL DNase I (Roche) for 30 minutes. This time is sufficient to observe its complete dissociation. The cell suspension is passed through a filter with 70µm pores and then washed in DMEM F12 (Lonza) via centrifugation at 200 g for 5 minutes then resuspension in fresh medium. 30 million cells are seeded in a 75 cm 2 culture flask (T75) in CnT-PR medium (CellnTec) supplemented with 100 U/mL of penicillin/streptamycin (pen/strep) and 10 µg/mL of gentamicin. EpiLife (ThermoFisher) medium and Dermacult (STEMCELL) were also used for epithelial cell culture.

For fibroblasts, the deep dermis remaining is cut into small pieces of a few millimeters with a scalpel then placed under stirring in a beaker containing a solution of 30mL RPMI, 1mL of DNase I and 330µL of collagenase I (Gibco) overnight in the incubator at 37°C, 5% CO_2. The next day, the digested dermis is passed through a 70µm filter. It is washed 3 times in DMEM. The cell suspension obtained is inoculated at 50 million per T75 in complete DMEM medium.
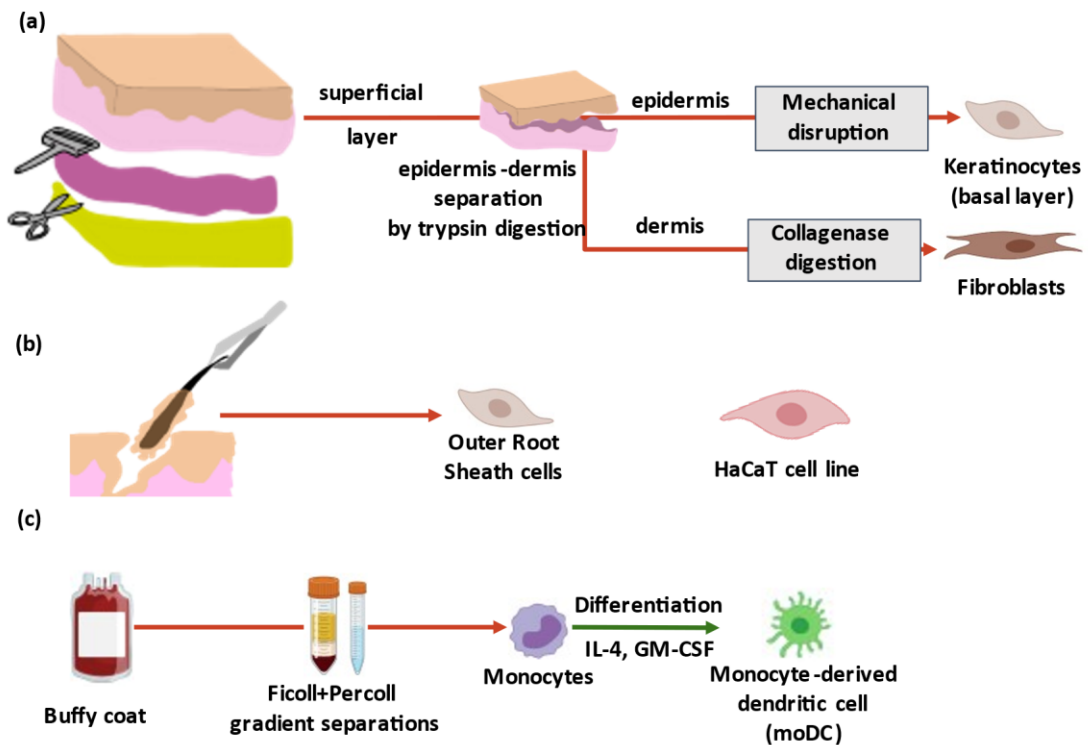
Figure 21. Cell cultures for 3D human skin reconstruction.

(a) Healthy skin samples were obtained from surgical waste (abdominoplasties) performed at the Sainte-Anne clinic (Strasbourg). Fibroblasts from the upper dermis (papillary) are privileged for their superior growth. (b) Differentiation of human dendritic cells from blood monocytes (moDCs).
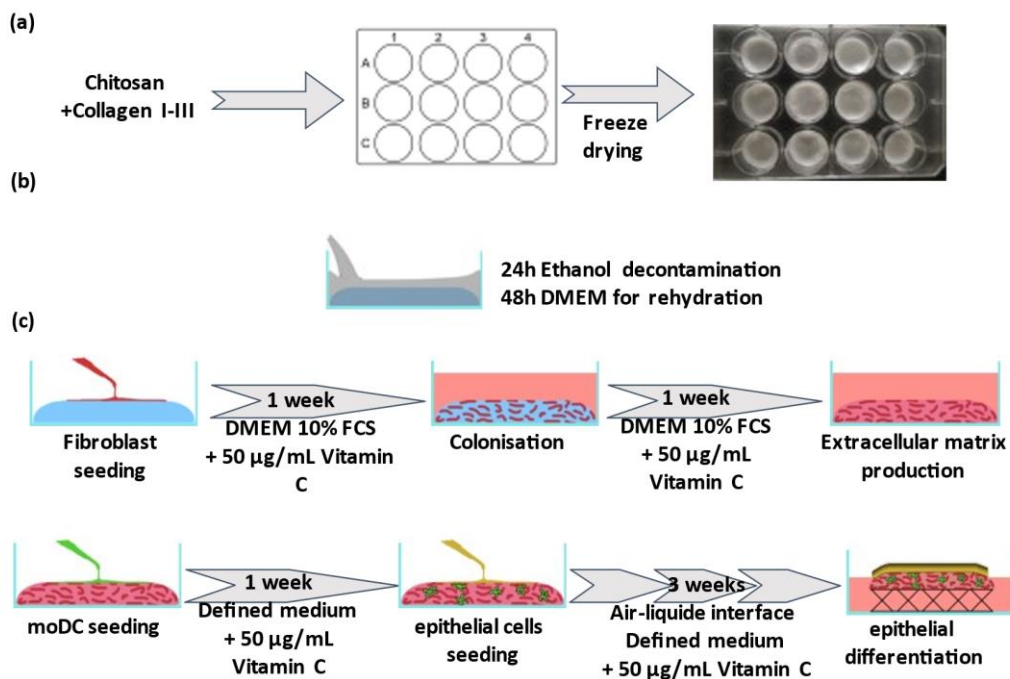
Figure 22. Immunocompetent 3D reconstructed skin model.

(a) Construction of collagen-chitosan matrices. (b) Preparation of the matrix for cell culture. (c) Fibroblasts, moDCs, epithelial cells (primary keratinocytes, HaCaT cell lines or ORS cells) are consecutively seeded over a 6-week colonization protocol.

Results

Three relevant HaCaT cell lineages were obtained from Dr. Michele Boniotto and PhD student Cécile Nait-Meddour: HaCaT WT, HaCaT NCSTN KO and HaCaT PSENEN KO, sporting the nonsense mutations described earlier. Indeed, HaCaT cells were previously utilized, instead of healthy human keratinocytes, as the building block for reconstructed full-thickness skin models[148]. We first cultured HaCaT cells in 2D to assess their general appearance, viability, and proliferative potential, ultimately gathering enough cells to seed the 3D supports. Mutated HaCaT cells showed no obvious viability or proliferative deficiency that could be related to the lack of γ-secretase. The next step involved seeding the wild-type HaCaT line onto 3D matrices containing fibroblasts and DCs. Seeding and culture procedures were not modified from the protocol that was set up for healthy human keratinocytes. The resulting HaCaT-based 3D models were characterized by immunofluorescence microscopy **(Figure 23)**. We subjected cryosections to staining for different epidermal markers, which were previously validated on fresh human skin samples: Keratin 14 (basal layer), Keratin 10 (differentiated epidermis), Filaggrin (upper layers) **(Figure 23a)**, α6 integrin/CD49f (lamina basale), and actin (stained by phalloidin) **(Figure 23b)**. 3D models were additionally stained for HLA-DR to reveal antigen-presenting cells, here the DCs.

Images of the HaCaT-based 3D models were compared with those obtained from healthy surgical skin explants **(Figure 23a-b)** or published previously by our team[144]. Phalloidin labelling reveals the actin cytoskeleton of cells within the model, showing that the whole sponge was indeed colonized **(Figure 23c, d)**. A strong CD49f staining was consistently seen, forming a line that likely corresponds to a lamina basale formed by the seeded HaCaT cells **(Figure 23c-f)**. We could find HLA-DR+ DCs within the dermal equivalent (colonized sponge) **(Figure 23e, f)**, which corresponded to the thicker part of the model. Conversely, the thinner part represented the epidermal equivalent that grew from HaCaT. Admittedly, this epidermal part appeared to display only one or two layers of cells, thereby questioning the ability of the HaCaT cells to develop into a multilayered epithelium in our model.
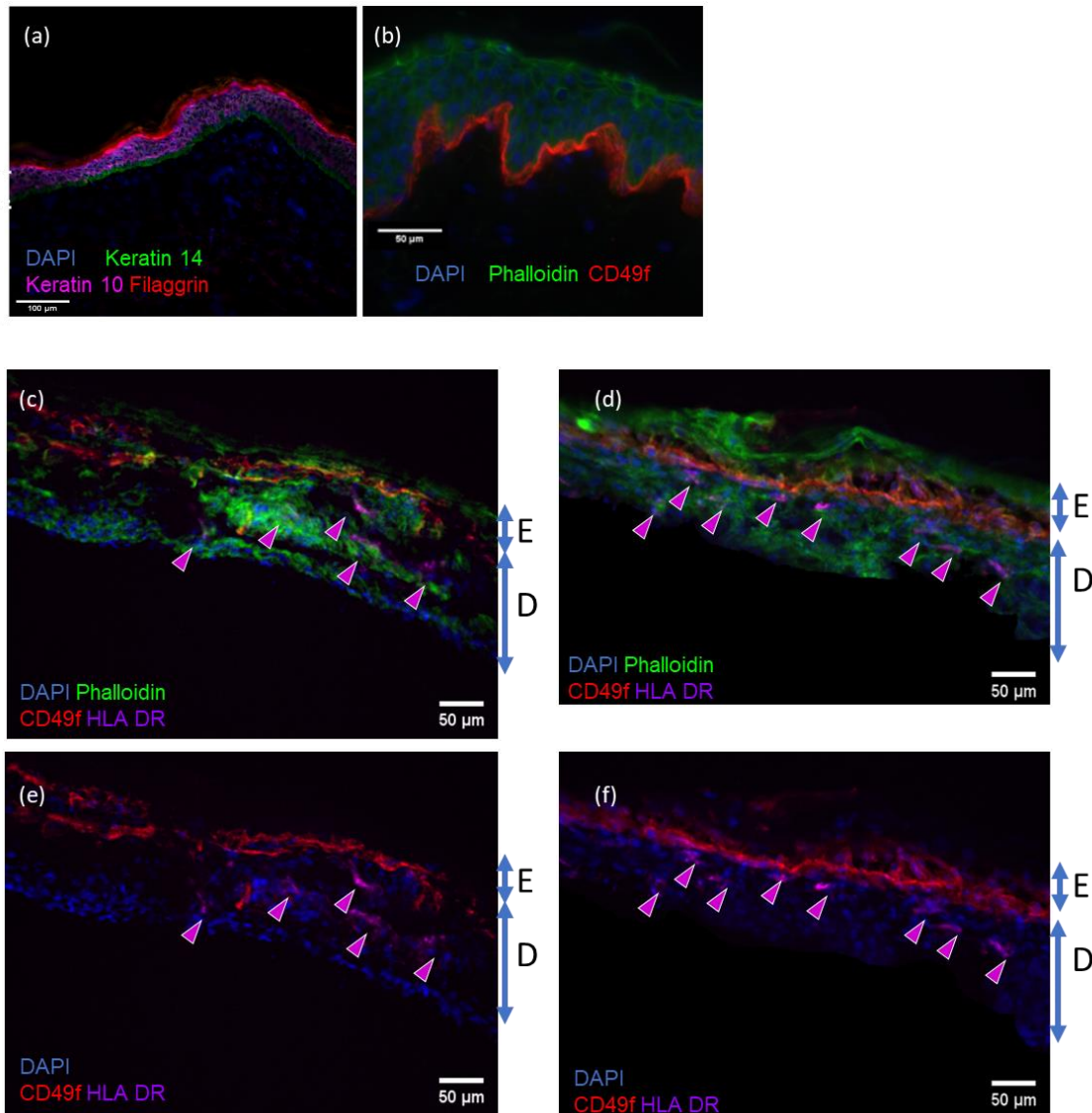
Figure 23. HaCaT cells form an epithelial layer atop the reconstructed dermis.

Immunofluorescence of 30µm-thick cryosections from human healthy skin (a, b) and 3D matrices seeded with human fibroblasts, human monocyte-derived DCs and wild-type HaCaT cells (d-f). Note that (c-e) and (d-f) correspond to two individual 3D models. D, dermal side (collagen sponge with fibroblasts and DCs); E, epidermal side (HaCaT cells).

Clinical partner Pr. Angelo Marzano (Milan) has identified two HS patients in the same family, a mother and her son bearing a yet unreported mutation of the DSP gene encoding desmoplakin (unpublished observations). The mother has one nonsense mutation, while the son has both alleles muted, precluding production of desmoplakin. Trans-epidermal water loss tests on the skin of patients showed a deleterious effect on skin barrier function (R. Gratton et al., manuscript in preparation). As barrier function failure could play an important role in HS onset, we decided to evaluate epithelial cells from these patients for our 3D skin reconstruction. ORS cells were extracted from plucked hairs, cultured at low passage, frozen and sent to our facilities. We first put the ORS cells in 2D culture to assess the culture purity, viability, and proliferation in the CnT medium **(Figure 24, left).** ORS cells had high mortality

rate when thawn and showed a very low proliferation rate. Mortality remained high during culture and passage, especially for the son's cells. At the observed rate of proliferation, we first deemed these ORS to be an unlikely candidate for 3D seeding, which requires a high number of viable cells. A change of the defined culture medium was initiated, switching from CnT-E™ to EpiLife™. EpiLife™ medium showed significant improvement over CnT for ORS expansion into nearly confluent cell cultures **(Figure 24, right)**.
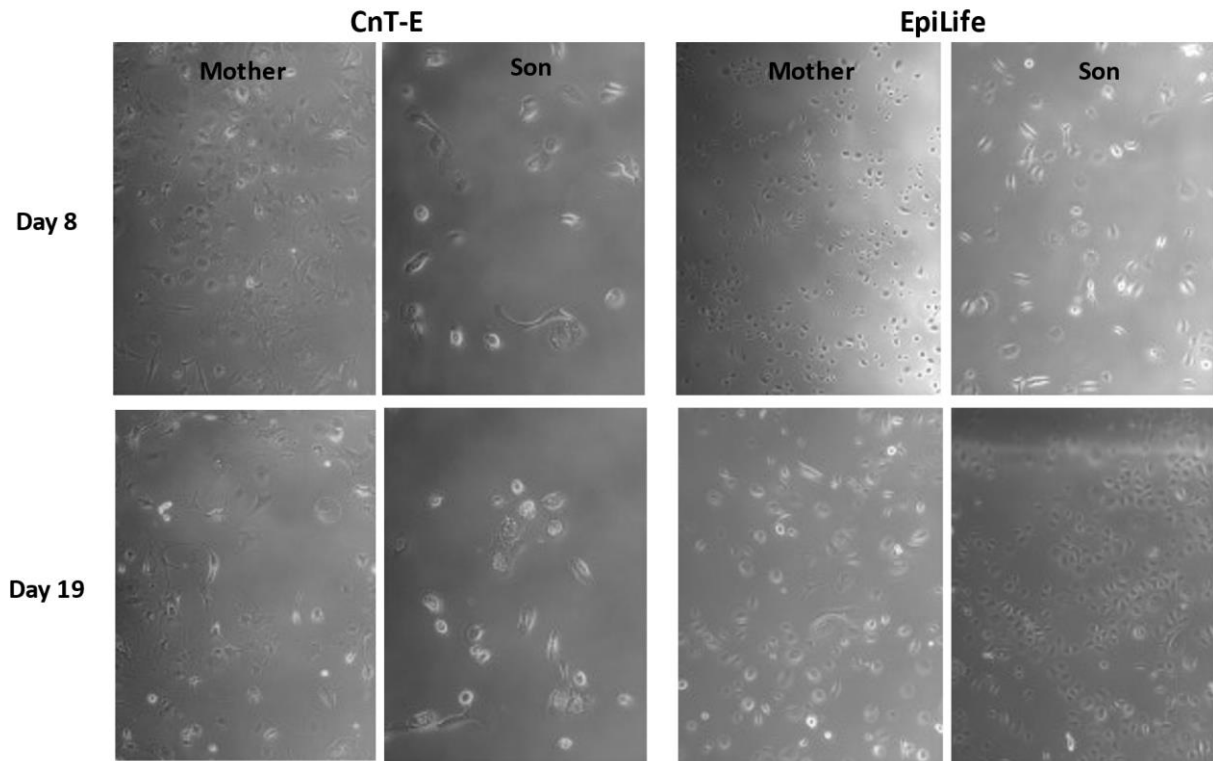
Figure 24. Outer root sheath cells only show robust expansion when cultured with the EpiLife medium.

Discussion

2D cultures of human primary keratinocytes and wild-type or mutated HaCaT cells routinely showed potent proliferation and resulted in large cell yields. Culture of ORS cells proved significantly more challenging, despite being, in essence, very similar to human basal keratinocytes. Different defined culture medium allowed a better expansion, yet the cell yields was very limited and not sufficient to seed ORS cells onto collagen sponges. The patient ORS that we had access to were characterized by a homozygous or heterozygous mutation of the DSP gene. This may have impacted proliferation because of disrupted cell-cell contact and the exchange of nutrient or secondary messengers important for the cells to survive and thrive in vitro.

3D cultures proved extremely challenging for several reasons and did not consistently result in physiologically relevant, full-thickness skin models. First, clinical sample collection agreement allowed to obtain blood and ORS cells from freshly plucked hair follicle. However, it did not include skin biopsies of uninvolved areas, from which basal keratinocytes could have been derived. We also tried to use HaCaT cells carrying mutations relevant to existing HS

familial cases. Nevertheless, both HaCaT and ORS cells may significantly differ from normal human keratinocytes, for which the 3D culture protocol was specifically designed.

Interestingly, in parallel to our full-thickness 3D skin model constructions, our partner Dr. Boniotto attempted to produce a simpler skin model, i.e. an epidermal reconstruction. This was based on the growth of keratinocytes on a collagen coating, followed by differentiation at the air-liquid interface. Similarly to our results, this approach was unfortunately unsuccessful when performed with wild-type or genetically modified HaCaT or with ORS cells from patients (data not shown). On the other hand, Dr. Boniotto and PhD student Ms. Nait-Meddour were recently able to develop hair follicle organoids from patient-derived iPS cells (manuscript in preparation), following a recently published method[149]. Keratinocytes can be extracted from these organoids, and our initial observations suggest a more potent expansion potential than ORS, like that of normal human keratinocytes. This represents an unexpected source of keratinocytes as well as fibroblasts that bear the same mutations as the patients. As a follow-up study of my PhD project, integration of these organoid-derived keratinocytes into an immunocompetent full-thickness skin model is currently under evaluation by Dr. V. Flacher and PhD student Ms. Annia Perez-Riveron.

Manuscript to be submitted:

Familial cases of hidradenitis suppurativa are associated with pronounced alterations of peripheral B cell and follicular T helper subsets

Context

As stated previously, my PhD project was strongly connected to the objectives pursued by the BATMAN European consortium, funded through the Agence Nationale de la Recherche and ERANet (ANR-18-PERM-0001) in the frame of the ERAPerMed 2018 call on personalized medicine. Partners in this project included Pr. Mathias Schmuth and Pr. Esther von Stebut, heads of the dermatology departments in Innsbruck (Austria) and Köln (Germany), respectively. They recruited an important cohort of HS patients, and detailed information about their background, in the frame of studies on blood cells and whole-exon sequencing.

Familial cases of hidradenitis suppurativa are associated with superior alterations of peripheral B cell and follicular T helper subsets

Wacym Boufenghour[1], Annia Pérez-Riveròn[1], Wolfram Jaschke[2], Michele Boniotto[3], Sergio Crovella[4] Esther von Stebut[5], Matthias Schmuth[2], Vincent Flacher[1*]

1 Laboratory CNRS UPR3572 Immunology, Immunopathology and Therapeutic Chemistry (I2CT) / Institut du Médicament de Strasbourg, Strasbourg, France.

2 Medical University of Innsbruck, Department of Dermatology, Venereology and Allergy, Anichstrasse 35, Innsbruck, Austria.

3 University Paris Est Créteil, INSERM, 94010, IMRB- Équipe Leboyer, Créteil, France.

4 University of Qatar, Biological Sciences Program, Department of Biological and Environmental Sciences, College of Arts and Sciences, Doha, Qatar.

5 Department of Dermatology, University of Cologne, Kerpenerstrasse 62, 50935 Köln, Germany.

* Correspondence: v.flacher@ibmc-cnrs.unistra.fr

Abstract

Hidradenitis suppurativa (HS) is a skin disease originating in the hair follicle. For yet unresolved reasons, chronic inflammation is perpetuated around this epidermal appendage, ultimately leading to tissue destruction, dermal invasion by the microbiota and deeply seated, painful scars. The massive immune infiltrate includes neutrophils, T cells and B cells that are expected to support the inflammatory reaction and dysbiosis. In particular, a potential role for autoantibodies and skin-infiltrating B cells has been recently proposed. In order to follow disease progression and to guide therapeutic intervention, HS patients are usually stratified according to severity scales, the Hurley and HIS4 grades. However, despite known associations of HS with genetic polymorphisms, the presence of several HS patients in a given family had not been considered in previous analyses of their immune responses. Here, we made use of two HS cohorts to seek after previously reported and novel features of circulating B and T cell subsets. The collected data was browsed with regard to severity grades and families concentrating several HS cases. Our analyses revealed that the blood of familial HS cases had more switched memory B cells, which also contained higher proportions of cutaneous leukocyte antigen (CLA)-expressing, skin-addressed cells. Differences between T helper subsets of healthy donors and HS patients were also more pronounced when CLA+ skin-addressed cells were considered, with a consistent decrease in Th1 cells. Finally, a sharp increase of follicular helper T cells characterized HS patients graded as Hurley stage II. Our findings provide novel insights into HS disease progression and shed light on patients with familial history of HS. We propose that this category of patients should be increasingly taken into consideration: indeed, in-depth analyses of their special features and genome wide association studies may prove helpful to distinguish key elements that characterize physiopathology of HS in broader populations.

Introduction

Hidradenitis suppurativa (HS) is an auto-inflammatory disease of the pilosebaceous unit, with lesions in the axilla, groin, breasts and thighs (Wollina et al., 2013). Currently estimated to affect 0.2% of the world population, HS has a high heterogeneity in relation to sex and origin of the patients, and a strong correlation with obesity and smoking (Sachdeva et al., 2021; Vaidya et al., 2017). At an early stage, patients display lesions may resemble other skin diseases such as psoriasis, leading to diagnosis delay average of five years in average. The current understanding of HS initiation points to a gradual process of inflammation triggered by a follicular occlusion of unknown origin. Follicular bursting and the entry of foreign material into the dermis expectedly alerts the local immune system, which recruits polymorphonuclear leukocytes into the affected area (Narla et al., 2021). The subsequently formed neutrophil extracellular traps enhance the inflammation and anchor it in time due to the presence of autoantibodies directed against them (Byrd et al., 2019; Carmona-Rivera et al., 2021). TNF-α inhibitors (Infliximab, Adalimumab) may reduce the inflammatory symptoms and tissue damage, yet the response to such treatments varies greatly. Later development of the disease ends up in a nearly complete destruction of the pilosebaceous unit and its surrounding tissue, causing irremediable alteration of the skin morphology. Painful, deep scars, nodules and keratinized ducts (tendrils) running through the dermis leave patients with few treatment options, eventually leading them to excision of large skin areas and the associated physical and psychological damage.

Multiple studies of HS patients allowed to uncover the principal pathological mechanisms and cellular targets. Cutaneous immune homeostasis notably relies on an immune shift towards effector T helper 17 (Th17) cells. They release IL-17, a pro-inflammatory cytokine with a key role in the protection against epithelial infection. Th17 cells can also produce IL-22, an important factor in epithelium homeostasis and wound healing. In HS lesional skin, IL-17 expression is increased (Melnik et al., 2018; Moran et al., 2017) whereas IL-22 expression is reduced (Wolk et al., 2011).

B cells also increasingly appear as an important actor in HS. Within lesional skin, CD20+ B cells cluster around plugged hair follicles (van der Zee et al., 2012). Differences were also found in peripheral blood B cell populations, with an increase of switched memory B cells (Musilova et al., 2020). Further studies established the presence of plasma cells in HS lesional skin, as well as the production of autoantibodies against citrullinated antigens (Byrd et al., 2019; Carmona-Rivera et al., 2021). Moreover, a strong transcriptomic signature and an elevation in IgG3, IgG1 and IgA1 antibodies were associated with HS (Carmona-Rivera et al., 2021; Hoffman et al., 2018).

There are established genetic predispositions to HS, evidenced by families in which numerous cases can be found, and several associations have been found, including, but not limited to, mutations in components of the gamma-secretase (Wang et al., 2010). Thus far, no study has evaluated whether patients from such families display significant alterations of their immune

responses. Here, based on a cohort including HS patients with or without affected relatives, we aimed at further defining in peripheral blood the B and T cell populations that characterize HS physiopathology. In particular, we interested in variations possibly associated with familial clustering of cases, as compared to sporadic cases.

Material and Methods

Blood sample collection and processing

Healthy controls were obtained from volunteers and buffy coats from the Etablissement Français du Sang (Strasbourg, France). Hospitals in Köln, Germany and Innsbruck, Austria admitted HS patients and their family members:

- Sporadic: 28 patients without any other identified HS case in the family.
- Familial: 35 patients from 27 different families declared at least one parent or sibling with HS manifestations. For 22 of these families, only one individual could be analyzed. In 3 families, one donor without HS agreed to give blood samples for the study. Family trees of these patients are presented in **Figure S1**.

14 mL of blood were sampled in sterile heparin-coated tubes, conditioned with 4°C cold packs in multiple layers of protection and shipped over to Strasbourg, France within 24 to 48 hours. Upon reception, samples were immediately unpacked and processed as follow. Each blood sample was separately diluted in half with SE buffer (PBS 2% fetal calf serum, 5mM EDTA) in a Falcon 50. SepMate™ 50mL tubes and standard protocol were used for cell separation. 15 mL of Ficoll was carefully deposited at the bottom of the tube, SE-diluted blood was then laid on top of the Ficoll. Tubes were centrifuged at 1500g for 20 min, with full brakes on. After centrifugation, all the red blood cells were pelleted at the bottom of the SepMate™ tube, allowing to easily collect the upper layer with peripheral blood mononuclear cells (PBMCs) by pouring the tube into a fresh 50mL tube. After a second centrifugation at 500g for 5 min the supernatant was discarded, the pellet resuspended in 10mL of SE and the cells were counted on a Malassez slide. After a second centrifugation, the pellet was resuspended again in SE to reach 10 million cells per mL.

Flow cytometry

Cells were seeded at 500 000 per well on a V-bottom plate and centrifuged to discard the SE. Pellets were resuspended using antibodies diluted in SE buffer **(Table 1)**. Incubation was performed for 20 min at 4°C away from light. Cells were washed once in SE and DAPI was added to the final 200µL of SE. Cell fluorescence was measured and recorded using a Beckman Coulter Gallios 3-lasers flow cytometer. Resulting data was analyzed with FlowJo 10 (Becton-Dickinson).

Human skin explants

Skin specimens were obtained from anonymized healthy subjects undergoing abdominal reduction, with written informed consent and institutional review board approval, in agreement with the Helsinki Declaration and French legislation. 4cm², ~1mm-thick biopsies

were placed at air-liquid interface onto a 40µm cell strainer (Biologix) in 6mL RPMI1640 medium supplemented with 10µg/mL gentamycin, 100U/mL penicillin, 100µg/mL streptomycin, 10mM HEPES (Lonza) and 10% fetal calf serum (Dutscher). After 3 days, the cells that exited the explant were collected from each well and analyzed by flow cytometry.

Antibody	Supplier	Clone	Reference
Anti-CD19 PerCP-vio770	Miltenyi	LT19	130-113-171
Anti-IgD FITC	BD Pharmingen	IA6-2	555778
Anti-CD27 APC	BD Pharmingen	M-T271	558664
Anti-CD38 AF700	Biolegend	HIT2	303524
Anti-CLA PE-Cy7	Biolegend	HECA-452	321315
Anti-CD4 APC-vio770	Miltenyi	REA623	130-113-223
Anti-CXCR5 FITC	Miltenyi	REA103	130-098-418
Anti-CD45RA PE-vio615	Miltenyi	HI100	130-118-789
Anti-CCR6 PE	Miltenyi	11A9	130-120-458
Anti-CXCR3 APC	Miltenyi	REA232	130-120-450
Anti-CD8 PE	BD Pharmingen	RPA-T8	555367
Anti-CD3 AF700	BD Pharmingen	UCHT1	557943

Table 1: Labelling antibodies for flow cytometry

Results

Proportions of peripheral B cells and their subsets are globally unaffected in HS patients

We first set out to determine the proportion of B cells in the peripheral blood of healthy donors and HS patients. Unexpectedly, there was no significant difference for the total percentage of B cells among PBMCs **(Figure 1a)**. To further dissect this, we interested in B cell subsets. Specifically, a previous report showed elevated proportions of plasmablasts and switched memory B cells in the blood of HS patients (Musilova et al., 2020). We used CD38 staining that labels plasmablasts as well as antibody-secreting plasma cells. Yet, plasmablasts were found in similar proportions in healthy donors and HS patient **(Figure 1b)**. Finally, B cells were split into four subpopulations defined by the IgD and CD27 surface markers (IgD+ CD27- naïve, IgD+ CD27+ unswitched, IgD- CD27- switched, IgD- CD27+ switched memory; **Figure 1c**). However, none of the B cell subsets showed detectable alterations in HS patients **(Figure 1d)**.

Since changes in immune cell populations may be related to different stages of the disease, total B cell percentages were plotted in relation to each patient's reported Hurley's stage or IHS4 score. We noticed an important, yet nonsignificant decrease of B cells in stage III patients, as compared to stage I **(Figure 1e)**. When the IHS4 scoring system was taken into consideration, a similar trend appeared between "mild" and "severe" stages **(Figure S2a)**. Focusing on switched memory cells, we could not find any association with a defined Hurley **(Figure 1f)** or IHS4 **(Figure S2b)** stage.

Finally, many of the samples were collected during a period of intensive vaccination campaign against SARS-CoV-2, and adult vaccination against tick-borne encephalitis virus is relatively frequent in Austria. Therefore, it was important to verify whether the proportions of naïve, switched, switched memory and plasmablasts among B cells might be associated with a recent vaccination event. However, we could not demonstrate any correlation between these proportions and the time following the latest vaccination **(Figure S3)**.

Therefore, on first estimation, our results do not appear to recapitulate previous reports of elevated total and subsets of blood B cells in HS patients, independently of the disease stage considered.

Discrimination of familial cases highlights an increase of switched memory B cells

These intriguing findings prompted us to further investigate the characteristics of our cohort. Indeed, the HS patients that we analyzed were in parallel recruited for a whole exon sequencing study aiming at the identification of novel HS-associated genetic polymorphisms, in the frame of the BATMAN project (Tricarico et al., 2022). Therefore, HS patients followed at the dermatology clinics of Innsbruck and Köln were asked for the occurrence of the disease in closely related family members. This allowed us to discriminate and compare patients with ("familial cases") or without ("sporadic cases") affected relatives. The mean age and sex ratio of the affected familial cases (mean±SEM: 43.47±12.08; 56% females) and sporadic cases (39.31± 11.58; 53% females) were similar.

Thus, we analyzed blood from several members (affected or not) of 5 families and from 16 individuals who reported relatives with diagnosed HS. Neither total B cells nor plasmablasts

were changed in proportions when the blood samples of sporadic and familial patients were compared **(Figure 2a/b)**. Nevertheless, familial cases had significantly more switched memory cells than sporadic cases and healthy cases **(Figure 2c)**. We defined a threshold of 28% switched memory cells, derived from the mean+standard deviation of their proportions in healthy donors (27.47%) and sporadic cases (27.05%), in order to highlight familial cases with significantly higher levels of this subset **(Figure 2d)**. Based on this, we found 7 families with patients showing outstanding percentages of switched memory cells **(Figure 2e)**, as opposed to 13 families with lower levels **(Figure 2f)**. Therefore, it is possible that the more important proportion of switched memory B cells in familial cases reflects that of patients of specific families with particularly high levels of this population.

Expression of CLA by switched memory B cells highlights a bias towards skin infiltration

The B cell infiltration found within inflammatory lesions of HS patients is increasingly considered for its potential involvement in disease progression (Byrd et al., 2019; Frew et al., 2020; Gudjonsson et al., 2020; Hoffman et al., 2018; Musilova et al., 2020). Since such infiltrates may be mirrored by alterations in blood B cells, we sought parameters that could be in line with the particular fate of B cells. CD162/PSGL-1 is a selectin involved in extravasation of leukocytes from the blood into inflamed tissues. CLA is a post-translational modification of PSGL-1 which can be detected by a specific antibody and allows to identify skin-addressed lymphocytes (Fuhlbrigge et al., 1997; de Jesús-Gil et al., 2021). By flow cytometry, we could verify CLA expression on a subset of in peripheral blood CD4+ T cells and on the majority of CD4+ T cells isolated from healthy skin **(Figure 3a)**. Interestingly, we found that a small subset of blood B cells also showed CLA expression **(Figure 3b)**. CLA+ B cells were slightly increased in familial cases as compared with the control groups **(Figure 3c)**. More strikingly, familial cases had a larger proportion of CLA+ switched memory B cells than healthy donors **(Figure 3d)**. Thus, in addition to increased proportions of switched memory cells, familial cases may be distinguished from other HS patients by the higher potential of this B cell subset to reach skin lesions.

Follicular helper T cells are increased in Hurley stage II patients

Next, we interested in functional subsets of blood T cells. In addition to memory T cells, we investigated follicular helper T (Tfh) cells, which are instrumental in the initiation and control of B cell responses. As shown by flow cytometry, CD45RA- memory CD4+ T cells include a population of CXCR5+ Tfh cells **(Figure 4a)**. However, neither memory nor Tfh cells were affected in any group of HS patient **(Figure 4b/c)**. Then, in the light of our findings on B cells, we estimated the proportion of CLA-expressing cells among memory T and Tfh cells. Again, there was no difference between healthy donors, sporadic and familial HS cases **(Figure 4d/e)**.

Next, we compared the levels of memory and Tfh cells with the Hurley and IHS4 stage of the patients. Memory CD4+ T cells were comparable at any stage with the levels observed in healthy donors **(Figure 4f and Figure S4a)**. On the other hand, the presence of Tfh cells appeared to peak in patients diagnosed with Hurley stage II **(Figure 4g)**. Intriguingly, higher

Tfh levels did not relate with any stage when the IHS4 scale was used to categorize the same patients **(Figure S4b)**.

Both memory T cells and Tfh cells can be further discriminated by their expression of chemokine receptors CXCR3 and CCR6. Considering previous findings on a Th17 bias of immune responses in HS (Moran et al., 2017), we quantified the relative proportions of CXCR3+ CCR6- Th1/Tfh1, CXCR3- CCR6- Th2/Tfh2 and CXCR3- CCR6+ Th17/Tfh17 **(Figure 5a)**. Yet, these proportions were identical in healthy donors and HS patients **(Figure 5b/c)**. When CLA+ skin-addressed cells were considered, we observed a decrease in Th1 cells and a nonsignificant increase of Th17 in HS patients **(Figure 5d)**. However, no such differences were visible for CLA+ Tfh subsets **(Figure 5e)**. We conclude that familial HS-related alterations of Th subsets may be exacerbated when skin-addressed cells are considered.

Discussion

Here, in order to uncover crucial hints about the disease development, we decided to investigate B and T cell subsets in the blood of HS patients with regard to (1) disease stage, using both Hurley and IHS4 scores and (2) families with clustered HS cases. Both parameters prove useful for data stratification. Indeed, Hurley stage II was characterized by high levels of Tfh cells, whereas a decrease of total circulating B cells may be associated with stage III. As opposed to sporadic cases, familial HS cases could be distinguished by a pronounced increase in switched memory B cells. We also found that CLA expression, a hallmark of skin-addressed leukocyte populations, reveals key features of these subsets in HS patients, such as increased switched memory B cells and decrease of Th1 cells.

Our initial analyses were performed on the bulk of patients in the cohort. However, the results did not match previous reports on B and T cell subset proportions in HS patients. Differences may be explained by the different origin and size of the cohort evaluated. Nevertheless, since immune responses in an autoinflammatory syndrome such as HS are expected to be linked with the severity of the disease, we decided to segregate patients according to their Hurley or IHS4 scores. Yet, most of the parameters that we analyzed did not correlate with disease stage. Based on the Hurley scoring system, we could however demonstrate that disease severity may be linked to specific alterations. Most strikingly, stage II patients displayed high rates of Tfh cells, whereas total B cells tend to decrease in stage III. Intriguingly, segregation of patients by the IHS4 scores did not uncover similar findings, which might be explained by the intrinsic differences in the scoring systems. The increased presence of Tfh cells in Hurley stage II patients may reflect an important step of disease development. Further analysis is required to confirm whether the loss of B cells is characteristic of late disease stages, and not related to other features of the patients or their therapeutic regimen.

To further address discrepancies with the previous literature, we interested in patients from families where HS was reported to affect several members. Taking this parameter into consideration allowed us to highlight clear differences between familial and sporadic cases. Overall, familial HS cases had more switched memory cells, although this may be attributed

to a minor proportion of the families with high ratios of this subset. Moreover, switched memory B cells also contained higher proportions of CLA-expressing cells. This is in support of a specific addressing of pathogenic B cells into skin lesions, although the role of such cells in the pathophysiology of HS remains unclear.

Our findings may be of great interest in the future design of therapeutic strategies that address this unresolved aspect of pathophysiology. Currently, transcriptomic and genomic analyses are being performed on samples from the cohort, which will complement the present data and allow us to dissect the mechanisms at play in the development of T and B cell responses.

Limitations of the study

Skin biopsies could not be collected to match blood samples. In addition to the specific expression of chemokine receptors, the Th/Tfh subsets were not confirmed by in vitro stimulation assays followed by cytokine production measurements. Hair samples from the familial cases were subjected to whole exon sequencing, which is still under analysis. Therefore, we are currently unable to consider the data on blood B and T cell subsets in the light of possibly related mutations.

Bibliography

Byrd, A.S., C. Carmona-Rivera, L.J. O'Neil, P.M. Carlucci, C. Cisar, A.Z. Rosenberg, M.L. Kerns, J.A. Caffrey, S.M. Milner, J.M. Sacks, O. Aliu, K.P. Broderick, J.S. Reichner, L.S. Miller, S. Kang, W.H. Robinson, G.A. Okoye, and M.J. Kaplan. 2019. Neutrophil extracellular traps, B cells, and type I interferons contribute to immune dysregulation in hidradenitis suppurativa. *Sci Transl Med*. 11:eaav5908. doi:10.1126/scitranslmed.aav5908.

Carmona-Rivera, C., L.J. O'Neil, E. Patino-Martinez, W.D. Shipman, C. Zhu, Q.-Z. Li, M.L. Kerns, L.A. Barnes, J.A. Caffrey, S. Kang, M.J. Kaplan, G.A. Okoye, and A.S. Byrd. 2021. Autoantibodies Present in Hidradenitis Suppurativa Correlate with Disease Severity and Promote the Release of Proinflammatory Cytokines in Macrophages. *J Invest Dermatol*. S0022-202X(21)02286–7. doi:10.1016/j.jid.2021.07.187.

Frew, J.W., D. Grand, K. Navrazhina, and J.G. Krueger. 2020. Beyond antibodies: B cells in Hidradenitis Suppurativa: Bystanders, contributors or therapeutic targets? *Exp Dermatol*. 29:509–515. doi:10.1111/exd.14092.

Fuhlbrigge, R.C., J.D. Kieffer, D. Armerding, and T.S. Kupper. 1997. Cutaneous lymphocyte antigen is a specialized form of PSGL- 1 expressed on skin-homing T cells. *Nature*. 389:978–981.

Gudjonsson, J.E., L.C. Tsoi, F. Ma, A.C. Billi, K.R. van Straalen, A.R.J.V. Vossen, H.H. van der Zee, P.W. Harms, R. Wasikowski, C.M. Yee, S.M. Rizvi, X. Xing, E. Xing, O. Plazyo, C. Zeng, M.T. Patrick, M.M. Lowe, R.E. Burney, J.H. Kozlow, J.R. Cherry-Bukowiec, Y. Jiang, J. Kirma, S. Weidinger, K.C. Cushing, M.D. Rosenblum, C. Berthier, A.S. MacLeod, J.J. Voorhees, F. Wen, J.M. Kahlenberg, E. Maverakis, R.L. Modlin, and E.P. Prens. 2020. Contribution of plasma cells and B cells to hidradenitis suppurativa pathogenesis. *JCI Insight*. 5:e139930, 139930. doi:10.1172/jci.insight.139930.

Hoffman, L.K., L.E. Tomalin, G. Schultz, M.D. Howell, N. Anandasabapathy, A. Alavi, M. Suárez-Fariñas, and M.A. Lowes. 2018. Integrating the skin and blood transcriptomes and serum proteome in hidradenitis suppurativa reveals complement dysregulation and a plasma cell signature. *PLoS One*. 13:e0203672. doi:10.1371/journal.pone.0203672.

de Jesús-Gil, C., L. Sans-de SanNicolàs, I. García-Jiménez, M. Ferran, A. Celada, A. Chiriac, R.M. Pujol, and L.F. Santamaria-Babí. 2021. The Translational Relevance of Human Circulating Memory Cutaneous Lymphocyte-Associated Antigen Positive T Cells in Inflammatory Skin Disorders. *Front Immunol*. 12:652613. doi:10.3389/fimmu.2021.652613.

Melnik, B.C., S.M. John, W. Chen, and G. Plewig. 2018. T helper 17 cell/regulatory T-cell imbalance in hidradenitis suppurativa/acne inversa: the link to hair follicle dissection, obesity, smoking and autoimmune comorbidities. *Br J Dermatol*. 179:260–272. doi:10.1111/bjd.16561.

Moran, B., C.M. Sweeney, R. Hughes, A. Malara, S. Kirthi, A.-M. Tobin, B. Kirby, and J.M. Fletcher. 2017. Hidradenitis Suppurativa Is Characterized by Dysregulation of the

Th17:Treg Cell Axis, Which Is Corrected by Anti-TNF Therapy. *J Invest Dermatol*. 137:2389–2395. doi:10.1016/j.jid.2017.05.033.

Musilova, J., B. Moran, C.M. Sweeney, A. Malara, A. Zaborowski, R. Hughes, D.C. Winter, J.M. Fletcher, and B. Kirby. 2020. Enrichment of Plasma Cells in the Peripheral Blood and Skin of Patients with Hidradenitis Suppurativa. *J Invest Dermatol*. 140:1091-1094.e2. doi:10.1016/j.jid.2019.08.453.

Narla, S., M. Azzam, S. Townsend, G. Vellaichamy, A.V. Marzano, A. Alavi, M.A. Lowes, and I.H. Hamzavi. 2021. Identifying key components and therapeutic targets of the immune system in hidradenitis suppurativa with an emphasis on neutrophils. *Br J Dermatol*. 184:1004–1013. doi:10.1111/bjd.19538.

Sachdeva, M., M. Shah, and A. Alavi. 2021. Race-Specific Prevalence of Hidradenitis Suppurativa. *J Cutan Med Surg*. 25:177–187. doi:10.1177/1203475420972348.

Tricarico, P.M., C. Moltrasio, A. Gradišek, A.V. Marzano, V. Flacher, W. Boufenghour, E. von Stebut, M. Schmuth, W. Jaschke, M. Gams, M. Boniotto, and S. Crovella. 2022. Holistic health record for Hidradenitis suppurativa patients. *Sci Rep*. 12:8415. doi:10.1038/s41598-022-11910-5.

Vaidya, T., R. Vangipuram, and A. Alikhan. 2017. Examining the race-specific prevalence of hidradenitis suppurativa at a large academic center; results from a retrospective chart review. *Dermatol Online J*. 23:13030/qt9xc0n0z1.

Wang, B., W. Yang, W. Wen, J. Sun, B. Su, B. Liu, D. Ma, D. Lv, Y. Wen, T. Qu, M. Chen, M. Sun, Y. Shen, and X. Zhang. 2010. Gamma-secretase gene mutations in familial acne inversa. *Science*. 330:1065. doi:10.1126/science.1196284.

Wolk, K., K. Warszawska, C. Hoeflich, E. Witte, S. Schneider-Burrus, K. Witte, S. Kunz, A. Buss, H.J. Roewert, M. Krause, A. Lukowsky, H.-D. Volk, W. Sterry, and R. Sabat. 2011. Deficiency of IL-22 contributes to a chronic inflammatory disease: pathogenetic mechanisms in acne inversa. *J Immunol*. 186:1228–1239. doi:10.4049/jimmunol.0903907.

Wollina, U., A. Koch, B. Heinig, T. Kittner, and A. Nowak. 2013. Acne inversa (Hidradenitis suppurativa): A review with a focus on pathogenesis and treatment. *Indian Dermatol Online J*. 4:2–11. doi:10.4103/2229-5178.105454.

van der Zee, H.H., J.D. Laman, J. Boer, and E.P. Prens. 2012. Hidradenitis suppurativa: viewpoint on clinical phenotyping, pathogenesis and novel treatments. *Exp Dermatol.* 21:735–739. doi:10.1111/j.1600-0625.2012.01552.x.
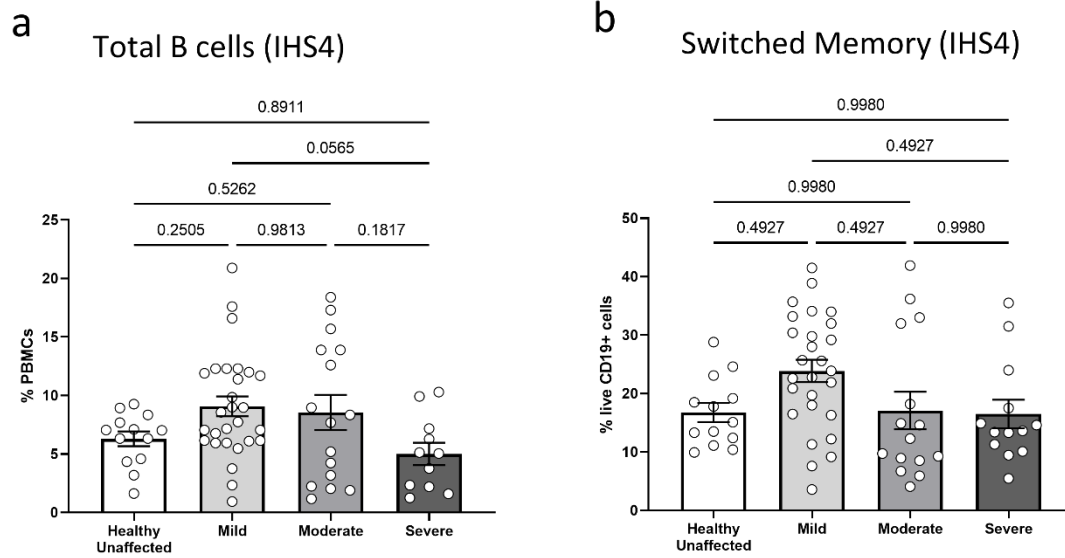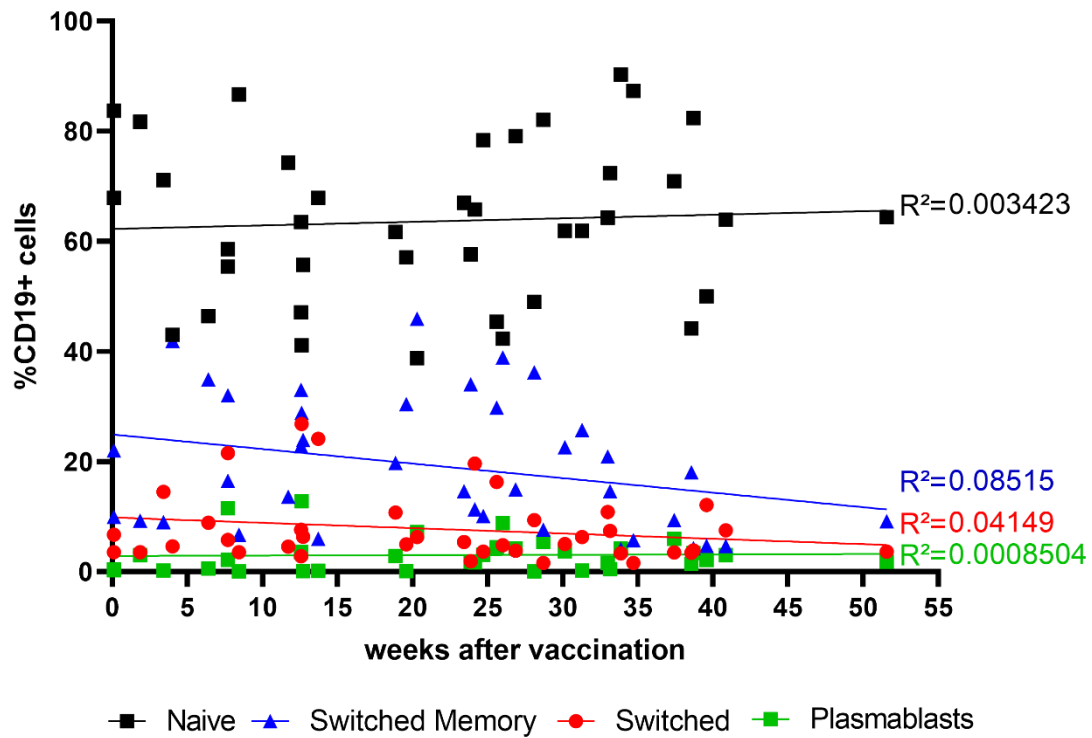
Figures
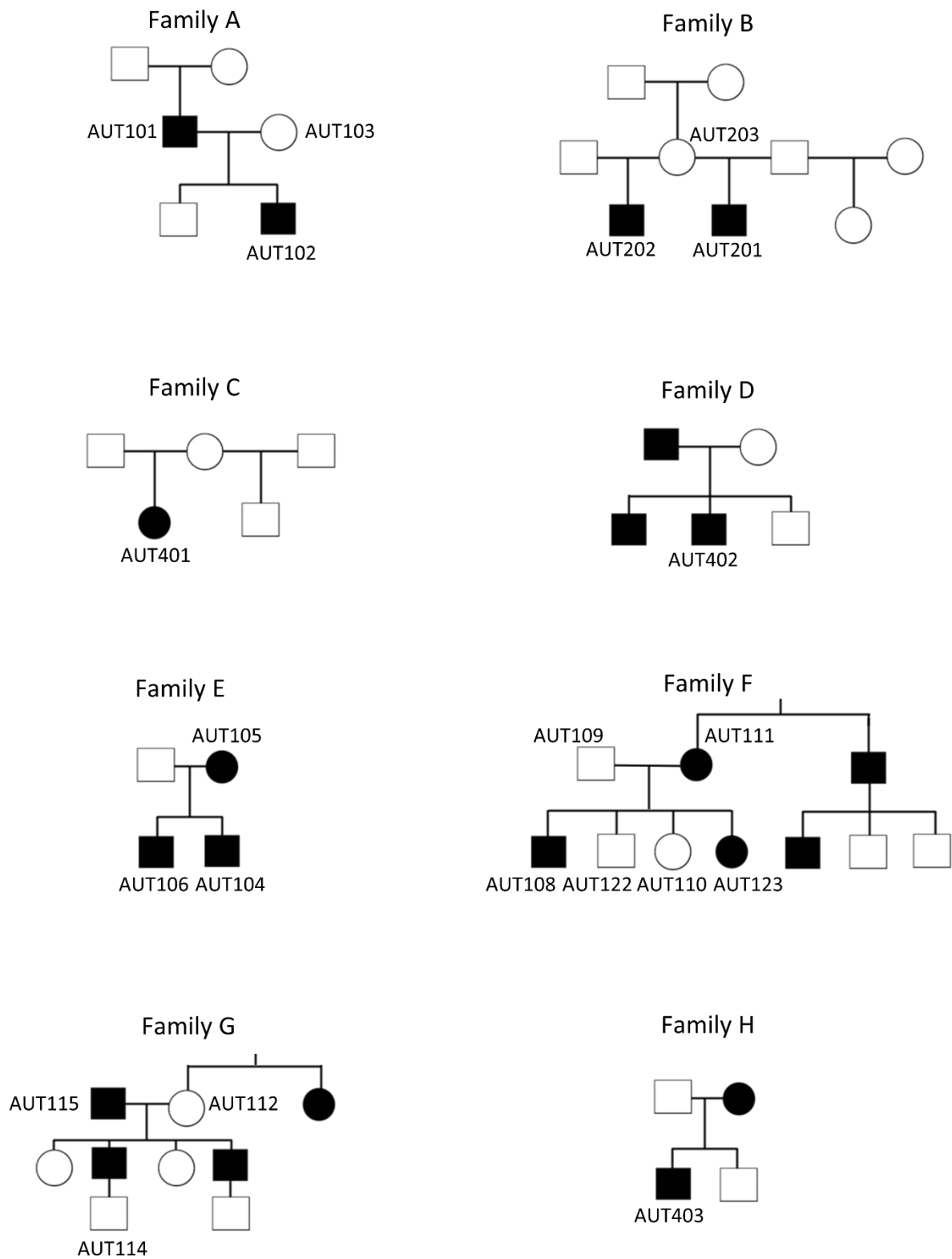
Figure S1: Familial pedigrees of HS patients recruited in the study. Circles, women; squares, men; black symbols, affected family members. Each patient and their relatives from which blood has been sampled are designated by anonymized identifiers (AUTxxx).
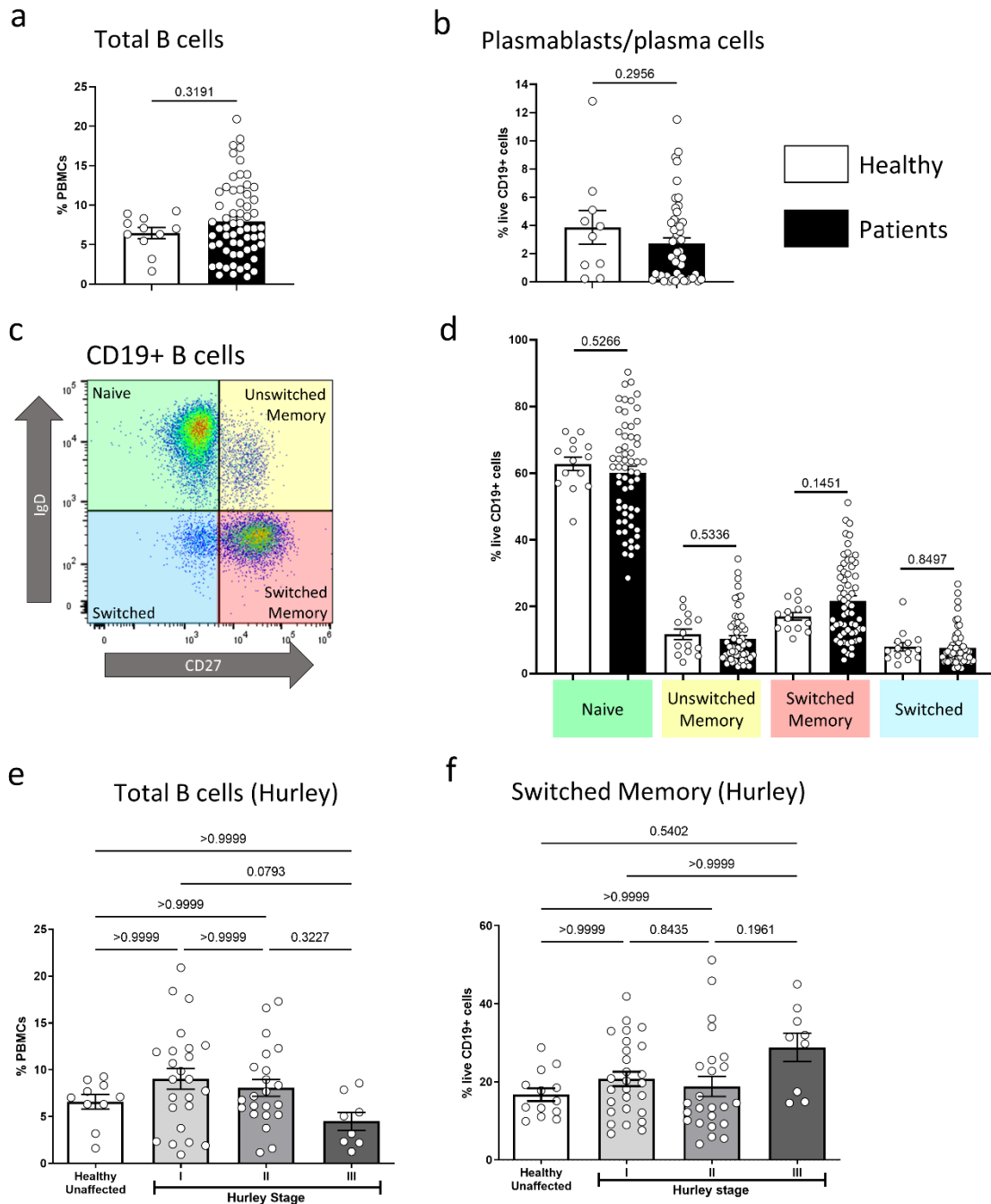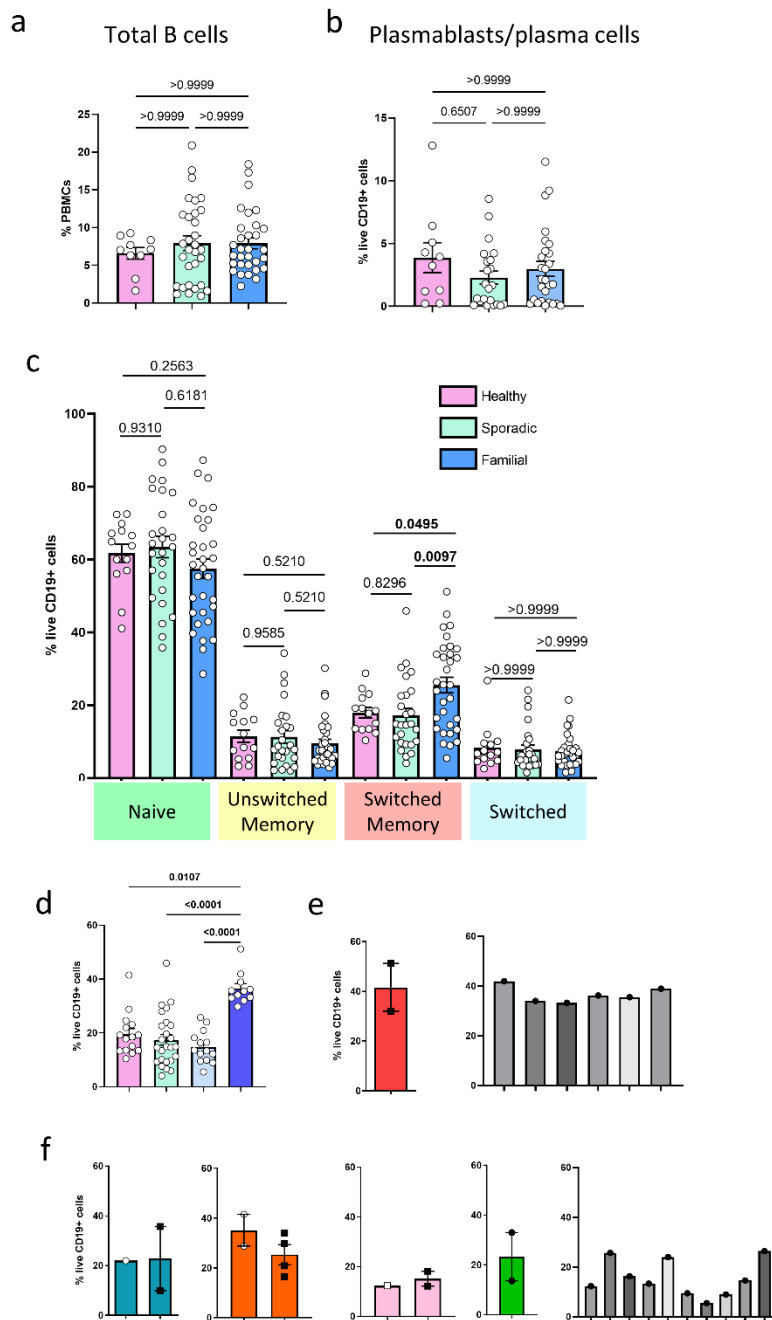
Figure 1: B cell subset proportions are similar in healthy donors and hidradenitis suppurativa patients. B cells were analyzed in the blood of healthy donors and acne inversa **(a)** Proportion of live B cells (CD19+) out of PBMCs **(b)** Proportion of plasmablasts/plasma cells (CD38+ CD19+) out of PBMCs. **(c)** Gating of four defined B cell subpopulations: Naïve (IgD+ CD27-), Unswitched Memory (IgD+ CD27+), Switched Memory (IgD- CD27+=, Switched (IgD- CD27-). **(d)** Proportions of B cell subsets. Next, patients were classified according to Hurley stages (I, II, III). **(e)** Percentage of B cells out of PBMCs. **(f)** Percentage of Switched Memory cells out of total B cells. Statistical comparisons used Mann-Whitney tests (a, b, d) and Kruskal-Wallis tests followed by Dunn's post-hoc test for multiple comparisons (e,f). For each comparison, p values are indicated (p>0.05, nonsignificant difference).

Figure S2: Higher levels of switched memory cells do not correlate with specific IHS4 stages. Patients were classified according to IHS4 scaling (mild, moderate, severe). **(a)** Percentage of B cells out of PBMCs. **(b)** Percentage of Switched Memory cells out of total B cells. Statistical comparisons used Kruskal-Wallis tests followed by Dunn's post-hoc test for multiple comparisons. For each comparison, p values are indicated (p>0.05, nonsignificant difference).

Figure S3: Vaccination does not elicit time-dependent changes in B cell subsets. Proportions of B cell subsets (Naive, Switched Memory, Switched and Plasmablasts) relative to the time period elapsed since a recent vaccination reported by the patients. Linear correlation was performed on each subset and R^2 were calculated.

Figure 2: B cell subset proportions are altered in patients with familial history of hidradenitis suppurativa. B cells were analyzed in the blood of healthy donors and acne inversa patients without (sporadic) or with familial history of the disease. **(a)** Proportion of live B cells (CD19+) out of PBMCs. **(b)** Proportion of plasmablasts/plasma cells (CD38+ CD19+) out of PBMCs. **(c)** Proportions of four defined B cell subpopulations: Naïve (IgD+ CD27-), Unswitched Memory (IgD+ CD27+), Switched Memory (IgD- CD27+=, Switched (IgD- CD27-). **(d)** Comparison of healthy donors, sporadic cases and familial cases with low (light blue) or high (dark blue) proportions of switched memory cells. **(e,f)** Families (colored bars) and individual familial cases (grey bars) with high **(d)** or low **(e)** proportions of switched memory B cells. Statistical comparisons used Kruskal-Wallis tests followed by Dunn's post-hoc test for multiple comparisons. For each comparison, p values are indicated (p>0.05, nonsignificant difference).
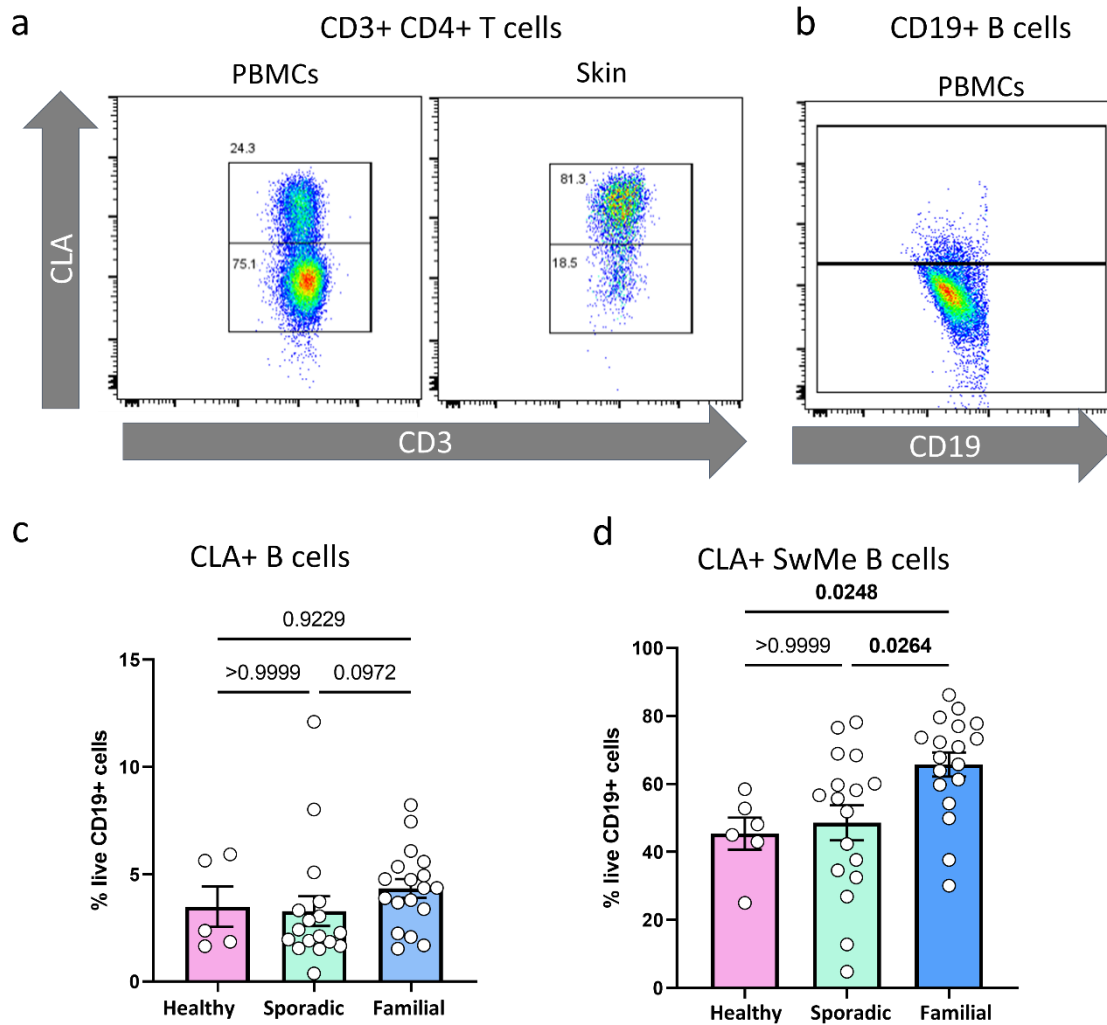
Figure 3: CLA+ Switched memory B cells are most strongly increased in the familial HS cases. **(a)** Representative CLA staining of CD3+ CD4+ cells from either PBMCs or skin explants of healthy donors. **(b)** Representative CLA staining of CD19+ B cells from PBMCs of healthy donors. **(c)** Proportion of CLA+ cells among B cells of healthy donors, sporadic and familial cases. **(d)** Proportion of CLA+ B cells with switched memory phenotype (IgD- C27+) in PBMCs of healthy donors, sporadic and familial HS cases. Statistical comparisons used Kruskal-Wallis tests followed by Dunn's post-hoc test for multiple comparisons. For each comparison, p values are indicated (p>0.05, nonsignificant difference).
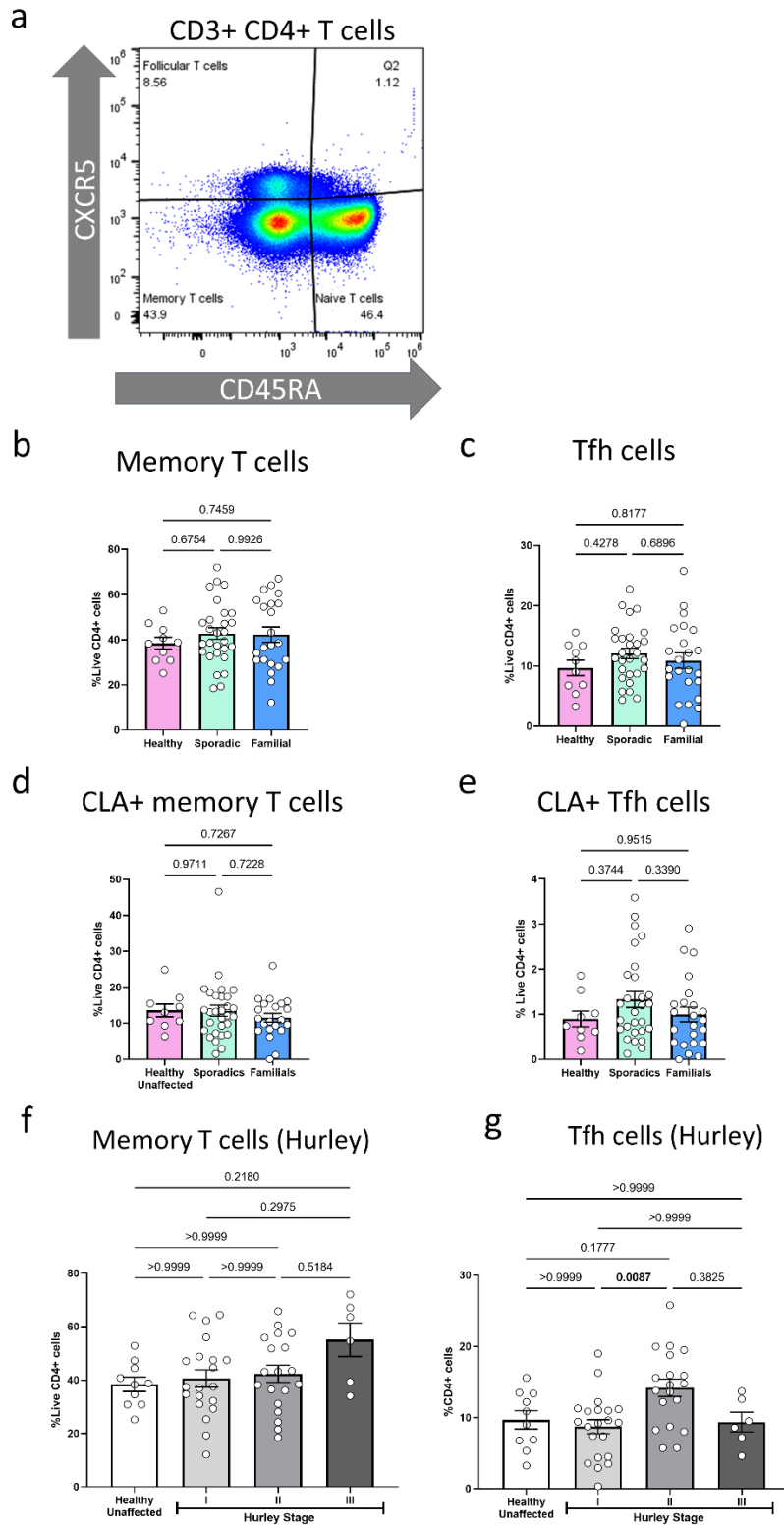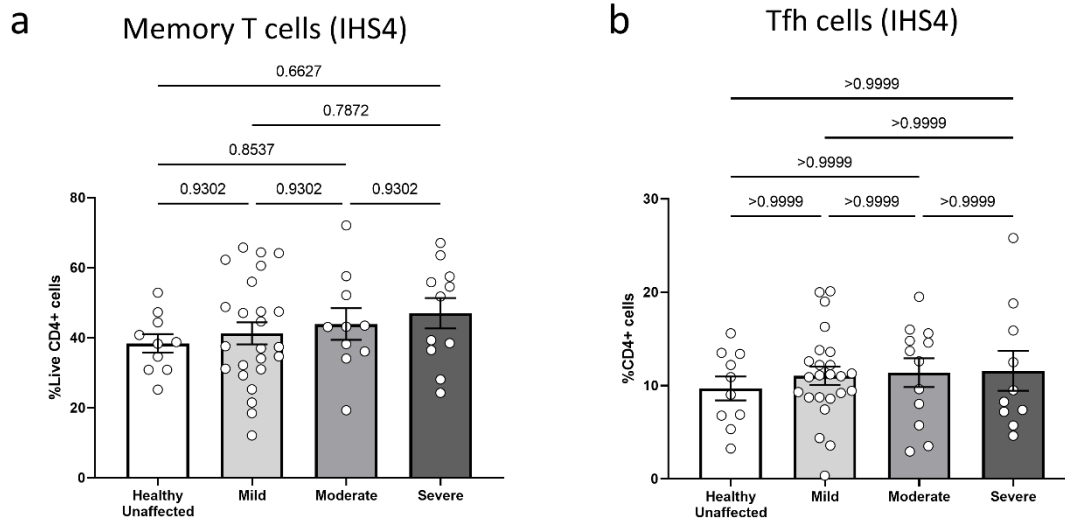
Figure 4: T cells of familial HS cases do not display changes in memory, Tfh and CLA+ cells.
Statistical comparisons used Kruskal-Wallis tests followed by Dunn's post-hoc test for multiple comparisons. For each comparison, p values are indicated (p>0.05, nonsignificant difference).

Figure S4: T cell subset proportions do not correlate with specific IHS4 stages. Patients were classified according to IHS4 scaling (mild, moderate, severe). **(a)** Percentage of CD45RA- CD4+ memory T cells out of PBMCs. **(b)** Percentage of CD45RA- CXCR5+ follicular helper T cells out of total T cells. Statistical comparisons used Kruskal-Wallis tests followed by Dunn's post-hoc test for multiple comparisons. For each comparison, p values are indicated (p>0.05, nonsignificant difference).
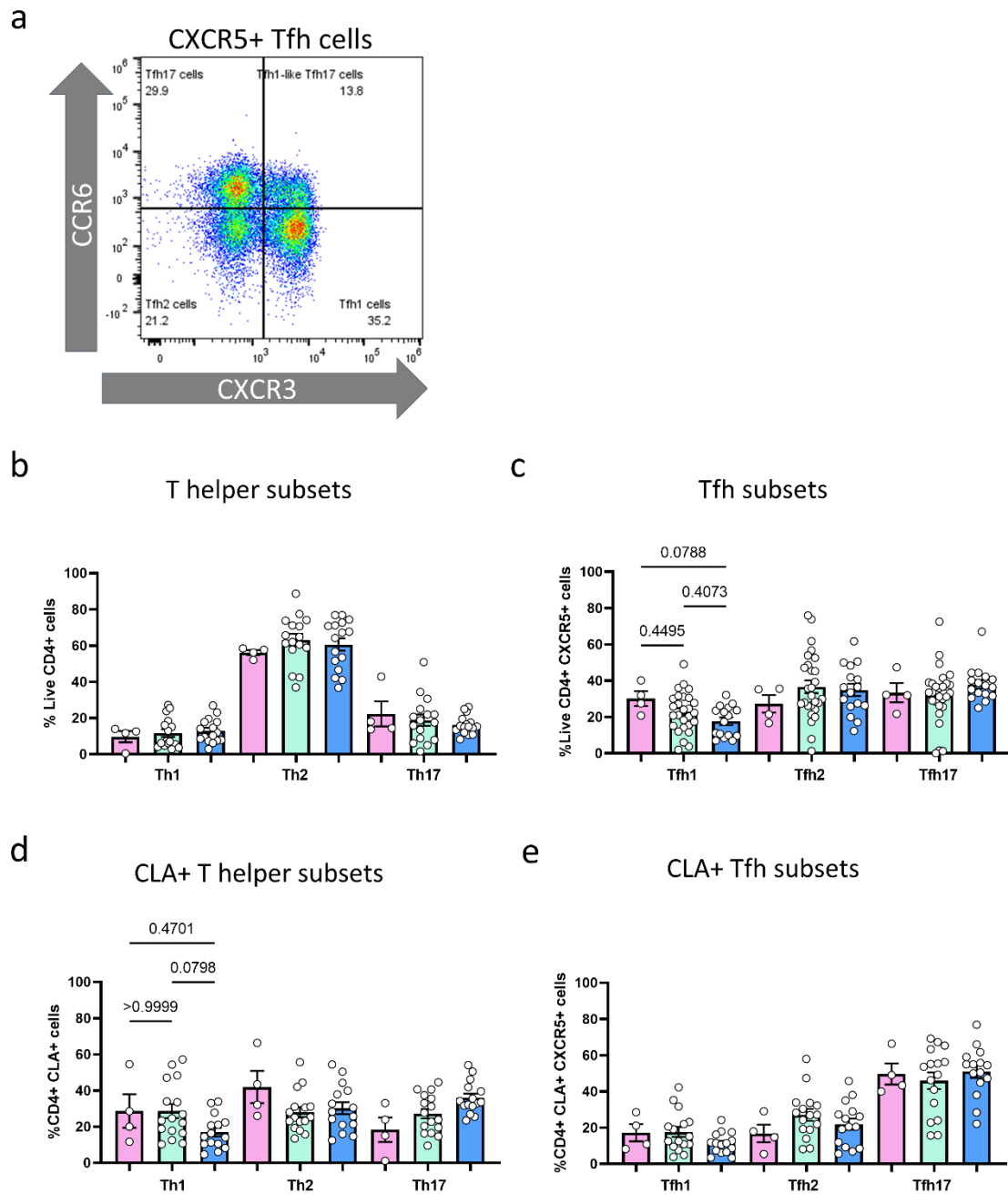
Figure 5: Functional subsets of Th and Tfh cells are similar in healthy donors and HS patients, with the exception of skin-addressed Th1 cells. (a) Discrimination by flow cytometry of functional CD4+ T cells. A representative example shows CXCR5+ Tfh cells further defined as CXCR3+ CCR6- Tfh1, CXCR3- CCR6- Tfh2 and CXCR3- CCR6+ Tfh17. Memory Th1/2/17 cells were identified by a similar gating strategy. **(b)** Proportions of Th1/2/17 subsets among CD4+ T cells. **(c)** Proportion of Tfh1/2/17 subsets among total Tfh cells. **(d)** Proportions of Th1/2/17 subsets among CLA+ CD4+ T cells**. (e)** Proportion of Tfh1/2/17 subsets among CLA+ Tfh cells. Statistical comparisons used Kruskal-Wallis tests followed by Dunn's post-hoc test for multiple comparisons. For each comparison, p values are indicated (p>0.05, nonsignificant difference).

scientific reports

OPEN

Holistic health record for Hidradenitis suppurativa patients

Paola Maura Tricarico[1]✉, Chiara Moltrasio[2,3], Anton Gradišek[4], Angelo V Marzano[2,5], Vincent Flacher[6], Wacym Boufenghour[6], Esther von Stebut[7], Matthias Schmuth[8], Wolfram Jaschke[8], Matjaž Gams[4], Michele Boniotto[9] & Sergio Crovella[10]

Hidradenitis suppurativa (HS) is a recurrent inflammatory skin disease with a complex etiopathogenesis whose treatment poses a challenge in the clinical practice. Here, we present a novel integrated pipeline produced by the European consortium BATMAN (Biomolecular Analysis for Tailored Medicine in Acne iNversa) aimed at investigating the molecular pathways involved in HS by developing new diagnosis algorithms and building cellular models to pave the way for personalized treatments. The objectives of our european Consortium are the following: (1) identify genetic variants and alterations in biological pathways associated with HS susceptibility, severity and response to treatment; (2) design in vitro two-dimensional epithelial cell and tri-dimensional skin models to unravel the HS molecular mechanisms; and (3) produce holistic health records HHR to complement medical observations by developing a smartphone application to monitor patients remotely. Dermatologists, geneticists, immunologists, molecular cell biologists, and computer science experts constitute the BATMAN consortium. Using a highly integrated approach, the BATMAN international team will identify novel biomarkers for HS diagnosis and generate new biological and technological tools to be used by the clinical community to assess HS severity, choose the most suitable therapy and follow the outcome.

Hidradenitis suppurativa (HS), also known as acne inversa, is a chronic, inflammatory, recurrent, debilitating skin disease. With a prevalence in Europe of 0.8 (varying between 0.5% and 1.3%) and a diagnosis often underestimated and usually delayed up to 7.2 ± 8.7 years, HS can't be considered as a rare disease[1] [https://www.orpha.net/consor/cgi-bin/OC_Exp.php?lng=en&Expert=387 Women are more frequently affected than men (female:male ratio, 3:1) and have more likely genitofemoral lesions[2]. The disease onset occurs usually during adolescence or early adulthood, resulting in frustration, embarrassment and depression. Very often, the severe forms start manifesting in early adolescence/puberty thus resulting in several inflammatory lesions over the years. Thus, early diagnosis and adequate, stage-adapted therapy is essential to avoid a destructive course of disease. Clinically, HS is characterized by inflammatory nodules that progress into abscesses and draining tunnels with foul smelling[3].

HS is usually a sporadic disease, but may occur as a familial disorder[4]. A familial form is reported in 40% of cases showing an autosomal dominant mode of inheritance with incomplete penetrance in some cases[2,5]. In a minority of patients, HS can be associated with other immune-mediated inflammatory diseases or inherited conditions, presenting as "syndromic" HS[6]. The main autoinflammatory syndromes characterized by the presence of HS are pyoderma gangrenosum (PG), acne and suppurative hidradenitis (PASH), pyogenic arthritis, PG, acne

[1]Department of Advanced Diagnostics, Institute for Maternal and Child Health - IRCCS Burlo Garofolo, Trieste, Italy. [2]Dermatology Unit, Fondazione IRCCS Ca' Granda Ospedale Maggiore Policlinico, Milan, Italy. [3]Department of Medical Surgical and Health Sciences, University of Trieste, Trieste, Italy. [4]Department of Intelligent System, Jožef Stefan Institute, Jamova Cesta 39, 1000 Ljubljana, Slovenia. [5]Department of Pathophysiology and Transplantation, Università Degli Studi Di Milano, Milan, Italy. [6]Laboratory CNRS I2CT/UPR3572 Immunology, Immunopathology and Therapeutic Chemistry, Strasbourg Drug Discovery and Development Institute (IMS), Institut de Biologie Moléculaire Et Cellulaire, University of Strasbourg, Strasbourg, France. [7]Department of Dermatology, University of Cologne, Kerpenerstr. 62, 50935 Cologne, Germany. [8]Department of Dermatology, Venereology and Allergy, Medical University of Innsbruck, Anichstrasse 35, Innsbruck, Austria. [9]INSERM, IMRB, Translational Neuropsychiatry, F-94010, University Paris Est Créteil, Créteil, France. [10]Biological Sciences Program, Department of Biological and Environmental Sciences, College of Arts and Sciences, University of Qatar, Doha, Qatar. ✉email: tricaricopa@gmail.com

1

and suppurative hidradenitis (PAPASH), psoriatic arthritis, PG, acne and suppurative hidradenitis (PsAPASH), pustular psoriasis, arthritis, PG, synovitis, acne and suppurative hidradenitis (PsAPSASH) and PG, acne, suppurative hidradenitis, and ankylosing spondylitis (PASS)[7].

Cigarette smoking and obesity are crucial trigger factors in HS and both have been directly correlated with the severity of this disease. Although clinically follicular hyperkeratosis and bacterial superinfection are common features, the molecular pathogenesis of HS remains to be clarified. Therefore, HS treatment is somehow empirical and includes topical (antibiotics, keratolytics, antiseptics), intralesional (corticosteroids), surgical (deroofing, wide local excision), and systemic (antibiotics, retinoids, biologics, immunosuppressants, metformin, antiandrogens) interventions. In particular, biologics, i.e. antibodies directed against TNF-alpha, IL-17, IL-23, IL-1, and latest generation immunosuppressants, i.e. JAK-inhibitors, are promising options awaiting a better pathogenetic rationale and a P4 medicine approach (predictive, preventative, personalized, participatory) to be introduced in the routine clinical practice.

Taking into account the current gap of knowledge in HS etio-pathogenesis, patients' efficient and timely diagnosis as well as tailored clinical follow-up, the purpose of this manuscript is to present a novel integrated pipeline produced by the ERAPerMed European consortium BATMAN (Biomolecular Analysis for Tailored Medicine in Acne iNversa) aimed at increasing the knowledge in HS etio-pathogenesis with the objective of translating the findings in the tailored clinical follow-up of HS patients.

The BATMAN consortium has been constituted joining the efforts of dermatologists with three active clinical Units from Milano (Italy), Innsbruck (Austria) and Cologne (Germany), geneticists (Trieste, Italy), immunologists and molecular cell biologists (Paris and Strasbourg, France) with the pivotal participation of informatics technology (IT) partners (Ljubljana, Slovenia).

In detail, this European Consortium aims at:

1. identifying genetic variants and alterations in biological pathways associated with HS susceptibility, severity and response to treatment;
2. designing in vitro two-dimensional epithelial cell and tri-dimensional skin models to unravel the HS molecular mechanisms;
3. producing holistic health records (HHR) to complement medical observations by developing a smartphone application to remotely monitor the physical and psychological wellbeing of patients and advise them on physical activity and dietary and smoking habits.

Here we will describe the main activities developed by different members of the Consortium including the IT approach that, integrating medical records, genetic results, immunology and cell biology findings will contribute to providing a tailored diagnosis for HS patients as well as paving the way for personalized treatments, thus starting to respond to the main patients' needs and changing the patients' care strategies used in clinical practice.

Aim 1: Identify genetic variants and alterations in biological pathways associated with HS susceptibility, severity and response to treatment

Genetic diagnosis of diseases requires a physical examination, personal medical history records, family health history and laboratory tests, including genetic testing. The occurrence of the same condition among family members is the key factor to be considered: pedigree analysis of the families with more than one member affected is the key clue for determining the patterns of disease inheritance.

As mentioned above, HS familial cases are reported in 40% of cases, more than one-third of patients. Whether HS manifests as an inherited disease and what is the frequency depends upon several factors: difficult and often delayed diagnosis of HS, caused by the lack of knowledge of this disease, absence of personal and family health history investigation, incomplete penetrance of this disease and also the unwillingness of other family members to participate in the study[5].

Genetic mutations in the γ-secretase enzyme subunits (*NCSTN*, *PSEN1*, *PSENEN*) have been reported in HS familial cases suggesting that HS could be considered a monogenic disease with autosomal dominant inheritance pattern and incomplete penetrance. Mutations in these genes lead to an impairment of the Notch pathway and/or of inflammasome signaling[8,9].

Whole exome sequencing (WES) of 11 HS families has been performed by P. Theut Riis et al.[10] The authors reported several variants of uncertain significance that segregated with the disease within these families. These findings suggest that familial HS can be regarded as a polygenic autoinflammatory condition and, only in a minority of cases, as a monogenic disease[10]. Despite this, further studies and functional validations are necessary to highlight the genetic landscape of familial HS.

In a cross-sectional study in a Dutch twin cohort, Van Straalen et al. observed an high heritability of HS (77%) and also environmental factors as significant contributors to the susceptibility of this disease, supporting a multifactorial etiology of this skin disorder[11].

In sporadic and syndromic HS cases, the contribution of genetic factors is still an active research area, and several genetic/functional studies are ongoing to unravel the pathogenesis of HS and its syndromic forms. A range of genetic changes have been associated with HS pathogenesis, including variations in genes involved in autoinflammation, vitamin D metabolism and keratinization pathway[12].

The Table 1 shows all the genes involved in HS known to date.

So, it's a widely accepted fact that genetics plays a role in the susceptibility to develop HS and to modulate the clinical phenotype. Moreover, patients' genetic background can have an impact in pharmacogenetics/pharmacogenomics; indeed, this kind of research is important to understand the genetic influence on the organism response to different drugs, different doses, and the timing of drugs' elimination.

Gene	Encoding protein	Disease	References
APH1B	Aph-1 homolog B	Familial HS	10
DEFB103	Defensin Beta 3 (hBD3)	Sporadic HS	13
DEFB4	Defensin Beta 2 (hBD2)	Sporadic HS	13
FGFR2	Fibroblast Growth Factor Receptor	Sporadic HS + Nevus comedonicus and Syndromic HS	4,14
GJB2	Gap Junction Protein Beta 2, Connexin-26	Sporadic HS + Keratitis-ichthyosis-deafness syndrome and Syndromic HS	14, 15
IL-12Rb1	Interleukin-12 Receptor Subunit Beta-1	Sporadic HS	16
LPIN2	Lipin 2	Sporadic HS	12
MEFV	MEFV innate immunity regulator	Familial HS and Syndromic HS	4, 12, 17
MYD88	Myeloid Differentiation Primary Response Protein MyD88	Sporadic HS	18
NCSTN	Nicastrin	Familial HS, Syndromic HS and HS + Dowling-Degos disease	4, 15, 19, 20
NLRC4	NLR Family CARD Domain Containing 4	Syndromic HS	15
NLRP12	NLR Family Pyrin Domain Containing 12	Syndromic HS	12
NLRP3	NLR Family Pyrin Domain Containing 3	Syndromic HS	12
NOD2	Nucleotide Binding Oligomerization Domain Containing 2	Familial HS and Syndromic HS	12, 15, 17, 19
OCRL1	Inositol polyphosphate 5-phosphatase	Sporadic HS + Dent disease 2	21
OTULIN	OTU Deubiquitinase With Linear Linkage Specificity	Syndromic HS	15
POFUT1	Protein O-Fucosyltransferase 1	Syndromic HS and HS + Dowling-Degos disease	4, 19, 22
PSEN1	Presenilin 1	Familial HS	9, 23
PSENEN	Presenilin Enhancer Protein 2	Familial HS, Syndromic HS and HS + Dowling-Degos disease	9, 19, 24, 25
PSTPIP1	Proline-Serine-Threonine Phosphatase Interacting Protein 1	Syndromic HS	15, 19, 26, 27
TNF	Tumor Necrosis Factor	Sporadic HS	28
WDR1	WD Repeat Domain 1	Syndromic HS	15

Table 1.. Summary of the genes involved in HS.

Liu et al. performed GWAS, designed for HS response to adalimumab (anti-TNFa), in 445 HS patients; the authors identified a single-nucleotide polymorphism (SNP) (rs59532114) in the intron (chr18:63162799, GRCh38.p13) of the BCL2 gene, associated with adalimumab response[29]. This SNP minor A allele is associated with increased BCL2 gene expression and its augmented protein level in the hair follicle, thus suggesting a potential role of apoptosis' regulation in the pathophysiology of adalimumab response in HS patients.

Previously, the same authors observed that HLA-DRB1*03 and HLA-DRB1*011 allele conferred an increased risk for developing anti-adalimumab antibodies in HS patients, while HLA-DQB1*05, HLA-DRB1*01 and HLA-DRB1*07 allele might protect against anti-adalimumab antibodies formation[30]. The formation of anti-drug antibodies to adalimumab can lead to its therapeutic ineffectiveness and these findings can lead the switch to other, more effective therapies.

So, genetically guided decisions of tailored therapies aim to enhance treatment success rate with a consequent improvement of patients' quality of life.

The discovery of differentially expressed genes (DEGs) that induce alterations in biological molecular pathways is highly necessary for improving understanding of HS pathogenesis and also of HS treatment. Coates M. et al. observed a dysregulation of antimicrobial peptides between lesional and unaffected skin of HS patients, analyzing HS skin transcriptomes from previously published studies. This observation allowed to confirm the key role of the innate immunity in the HS pathogenesis and also to pave the way for development of new therapies based on supplementation/activation of antimicrobial peptides[31]. On the other hand, Mariottoni et al. identified an upregulation of genes involved in interferon and antimicrobial defense signaling. They also observed monocyte/macrophage dysregulation, with single cell RNA sequencing (scRNA-seq) analysis of skin tissue; according to the authors this observation could pave the way for the identification of potential novel therapeutic targets[32].

Considering all these findings, HS has no clear and well-defined mode of inheritance, due to the polygenic and multifactorial nature of the disease. Thus, the following question arises: how far are we from the identification of genetic variants useful for disease's mechanistic understanding as well as for personalized diagnosis and treatment? Could the integration of data between genetic variants and DEGs help to understand HS pathogenesis? How genetics can help in sporadic and syndromic cases?

In the attempt of contributing to unraveling these questions, the dermatologists of the BATMAN consortium, collected and accurately clinically phenotyped HS familial and sporadic cases, as well as syndromic HS. Saliva is collected from all HS patients for DNA extraction in order to perform genetic analyses (single nucleotide polymorphisms arrays and/or whole exome sequencing); instead, skin punch biopsies are collected only from HS familial and syndromic cases in order to identify DEGs and perform histological analyses.

Aim 1: Methods

Patients recruitment. The inclusion criteria for patient enrollment are the compliance to the diagnostic criteria for HS. Three criteria must be fulfilled:

1. 1.Typical lesions: deep-seated painful nodules, abscesses, bridged scars and draining fistulae as well as open, tombstone double-ended comedones (pseudocomedones). Usually, multiple lesions are present that facilitate the diagnosis. It is, however, important to avoid misdiagnosis with nondiagnostic elements, such as simple folliculitis.
2. Predilection sites: axillae, inframammary and/or intermammary folds, groin, perineal region, or buttocks. Lesions may appear ectopically (i.e. face, trunk, ears) but they must involve the areas for which the disease has a predilection to meet the diagnosis.
3. History of chronicity and recurrence: temporary lesions initially recur in the predilection areas only to turn chronic later in the course of the disease. Two recurrences over a period of six months have been used as a useful diagnostic criterion.

All three criteria must be present for HS diagnosis, and considering the recurrence/chronicity, an observation period may be necessary before the definitive diagnosis[33].

Based on clinical observations, six phenotypes have been proposed: (1) regular, (2) frictional furunculoid, (3) scarring folliculitis, (4) conglobata, (5) ectopic and (6) syndromic[34]. However, Dudink et al. suggested that the ectopic and syndromic types do not have specific clinical features and could be categorized as one of the other phenotypes[35]. Finally, Frew et al. presented a revised phenotype classification system: (1) typical (previously regular subtype) and (2) atypical that includes scarring folliculitis and conglobata subtypes[36]. However, given the clinical heterogeneity of HS, further sub-classifications under the "atypical" need additional investigations. Syndromic disease has the potential to become a third classification. Patients with HS syndromic are characterized by concomitant manifestations, such as PG and arthritis; however, other clinical consensus are required to define the symptomatology sufficient for a syndromic phenotype diagnosis. It remains unclear whether a syndromic phenotype should remain restricted to PASH and PAPASH syndromes or if other autoimmune/autoinflammatory syndromes such as Familial Mediterranean Fever and Dowling Degos Disease should also be included[25,36,37].

Interestingly, familial HS cases show a severe disease phenotype not entirely matching with the one typical of "sporadic" HS, as mentioned above[38].

Accurate disease severity assessment and classification of HS patients are mandatory for guiding therapeutic decisions as well as for patient stratification. Zouboulis et al. have established IHS4 (International Hidradenitis Suppurativa Severity Score System), a dynamic HS score[39]. This IHS4 score (points) = (number of nodules multiplied by 1) + (number of abscesses multiplied by 2) + [number of draining tunnels (fistulae/sinuses) multiplied by 4]. A score of 3 or less signifies mild HS, a score of 4–10 corresponds to moderate HS and a score of 11 or higher reveals severe HS.

This proposed score can be used complementary and simultaneously with HiSCR (Hidradenitis suppurativa Clinical Response) score and both can be calculated easily in daily clinical practice and clinical trial settings.25 The HiSCR is defined as a ≥ 50% reduction in inflammatory lesion count (sum of abscesses and inflammatory nodules) and no increase in abscesses or draining fistulas in HS when compared with baseline. This score was only recently created but it is a promising clinical endpoint to evaluate therapeutic outcomes in patients with Hidradenitis suppurativa.

Sample collection. All biological samples are obtained, in all clinical centers, with written informed consent and institutional review board approval, in agreement with the Helsinki Declaration and local legislations (the study was approved by the institutional review boards of "Comitato Etico Unico Regionale of Friuli Venezia Giulia, Institute for Maternal and Child Health IRCCS Burlo Garofolo" Italy, of "Comitato etico Milano Area 2 IRCCS CA' GRANDA the Policlinico Maggiore Hospital" Italy, of "Medical University of Innsbruck" Austria and of "Medical University of Cologne" Germany).

In detail, from familial and syndromic HS cases the following samples are collected: saliva (for DNA extraction), skin punch biopsies (half for RNA extraction and other half for histological analysis), plucked terminal hairs (for two-dimensional epithelial cell model, aim 2) and blood cells (for three-dimensional skin model, aim 2); from sporadic HS cases saliva (for DNA extraction) is collected (Fig. 1).

Saliva is collected using the Oragene-DNA (Ottawa, Canada) kit, following the manufacturer's protocols, and stored at room temperature.

Skin biopsies are taken from lesional regions of HS patients. One half of the biopsy is placed directly in RNAlater (Qiagen, Hilden, Germany) and stored at − 20 °C; the other half of the biopsy is embedded in paraffin and maintained at room temperature.

Plucked terminal hairs in anagen phase are placed immediately in DMEM low calcium (Gibco, Thermo Fisher Scientific) with 1X gentamicin/amphotericin (Gibco, Thermo Fisher Scientific). Hairs can be stored at room temperature and can be processed up to three days after isolation.

B and T cell populations are analyzed by flow cytometry from fresh blood samples. Peripheral blood mononuclear cells (PBMCs) are stored in nitrogen and are used either as a source of monocytes (see 3D skin models) or in functional assessment of T cell responses.

Genetic analyses. DNA is extracted from saliva using the Oragene-DNA (Ottawa, Canada) kit following the manufacturer's protocols.
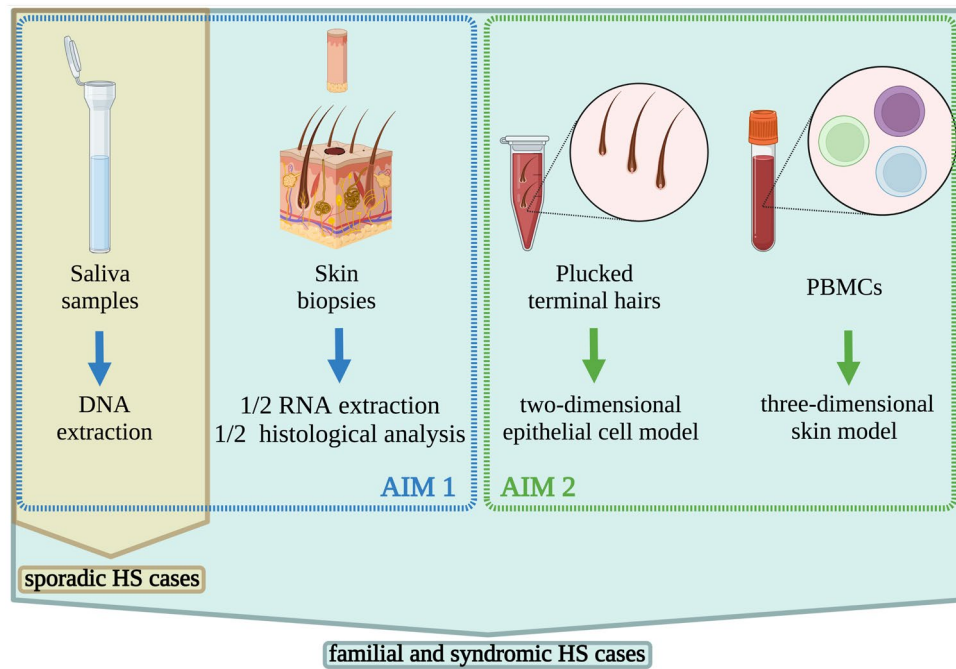
Figure 1. Schematic representation of samples collection. From familial and syndromic HS cases are collected: saliva for DNA extraction (AIM1), skin punch biopsies (AIM1) half for RNA extraction and other half for histological analysis, plucked terminal hairs (AIM2) for two-dimensional epithelial cell model, and blood cells (AIM2) for three-dimensional skin model; from sporadic HS cases saliva is collected.

Single nucleotide polymorphisms (SNPs) arrays, using the Illumina Infinium® Global Screening Array-24 v1.0 Kit, is performed on all recruited HS patients in order to identify:

1. Disease-shared genomic regions, comparing patients with healthy controls;
2. Disease severity, comparing patients stratified based on Hurley score;
3. Novel loci associated with successful response to anti-TNF treatment, comparing HS responders with non-responders based on HiSCR.

Moreover, all HS syndromic cases and selected HS familial cases, the most distant familiar HS cases (i.e. proband vs. cousin or vs. nephew), are further investigated by Whole Exome Sequencing (WES) searching for novel candidate genes/mutations. WES with 100X of expected coverage is performed in outsourcing by Macrogen (Seoul, Korea).

Transcriptome analyses. RNA is extracted from one half of skin biopsy with the RNeasy Lipid Tissue kit (Qiagen, Hilden, Germany) using TissueLyser II (Qiagen, Hilden, Germany), following the manufacturer's protocols. Transcriptome analysis is performed with RNA sequencing (RNAseq), in outsourcing by Macrogen (Seoul, Korea), in order to identify DEGs and alterations in biological molecular pathways, to confirm the genetic variations identified with WES.

Genomic and transcriptomics data integration. Single-omics datasets, such as genomic and transcriptomic, could fail to fully untangle the complexity of a disease, so HS can be better understood by integrating the multi-omics datasets. In detail, omics data integration will allow a broad characterization of the molecular mechanisms, an identification of key molecular pathways involved in HS susceptibility, onset, clinical course and severity. For this purpose, we have developed the PlatOMICs, a platform capable of automatically deciphering the information derived from the public repositories as well as from the scientific literature interpreting and integrating with the findings obtained by omics analysis in HS patients[40].

Skin histology and integrated OMICs data validation. The other half of skin biopsy is used to perform conventional histological analysis as well immunohistochemistry aimed at validating the genetic and transcriptomic data and to identify any variation in expression and localization of particular proteins.

Aim 2: Design in vitro two-dimensional epithelial cell and tri-dimensional skin models to unveil the molecular mechanisms occurring in HS pathogenesis

Two-dimensional epithelial cell model. Recently, apocrine sweat gland involvement in HS has been discarded. Neither differences in apocrine sweat gland size and density or in its morphology have been observed in HS patients. Infundibular plugging of the folliculosebaceous apocrine apparatus, on the other hand, has been observed in the early phase of the disease[41,42].

More recently, Dunstan et al. observed hyperplasia of the infundibular ORS, early "tendril" formation, and keratin plugging with infundibular dilatation in punch biopsies and excisional skins from 65 HS patients[43]. Interestingly, in fully developed lesions, cells expressing outer root sheath (ORS) markers, such as KRT17, 19 and nestin are capable of proliferating and infiltrating the dermis then differentiating in corneocyte (expressing KRT10), and form "cysts" filled with antigenic keratin. Dunstan et al. also identified KRT15, 19 and nestin positive cells in the tendrils thus showing that ORS cells are capable of an uncontrolled proliferation and invasiveness becoming corneocytes (KRT10+) or going back to the multipotency. This finding was corroborated by scRNA-seq performed earlier by Marohn et al.[44] The results from the scRNA-seq analysis revealed that cells forming tendrils shared common transcripts with the cells of infundibulum/sweat duct, therefore expressing high levels of genes specific for sweat and sebaceous glands, albeit their morphology and differentiation program resembled interfollicular keratinocytes.

Loss of hair follicle stem cells identity is a peculiar characteristic of HS, and it seems to be independent to the disease's varied inflammatory response that may be initiated by chemokines and cytokines expressed by cells in the tendrils and fueled by keratin spilled from the final cysts[43,44].

These findings imply that ORS cells could be the main culprit in HS. Two-dimensional ORS cultures have been already used to show an increased expression of inflammatory cytokines and chemokines in HS patients and decreased expression of the constitutive antimicrobial peptide beta defensin-1 (hBD-1)[45]. Transcriptome analysis of ORS cells, isolated from 6 HS patients and cultured in a defined medium, showed a differential expression of genes involved in cell proliferation and differentiation, and an upregulation of the DNA damage response and cell cycle G2/M checkpoint pathways in HS[46].

The main question here addressed is: how far can we go in personalizing HS patients' follow-up by using their biological material (i.e. ORS cells)? What are the advantages of designing personalized treatment based on cells from patients? What are the limitations (if any) or advantages related to ORS differentiation for each patient?

ORS cells present a non-invasive and autologous source of stem cells. Thus a model aiming to unveil the HS molecular mechanisms leading to the disorder should incorporate these cells as main actors. Isolating cells from a patient suffering from HS and comparing their properties with cells from a healthy control may be useful to characterize HS genetics (both at genome and transcriptome levels) and protein profiles. This could provide a solution in identifying new elements involved in this skin pathologic condition.

Two-dimensional collection and culture of ORS from HS patients have some major advantages. First, ORS bring us one step closer to a model organism to study the disease, and they are relatively easy to manipulate. Second, in contrast to blood cells and skin fibroblast, the latter requiring invasive extraction methods, ORS represent an easily accessible cell type thus providing an opportunity for patients to collect and send their own hair samples to the laboratory. This is important for HS patients who are eager to participate in HS research, but fell off from clinical follow-up as they were discouraged for absence of improvement in their condition. Third, ORS is very resourceful in terms of in vitro cultivation. It harbours a heterogeneous cell pool, including stem cells mainly present in the bulge area[47]. ORS can be isolated from hair follicles even after 5 days from hair plucking, allowing the time for transporting the cells from the clinical center to the laboratory just sending the cells conserved in appropriate medium by express courier. Remarkably, during the pandemics the possibility for the clinicians to send the ORS to the specialized laboratory by courier, allowed the continuity of the research.

Finally, ORS cells isolation doesn't need a long enzymatic digestion, commonly applied in skin samples in order to loosen the tissue around the follicles prior to dissection, which may damage the cells.

Some drawbacks in using ORS cells technique may also be observed. This technique is time consuming and an expensive method for cell isolation and amplification. In addition, primary cells may reach senescence and differentiation after 5–8 passages, which restrains its utilization for precision medicine.

In the BATMAN project ORS cells isolated from patients are being used to unveil the HS molecular mechanisms and to identify biological pathways affected by the disease thus helping in identifying novel genes associated with disease susceptibility. ORS cells present a non-invasive and endless autologous source of stem cells. Isolating cells from a patient suffering from HS and comparing their properties with cells from a healthy control may be useful to characterize HS genetic and protein profiles. This could present a solution in identifying new elements involved in the skin pathologic condition. Since HS phenotypes vary between patients, ORS cells should be ideally isolated from each patient willing to participate in the project. However, for this project we have chosen to collect hairs from familial and syndromic HS patients for whom WES has already been performed to identify and/or confirm a candidate genetic variant associated with the disease.

RNA sequencing of low passage ORS cells cultured in defined media can serve to identify DEGs that will be clustered in pathways and assembled with genetic findings by using AI tools.

Finally, it should be said that nowadays the ORS study approach is for research use only, and still far from being applied in the routine patients' follow-up due to the limitations mentioned above.

Three-dimensional skin models. Human models that accurately reproduce HS in vitro would represent a substantial asset for investigations on physiopathology, drug screening and personalized medicine approaches[48]. Ex vivo culture of patients' skin explants replicates known characteristics of the disease, and incubation with different HS-targeting drugs yielded responses that were consistent with clinical trial results[49,50]. Lesional skin

6
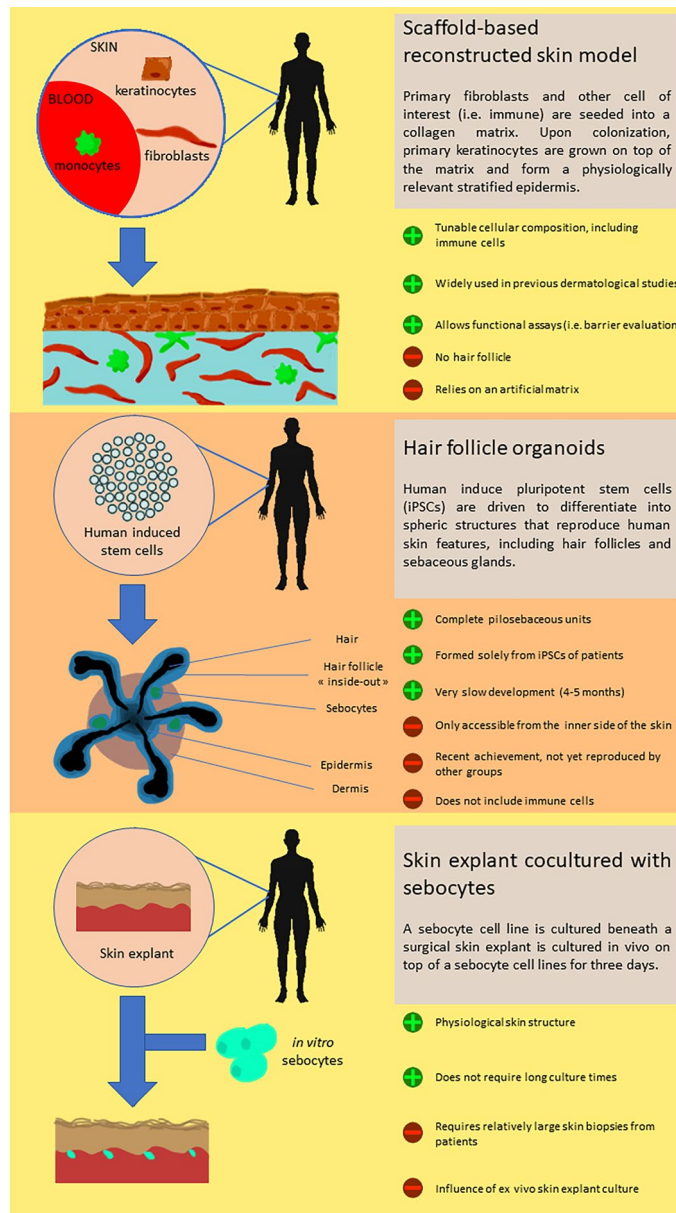
Figure 2. Representation of the three types of 3D skin models relevant for HS studies. The scaffold-based reconstructed skin model, the hair follicle organoids and the skin explant cocultured with sebocytes.

may be obtained upon surgical excision, which remains frequent for HS patients. Nevertheless, such samples are difficult to maintain in sterile culture conditions because they are highly septic. Collecting non-lesional skin biopsies may pose ethical issues if they are of a sufficient size to allow ex vivo assays. Therefore, there is a need for alternative models that could be grown from a limited amount of patients' cells.

Reconstructed skin models have evolved from tissue engineering methods, which initially aimed at reproducing a functional organ in vitro with the goal of transplanting it to compensate for a deficiency. For the skin, it started from the production of epidermal grafts for patients suffering extensive burns wounds. More recently, protocols using genetically modified keratinocytes have been implemented to correct genetic insufficiencies that dramatically alter the skin barrier function[51]. In parallel, similar culture techniques have been applied to generate in vitro models, and these tissue reconstructions are now often employed in research and in biosafety evaluations. Here, we will present different forms of 3D skin models (Fig. 2) and discuss the relevant features to resolve poorly understood aspects of HS pathogenesis.

As an interface organ, the organization of the skin is composed to create a physical barrier protecting against harmful substances and pathogens. The ultrastructure of the epidermal compartment can be convincingly reproduced by keratinocytes alone, which spontaneously stratify when cultured at the air–liquid interface. Commercially available healthy epidermis models (i.e. Episkin) can be challenged by chemical substances. This technique also led to building models from keratinocytes of atopic dermatitis patients[52]. In the context of HS, hair follicle

rupture and the subsequent dermal invasion by proinflammatory molecules and microorganisms might result from impairment of the barrier function. Even in the absence of a hair follicle, this fragility or increased permeability could be advantageously tested in an epidermal model constructed from HS patients with genetic defects suspected to alter the cohesion between keratinocytes. Moreover, gamma-secretase deficiencies associated with HS cases are expected to impact keratinocyte growth and might lead to aberrant epidermal formations when cultured in vitro. Complementing this approach by CRISPR/Cas9 genetic engineering would be an important tool to assess the effect of genetic alterations introduced in healthy cells. Conversely, if abnormal epidermal structure is observed with patient cells bearing a polymorphism of interest, CRISPR/Cas9 could be used to correct the mutation and determine how important it was in the anomaly.

By including a dermal compartment based on an artificial matrix, full-thickness skin models have an extended potential to reproduce more complex functions, i.e. innervation, vascularization or immunocompetence. In particular, immune barrier function of the skin requires a dense network of mononuclear phagocytes, which prevent pathogen invasion either by direct elimination (innate immunity) or by enabling the effector function of T and B cells (adaptive immunity). These sentinels comprise Langerhans cells (LCs) in the epidermis and different subsets of dendritic cells (DCs) and macrophages in the dermis[53]. To reproduce the key function of immunocompetence, several skin models integrate DCs, LCs or macrophages differentiated from hematopoietic stem cells of umbilical cord blood or peripheral blood monocytes[54,55]. Indeed, at least part of HS pathogenesis might be due to the patient's exacerbated potential to perpetuate inflammation in the skin, following a microbial challenge. This could be conveniently investigated in an immunocompetent 3D model, in which immune cells would be in a physiologically relevant position to interact with their neighbours, possibly leading to a self-fueling inflammation. The outcome of such experiments could be compared with the signature of surgically removed HS lesions by multiparameter analysis, i.e. single-cell transcriptomics. Unfortunately, neutrophils, which typically infiltrate HS lesions, remain very difficult to maintain ex vivo and therefore cannot be introduced in a skin model. Yet, one could expect to detect a strong expression of chemokines that attract neutrophils in a relevant HS skin model. Finally, the cutaneous environment (cellular contacts, soluble factors, microbiome) shapes the capacity of DCs to direct adaptive immune responses. In a skin model including monocyte-derived DCs from HS patients, we could evaluate their potential to bias T-cell differentiation towards Th17-dominated responses typical of this disease.

Despite constant efforts to ameliorate their complexity and physiological relevance, tissue-engineered skin models retain a major shortcoming so far: the absence of skin appendages. Notably, hair follicles are believed to play a central role in HS pathogenesis. They are located at the dermo-epidermal interface, constitute a dense epidermal niche, and their cyclic renewal must be tightly regulated to avoid structural dysfunction such as occlusion or rupture. Recently, a novel culture method has been able to produce skin organoids harbouring structurally relevant hair follicles[56]. This was done in the absence of a solid culture scaffold and relied on the self-organization capacity of precursor cells. Although constructing this model entails a long and complex procedure and still represents a challenge, yet this important innovation is likely to be included as a tool to study hair follicle-based diseases in the near future. Finally, these organoids expand from a limited number of easily accessible hair follicle stem cells which differentiate into a large variety of cell types. Therefore, enzymatically dissociated hair follicle organoids may represent a reliable source of keratinocytes and fibroblasts, which are obtained from invasive biopsies.

In the context of HS, another crucial part of the pilosebaceous unit is the sebaceous gland. Anomalies in this appendage are believed to play in follicular obstruction and dysbiosis. The influence of sebaceous glands can be mimicked in vitro by coculturing healthy skin explants with a sebocyte cell line[57]. This model has been recently applied to HS skin reconstruction, using patient cells[58]. Interestingly, the company Labskin Creations (Lyon, France) proposes a tissue-engineered model integrating hIPSC-derived sebocytes, which assemble as structurally relevant sebaceous glands in the dermal compartment (https://www.labskincreations.com/SeboSkin.aspx).

Aim 2: Methods

In vitro two-dimensional epithelial cell model. ORS cells isolated from plucked hairs are amplified and maintained following the protocol described by Rheinwald and Green in presence of feeder cells 3T3-J2 (kindly donated by Dr. Y. Barrandon) (Fig. 3)[59]. Cells are further expanded in a defined medium and we have had consistent results with EpilifeTM (ThermoFisher Scientific,Villebon-sur-Yvette, France), CNT-07 (CELLnTEC, Bern, Switzerland) and DermaCult™ Keratinocyte Expansion Medium (StemCell Technologies, Saint Égrève, France). After amplification cells are stored at − 150 °C for further use.

Cells with novel candidate mutations or with a mutation in genes already associated with HS are used to obtain Induced Pluripotent Stem Cells (iPSCs) (Fig. 3). Cells are reprogrammed using the CytoTune iPS 2.1 Sendai Reprogramming kit (ThermoFisher Scientific) with two different ratios of Sendai virus particles containing Yamanaka factors. Six to seven days after infection, cells are plated in 100-mm culture plates treated with gelatin and pre-seeded with irradiated Mouse Embryonic Fibroblasts (MEFs). iPSCs colonies are picked manually, subcloned, cultured and characterized following published protocols. Karyotyping of iPSC clones is performed by SNPs-microarray analysis and genetic mutation confirmed by Sanger sequencing.

Three-dimensional full-thickness skin model. iPSCs derived from ORS of HS patients are used to differentiate keratinocytes and fibroblasts. The cells incorporated in control models are obtained from healthy skin donors or from iPSCs with CRISPR/Cas9-corrected genetic variants. Innate immune sentinels, i.e. macrophages, dendritic cells and Langerhans cells, are derived in vitro from monocytes of healthy donors or HS patients. Fibroblasts and immune cells are sequentially introduced into a collagen-chitosan matrix, mimicking the dermal compartment. Then, keratinocytes are seeded on top of the matrix and allowed to differentiate into an epidermis
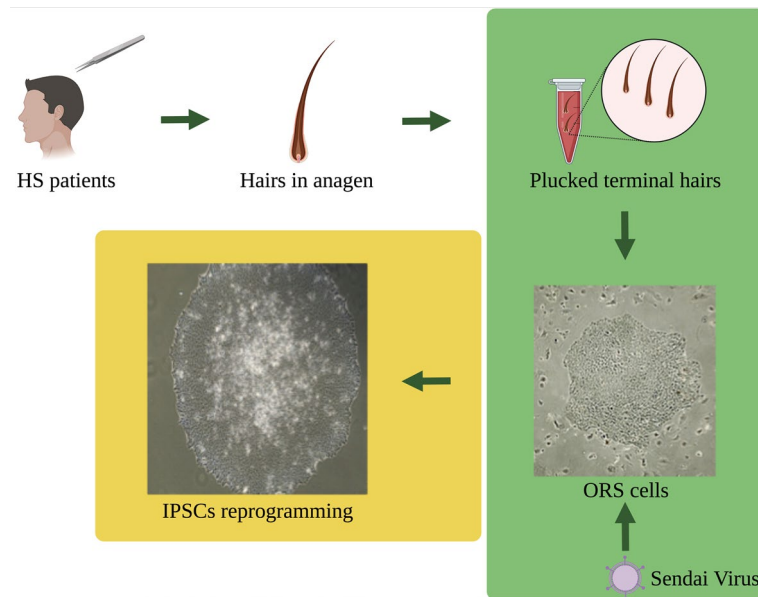
Figure 3. Schematic representation of hairs collection, ORS isolation and IPSCs reprogramming. Pluked termial hairs in anagen phase are collected from familial and syndromic HS cases. ORS cells isolated from plucker hair are aplificated and reprogrammated using Sendai virus to obtain Induced Pluripotent Stem Cells (iPSCs).

upon exposure to air–liquid interface. The resulting models are analyzed by immunohistochemistry, ELISA and flow cytometry.

Aim 3: Produce holistic health records (HHR) to complement medical observations by developing a smartphone application

The use of smartphone applications related to health has expanded substantially over the past decade, with smartphones being daily companions for a majority of the population. While most commonly-known health-related applications focus on aspects such as exercise ("fitness trackers") or nutrition, independent of involvement of a medical doctor, there is also a segment of application that has found its use in the clinical practice. In the field of dermatology, a recent review grouped the applications according to their functions as teledermatology, self-surveillance/diagnosis, disease guide, and general dermatology reference[59]. Considering the teledermatology applications, one approach uses a live consultation with a dermatologist, while the other one requires the patient to take a photo with the smartphone and send it to a server for a dermatologist to review later. Some of these applications are supported by national or other insurance plans[60].

Self-surveillance/diagnosis apps often harness the processing power of a smartphone in combination to its plethora of sensors. In dermatology, the most useful sensor is clearly the phone camera. Image recognition algorithms have been employed to detect and monitor skin cancer, and the applications run either automatically or in association with a dermatologist[61].

There is ongoing research on algorithms that are able to distinguish between different skin diseases. Pangti et al. developed a deep-learning method that was able to distinguish between 40 common conditions[62]. The study included hidradenitis suppurativa, where the algorithm achieved about 80% sensitivity and almost a 100% specificity in a cross-validation experiment.

The advantage of the self-surveillance/diagnosis approaches is their ability to provide the patient the information fast, without the need to visit a dermatologist. However, this is also a major shortcoming, since the algorithms have various degrees of accuracy in detection or classification, and furthermore can be biased based on the dataset that was used to train them. Coupled with the abundance of misinformation and unvetted applications, this calls for a very cautious handling of such applications, which should ideally only be used together with a professional medical counsel. As patients are typically not equipped to critically assess and evaluate the information found online, the doctors should work with them to educate them and to inform them where to find appropriate resources[60].

There are several online resources that provide dermatological information. For example, the Dermatology Atlas (https://play.google.com/store/apps/details?id=com.andromo.dev706301.app782141) and VisualDx (https://apps.apple.com/us/app/visualdx/id348177521) are applications that contain extensive collections of photographs of different conditions and are useful resources for both medical students and practicing doctors. Resources for patients are also available in different forms and typically also in the patient's language. An example is the Italian platform https://lapellesicura.it that offers information about several dermatological conditions, including HS.
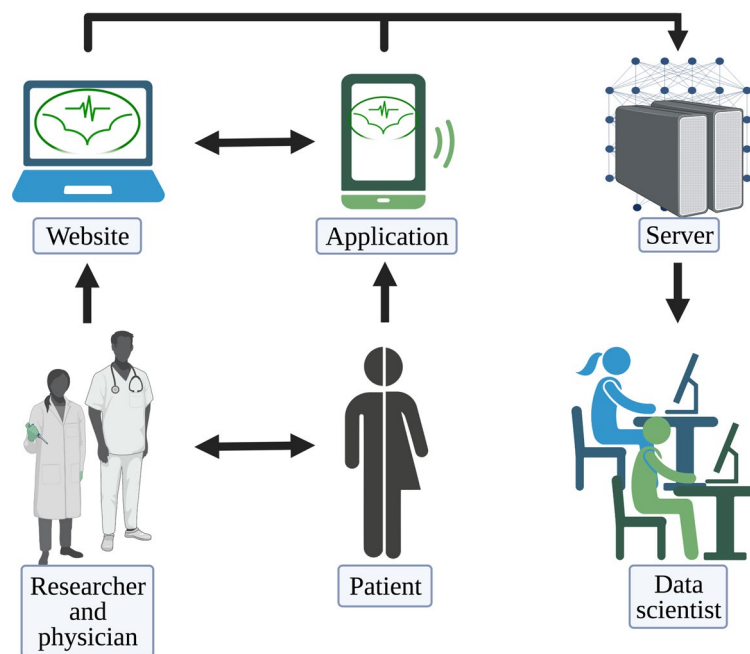
Figure 4. Schematic representation of AIM3. The interactions beetween physicians, patients and data scientists with the platform.

In the BATMAN project, a smartphone application (https://play.google.com/store/apps/details?id=si.ijs.batman&hl=en) and a web-based platform (https://batman-project.eu/) for research purposes were used, to collect patient data, in order to build a holistic picture of patients with Hidradenitis suppurativa.

It has been previously demonstrated that it is beneficial to look at the HS patients from different viewpoints: medical, functional genetic, and lifestyle. All three to some degree influence the occurrence and the severity of the medical condition, therefore it is beneficial for a doctor to have a look at the complete data, e.g. holistic data. For this purpose, we developed a web platform for doctors and patients, coupled to a smartphone application for the patients that allows us to obtain all three types of data (Fig. 4).

Aim 3: Methods

Medical data is obtained in the form of a standard electronic health record (EHR) and is uploaded into the platform by the physician, using a unique patient identifier. Genetic data, likewise, comes in a standard format and is uploaded using the same identifier.

Lifestyle data is collected in real time from the patients through a dedicated smartphone application, and is of two types. Self-reported data is obtained using questionnaires that the patient fills in when prompted. In the food preferences questionnaire, the patients report their dietary preferences, namely how often they eat certain types of food. This form is filled in by the patient only once in the study as it is expected that the preferences are unlikely to change during the duration of the pilot. Additional questions, that are asked only once, related to the alcohol consumption and smoking habits, whether they like to exercise in a company, and the daily hours of sleep. On the other hand, there are two questionnaires that the patient may be asked by the doctor to fill in on several occasions, to track the development of the medical condition. These are the Dermatological Quality of Life (DQoL) questionnaire and the Major Depression Inventory (MDI).

In addition to the self-reported data, the smartphone application records physical activity of the patient, which is done using a step counter plug-in. Physical activity is on one hand important as a way to cope with the HS and on the other hand, it can be used as a proxy by the doctor to see how severe the medical condition that the patient is currently experiencing is. Namely, as HS involves the lesions developing in the intertriginous body areas, pain is one of the most important problems; the patient will feel pain while moving, thus will likely rest more. Conversely, an increase in a patient's movement on a daily basis likely corresponds to a decrease in pain intensity and an improvement in HS and in the quality of life.

The communication between the smartphone and the platform takes place through a secure protocol. The doctor issues the patient a unique username and the password and the application only sends the answers to the questionnaires and aggregated daily activity data, ensuring that no additional information that could be used to identify the patient from that data (such as the IPs or location data) is shared with the platform. Since the study is carried out in the EU, a special care was paid to assure that all steps are GDPR-compliant[63]. The data used for analysis is thus anonymized, stripped of any possible personal identifiers—the medical doctor is the only person who knows the identity of their patients.

Future work could include adding supplementary information to the HHR. In studies of support groups on Facebook, Lombardo et al.[64,65] took advantage of the users' posts and comments to extract information about emotional states and social interactions. They also studied the correlations of emotional states with the time of the day or season of the year. Such automated emotion recognition is beneficial as it reduces the need for questionnaires, although the implementation of such type of patient monitoring is complicated due to privacy concerns. On the other hand, monitoring of stress using a wristband has already been explored[66]. A wristband as an activity-monitoring device has further advantages when compared to a smartphone, as the user can wear it all the time, even at night, and can record physiological data such as heart rate and sweating. The choice of the smartphone as patients' device to collect data, instead of the wristband is related to the need of using the most available tool (the vast majority of people do possess a smartphone); a wristband could be then provided to HS patients in the future, this wristband will be also linked to the smartphone to allow real-time communication between patients and the physicians.

Conclusions

As examples of BATMAN bench to patients' application of genetic analysis, based on integrated WES, we have been able to identify the biologic pathways associated with syndromic HS in patients from the IRCCS Ca' Granda Ospedale Maggiore Policlinico of Milan[67]. We identified genetic variants impairing the Vitamin D (calciferol) metabolism in HS patients[68]. Based on our findings the dermatologists started to administer Vitamin D to the patients, with a significant improvement of the skin conditions, thus ameliorating their quality of life. We also developed the PlatOMICs, a novel IT- based in house tool for OMICs integrated analysis, basically genomics and transcriptomics, in the context of skin diseases[40]; our PlatOMICs platform allows users, to integrate and re-analyze OMICs information, looking more in deep the molecular actors playing a role in the pathogenesis of HS and its syndromic forms. By analyzing the WES of 10 Unrelated Patients with Syndromic HS, we further concluded that syndromic HS can be considered as a polygenic autoinflammatory condition[15].

In addition to all of this, we must consider that the platform is built in a way that it allows for future extensions. For example, monitoring the daily activity of the patient can give the doctor direct feedback on how effective the current treatment is, and the DQoL and MDI questionnaires provide direct insight into the patient's mood. Using an in-app messaging function, the doctor can then send the patient's advice.

The BATMAN project is an European project with impact on the national health systems; our consortium is seeking to prompt interventions aimed at supporting HS patients, with particular attention to women and adolescents, promoting not only clinical or diagnostic actions but also support (i.e. psychological) for a better inclusion of HS patients in the social context, thus ameliorating their quality of life.

This project aims at providing early diagnosis and personalized clinical follow-up for HS patients by identifying novel biomarkers. We surmise that through genetic profiling and continuous monitoring of well-being using a dedicated application and platform, we can also propose novel stratification methods that clinicians can use to assess HS severity, choose the therapy and follow the outcome. Research on in vitro two-dimensional cell and tri-dimensional skin models support preclinical findings by validating genetic variants' role in HS and by generating novel models to understand pathophysiology allowing the exploration of different therapeutic approaches.

Data availability

Supporting data is available at SRA: https://www.ncbi.nlm.nih.gov/sra/PRJNA801118.

References

1. Saunte, D. M. et al. Diagnostic delay in Hidradenitis suppurativa is a global problem. Br. J. Dermatol 173, 1546–1549. https://doi.org/10.1111/bjd.14038 (2015).
2. Jemec, G. B. Clinical practice Hidradenitis suppurativa. N. Engl. J. Med. 366, 158–164. https://doi.org/10.1056/NEJMcp1014163 (2012).
3. Zouboulis, C. C. et al. Hidradenitis suppurativa/acne inversa: Criteria for diagnosis, severity assessment classification and disease evaluation. Dermatology 231, 184–190. https://doi.org/10.1159/000431175 (2015).
4. Zouboulis, C. C. et al. What causes Hidradenitis suppurativa? 15 years after. Exp. Dermatol. 29, 1154–1170. https://doi.org/10.1111/exd.14214 (2020).
5. Nikolakis, G. et al. Pathogenesis of Hidradenitis suppurativa/acne inversa. Hautarzt 72, 658–665. https://doi.org/10.1007/s00105-021-04853-x (2021).
6. Garcovich, S., Genovese, G., Moltrasio, C., Malvaso, D. & Marzano, A. V. PASH, PAPASH, PsAPASH, and PASS: The autoinflammatory syndromes of Hidradenitis suppurativa. Clin. Dermatol. 39, 240–247. https://doi.org/10.1016/j.clindermatol.2020.10.016 (2021).
7. Genovese, G., Moltrasio, C., Garcovich, S. & Marzano, A. V. PAPA spectrum disorders. G Ital Dermatol. Venereol. 155, 542–550. https://doi.org/10.23736/S0392-0488.20.06629-8 (2020).
8. Fitzsimmons, J. S., Guilbert, P. R. & Fitzsimmons, E. M. Evidence of genetic factors in Hidradenitis suppurativa. Br. J. Dermatol. 113, 1–8. https://doi.org/10.1111/j.1365-2133.1985.tb02037.x (1985).
9. Tricarico, P. M. et al. An integrated approach to unravel Hidradenitis suppurativa etiopathogenesis. Front. Immunol. 10, 892. https://doi.org/10.3389/fimmu.2019.00892 (2019).
10. Theut Riis, P. et al. Full exome sequencing of 11 families with Hidradenitis suppurativa. J. Eur. Acad. Dermatol. Venereol. 35, 1203–1211. https://doi.org/10.1111/jdv.17095 (2021).
11. van Straalen, K. R., Prens, E. P., Willemsen, G., Boomsma, D. I. & van der Zee, H. H. Contribution of genetics to the susceptibility to Hidradenitis suppurativa in a large cross-sectional Dutch twin cohort. JAMA Dermatol. 156, 1359–1362. https://doi.org/10.1001/jamadermatol.2020.3630 (2020).
12. Marzano, A. V. et al. Autoinflammation in pyoderma gangrenosum and its syndromic form (Pyoderma gangrenosum, acne and Suppurative hidradenitis). Br. J. Dermatol. 176, 1588–1598. https://doi.org/10.1111/bjd.15226 (2017).

nature portfolio 11

13. Giamarellos-Bourboulis, E. J. *et al.* High copy numbers of beta-defensin cluster on 8p231, confer genetic susceptibility, and modulate the physical course of Hidradenitis suppurativa/acne inversa. *J. Invest. Dermatol.* **136**, 1592–1598 (2016).

14. Higgins, R., Pink, A., Hunger, R., Yawalkar, N. & Navarini, A. A. Generalized comedones, acne, and Hidradenitis suppurativa in a patient with an FGFR2 missense mutation. *Front. Med. Lausanne* **4**, 16. https://doi.org/10.3389/fmed.2017.00016 (2017).

15. Marzano, A. V. *et al.* Whole-exome sequencing in 10 unrelated patients with syndromic Hidradenitis suppurativa: A preliminary step for a genotype-phenotype correlation. *Dermatology.* https://doi.org/10.1159/000521263 (2022).

16. Giatrakos, S. *et al.* Haplotypes of IL-12Rbeta1 impact on the clinical phenotype of Hidradenitis suppurativa. *Cytokine* **62**, 297–301. https://doi.org/10.1016/j.cyto.2013.03.008 (2013).

17. Jfri, A., Litvinov, I. V., Netchiporouk, E. & O'Brien, E. Novel variants of MEFV and NOD2 genes in familial hidradenitis suppurativa: A case report. *SAGE Open Med. Case Rep.* **8**, 2050313X20953113. https://doi.org/10.1177/2050313X20953113 (2020).

18. Kfoury, A., Virard, F., Renno, T. & Coste, I. Dual function of MyD88 in inflammation and oncogenesis: Implications for therapeutic intervention. *Curr. Opin. Oncol.* **26**, 86–91. https://doi.org/10.1097/CCO.0000000000000037 (2014).

19. Jfri, A. H., O'Brien, E. A., Litvinov, I. V., Alavi, A. & Netchiporouk, E. Hidradenitis suppurativa: Comprehensive review of predisposing genetic mutations and changes. *J. Cutan. Med. Surg.* **23**, 519–527. https://doi.org/10.1177/1203475419852049 (2019).

20. Garcovich, S. *et al.* Novel nicastrin mutation in Hidradenitis suppurativa-Dowling-Degos disease clinical phenotype: More than just clinical overlap?. *Br. J. Dermatol.* **183**, 758–759. https://doi.org/10.1111/bjd.19121 (2020).

21. Marzuillo, P. *et al.* Patients affected by dent disease 2 could be predisposed to Hidradenitis suppurativa. *J. Eur. Acad. Dermatol. Venereol.* **32**, e309–e311. https://doi.org/10.1111/jdv.14860 (2018).

22. Garcia-Gil, M. F. *et al.* A novel mutation in POFUT1 gene associated with Dowling-Degos disease and Hidradenitis suppurativa. *Int. J. Dermatol.* **60**, e25–e27. https://doi.org/10.1111/ijd.15092 (2021).

23. Haapasalo, A. & Kovacs, D. M. The many substrates of presenilin/gamma-secretase. *J. Alzheimers Dis.* **25**, 3–28. https://doi.org/10.3233/JAD-2011-101065 (2011).

24. Li, C. *et al.* PSENEN mutation carriers with co-manifestation of Acne Inversa (AI) and Dowling-Degos Disease (DDD): Is AI or DDD the Subphenotype?. *J. Invest. Dermatol.* **137**, 2234–2236. https://doi.org/10.1016/j.jid.2017.05.021 (2017).

25. Pavlovsky, M. *et al.* A phenotype combining Hidradenitis suppurativa with Dowling-Degos disease caused by a founder mutation in PSENEN. *Br. J. Dermatol.* **178**, 502–508. https://doi.org/10.1111/bjd.16000 (2018).

26. Marzano, A. V. *et al.* Pyogenic arthritis, pyoderma gangrenosum, acne, and hidradenitis suppurativa (PAPASH): A new autoinflammatory syndrome associated with a novel mutation of the PSTPIP1 gene. *JAMA Dermatol.* **149**, 762–764. https://doi.org/10.1001/jamadermatol.2013.2907 (2013).

27. Saito, N. *et al.* Novel PSTPIP1 gene mutation in Pyoderma gangrenosum, acne and Suppurative hidradenitis syndrome. *J. Dermatol.* **45**, e213–e214. https://doi.org/10.1111/1346-8138.14259 (2018).

28. Savva, A. *et al.* Impact of Toll-like receptor-4 and tumour necrosis factor gene polymorphisms in patients with Hidradenitis suppurativa. *Br. J. Dermatol.* **168**, 311–317. https://doi.org/10.1111/bjd.12105 (2013).

29. Liu, M. *et al.* A genetic variant in the BCL2 gene associates with adalimumab response in Hidradenitis suppurativa clinical trials and regulates expression of BCL2. *J. Invest. Dermatol.* **140**, 574-582.e572. https://doi.org/10.1016/j.jid.2019.06.152 (2020).

30. Liu, M. *et al.* Identification of HLA-DRB1 association to adalimumab immunogenicity. *PLoS ONE* **13**, e0195325. https://doi.org/10.1371/journal.pone.0195325 (2018).

31. Coates, M. *et al.* The skin transcriptome in Hidradenitis suppurativa uncovers an antimicrobial and sweat gland gene signature which has distinct overlap with wounded skin. *PLoS ONE* **14**, e0216249. https://doi.org/10.1371/journal.pone.0216249 (2019).

32. Mariottoni, P. *et al.* Single-Cell RNA sequencing reveals cellular and transcriptional changes associated with M1 macrophage polarization in Hidradenitis suppurativa. *Front. Med. (Lausanne)* **8**, 665873. https://doi.org/10.3389/fmed.2021.665873 (2021).

33. Revuz, J. E. & Jemec, G. B. Diagnosing Hidradenitis suppurativa. *Dermatol. Clin.* **34**, 1–5. https://doi.org/10.1016/j.det.2015.08.009 (2016).

34. van der Zee, H. H. & Jemec, G. B. New insights into the diagnosis of Hidradenitis suppurativa: Clinical presentations and phenotypes. *J. Am. Acad. Dermatol.* **73**, S23-26. https://doi.org/10.1016/j.jaad.2015.07.047 (2015).

35. Dudink, K. *et al.* Prevalence and clinical characteristics of Hidradenitis suppurativa phenotypes in a large dutch cohort. *Dermatology.* https://doi.org/10.1159/000518965 (2021).

36. Frew, J. W., Hawkes, J. E., Sullivan-Whalen, M., Gilleaudeau, P. & Krueger, J. G. Inter-rater reliability of phenotypes and exploratory genotype-phenotype analysis in inherited Hidradenitis suppurativa. *Br. J. Dermatol.* **181**, 566–571. https://doi.org/10.1111/bjd.17695 (2019).

37. Vural, S., Gundogdu, M., Kundakci, N. & Ruzicka, T. Familial mediterranean fever patients with Hidradenitis suppurativa. *Int. J. Dermatol.* **56**, 660–663. https://doi.org/10.1111/ijd.13503 (2017).

38. Seyed Jafari, S. M., Hunger, R. E. & Schlapbach, C. Hidradenitis suppurativa: Current understanding of pathogenic mechanisms and suggestion for treatment algorithm. *Front. Med. (Lausanne)* **7**, 68. https://doi.org/10.3389/fmed.2020.00068 (2020).

39. Zouboulis, C. C. *et al.* Development and validation of the International Hidradenitis suppurativa Severity Score System (IHS4), a novel dynamic scoring system to assess HS severity. *Br. J. Dermatol.* **177**, 1401–1409. https://doi.org/10.1111/bjd.15748 (2017).

40. Brandao, L. A. C. *et al.* Multiomics integration in skin diseases with alterations in notch signaling pathway: PlatOMICs phase 1 deployment. *Int. J. Mol. Sci.* https://doi.org/10.3390/ijms22041523 (2021).

41. von Laffert, M. *et al.* Hidradenitis suppurativa (acne inversa): Early inflammatory events at terminal follicles and at interfollicular epidermis. *Exp. Dermatol.* **19**, 533–537. https://doi.org/10.1111/j.1600-0625.2009.00915.x (2010).

42. von Laffert, M., Stadie, V., Ulrich, J., Marsch, W. C. & Wohlrab, J. Morphology of pilonidal sinus disease: Some evidence of its being a unilocalized type of Hidradenitis suppurativa. *Dermatology* **223**, 349–355. https://doi.org/10.1159/000335373 (2011).

43. Dunstan, R. W. *et al.* Histologic progression of acne inversa/hidradenitis suppurativa: Implications for future investigations and therapeutic intervention. *Exp. Dermatol.* **30**, 820–830. https://doi.org/10.1111/exd.14273 (2021).

44. Marohn, M. *et al.* Defining epidermal stem cell fate infidelity and immunogenicity in Hidradenitis suppurativa at the single-cell resolution. *bioRxiv* https://doi.org/10.1101/2020.04.21.053611 (2020).

45. Hotz, C. *et al.* Intrinsic defect in keratinocyte function leads to inflammation in Hidradenitis suppurativa. *J. Invest. Dermatol.* **136**, 1768–1780. https://doi.org/10.1016/j.jid.2016.04.036 (2016).

46. Orvain, C. *et al.* Hair follicle stem cell replication stress drives IFI16/STING-dependent inflammation in Hidradenitis suppurativa. *J. Clin. Invest.* **130**, 3777–3790. https://doi.org/10.1172/JCI131180 (2020).

47. Li, H. *et al.* The middle part of the plucked hair follicle outer root sheath is identified as an area rich in lineage-specific stem cell markers. *Biomolecules.* https://doi.org/10.3390/biom11020154 (2021).

48. Zouboulis, C. C. Ex vivo human models of Hidradenitis suppurativa/acne inversa for laboratory research and drug screening. *Br. J. Dermatol* **181**, 244–246. https://doi.org/10.1111/bjd.18173 (2019).

49. Sanchez, J. *et al.* Matrix remodelling and MMP expression/activation are associated with Hidradenitis suppurativa skin inflammation. *Exp. Dermatol.* **28**, 593–600. https://doi.org/10.1111/exd.13919 (2019).

50. Vossen, A., Ardon, C. B., van der Zee, H. H., Lubberts, E. & Prens, E. P. The anti-inflammatory potency of biologics targeting tumour necrosis factor-alpha, interleukin (IL)-17A, IL-12/23 and CD20 in Hidradenitis suppurativa: An ex vivo study. *Br. J. Dermatol.* **181**, 314–323. https://doi.org/10.1111/bjd.17641 (2019).

51. Jayarajan, V., Kounatidou, E., Qasim, W. & Di, W. L. Ex vivo gene modification therapy for genetic skin diseases-recent advances in gene modification technologies and delivery. *Exp. Dermatol.* **30**, 887–896. https://doi.org/10.1111/exd.14314 (2021).

nature portfolio 12

52. Blunder, S. *et al.* Alterations in epidermal eicosanoid metabolism contribute to inflammation and impaired late differentiation in FLG-mutated atopic dermatitis. *J. Invest. Dermatol.* **137**, 706–715. https://doi.org/10.1016/j.jid.2016.09.034 (2017).

53. Kabashima, K., Honda, T., Ginhoux, F. & Egawa, G. The immunological anatomy of the skin. *Nat. Rev. Immunol.* **19**, 19–30. https://doi.org/10.1038/s41577-018-0084-5 (2019).

54. Dezutter-Dambuyant, C. *et al.* Evolutive skin reconstructions: From the dermal collagen-glycosaminoglycan-chitosane substrate to an immunocompetent reconstructed skin. *Biomed. Mater. Eng.* **16**, S85-94 (2006).

55. Bechetoille, N., Andre, V., Valladeau, J., Perrier, E. & Dezutter-Dambuyant, C. Mixed Langerhans cell and interstitial/dermal dendritic cell subsets emanating from monocytes in Th2-mediated inflammatory conditions respond differently to proinflammatory stimuli. *J. Leukoc. Biol.* **80**, 45–58. https://doi.org/10.1189/jlb.0205109 (2006).

56. Lee, J. *et al.* Hair-bearing human skin generated entirely from pluripotent stem cells. *Nature* **582**, 399–404. https://doi.org/10.1038/s41586-020-2352-3 (2020).

57. Nikolakis, G. *et al.* Ex vivo human skin and SZ95 sebocytes exhibit a homoeostatic interaction in a novel coculture contact model. *Exp. Dermatol.* **24**, 497–502. https://doi.org/10.1111/exd.12712 (2015).

58. Hou, X. *et al.* 3D-seboskin model for human ex vivo studies of hidradenitis suppurativa/acne inversa. *Dermatology.* https://doi.org/10.1159/000515955 (2021).

59. Rheinwald, J. G. & Green, H. Epidermal growth factor and the multiplication of cultured human epidermal keratinocytes. *Nature* **265**, 421–424. https://doi.org/10.1038/265421a0 (1977).

60. Flaten, H. K., St Claire, C., Schlager, E., Dunnick, C. A. & Dellavalle, R. P. Growth of mobile applications in dermatology—2017 update. *Dermatol. Online J.* **24**, 1 (2018).

61. Kong, F. W., Horsham, C., Ngoo, A., Soyer, H. P. & Janda, M. Review of smartphone mobile applications for skin cancer detection: What are the changes in availability, functionality, and costs to users over time?. *Int. J. Dermatol.* **60**, 289–308. https://doi.org/10.1111/ijd.15132 (2021).

62. Pangti, R. *et al.* A machine learning-based, decision support, mobile phone application for diagnosis of common dermatological diseases. *J. Eur. Acad. Dermatol. Venereol.* **35**, 536–545. https://doi.org/10.1111/jdv.16967 (2021).

63. Gradišek, G. G. V. A. Data protection impact assessment case study for a research project using artificial intelligence on patient data. *Informatica* **44**, 383–391 (2020).

64. Lombardo, G., Fornacciari, P., Mordonini, M., Sani, L. & Tomaiuolo, M. A combined approach for the analysis of support groups on Facebook—The case of patients of Hidradenitis suppurativa. *Multimed. Tools Appl.* https://doi.org/10.1007/s11042-018-6512-5 (2019).

65. Lombardo, G. *et al.* Dynamics of emotions and relations in a facebook group of patients with Hidradenitis suppurativa. *Smart Objects Technol. Soc. Good* https://doi.org/10.1007/978-3-319-76111-4_27 (2017).

66. Gjoreski, M., Lustrek, M., Gams, M. & Gjoreski, H. Monitoring stress with a wrist device using context. *J. Biomed. Inform.* **73**, 159–170. https://doi.org/10.1016/j.jbi.2017.08.006 (2017).

67. Brandao, L. *et al.* Altered keratinization and vitamin D metabolism may be key pathogenetic pathways in syndromic Hidradenitis suppurativa: A novel whole exome sequencing approach. *J. Dermatol. Sci.* **99**, 17–22. https://doi.org/10.1016/j.jdermsci.2020.05.004 (2020).

68. Moltrasio, C. *et al.* 25-Hydroxyvitamin D serum levels inversely correlate to disease severity and serum C-reactive protein levels in patients with Hidradenitis suppurativa. *J. Dermatol.* **48**, 715–717. https://doi.org/10.1111/1346-8138.15797 (2021).

Acknowledgements

Author contributions

A.V.M., E.v.S., M.S., P.T.M., S.C. and W.J. contributed to patients' clinical description, P.T.M., C.M., A.V.M. and S.C. contributed to AIM1; M.B., V.F. and W.B. contributed to AIM2; A.G. and M.G. contributed to AIM3; P.T.M., V.F. and W.B. generated images; P.M.T. and S.C. drafted and revised the manuscript. All authors have read the manuscript and agree to its content.

Competing interests

The authors declare no competing interests.

Additional information

Correspondence and requests for materials should be addressed to P.M.T.

Reprints and permissions information is available at www.nature.com/reprints.

Publisher's note Springer Nature remains neutral with regard to jurisdictional claims in published maps and institutional affiliations.

CONCLUSION

Hidradenitis suppurativa has been gaining increased interest over the last decade both from the research and medical communities, as it represents a challenging disease to tackle. Said disease touches around 40 million people worldwide with little treatment currently available, most oriented toward symptoms relief more than being a permanent cure. HS symptoms, pain, nodules and scarring on the skin surface, are hard to discern from other skin diseases until the later stages where disease progression becomes severe and patient quality of life drastically reduced. To face such a cunning and damaging foe for humanity, the BATMAN European consortium was raised: combining the specialized skills and modern methods of medical and research teams around Europe. As a part of BATMAN, we were first tasked with developing laboratory models of HS: one of the main barriers of studying HS lies in the lack of readily available research models, be it *in vitro* or *in vivo*. While several mice models are good candidates to explore some aspects of HS, no specific model able to replicate the key physiopathological of the disease exists currently. Later, our tasking expanded to include analyses from HS patient blood samples: As some recent cohort studies emerged on the immune response of HS and found several novel potential hallmarks that deserved investigation on the patients recruited via BATMAN-embedded teams.

We first worked using the previous collective experience acquired from reconstructed human skin using 3D scaffolds. The goal was to assess the feasibility of skin models using patient material, or conditions relevant to HS, uncovering defects in the reconstructed skin underlying the disease onset. The use of HaCaT cell line proved easier to handle for culture in comparison to normal human keratinocytes (NHK) or even outer root sheath (ORS) cells, who proved to be significantly more fragile in culture. HaCaT cells also proved capable of colonizing and growing in our 3D scaffolds. However, the highly proliferative and calcium-sensitive nature of HaCaT created some challenges in the 3D culture protocol. Instances of HaCaT cells over proliferating and not producing any coherent epithelium were noticed. It is unknown if the default protocol has an impact on HaCaT differentiation in 3D culture, where differentiation should be induced by contact with the air. The 3D scaffold themselves were extremely to handle. First produced matrices were all homemade, using a small lyophilizer to "rise" the chitin-collagen mix into matrices. This step produced unstandardized sponges, with variable mesh quality that affected cell colonization. The use of an industrial lyophilizer from the Aerial company solved this issue. Furthermore, the whole manufacturing process was performed in unsterile conditions. While ethanol treatment worked in most cases, contaminations were a constant trouble during the entire length of the experiments. Some trialed matrices variants, with a thinner or thicker chitin mesh, were also harder to colonize by epithelial cells, however this issue was quickly solved by standardizing on a single thickness. Overall, the scaffolds offered a decent support for skin 3D culture and can be relevant as an HS model: First, with the ability to seed immune cells inside and study patient immune system via the production of cytokines or the orientation of T cells. Epithelial cell proliferation is an acknowledged issue in HS and while we cannot yet grow a hair follicle on the matrices, they are enough to provide a support to study patient keratinocytes behavior. In the long term, it is even possible to imagine a personalized diagnostic tool using these matrices, if necessary.

We further explored the possibility of designing a mice model that could replicate some aspects of HS *in vivo*. We focused on the inflammatory aspect of HS, represented by a strong neutrophilic infiltrate around the hair follicles. Mice models already at hand allowed to specifically target the hair follicle using a tamoxifen-inducible Sox9-creERT2, which specifically affected the upper part of the hair follicle. Knocking-down the autophagy pathway in these mice via our Sox9-Atg5 model did not produce alterations of the hair follicle or the immune infiltrate recruited after stimulation. While Atg5 is an important actor of autophagy, redundancies exist to safeguard this vital process, and it isn't excluded the deletion was not enough to deter autophagic function. The use of an inhibitor of the γ-secretase proved more efficient at disrupting autophagy in the hair follicle subsets but not the interfollicular keratinocytes, although it did not specifically target the hair follicle. Autophagy impairment was one consequence of the γ-secretase mutations *in vitro*, an unexpected one, and has not yet been revealed in HS etiology. Disabling such an important enzyme most likely had further consequences on physiology beyond autophagy worth exploring, therefore further efforts should be focused on the γ-secretase itself instead.

Finally, we used flow cytometry to study the lymphocyte blood populations of HS patients. Starting from the fresh discovery of B cells and antibodies in HS patients, we focused on describing the different blood subsets of B and T cells. We first observed no abnormality in subset proportions compared to non-HS affected individuals. However, when focusing on CLA+ cells, expressed on more than 90% of skin-homing T lymphocytes, we spotted different tendencies between controls and patients. To further explore HS patient CLA T cells function, we tried several PMA-Ionomycin stimulation assays from unfrozen PBMCs and try to assess the cytokines they expressed. Furthermore, we confirmed B cells express CLA on their surface, and that skin B cells express CLA in a similar proportion than T cells. B cells also produced different proportions in familial cases, whereas sporadic cases were not affected. The segregation of patients from familial to sporadic is always subject to caution, as the only difference is the knowledge of familial history of HS. As the disease is known to be under diagnosed, the possibility of sporadic patients having a familial history remains, and only proper genotyping of the patient and their family members could resolve this issue. The use of the CLA marker should be encouraged for further studies about HS patient blood and can be easily expanded to B cells subsets. While we found little differences in the B cell subsets, we did not study the antibody they produced. In the wake of the discovery of autoantibodies in HS patients' skin, it would be relevant to investigate the antibodies found in the blood, their class, concentration, and their relation to CLA B cells.

In the long term we can see this corpus of data contributing further to the understanding of HS. First, future developments of the 3D skin culture models are expected to open the door to understanding minute differences characteristic of patient disease progression. This could speed up the screening of potential drugs aimed at alleviated or stopping the abnormal epithelial proliferation. In the context of an immunologically competent model, the fundamental and pharmaceutical research already possible on the epithelium can be extended to the immune reaction within HS. While the *in vitro* model offers

a fully human model, no complex disease can be well understood without *in vivo* approaches, especially because if related to hair follicles, a complex structure which, despite recent developments, remains difficult to mimic *in vitro*. To this day, no comprehensive mouse model of HS exists. Finally, the role and specificities of innate and adaptive immune reactions in HS remains unclear. Deciphering disease complexity from a simple blood sampling would significantly help clinicians confirm their diagnosis and orient their choice of therapy, a concept already put into practice in various auto-immune diseases. Sadly, blood markers of HS are not currently used in diagnosis, in part because of the local nature of the disease: being specific to certain regions of the skin, most markers will focus there and require a skin biopsy to properly confirm an HS diagnosis. Obviously, this is also due to a lack of critical knowledge to leverage blood markers related to HS. Altogether, we believe that future research on HS should rely on all these different approaches, to reach meaningful results which could be translatable to patients.

Bibliography

1. Dhouailly, D. A new scenario for the evolutionary origin of hair, feather, and avian scales. *J. Anat.* **214**, 587–606 (2009).

2. Gilbert, S. F. The Epidermis and the Origin of Cutaneous Structures. *Dev. Biol. 6th Ed.* (2000).

3. Santos, M. D. *et al.* Perlecan expression influences the keratin 15-positive cell population fate in the epidermis of aging skin. *Aging* **8**, 751–768 (2016).

4. Kaidbey, K. H., Agin, P. P., Sayre, R. M. & Kligman, A. M. Photoprotection by melanin—a comparison of black and Caucasian skin. *J. Am. Acad. Dermatol.* **1**, 249–260 (1979).

5. Szabo, G. The regional anatomy of the human integument with special reference to the distribution of hair follicles, sweat glands and melanocytes. *Philos. Trans. R. Soc. Lond. B. Biol. Sci.* **252**, 447–485 (1997).

6. Jupe, S. Melanin biosynthesis. *Reactome - Curated Knowledgebase Biol. Pathw.* **52**, (2015).

7. Ando, H. *et al.* Melanosomes are transferred from melanocytes to keratinocytes through the processes of packaging, release, uptake, and dispersion. *J. Invest. Dermatol.* **132**, 1222–1229 (2012).

8. Yousef, H., Alhajj, M. & Sharma, S. Anatomy, Skin (Integument), Epidermis. in *StatPearls* (StatPearls Publishing, 2022).

9. Stratum Granulosum and Stratum Corneum. http://medcell.org/histology/skin_lab/granulosum_and_corneum.php.

10. Simpson, C. L. *et al.* NIX initiates mitochondrial fragmentation via DRP1 to drive epidermal differentiation. *Cell Rep.* **34**, 108689 (2021).

11. Bianconi, E. *et al.* An estimation of the number of cells in the human body. *Ann. Hum. Biol.* **40**, 463–471 (2013).

12. Sender, R., Fuchs, S. & Milo, R. Revised Estimates for the Number of Human and Bacteria Cells in the Body. *PLoS Biol.* **14**, e1002533 (2016).

13.   Yoo, J. Y., Groer, M., Dutra, S. V. O., Sarkar, A. & McSkimming, D. I. Gut Microbiota and Immune System Interactions. *Microorganisms* **8**, 1587 (2020).

14.   Rowland, I. *et al.* Gut microbiota functions: metabolism of nutrients and other food components. *Eur. J. Nutr.* **57**, 1–24 (2018).

15.   Hoff, S., Oyoshi, M. K., Macpherson, A. & Geha, R. S. The microbiota is important for IL-17A expression and neutrophil infiltration in lesional skin of Flg(ft/ft) mice. *Clin. Immunol. Orlando Fla* **156**, 128–130 (2015).

16.   Li, H. *et al.* Mucosal or systemic microbiota exposures shape the B cell repertoire. *Nature* **584**, 274–278 (2020).

17.   Cogen, A. L., Nizet, V. & Gallo, R. L. Skin microbiota: a source of disease or defence? *Br. J. Dermatol.* **158**, 442–455 (2008).

18.   Holzer, P. & Farzi, A. Neuropeptides and the Microbiota-Gut-Brain Axis. *Adv. Exp. Med. Biol.* **817**, 195–219 (2014).

19.   Ríos-Covian, D., Langella, P. & Martín, R. From Short- to Long-Term Effects of C-Section Delivery on Microbiome Establishment and Host Health. *Microorganisms* **9**, 2122 (2021).

20.   Jacobson, A. *et al.* A gut commensal-produced metabolite mediates colonization resistance to Salmonella infection. *Cell Host Microbe* **24**, 296–307.e7 (2018).

21.   Swaney, M. H. & Kalan, L. R. Living in Your Skin: Microbes, Molecules, and Mechanisms. *Infect. Immun.* **89**, e00695-20 (2021).

22.   Bartolomaeus, H. *et al.* Short-Chain Fatty Acid Propionate Protects From Hypertensive Cardiovascular Damage. *Circulation* **139**, 1407–1421 (2019).

23.   Haghikia, A. *et al.* Propionate attenuates atherosclerosis by immune-dependent regulation of intestinal cholesterol metabolism. *Eur. Heart J.* **43**, 518–533 (2022).

24.   Serger, E. *et al.* The gut metabolite indole-3 propionate promotes nerve regeneration and repair. *Nature* **607**, 585–592 (2022).

25.   Kabashima, K., Honda, T., Ginhoux, F. & Egawa, G. The immunological anatomy of the skin. *Nat. Rev. Immunol.* **19**, 19–30 (2019).

26. Cordier-Dirikoc, S. *et al.* Dermal fibroblasts are the key sensors of aseptic skin inflammation through interleukin 1 release by lesioned keratinocytes. *Front. Immunol.* **13**, 984045 (2022).

27. Ferrer, R. A. *et al.* Dermal Fibroblasts Promote Alternative Macrophage Activation Improving Impaired Wound Healing. *J. Invest. Dermatol.* **137**, 941–950 (2017).

28. Stunova, A. & Vistejnova, L. Dermal fibroblasts—A heterogeneous population with regulatory function in wound healing. *Cytokine Growth Factor Rev.* **39**, 137–150 (2018).

29. Sorrell, J. M. & Caplan, A. I. Fibroblast heterogeneity: more than skin deep. *J. Cell Sci.* **117**, 667–675 (2004).

30. Marzvanyan, A. & Alhawaj, A. F. Physiology, Sensory Receptors. in *StatPearls* (StatPearls Publishing, 2022).

31. Henley, C. Touch: The Skin. (2021).

32. Jamora, C., DasGupta, R., Kocieniewski, P. & Fuchs, E. Links between signal transduction, transcription and adhesion in epithelial bud development. *Nature* **422**, 317–322 (2003).

33. Botchkarev, V. A. & Fessing, M. Y. Edar signaling in the control of hair follicle development. *J. Investig. Dermatol. Symp. Proc.* **10**, 247–251 (2005).

34. Tan, J. *et al.* The adaptive variant EDARV370A is associated with straight hair in East Asians. *Hum. Genet.* **132**, 1187–1191 (2013).

35. Kamberov, Y. G. *et al.* Modeling recent human evolution in mice by expression of a selected EDAR variant. *Cell* **152**, 691–702 (2013).

36. Eckhart, L. *et al.* Identification of reptilian genes encoding hair keratin-like proteins suggests a new scenario for the evolutionary origin of hair. *Proc. Natl. Acad. Sci.* **105**, 18419–18423 (2008).

37. Koch, S. L., Tridico, S. R., Bernard, B. A., Shriver, M. D. & Jablonski, N. G. The biology of human hair: A multidisciplinary review. *Am. J. Hum. Biol.* **32**, (2020).

38. Robbins, C. R. *Chemical and Physical Behavior of Human Hair*. (Springer New York, 1988). doi:10.1007/978-1-4757-2009-9.

39. Rogers, G. E. Known and Unknown Features of Hair Cuticle Structure: A Brief Review. *Cosmetics* **6**, 32 (2019).

40. Lenoir, M.-C., Bernard, B. A., Pautrat, G., Darmon, M. & Shroot, B. Outer root sheath cells of human hair follicle are able to regenerate a fully differentiated epidermis in vitro. *Dev. Biol.* **130**, 610–620 (1988).

41. Myung, P. & Ito, M. Dissecting the bulge in hair regeneration. *J. Clin. Invest.* **122**, 448–454 (2012).

42. Ohyama, M. Hair follicle bulge: A fascinating reservoir of epithelial stem cells. *J. Dermatol. Sci.* **46**, 81–89 (2007).

43. Cartron, M. L. *et al.* Bactericidal Activity of the Human Skin Fatty Acid cis-6-Hexadecanoic Acid on Staphylococcus aureus. *Antimicrob. Agents Chemother.* **58**, 3599–3609 (2014).

44. Kobayashi, T. *et al.* Homeostatic Control of Sebaceous Glands by Innate Lymphoid Cells Regulates Commensal Bacteria Equilibrium. *Cell* **176**, 982–997.e16 (2019).

45. Packer, L., Weber, S. U. & Thiele, J. J. Sebaceous Gland Secretion is a Major Physiologic Route of Vitamin E Delivery to Skin. *J. Invest. Dermatol.* **113**, 1006–1010 (1999).

46. Makrantonaki, E., Ganceviciene, R. & Zouboulis, C. An update on the role of the sebaceous gland in the pathogenesis of acne. *Dermatoendocrinol.* **3**, 41–49 (2011).

47. Lousada, M. B. *et al.* Exploring the human hair follicle microbiome*. *Br. J. Dermatol.* **184**, 802–815 (2021).

48. Ho, B. S.-Y. *et al.* Microbiome in the hair follicle of androgenetic alopecia patients. *PLOS ONE* **14**, e0216330 (2019).

49. Lacey, N., Russell-Hallinan, A., Zouboulis, C. C. & Powell, F. C. Demodex mites modulate sebocyte immune reaction: possible role in the pathogenesis of rosacea. *Br. J. Dermatol.* **179**, 420–430 (2018).

50. Beseris, E. A., Naleway, S. E. & Carrier, D. R. Impact Protection Potential of Mammalian Hair: Testing the Pugilism Hypothesis for the Evolution of Human Facial Hair. *Integr. Org. Biol.* **2**, obaa005 (2020).

51. Su, Y. & Richmond, A. Chemokine Regulation of Neutrophil Infiltration of Skin Wounds. *Adv. Wound Care* **4**, 631–640 (2015).

52. Summers, C. *et al.* Neutrophil kinetics in health and disease. *Trends Immunol.* **31**, 318–324 (2010).

53. Wang, J. *et al.* Visualizing the function and fate of neutrophils in sterile injury and repair. *Science* **358**, 111–116 (2017).

54. Segal, A. W. How Neutrophils Kill Microbes. *Annu. Rev. Immunol.* **23**, 197 (2005).

55. Lacy, P. Mechanisms of Degranulation in Neutrophils. *Allergy Asthma Clin. Immunol. Off. J. Can. Soc. Allergy Clin. Immunol.* **2**, 98–108 (2006).

56. Farnaud, S. & Evans, R. W. Lactoferrin—a multifunctional protein with antimicrobial properties. *Mol. Immunol.* **40**, 395–405 (2003).

57. Lee, H. S. & Kim, W. J. The Role of Matrix Metalloproteinase in Inflammation with a Focus on Infectious Diseases. *Int. J. Mol. Sci.* **23**, 10546 (2022).

58. Pearce, E. J. & Everts, B. Dendritic cell metabolism. *Nat. Rev. Immunol.* **15**, 18–29 (2015).

59. Kissenpfennig, A. & Malissen, B. Langerhans cells--revisiting the paradigm using genetically engineered mice. *Trends Immunol.* **27**, 132–139 (2006).

60. Doebel, T., Voisin, B. & Nagao, K. Langerhans Cells - The Macrophage in Dendritic Cell Clothing. *Trends Immunol.* **38**, 817–828 (2017).

61. Homey, B. *et al.* CCL27-CCR10 interactions regulate T cell-mediated skin inflammation. *Nat. Med.* **8**, 157–165 (2002).

62. Scholz, F. *et al.* Constitutive expression and regulated release of the transmembrane chemokine CXCL16 in human and murine skin. *J. Invest. Dermatol.* **127**, 1444–1455 (2007).

63.   Wang, Z.-S. *et al.* Prevalence of Acne Inversa (Hidradenitis Suppurativa) in China: A Nationwide Cross-Sectional Epidemiological Study. *Int. J. Dermatol. Venereol.* **5**, 1–7 (2022).

64.   Patterson, A. T., Tian, F. T., Elston, D. M. & Kaffenberger, B. H. Occluded Cigarette Smoke Exposure Causing Localized Chloracne-Like Comedones. *Dermatology* **231**, 322–325 (2015).

65.   Mintoff, D. *et al.* Obesity and Hidradenitis Suppurativa: Targeting meta-inflammation for therapeutic gain? *Clin. Exp. Dermatol.* llad182 (2023) doi:10.1093/ced/llad182.

66.   Cannistrà, C., Finocchi, V., Trivisonno, A. & Tambasco, D. New perspectives in the treatment of hidradenitis suppurativa: Surgery and brewer's yeast–exclusion diet. *Surgery* **154**, 1126–1130 (2013).

67.   Langan, E. A. *et al.* The Role of the Cutaneous Microbiome in Hidradenitis Suppurativa-Light at the End of the Microbiological Tunnel. *Int. J. Mol. Sci.* **21**, E1205 (2020).

68.   Williams, S. C., Frew, J. W. & Krueger, J. G. A systematic review and critical appraisal of metagenomic and culture studies in hidradenitis suppurativa. *Exp. Dermatol.* **30**, 1388–1397 (2021).

69.   Abirached, D. G. *et al.* COMITÉ DE LECTURE/RÉDACTION. (2018).

70.   B, H. *et al.* Hurley Staging Refined: A Proposal by the Dutch Hidradenitis Suppurativa Expert Group. *Acta Derm. Venereol.* **97**, (2017).

71.   Zouboulis, C. C. *et al.* Development and validation of the International Hidradenitis Suppurativa Severity Score System (IHS4), a novel dynamic scoring system to assess HS severity. *Br. J. Dermatol.* **177**, 1401–1409 (2017).

72.   Fougerousse, A.-C., Maccari, F., Guillem, P. & Reguiai, Z. Antibiotic Treatment for Hidradenitis Suppurativa in France: A Practice Survey. *Clin. Cosmet. Investig. Dermatol.* **Volume 15**, 2641–2645 (2022).

73.   Mendonça, C. O. & Griffiths, C. E. M. Clindamycin and rifampicin combination therapy for hidradenitis suppurativa. *Br. J. Dermatol.* **154**, 977–978 (2006).

74. Babbush, K. M., Andriano, T. M. & Cohen, S. R. Antiandrogen therapy in hidradenitis suppurativa: finasteride for females. *Clin. Exp. Dermatol.* **47**, 86–92 (2022).

75. Sakyanun, P., Vongvanichvathana, T. & Lertsanguansinchai, P. Radiation therapy in chronic hidradenitis suppurativa: case report. *Radiat. Oncol. J.* **40**, 79–85 (2022).

76. Zouboulis, C. C. *et al.* What causes hidradenitis suppurativa?—15 years after. *Exp. Dermatol.* **29**, 1154–1170 (2020).

77. Pink, A. E., Simpson, M. A., Desai, N., Trembath, R. C. & Barker, J. N. W. γ-Secretase Mutations in Hidradenitis Suppurativa: New Insights into Disease Pathogenesis. *J. Invest. Dermatol.* **133**, 601–607 (2013).

78. Duchatelet, S. *et al.* Low Prevalence of GSC Gene Mutations in a Large Cohort of Predominantly Caucasian Patients with Hidradenitis Suppurativa. *J. Invest. Dermatol.* **140**, 2085–2088.e14 (2020).

79. von der Werth, J. & Williams, H. The natural history of hidradenitis suppurativa. *J. Eur. Acad. Dermatol. Venereol.* **14**, 389–392 (2000).

80. Karagiannidis, I., Nikolakis, G., Sabat, R. & Zouboulis, C. C. Hidradenitis suppurativa/Acne inversa: an endocrine skin disorder? *Rev. Endocr. Metab. Disord.* **17**, 335–341 (2016).

81. Nisar, S. *et al.* Further Histological and Cellular Characterization of Hidradenitis Suppurativa in 11 Patients. **19**, 14.

82. van der Zee, H. H. *et al.* Alterations in leucocyte subsets and histomorphology in normal-appearing perilesional skin and early and chronic hidradenitis suppurativa lesions: HS histomorphology and leucocyte subsets. *Br. J. Dermatol.* **166**, 98–106 (2012).

83. Danby, F. W., Jemec, G. B. E., Marsch, W. Ch. & von Laffert, M. Preliminary findings suggest hidradenitis suppurativa may be due to defective follicular support: HS with defective follicular support. *Br. J. Dermatol.* **168**, 1034–1039 (2013).

84. Naik, H. B., Jo, J.-H., Paul, M. & Kong, H. H. Skin Microbiota Perturbations Are Distinct and Disease Severity-Dependent in Hidradenitis Suppurativa. *J. Invest. Dermatol.* **140,** 922-925.e3 (2020).

85. Dunstan, R. W. *et al.* Histologic progression of acne inversa/hidradenitis suppurativa: Implications for future investigations and therapeutic intervention. *Exp. Dermatol.* **30,** 820–830 (2021).

86. Orvain, C. *et al.* Hair follicle stem cell replication stress drives IFI16/STING-dependent inflammation in hidradenitis suppurativa. *J. Clin. Invest.* **130,** 3777–3790 (2020).

87. Holm Nielsen, S. *et al.* Biomarkers of Tissue Turnover and Systemic Inflammation Are Associated with Disease Severity and Activity in Patients with Hidradenitis Suppurativa. *J. Invest. Dermatol.* S0022202X22019054 (2022) doi:10.1016/j.jid.2022.08.049.

88. Byrd, A. S. *et al.* Neutrophil extracellular traps, B cells, and type I interferons contribute to immune dysregulation in hidradenitis suppurativa. *Sci. Transl. Med.* **11,** eaav5908 (2019).

89. Melnik, B. C., John, S. M., Chen, W. & Plewig, G. T helper 17 cell/regulatory T-cell imbalance in hidradenitis suppurativa/acne inversa: the link to hair follicle dissection, obesity, smoking and autoimmune comorbidities. *Br. J. Dermatol.* (2018) doi:10.1111/bjd.16561.

90. Narla, S. *et al.* Identifying key components and therapeutic targets of the immune system in hidradenitis suppurativa with an emphasis on neutrophils. *Br. J. Dermatol.* **184,** 1004–1013 (2021).

91. Carmona-Rivera, C. *et al.* Autoantibodies Present in Hidradenitis Suppurativa Correlate with Disease Severity and Promote the Release of Proinflammatory Cytokines in Macrophages. *J. Invest. Dermatol.* **142,** 924–935 (2022).

92. Gudjonsson, J. E. *et al.* Contribution of plasma cells and B cells to hidradenitis suppurativa pathogenesis. *JCI Insight* **5,** e139930 (2020).

93. Musilova, J. *et al.* Enrichment of Plasma Cells in the Peripheral Blood and Skin of Patients with Hidradenitis Suppurativa. *J. Invest. Dermatol.* **140**, 1091–1094.e2 (2020).

94. Witte-Händel, E. *et al.* The IL-1 Pathway Is Hyperactive in Hidradenitis Suppurativa and Contributes to Skin Infiltration and Destruction. *J. Invest. Dermatol.* **139**, 1294–1305 (2019).

95. Moran, B. *et al.* Hidradenitis Suppurativa Is Characterized by Dysregulation of the Th17:Treg Cell Axis, Which Is Corrected by Anti-TNF Therapy. *J. Invest. Dermatol.* **137**, 2389–2395 (2017).

96. Mitsdoerffer, M. *et al.* Proinflammatory T helper type 17 cells are effective B-cell helpers. *Proc. Natl. Acad. Sci. U. S. A.* **107**, 14292–14297 (2010).

97. Grand, D., Navrazhina, K. & Frew, J. W. Integrating complement into the molecular pathogenesis of Hidradenitis Suppurativa. *Exp. Dermatol.* **29**, 86–92 (2020).

98. Hoffman, L. K. *et al.* Integrating the skin and blood transcriptomes and serum proteome in hidradenitis suppurativa reveals complement dysregulation and a plasma cell signature. *PLOS ONE* **13**, e0203672 (2018).

99. Katz, Y., Nadiv, O., Rapoport, M. J. & Loos, M. IL-17 regulates gene expression and protein synthesis of the complement system, C3 and factor B, in skin fibroblasts. *Clin. Exp. Immunol.* **120**, 22–29 (2001).

100. Souwer, Y. *et al.* Human TH17 cell development requires processing of dendritic cell-derived CXCL8 by neutrophil elastase. *J. Allergy Clin. Immunol.* **141**, 2286-2289.e5 (2018).

101. Schwartzman, R. M. & Maguire, H. G. Staphylococcal Apocrine Gland Infections in the Dog (Canine Hidradenitis Suppurativa). *Br. Vet. J.* **125**, 121–127 (1969).

102. Tricarico, P. M. *et al.* Holistic health record for Hidradenitis suppurativa patients. *Sci. Rep.* **12**, 8415 (2022).

103. Quartey, Q. Q. *et al.* Lessons learned from the development of a hidradenitis suppurativa xenograft mouse model. *Clin. Exp. Dermatol.* **45**, 202–206 (2020).

104. Yang, J. *et al.* Keratin 5-Cre-driven deletion of Ncstn in an acne inversa-like mouse model leads to a markedly increased IL-36a and Sprr2 expression. *Front. Med.* **14**, 305–317 (2020).

105. Joost, S. *et al.* The Molecular Anatomy of Mouse Skin during Hair Growth and Rest. *Cell Stem Cell* **26**, 441-457.e7 (2020).

106. Vauclair, S., Nicolas, M., Barrandon, Y. & Radtke, F. Notch1 is essential for postnatal hair follicle development and homeostasis. *Dev. Biol.* **284**, 184–193 (2005).

107. Pan, Y. *et al.* □-Secretase Functions through Notch Signaling. *Dev. Cell* 13.

108. Demehri, S. & Kopan, R. Notch signaling in bulge stem cells is not required for selection of hair follicle fate. *Development* **136**, 891–896 (2009).

109. Aubin-Houzelstein, G. Notch Signaling and the Developing Hair Follicle. in *Notch Signaling in Embryology and Cancer* (eds. Reichrath, J. & Reichrath, S.) vol. 727 142–160 (Springer US, 2012).

110. Faraji Zonooz, M. *et al.* Whole Genome Linkage Analysis Followed by Whole Exome Sequencing Identifies Nicastrin (NCSTN) as a Causative Gene in a Multiplex Family with γ-Secretase Spectrum of Autoinflammatory Skin Phenotypes. *J. Invest. Dermatol.* **136**, 1283–1286 (2016).

111. Pink, A. E. *et al.* Mutations in the γ-Secretase Genes NCSTN , PSENEN , and PSEN1 Underlie Rare Forms of Hidradenitis Suppurativa (Acne Inversa). *J. Invest. Dermatol.* **132**, 2459–2461 (2012).

112. Wang, B. *et al.* Gamma-secretase gene mutations in familial acne inversa. *Science* **330**, 1065 (2010).

113. Nakamizo, S. *et al.* High-fat diet induces a predisposition to follicular hyperkeratosis and neutrophilic folliculitis in mice. *J. Allergy Clin. Immunol.* **148**, 473-485.e10 (2021).

114. Sakamoto, K. *et al.* Disruption of the endopeptidase ADAM10-Notch signaling axis leads to skin dysbiosis and innate lymphoid cell-mediated hair follicle destruction. *Immunity* **54**, 2321-2337.e10 (2021).

115. Abu Rached, N. *et al.* The Role of Hormones in Hidradenitis Suppurativa: A Systematic Review. *Int. J. Mol. Sci.* **23**, 15250 (2022).

116. Garg, A., Papagermanos, V., Midura, M. & Strunk, A. Incidence of hidradenitis suppurativa among tobacco smokers: a population-based retrospective analysis in the U.S.A. *Br. J. Dermatol.* **178**, 709–714 (2018).

117. Jemec, G. B. E., Thomsen, B. M. & Hansen, U. The homogeneity of hidradenitis suppurativa lesions. *APMIS* **105**, 378–383 (1997).

118. Takeshige, K., Baba, M., Tsuboi, S., Noda, T. & Ohsumi, Y. Autophagy in yeast demonstrated with proteinase-deficient mutants and conditions for its induction. *J. Cell Biol.* **119**, 301–311 (1992).

119. Lysosomes, Autophagy | Learn Science at Scitable. https://www.nature.com/scitable/topicpage/the-discovery-of-lysosomes-and-autophagy-14199828/.

120. Clarke, A. J. & Simon, A. K. Autophagy in the renewal, differentiation and homeostasis of immune cells. *Nat. Rev. Immunol.* **19**, 170–183 (2019).

121. Eckhart, L., Tschachler, E. & Gruber, F. Autophagic Control of Skin Aging. *Front. Cell Dev. Biol.* **7**, 143 (2019).

122. Green, D. R., Oguin, T. H. & Martinez, J. The clearance of dying cells: table for two. *Cell Death Differ.* **23**, 915–926 (2016).

123. Chai, M. *et al.* Stimulation of Hair Growth by Small Molecules that Activate Autophagy. *Cell Rep.* **27**, 3413-3421.e3 (2019).

124. Parodi, C. *et al.* Autophagy is essential for maintaining the growth of a human (mini-)organ: Evidence from scalp hair follicle organ culture. *PLOS Biol.* **16**, e2002864 (2018).

125. Liao, X. *et al.* Macrophage Autophagy Plays a Protective Role in Advanced Atherosclerosis. *Cell Metab.* **15**, 545–553 (2012).

126. Wang, M., Qu, S., Ma, J., Wang, X. & Yang, Y. Metformin Suppresses LPS-Induced Inflammatory Responses in Macrophage and Ameliorates Allergic

Contact Dermatitis in Mice *via* Autophagy. *Biol. Pharm. Bull.* **43**, 129–137 (2020).

127. Haapasalo, A. & Kovacs, D. M. The Many Substrates of Presenilin/γ-Secretase. *J. Alzheimers Dis.* **25**, 3–28 (2011).

128. Bae, S. *et al.* Notch Signaling in Hair Follicle Development. *Asian J. Beauty Cosmetol.* **15**, 377–386 (2017).

129. AlMuraikhi, N. *et al.* Notch Signaling Inhibition by LY411575 Attenuates Osteoblast Differentiation and Decreased Ectopic Bone Formation Capacity of Human Skeletal (Mesenchymal) Stem Cells. *Stem Cells Int.* **2019**, 1–12 (2019).

130. Bigas, A. & Espinosa, L. Hematopoietic stem cells: to be or Notch to be. *Blood* **119**, 3226–3235 (2012).

131. Pavlovsky, M. *et al.* A phenotype combining hidradenitis suppurativa with Dowling-Degos disease caused by a founder mutation in *PSENEN*. *Br. J. Dermatol.* **178**, 502–508 (2018).

132. Takeichi, T. *et al.* A novel *NCSTN* missense mutation in the signal peptide domain causes hidradenitis suppurativa, which has features characteristic of an autoinflammatory keratinization disease. *Br. J. Dermatol.* **182**, 491–493 (2020).

133. Jfri, A. H., O'Brien, E. A., Litvinov, I. V., Alavi, A. & Netchiporouk, E. Hidradenitis Suppurativa: Comprehensive Review of Predisposing Genetic Mutations and Changes. *J. Cutan. Med. Surg.* **23**, 519–527 (2019).

134. Arnold, J. *et al.* Autophagy is dispensable for B-cell development but essential for humoral autoimmune responses. *Cell Death Differ.* **23**, 853–864 (2016).

135. Zahner, S. P. *et al.* Conditional deletion of TGF-βR1 using Langerin-Cre mice results in Langerhans cell deficiency and reduced contact hypersensitivity. *J. Immunol. Baltim. Md 1950* **187**, 5069–5076 (2011).

136. Letronne, F. ADAM30 and APP metabolism: an involment in Alzheimer's disease physiopathological development. (2014).

137. Garcovich, S. *et al.* Novel nicastrin mutation in hidradenitis suppurativa-Dowling-Degos disease clinical phenotype: more than just clinical overlap? *Br. J. Dermatol.* **183**, 758–759 (2020).

138. Mesa, K. R. *et al.* Niche-induced cell death and epithelial phagocytosis regulate hair follicle stem cell pool. *Nature* **522**, 94–97 (2015).

139. Vidal, V. P. I. *et al.* Sox9 Is Essential for Outer Root Sheath Differentiation and the Formation of the Hair Stem Cell Compartment. *Curr. Biol.* **15**, 1340–1351 (2005).

140. Nowak, J. A., Polak, L., Pasolli, H. A. & Fuchs, E. Hair Follicle Stem Cells Are Specified and Function in Early Skin Morphogenesis. *Cell Stem Cell* **3**, 33–43 (2008).

141. Bohin, N., Carlson, E. A. & Samuelson, L. C. Genome Toxicity and Impaired Stem Cell Function after Conditional Activation of CreERT2 in the Intestine. *Stem Cell Rep.* **11**, 1337–1346 (2018).

142. Furuyama, K. *et al.* Continuous cell supply from a Sox9-expressing progenitor zone in adult liver, exocrine pancreas and intestine. *Nat. Genet.* **43**, 34–41 (2011).

143. Bechetoille, N. *et al.* A new organotypic model containing dermal-type macrophages. *Exp. Dermatol.* **20**, 1035–1037 (2011).

144. Muller, Q. *et al.* Development of an innervated tissue-engineered skin with human sensory neurons and Schwann cells differentiated from iPS cells. *Acta Biomater.* **82**, 93–101 (2018).

145. Muller, Q., Berthod, F. & Flacher, V. [Tridimensional in vitro models of nervous and immune systems in the skin]. *Med. Sci. MS* **37**, 68–76 (2021).

146. Hotz, C. *et al.* Intrinsic Defect in Keratinocyte Function Leads to Inflammation in Hidradenitis Suppurativa. *J. Invest. Dermatol.* **136**, 1768–1780 (2016).

147. Blais, M., Grenier, M. & Berthod, F. Improvement of nerve regeneration in tissue-engineered skin enriched with schwann cells. *J. Invest. Dermatol.* **129**, 2895–2900 (2009).

148. Boelsma, E., Verhoeven, M. C. H. & Ponec, M. Reconstruction of a Human Skin Equivalent Using a Spontaneously Transformed Keratinocyte Cell Line (HaCaT). *J. Invest. Dermatol.* **112,** 489–498 (1999).

149. Koehler, K. R. *et al.* Generation of inner ear organoids containing functional hair cells from human pluripotent stem cells. *Nat. Biotechnol.* **35,** 583–589 (2017).

ANNEXES

Annex 1 :

Manuscript in revision

Epidermal maintenance of Langerhans cells relies on autophagy-regulated lipid metabolism.

Context

The maintenance of Langerhans cells (LCs) within the epidermis is crucial for their role in immunosurveillance. Therefore, LCs are adapted to the metabolic specificities of the epidermal microenvironment, i.e. hypoxia, limited nutrient supplies and exposure to UV radiations. We hypothesized that such adaptations may imply a role for autophagy in regulating LC survival. I participated in a joint project of Drs. Vincent Flacher and Frédéric Gros (INSERM UMRS1109, Strasbourg), in which the CRE-mediated deletion of *Atg5* was targeted to LCs through their specific expression of Langerin/CD207. I have notably worked on metabolic analysis of LCs by Seahorse, as well as assays that addressed the proinflammatory potential of autophagy-deficient LCs. The manuscript, also available in bioRxiv, has been submitted to the Journal of Experimental Medicine and is currently in revision.

Epidermal maintenance of Langerhans cells relies on autophagy-regulated lipid metabolism

Florent Arbogast[1,2], Raquel Sal-Carro[1], Wacym Boufenghour[1], Quentin Frenger[2,9], Delphine Bouis[1], Louise Filippi De La Palavesa[1], Jean-Daniel Fauny[1], Olivier Griso[4], Hélène Puccio[4], Rebecca Fima[5], Thierry Huby[5], Emmanuel L. Gautier[5], Anne Molitor[3], Raphaël Carapito[3,6], Seiamak Bahram[3,6], Nikolaus Romani[7], Björn E. Clausen[8], Benjamin Voisin[1], Christopher G. Mueller[1], Frédéric Gros[1,2,9]*, Vincent Flacher[1]*

1 Laboratory CNRS I²CT/UPR3572 Immunology, Immunopathology and Therapeutic Chemistry, Strasbourg Drug Discovery and Development Institute (IMS), Institut de Biologie Moléculaire et Cellulaire, Strasbourg, France.

2 Université de Strasbourg, Strasbourg, France.

3 Laboratoire d'Immunorhumatologie Moléculaire, Plateforme GENOMAX, INSERM UMR_S 1109, Faculté de Médecine, Fédération Hospitalo-Universitaire OMICARE, ITI TRANSPLANTEX NG, Université de Strasbourg, 67085, Strasbourg, France. Strasbourg Federation of Translational Medicine (FMTS), Strasbourg University, Strasbourg, France.

4 INSERM U1258 / CNRS UMR7104, Institut de Génétique et de Biologie Moléculaire et Cellulaire, Illkirch, France.

5 Sorbonne Université, INSERM UMR_S 1166 ICAN, Paris, France.

6 Service d'Immunologie Biologique, Plateau Technique de Biologie, Pôle de Biologie, Nouvel Hôpital Civil, Hôpitaux Universitaires de Strasbourg, Strasbourg, France.

7 Department of Dermatology, Venereology and Allergology, Medical University of Innsbruck, Innsbruck, Austria.

8 Institute for Molecular Medicine and Paul Klein Center for Immunotherapy (PKZI), University Medical Center of the Johannes Gutenberg-University Mainz, Mainz, Germany.

9 Present address: INSERM UMR_S 1109 Immunorhumatologie Moléculaire, Fédération de Médecine Translationnelle de Strasbourg (FMTS), ITI Transplantex NG, Centre de Recherche en Biomédecine de Strasbourg (CRBS), Faculté des Sciences de la Vie, Université de Strasbourg, Strasbourg, France.

* Correspondance : f.gros@unistra.fr, v.flacher@ibmc-cnrs.unistra.fr

ABSTRACT (149 words)

Macroautophagy (often-named autophagy), a catabolic process involving autophagy-related (*Atg*) genes, prevents accumulation of harmful cytoplasmic components and mobilizes energy reserves in long-lived and self-renewing cells. Autophagy deficiency affects antigen presentation in conventional dendritic cells (DCs) without impacting their survival. However, previous studies did not address epidermal Langerhans cells (LCs), a proliferating skin DC subset with extended lifespan. Here, we demonstrate that deletion of either *Atg5* or *Atg7* in LCs leads to their gradual depletion. ATG5-deficient LCs showed metabolic dysregulation and accumulated neutral lipids. Despite increased mitochondrial respiratory capacity, they were unable to process lipids, eventually leading them to ferroptosis. Metabolically impaired LCs upregulated proinflammatory transcripts, in line with exacerbated inflammasome-dependent priming. Moreover, they decreased expression of neuronal interaction receptors, in line with a reduction of epidermal nerves upon LC depletion. Altogether, autophagy represents a critical regulator of lipid storage and metabolism in LCs, allowing their maintenance in the epidermis.

GRAPHICAL ABSTRACT
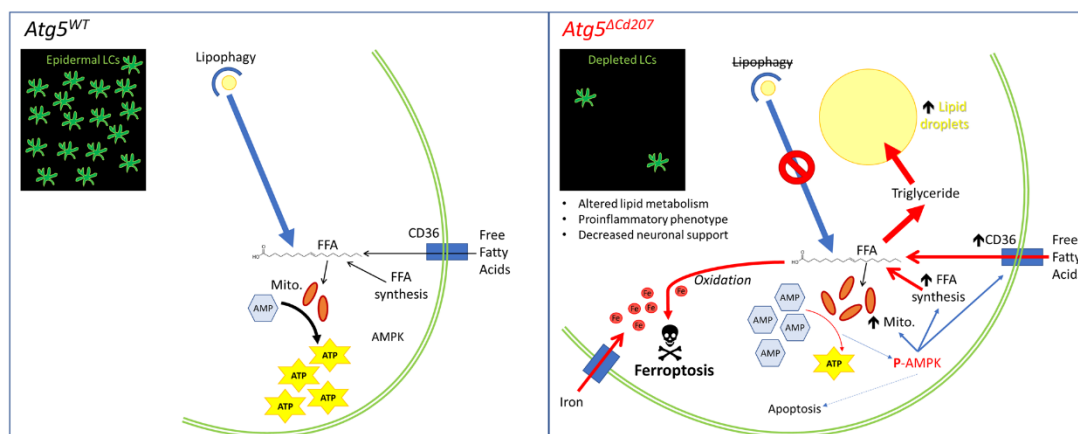
KEYWORDS

Autophagy, Langerhans cells, skin, homeostasis, lipid droplets, ferroptosis, metabolism

ABBREVIATIONS

2-NBDG: 2-(N-(7-Nitrobenz-2-oxa-1,3-diazol-4-yl) Amino)-2-Deoxyglucose

AMPK: AMP-activated protein kinase

APCs: Antigen-presenting cells

Atg: Autophagy-related genes

DCs: Dendritic cells

cDCs: Conventional dendritic cells

DETCs: Dendritic epidermal T cells

ER: Endoplasmic Reticulum

FCS: fetal calf serum

IRE1: Inositol-requiring enzyme 1

LCs: Langerhans cells

LN: Lymph nodes

MHC-II: Major histocompatibility complex

MT: Mitotracker

ROS: reactive oxygen species

UPR: Unfolded protein response

TGF-β1: Tumor growth factor β 1

Xbp1: X-box binding protein 1

Manuscript length: 38177 characters (without spaces, methods and references)

INTRODUCTION

Langerhans cells (LCs) are resident antigen-presenting cells (APCs) of the epidermis (Doebel et al., 2017; Kaplan, 2017). LCs arise from hematopoietic precursors that emerge from the yolk sac and the fetal liver to colonise the skin before birth (Hoeffel et al., 2012). There, they are maintained lifelong by local proliferation (Merad et al., 2002). LCs exhibit an exceptional longevity, with a half-life of several weeks, whereas other dendritic cells (DCs) are replenished from bone marrow precursors within days (Kamath et al., 2002). Possibly as a consequence of UV exposure, LCs are endowed with a potent DNA-repair capacity, allowing the survival of at least a pool of self-renewing cells upon gamma irradiation (Price et al., 2015). Despite free diffusion of glucose from the blood into the lowest layers of the epidermis, their position in the stratum granulosum implies a limited supply of nutrients, which must be metabolised in a very hypoxic environment (Bedogni et al., 2005). Similar to other cutaneous DC subsets, LCs migrate to lymph nodes (LNs) following microorganism recognition or irradiation. There, they contribute, as conventional dendritic cells (cDC), to antigen presentation and differentiation of CD4^{+} and CD8^{+} T cells, either driving immune activation or tolerance (Bedoui et al., 2009; Flacher et al., 2014; Igyarto et al., 2011). LCs are among the first APCs that sense skin infections (Kashem et al., 2015) and are involved in inflammatory disorders such as psoriasis (Singh et al., 2016). Therefore, a deeper understanding of their homeostasis appears critical.

Autophagy is a conserved mechanism of self-digestion, allowing the engulfment of cytoplasmic content into double-membrane vesicles, which fuse with lysosomes for degradation and recycling of the sequestered content (Arbogast et al., 2018; Clarke and Simon, 2018). The core autophagy proteins are encoded by autophagy-related (*Atg*) genes. Autophagy is promoted under energetic stress notably trough the inhibition of the PI3K/AKT/mTOR pathway (Galluzzi et al., 2014). Autophagy also contributes to metabolic equilibrium in homeostatic conditions as it is a key process to support energy provision. For cells relying on oxidative phosphorylation to generate ATP, autophagy contributes to maintain a functional mitochondrial pool through degradation of defective mitochondria and to mobilize fatty acids through degradation of lipid droplets in a process called lipophagy (Kim et al., 2014). To support homeostasis, autophagy also acts as a quality-control mechanism during the unfolded protein response (UPR), preventing the accumulation of misfolded protein aggregates and degrading excess or damaged endoplasmic reticulum (ER) (Anding and Baehrecke, 2017). These housekeeping forms of autophagy are particularly important in long-lived and self-renewing cells. In the immune system, B-1 B cells, memory B and T cells as well as plasma cells rely on autophagy for their maintenance (Arbogast et al., 2018; Arnold et al., 2016; Clarke et al., 2018; Murera et al., 2018; Pengo et al., 2013; Xu et al., 2014). ATG proteins are also involved in several non-autophagic processes such as LC3-associated phagocytosis (LAP). LAP requires Rubicon (*Rubcn*) to form an initiation complex, and is involved in microorganism clearance, efferocytosis and antigen presentation, which are highly relevant for DCs (Heckmann and Green, 2019; Munz, 2015). Notably, autophagy impairment in DCs notably leads to defective CD4^{+} and CD8^{+} T cell responses (Alissafi et al., 2017; Lee et al., 2010; Mintern et al., 2015; Weindel et al., 2017).

Overall, selective deletion of *Atg* genes in macrophages and DCs has demonstrated that autophagy modulates pathogen resistance, antigen presentation, and proinflammatory signals, i.e. inflammasome activity (Bah and Vergne, 2017; Ghislat and Lawrence, 2018; Valecka et al., 2018; Takahama et al., 2018). Similarly, recent reports focused on LCs support a role of autophagy in the regulation of inflammatory responses (Müller et al., 2020; Said et al., 2014) and in the immune response against intracellular bacteria (Dang et al., 2019). Moreover, autophagy proteins participate in the intracellular routing of human immunodeficiency virus (HIV) particles towards degradative compartments in human LCs upon Langerin/CD207-mediated uptake (Ribeiro et al., 2016). Interestingly, enhancing autophagy by pharmacological agents limits HIV-1 mucosal infection and replication (Cloherty et al., 2021). Yet, non-autophagic roles of ATG proteins cannot be ruled out to explain these results.

Thus far, autophagy defects were only assessed in cDCs, in which antigen presentation, but not cell survival, was affected. (Lee et al., 2010; Mintern et al., 2015; Oh and Lee, 2019). No information is currently available on the consequences of constitutive autophagy impairment for LCs *in vivo*. Since LCs are self-renewing, long-lived APCs that are exposed to low availability of nutrients, UV irradiation or stress related to infection, we hypothesized that efficient autophagy might be a key element supporting their maintenance in the epidermis. To investigate this, we generated *Cd207*-specific deletion of *Atg5* in order to define primary roles of autophagy and related processes in LC biology.

RESULTS

ATG5 is necessary for Langerhans cell network maintenance.

Since evidence for autophagosomes in primary LCs has been so far limited (Ribeiro et al., 2016), we first verified whether LCs from digested murine epidermis comprise such compartments. Electron microscopy of LCs, including original images and reanalysis of previously published samples (Schuler and Steinman, 1985), allowed the identification of double-membrane compartments as well as crescent-shape structures reminiscent of incipient phagophores and isolation membranes. The diameter of the autophagosomes was between 400 and 600nm **(Figure S1)**. In line with this observation, LC3 staining by immunofluorescence revealed positive compartments within LCs **(Figure 1A, upper panels)**. When LCs were treated with hydroxychloroquine to block lysosomal degradation of autophagosomes, we observed an accumulation of membrane-associated LC3 by flow cytometry, thereby demonstrating autophagic flux **(Figure 1B, upper panel)**. Altogether, this showed constitutive autophagic activity in LCs of wild-type mice.

To determine the function of autophagy in LCs *in vivo* we generated *Cd207-cre x Atg5$^{flox/-}$* (*Atg5$^{\Delta Cd207}$*) mice, in which the essential autophagy gene *Atg5* is deleted by CRE-mediated recombination in cells expressing CD207 **(Figure S2A)**. Efficiency of the deletion was verified by RT-qPCR of LCs sorted from the mouse epidermis **(Figure S2B)** and from skin-draining LNs of 4-week-old mice **(Figure S2C, D)**. This confirmed that the breeding strategy resulted in an optimal deletion efficiency, as *Atg5* mRNA was undetectable in LCs from *Atg5$^{\Delta Cd207}$* mice, as compared with LCs from *Atg5$^{flox/+}$* and *Cd207-cre x Atg5$^{flox/+}$* control animals (respectively referred to as *Atg5^{WT}* and *Atg5$^{WT/\Delta}$* below). With respect to migratory dermal DCs isolated from LNs of *Atg5$^{\Delta Cd207}$* mice, *Atg5* mRNA was absent from CD103$^+$ dermal cDC1, which also express CD207 (Henri et al., 2010), but, as expected, it was still present in CD207$^-$ MHCII^{high} dermal DCs **(Figure S2D)**.

To address whether the deletion of *Atg5* leads to autophagy impairment in LCs, formation of autophagic compartments was assessed by LC3 immunostaining. LC3$^+$ punctate staining in the cytoplasm of *Atg5^{WT}* LCs was clearly visible, whereas LC3 staining was diffuse in LCs from *Atg5$^{\Delta Cd207}$* mice **(Figure 1A, lower panels, and Supplementary Videos SV1, SV2)**. This reflects the expected consequences of ATG5 deficiency, i.e. the absence of LC3 conjugation with phosphatidylethanolamine (LC3-II) and lack of integration into autophagic compartments. Since this accumulation of LC3$^+$ vesicles may also reveal an impaired degradation of autophagosomes, the acidification and lysosomal load were quantified by Lysosensor and Lysotracker probes, respectively. We could thus verify that it was unperturbed in the absence of ATG5 **(Figure S3)**. Finally, we observed that autophagic flux was abolished in LCs of *Atg5$^{\Delta Cd207}$* mice **(Figure 1B, lower panel)**. This shows that ATG5 deletion leads to autophagy impairment in LCs.

To monitor the possible involvement of autophagy in the homeostatic maintenance of LCs under steady state conditions, we evaluated their epidermal network at different ages. Since CD207 expression in MHCII$^+$ epidermal LC precursors is completed around 7-10 days after birth

(Tripp et al., 2004), we assessed the proportion of MHCII$^+$ TCRγδ$^-$ CD207$^+$ LCs among CD45$^+$ epidermal cells by flow cytometry from 10 days until 9 months of age **(Figure 1C)**. The basal proportion of LCs at 10 days was comparable for mice of all genotypes, suggesting that no major defect occurs in the seeding of MHCII$^+$ CD207$^-$ embryonic LC precursors in the epidermis, which also corresponds to the expected kinetics of *Cd207* promoter activity and CRE expression (Tripp et al., 2004) **(Figure 1D)**. In *Atg5^{WT}* and *Atg5$^{WT/Δ}$* mice, we observed a moderate increase of LCs until 6-12 weeks, followed by a decrease in aging mice. Nevertheless, the proportion of LCs diminished sharply around 2-4 weeks of age in the epidermis of *Atg5^{ΔCd207}*, eventually stabilizing at around 5% of epidermal CD45$^+$ leukocytes at 9 months.

To reinforce the conclusion that the loss of LCs is due to impaired autophagy and not other ATG5-related cellular homeostatic dysfunctions, we generated *Cd207-cre x Atg7$^{flox/flox}$* (*Atg7^{ΔCd207}*) mice and compared their epidermal cell suspensions with that of *Atg7$^{flox/flox}$* (*Atg7^{WT}*) mice. Similar to our findings with *Atg5^{ΔCd207}* mice, ATG7 deficiency resulted in a significant depletion of LCs from the epidermis of mice older than 10 weeks **(Figure 1E)**. Thus, we can exclude effects only linked to ATG5, such as direct regulation of apoptosis independently of the autophagy machinery (Galluzzi et al., 2014). Additionally, we could exclude a role for LAP or other endocytic processes requiring ATG5, as the epidermal network of LCs appeared unaffected in Rubicon-deficient mice **(Figure S4).**

We then performed an immunofluorescent staining of the LC network in epidermal sheets prepared from ear skin of *Atg5^{ΔCd207}* and control mice **(Figure 1F)**. We did not observe any obvious difference in the LC network in 3-week-old mice, regardless of their genotype. However, and in accordance with flow cytometry results, very few LCs were visible in 6-month-old *Atg5^{ΔCd207}* mice. Interestingly, LCs remaining in older mice were often assembled in disseminated patches. This pattern is reminiscent of the network reconstitution that occurs through slow *in situ* LC proliferation following induced depletion in Langerin-DTR mice (Bennett et al., 2005). Indeed, LCs ensure the integrity of their epidermal network by self-renewal (Chorro et al., 2009; Ghigo et al., 2013). Consequently, we assessed the proliferative capacity of ATG5-deficient LCs by 5-bromo-2'-deoxyuridine (BrdU) incorporation and Ki-67 staining by flow cytometry **(Figure 1G)**. We observed proliferation rates consistent with our previous observations in 4-week-old mice (Voisin et al., 2019), with comparable percentages of BrdU$^+$ and Ki-67$^+$ LCs in *Atg5^{ΔCd207}* and control *Atg5^{WT}* mice, thereby concluding that autophagy deficiency does not prevent maintenance of the LC network by a major proliferative impairment. On the other hand, LCs of 6-month-old *Atg5^{ΔCd207}* mice displayed higher proliferation rates, presumably because of homeostatic compensation for the depletion of their epidermal niche.

Finally, since dermal cDC1 also express CD207 and showed deletion of *Atg5* in *Atg5^{ΔCd207}* mice **(Figure S2D)**, we quantified LC and cDC1 populations among total MHCII$^+$ CD11c$^+$ skin DCs. As expected, a decrease was evident for LCs present in whole skin suspensions, while the proportion of cDC1 among skin DCs was rather slightly increased **(Figure S5A,B)**. Thus, the core autophagic machinery is dispensable for the maintenance of dermal cDC1, yet appears essential to LCs.

ATG5-deficient Langerhans cells undergo apoptosis.

Since their self-renewal was not affected, the loss of ATG5-deficient LCs might be explained by an enhance emigration into lymph nodes or by increased cell death. LCs, as other DCs of peripheral tissues, undergo maturation and migrate to skin-draining LNs following inflammatory signals (Doebel et al., 2017; Kaplan, 2017). Alternatively, spontaneous maturation of LCs may result from disrupted TGF-β signalling, which, under physiological conditions, is required to maintain an immature state (Bobr et al., 2012; Kel et al., 2010). In both cases, an increased expression of maturation markers MHC-II and CD86 can be observed prior to the departure of LCs from the epidermis. We thus verified whether autophagy impairment might prompt spontaneous LC maturation. MHC-II and CD86 expression by LCs in the epidermis did not show any variation in $Atg5^{\Delta Cd207}$ compared to control mice **(Figure 2A, B)**. Moreover, because an overt LC emigration from the epidermis would lead to a noticeable accumulation in LNs, we determined LC numbers in inguinal and brachial LNs of 6-week-old mice. We observed instead a trend towards a decrease, only significant in percentage for LCs from $Atg5^{\Delta Cd207}$ mice **(Figure 2C, D)**. A similar pattern was observed for dermal cDC1 that also express CD207. As expected, no differences were detected for CD207⁻ dermal DC subsets that lack ATG5 deletion. Taken together, these results exclude that impaired autophagy leads to a massive spontaneous maturation and migration of LCs.

Finally, using flow cytometry, we addressed whether the absence of *Atg5* might lead to increased apoptosis by measuring the proportion of LCs with active caspase-3. Interestingly, this major effector of apoptosis was detected markedly induced in ATG5-deficient LCs, both in the epidermis and in LNs **(Figure 2E)**. Altogether, these results demonstrate that reduced cell division or increased maturation cannot account for LC network disintegration, whereas ATG5 appears crucial, even in the steady state, for LC survival.

ATG5-deficient Langerhans cells show limited endoplasmic reticulum stress.

Functional autophagy is required for the maintenance of the endoplasmic reticulum (ER). ER damage triggers the inositol-requiring enzyme 1 (IRE1)/X-box binding protein 1 (Xbp1) axis of the Unfolded Protein Response (UPR), which is a master regulator of DC survival and maturation (Cubillos-Ruiz et al., 2015; Grootjans et al., 2016; Tavernier et al., 2017). Autophagy regulates ER swelling, protein aggregation and thereby limits the extent of the UPR (Song et al., 2018). In line with this, exposure of wild-type LCs to the phosphatidylinositol-3-kinase inhibitor, wortmannin, which inhibits the initiation of the autophagosome formation, resulted in an increased labelling by ER-tracker **(Figure S6A)**. Therefore, we stained LCs from 3-week-old mice with ER-tracker, a fluorescent dye specific for ER membranes. Flow cytometry analysis showed a significantly increased ER-tracker staining in LCs of $Atg5^{\Delta Cd207}$ compared to wild-type mice **(Figure S6B)**. In line with this, confocal microscopy revealed an expanded ER compartment in these cells **(Figure S6C and Supplementary Videos SV3, SV4)**. These signs of ER expansion prompted us to study whether the expression of key intermediates of the UPR pathway might be elevated. Quantitative PCR was performed for *Ern1*, total *Xbp1*, spliced *Xbp1* and *Ddit3* mRNA. However, none of these genes showed

increased expression, demonstrating that the UPR pathway was not constitutively engaged **(Figure S6D)**. Therefore, we conclude that ATG5-deficient LCs can cope with the observed ER swelling, which does not trigger a massive UPR that could lead to cell death.

Autophagy-deficient Langerhans cells accumulate intracellular lipid storage

To identify dysregulated gene expression patterns that could be linked with impaired autophagy, RNA sequencing was performed on epidermal LCs sorted from 3-week-old $Atg5^{\Delta Cd207}$ or $Atg5^{WT}$ control mice. Analysis of $Atg5$ mRNA sequencing reads confirmed the deletion of exon 3 in LCs upon CRE-mediated recombination **(Figure S7A)**. Principal component analysis revealed clear differences in transcriptomic profiles between $Atg5^{\Delta Cd207}$ and $Atg5^{WT}$ mice **(Figure S7B)**. Differentially expressed genes in $Atg5^{\Delta Cd207}$ LCs included 673 upregulated and 629 downregulated genes **(Table 2, Figure S7C, D)**. Gene ontology pathway enrichment analysis suggested in particular a dysregulation of cellular metabolism (GO:0046942, GO:0043269, GO:0044272, GO:0051186, GO:0046085, GO:1901615, GO:0015711, GO:0009166, GO:0007584; **Figure S7E)**.

Autophagy regulates cellular lipid metabolism by lipophagy, which has a crucial role in balancing energy supply in both steady state and under metabolic stress. Lipophagy mediates lysosomal degradation of proteins that coat cytoplasmic lipid droplets, and lipolysis of triglycerides, thus liberating free fatty acids to be consumed by beta-oxidation in mitochondria (Kounakis et al., 2019). Accordingly, LCs of $Atg5^{\Delta Cd207}$ mice modulated the expression of several genes encoding actors of lipidic metabolism pathways **(Figure 3A)**. We noticed upregulation of mRNA of the solute carrier (SLC) family transporters MCT-4/SLC16A3 (lactate), SLC7A11 (cystein, glutamate) and SLC7A2 (lysine, arginine), which import molecules that directly or indirectly provide substrates to the tricarboxylic acid cycle. Upregulated expression of *Acss1* and *Acss2* (Acyl-CoA Synthetase Short Chain Family Member 1 and 2) is expected to favour synthesis of Acetyl-CoA, which can either be converted into lipids or fuel mitochondrial beta-oxidation. Fatty acid synthesis and energy storage in the form of lipid droplets appears to be favoured in ATG5-deficient LCs, as hinted by the upregulation of *Gyk*, encoding the Glycerol kinase which catalyses triglyceride synthesis, and *Acsl3,* encoding the Acyl-CoA Synthetase Long Chain Family Member 3, a key enzyme for neutral lipid generation (Gao et al., 2019).

To determine whether lipid storage was deregulated in autophagy-deficient LCs, epidermal cell suspensions were exposed to Bodipy, a lipid staining dye that targets neutral lipid-rich vesicles, which then can be quantified by flow cytometry. We first validated this experimental approach by treating wild-type LCs with etomoxir, a carnitine palmitoyltransferase I inhibitor that blocks the import of activated free fatty acids (acyl-CoA) by mitochondria. As expected, etomoxir treatment resulted in a stronger intensity of Bodipy staining, reflecting higher neutral lipid storage **(Figure 3B)**. Interestingly, treating LCs with the autophagy inhibitor wortmannin also resulted in an increased Bodipy staining suggesting constitutive lipophagy in LCs **(Figure 3C)**. We then found that $Atg5^{\Delta Cd207}$ LCs retained more Bodipy as compared with LCs of control mice **(Figure 3D)**. We consistently observed by confocal microscopy that LCs of

Atg5^{ΔCd207} contained more Bodipy-positive vesicular structures that could correspond to lipid droplets **(Figure 3E and Supplementary Videos SV5, SV6)**. Perilipin-1 staining in LCs allowed to unequivocally identify lipid droplets, confirming that autophagy deficiency resulted in an abnormal increase in neutral lipid storage **(Figure 3F)**. Thus, enlargement of the ER may be a direct consequence of lipid droplets budding from this compartment.

Disrupted lipid metabolism in autophagy-deficient Langerhans cells

ATG5 deficiency might lead to an accumulation of intracellular lipids if energy production in LCs strongly relies on lipophagy to mobilize these storage units and produce energy by the beta-oxidation pathway (Kounakis et al., 2019). To assess the energy production in LCs, we focused on AMP-activated protein kinase (AMPK), a master regulator of energetic metabolism, which is phosphorylated on residues T183/T172 when ATP/AMP ratios decline (Herzig and Shaw, 2018). As measured by flow cytometry, AMPK phosphorylation was indeed increased in LCs from *Atg5^{ΔCd207}* mice **(Figure 4A)**. Downstream of AMPK phosphorylation, import of glucose to support glycolysis, or fatty acid uptake and synthesis can be induced to help restore optimal ATP production. To quantify the glucose uptake intensity, we first monitored the expression of the glucose transporter GLUT-1 by LCs. However, no difference could be observed between LCs of *Atg5^{ΔCd207}* mice and control mice **(Figure 4B)**. Next, we quantified the glucose uptake of these cells using 2-(N-(7-Nitrobenz-2-oxa-1,3-diazol-4-yl) Amino)-2-Deoxyglucose (2-NBDG), a fluorescent glucose analogue which can be tracked by flow cytometry. In line with the unmodified GLUT-1 expression, autophagy-deficient LCs were not more efficient at capturing glucose than LCs of wild-type mice **(Figure 4C)**. On the other hand, LCs from *Atg5^{ΔCd207}* mice exhibited a stronger expression of CD36 **(Figure 4D)**. This scavenger receptor has a key role in the capture of free fatty acids and lipids, which was indeed increased when LCs incubated with Bodipy-labelled C16 fatty acid **(Figure 4E)**. Altogether, these assays demonstrate that autophagy-deficient LCs show a deficit in energy production, despite an increased ability to capture and store lipids.

To evaluate whether a lack of autophagy affects oxidative phosphorylation in LCs, we quantified metabolic flux of LCs exposed to a series of inhibitors of mitochondrial respiratory complexes **(Figure 4F)**. The decrease of oxygen consumption rates for wild-type and ATG5-deficient LCs upon oligomycin treatment was similar to that of bone marrow-derived DCs (BMDCs), indicating a similar basal production of ATP at steady state **(Figure 4G: ATP)**. Wild-type LCs and BMDCs also displayed a comparable profile after exposure to FCCP, which unleashes the maximal respiratory capacity of a cell. On the other hand, LCs of *Atg5^{ΔCd207}* mice reacted to FCCP by a strikingly prominent peak of their oxygen consumption **(Figure 4G: Max)**. This implies that, in the absence of autophagy, the potential of LCs to mobilize oxidative phosphorylation, also called spare respiratory capacity, had massively increased **(Figure 4G: SRC)**. Despite this, ATG5-deficient LCs appeared unable to use this capacity to promote ATP production **(Figure 4G: ATP)**. The respiratory capacity of a cell relies on mitochondria, and transcriptome analysis demonstrated that mitochondria-related genes were differentially regulated upon loss of autophagy **(Figure 4H)**. Thus, we performed a double staining with mitotracker (MT) Green and Deep Red on LCs extracted from 3-week-old mice. While MT Deep

Red is sensitive to mitochondrial membrane potential, MT Green stains mitochondrial membranes independently of the membrane potential, thus allowing normalization of the membrane potential to the mitochondrial load. An increased mitochondrial mass was detected **(Figure 4I)**, in line with the increased capacity of energy production that we measured by the mitochondrial stress assay. ATG5-deficient LCs did not display decreased membrane potential **(Figure S8A)**, suggesting that mitochondrial function was preserved. Mitophagy is a key process to eliminate defective mitochondria, in particular when they produce reactive oxygen species (ROS). We used Mitosox staining to quantify ROS produced under altered mitochondria function, but this assay did not reveal any difference between $Atg5^{\Delta Cd207}$ and $Atg5^{WT}$ mice **(Figure S8B)**. All things considered, since mitochondria and lysosomes of autophagy-deficient LCs remained functional, we conclude that shortage in the lipophagy-dependent fatty acid supply could not be compensated by increased mitochondrial mass.

Ferroptosis results from lipid oxidation in ATG5-deficient Langerhans cells

Mitosox detects superoxide $O_2\cdot-$, yet other ROS may cause cellular damage and death, i.e. H_2O_2 and $HO\cdot$. Interestingly, ATG5-deficient LCs showed upregulated transcription of *Gss* (Glutathione-S Synthetase), *Slc7a11* (Cysteine/glutamate antiporter xCT), *Esd* (S-formylglutathione hydrolase) and *Gclm* (Glutamate-Cysteine Ligase Modifier Subunit), which are key elements in the glutathione-dependent response to ROS **(Figure 4J)**. The glutathione pathway is notably involved in preventing ferroptosis, in which cell death occurs as a consequence of iron-dependent lipid peroxidation (Stockwell, 2022). In favour of this hypothesis, we noticed several genes that showed significant moderate or high (more than two-fold) upregulation in ATG5-deficient LCs. These genes included ferroptosis-related genes such as *Hfe* (Homeostatic iron regulator), *Tfrc* (Transferrin receptor protein 1), *Ftl1* (Ferritin Light Chain), *Slc7a1* (Solute Carrier Family 7 Member 1), *Sat1* (Spermidine/Spermine N1-Acetyltransferase 1), *Lpcat3* (Lysophosphatidylcholine Acyltransferase 3). Finally, elevated expression of *Ptgs2* (Prostaglandin-Endoperoxide Synthase 2/Cyclooxygenase 2), and *Acsl4* (acyl-CoA synthetase long-chain family member 4) is considered as a strong indication of ongoing ferroptosis.

To confirm that lipid peroxidation occurs in the absence of functional autophagy, LCs were exposed to Bodipy-C11, a derivative of undecanoic acid that emits fluorescence upon oxidation. As expected, upon treatment with this compound, LCs harvested from $Atg5^{\Delta Cd207}$ mice displayed significantly higher fluorescence intensity than LCs of $Atg5^{WT}$ mice **(Figure 4K)**. Thus, our results indicate that oxidation of the lipids accumulated in ATG5-deficient LCs leads them to ferroptosis, thereby contributing to their progressive depletion from the epidermis.

Langerhans cells under metabolic stress alter cutaneous homeostasis

Besides metabolic imbalance, RNA sequencing revealed dysregulation of inflammation-related genes **(Figures S6E and 5A)**. In particular, autophagy-deficient LCs increased their expression of mRNA encoding IL-1α and chemokines CXCL1, CXCL2 and CXCL3, known to attract neutrophils through CXCR2. Despite this observation, no obvious signs of inflammation

were observed on the skin of $Atg5^{\Delta Cd207}$ mice: when analysing ear skin of 3-week-old mice for myeloid infiltrates **(Figure 5B)**, the proportions of Gr1$^+$ Ly6G$^+$ neutrophils or Gr1^{low} Ly6G$^-$ monocytes did not differ between $Atg5^{WT}$ and $Atg5^{\Delta Cd207}$ mice **(Figure 5C)**. Since NRLP3, a key inflammasome component, was markedly upregulated in LCs of $Atg5^{\Delta Cd207}$ mice, we challenged this pathway by injecting intradermally a small dose of alum hydroxide into the ears of 3-week-old mice. In $Atg5^{WT}$ mice, this resulted in only a modest increase of neutrophils **(Figure 5C)**, whereas monocytes were not significantly attracted **(Figure 5D)**. In contrast, alum hydroxide injection was able to drive monocyte infiltration into the ears of $Atg5^{\Delta Cd207}$ mice **(Figure 5D;** fold increases: x2.95 for $Atg5^{WT}$ and x8.86 for $Atg5^{\Delta Cd207}$). This outcome suggests that the presence of autophagy-deficient LCs increases sensitivity to proinflammatory challenge.

Several reports showed that a long-term absence of LCs leads to a decrease of intraepidermal nerve endings, although the pathways governing this remains unidentified (Zhang et al., 2021; Doss and Smith, 2014). Interestingly, autophagy-deficient LCs downregulated a set of genes involved in neuronal interactions and axonal guidance (GO:0045664, GO:0050808, GO:0071526, GO:0030031; **Figures S6E and 5E)**. Thus, we sought to investigate the epidermal neuronal network of mice aged 6 months and older. Since neuronal development is particularly sensitive to autophagy impairment (Hara et al., 2006), we chose to compare the density of LCs and epidermal sensory neurons of $Atg5^{WT}$ and $Atg5^{\Delta Cd207}$ mice with that of heterozygous $Atg5^{WT/-}$ mice **(Figure 5F)**. As expected for mice of this age, we observed a decrease in LC density in $Atg5^{\Delta Cd207}$ epidermis, but not in control mice **(Figure 5G)**. In parallel, quantification of β3-tubulin staining demonstrated that only $Atg5^{\Delta Cd207}$ mice presented significantly less epidermal nerve endings as compared to $Atg5^{WT}$ mice, although a slight reduction was observed in $Atg5^{WT/-}$ mice **(Figure 5H)**. Intriguingly, there was a stronger correlation of LC numbers with the density of epidermal nerve endings in $Atg5^{WT/-}$ and $Atg5^{WT}$ mice than in $Atg5^{\Delta Cd207}$ mice with complete deletion of $Atg5$ in LCs **(Figure S9).** This may imply that the remaining autophagy-deficient LCs were unable to support neuronal epidermal growth, in line with their decreased neuron-related transcripts. Altogether, in accordance with previous findings, LCs appear to play a crucial role in the extension of sensory neurons into the epidermis. Furthermore, the metabolic stress resulting from reduced autophagy may have an impact on the epidermal neuronal network.

DISCUSSION

In contrast to other types of DCs, epidermal LCs self-renew to maintain their population and they are exposed in the steady state to environmental conditions (hypoxia, irradiation) that may favour autophagy. We report here a major role for autophagy in LC homeostasis. When deprived of the key autophagy mediator ATG5, LCs displayed clear signs of lipid-related metabolic stress and underwent progressive depletion from the epidermis. They enhanced cutaneous immune infiltration upon inflammasome priming, and showed decreased transcription of innervation regulators, which is in accordance with a decreased network of epidermal nerves when these mice were aging.

The depletion of LCs was not due to their emigration or decreased proliferation, suggesting cell death as the most likely explanation. Our analyses excluded a significant contribution of the ER stress response and major mitochondrial damages. In the absence of autophagy, ferroptosis, implied from the upregulation of relevant detoxification pathways, was a consequence of uncontrolled supply of lipids and their peroxidation by ROS. Apoptosis may also occur in a relatively low proportion of ATG5-deficient LCs, as a result of the critically low ATP:AMP ratio (Liang et al., 2007) revealed by increased phosphorylation of AMPK.

The similar depletion of LCs observed using *Cd207*-specific *Atg7* deletion supports the idea that ATG5-dependent, non-autophagic functions, are not directly involved in the maintenance of LCs. We could also rule out lysosomal alterations or the impairment for endocytic mechanisms such as LAP, since the LC network appeared unperturbed in *Rubcn*^{-/-} mice. The importance of autophagy for other skin DC subsets *in vivo* has been investigated previously. An earlier report did not find any consequence on the maintenance for CD207^{+} cDC1, in line with our findings (Lee et al., 2010), although the absence of Vps34, which plays a role in autophagy and other biological pathways, resulted in the depletion of splenic cDC1 (Parekh et al., 2017). Recently, LAP in dermal cDC2 was found to be required to limit inflammation after UV exposure, without reported consequences on their homeostasis (Sil et al., 2020). Nevertheless, the ontogeny and features of LCs differ strikingly from those of other DC subsets (Doebel et al., 2017). Surprisingly, LCs had a continuous presence in skin-draining LNs, despite their depletion from the epidermis. This could be due to LCs remaining proliferative in older mice , which allowed the steady-state flux of LCs towards LNs to be kept constant. Emigration to LNs also entails a major environmental change as compared to the epidermis, and this may be beneficial to extended survival of LCs.

The metabolic requirements of LCs have never been studied and can only be extrapolated from those of keratinocytes nearby. In the epidermal layer where they reside, LCs are distant from dermal blood capillaries and have limited access to glucose and oxygen. Interestingly, epidermal hypoxia appears to regulate the functional properties of human LCs (Pierobon et al., 2016). Hypoxic tissues exhibit low levels of phosphorylated Akt (Bedogni et al., 2005), which is expected to promote autophagy. LCs attempted to compensate autophagy impairment by inhibiting the PI3K/Akt pathway: they decreased expression of Inositol-3-phosphate synthase 1 (*Isyna1*) and of TNF-α-induced protein 8-like protein 3 (*Tnfaip8l3*), which shuttles PIP2 and PIP3 across the plasma membrane (Fayngerts et al., 2014), whereas Protein Kinase C beta (*Prkcb*) was upregulated.

Although historically autophagy has been shown to be regulated through mTOR complex (in particular under energetic stress), it is now clear that several induction pathways coexist with constitutive activity, especially in immune cells. Intriguingly, progressive disappearance of epidermal LCs at a young age has been reported in mice with selective disruption of critical intermediates of the mTOR pathway (Kellersch and Brocker, 2013; Sparber et al., 2015, 2014). Therefore, since mTOR is recognized as a negative regulator of autophagy, it could be interpreted that excessive autophagy is detrimental to LCs. However, autophagy has not been investigated in these mouse models. In addition, mTOR regulates many other cellular

processes and, beyond autophagy, is critical to survival, lysosomal trafficking or cytokine signalling pathways. By impairing the recycling of receptors through lysosomes, LAMTOR2 deletion leads to a defect in TGF-β signalling, which is essential for the differentiation of LCs (Kaplan et al., 2007). Moreover, LCs deficient in Raptor, an adaptor of the mTOR complex 1, leave the epidermis, which may also result from an impaired TGF-β signalling that normally maintains the epidermal LC network by restricting their spontaneous migration to skin-draining LNs (Kel et al., 2010; Bobr et al., 2012). Altogether, there is no direct evidence to date that the deleterious impact of genetic ablations affecting the mTOR pathway in LCs may depend solely on altered autophagy.

ATG5-deficient LCs displayed an accumulation of lipid droplets that likely resulted from impaired lipophagy. Of note, a similar phenotype was recently reported for LCs of psoriatic lesions in both patients and mouse models (Zhang et al., 2022). In the absence of autophagy, LCs did not promote glycolysis and were unable to take advantage of their increased respiratory capacity linked to higher mitochondrial mass, highlighting the critical importance of lipophagy for their energy production. The limited ER swelling observed in our model, which was not sufficient to trigger the UPR pathway in LCs, may be related to defective energy mobilisation from lipid storage (Cubillos-Ruiz et al., 2015; Velázquez et al., 2016), multiple budding of lipid droplets (Gao et al., 2019) or modification of ER membrane dynamics following lipid peroxidation (Agmon et al., 2018). Accumulation of lipid droplets as a result of an impaired autophagy machinery has been observed in other cell types that rely on lipophagy. This catabolic process is key in the development of neutrophils (Riffelmacher et al., 2017). Of note, DCs derived from $Atg5^{-/-}$ bone marrow display elevated CD36 expression and lipid droplets, although no cell death was reported during the time frame of this *in vitro* experiment (Oh and Lee, 2019). Yet, the lifespan of bone marrow-derived or conventional DCs is not comparable to that of LCs, for alterations in lipid metabolism may have deleterious consequences when they accumulate in the long term. Considering that CD207 is expressed in LCs about 10 days after birth (Tripp et al., 2004), the time period at which LC depletion becomes visible (around 20 days of age) suggests that they cannot survive more than 2 weeks to autophagy deficiency in the steady state. This represents a relatively short delay as compared to other, unrelated cell types previously found to rely on autophagy, i.e. B-1 B cells that survive 6 weeks after deletion of *Atg5* (Clarke et al., 2018).

Some features of LCs are reminiscent of tissue-resident macrophages (Doebel et al., 2017). Although autophagy regulates many functions of macrophages, it was not considered to play a prominent role in their homeostatic maintenance (Wu and Lu, 2019). It was only recently reported that a lack of autophagy affects the survival of a subset of peritoneal macrophages (Xia et al., 2020). Interestingly, similar to steady-state LCs, this subset is of embryonic rather than monocytic origin. It remains to be demonstrated whether the dependence on autophagy can be associated with the origin and/or long-term residency for macrophages within other organs.

The consequences for the epidermis of a long-term absence of LCs have been investigated through constitutive diphtheria toxin-mediated depletion in the huLangerin-DTA mouse strain

(Su et al., 2020; Zhang et al., 2021). However, since LCs are absent from birth, it is difficult to identify which of the genes that they normally express may affect epidermal homeostasis. Here, we were able to document transcriptome alterations of ATG5-deficient LCs that are still present in young mice, albeit in a metabolically stressed state. First and foremost, our data suggested a potential for supporting inflammation. Immune infiltration did not occur spontaneously, which could be explained by the fact that autophagy-deficient LCs progressively disappear, limiting their capacity to induce inflammation. Nevertheless, a challenge by inflammasome agonist alum hydroxide resulted in a larger immune infiltration, especially involving monocytes, in mice where LCs were impaired for autophagy. Secondly, several genes involved in neuronal interactions were downregulated by ATG5-deficient LCs, including EPH receptor A1, Semaphorin 4A, Neuropilin-1 and Neuregulin-1. The long-term absence of LCs in our model led to a decrease of epidermal nerve endings. These findings thus represent a milestone for future investigations on neuroimmune interactions, considering the putative role of LCs and dermal macrophages (Kolter et al., 2019) in regulating sensory neuron growth and repair in the skin.

Altogether, we shed light on the metabolic adaptations of LCs that ensure their long-lasting tissue residency. It will be of great interest to translate these findings in the context of human skin diseases, considering that lipid supply and autophagy capacity of LCs may perturb their homeostasis and favour inflammation.

MATERIAL AND METHODS

Mice

Mice were bred and maintained on a C57BL/6J background at the animal facility of the Institut de Biologie Moléculaire et Cellulaire (IBMC). *Atg5$^{flox/flox}$* and *Cd207-cre* mice were gifted by N. Mizushima and B.E. Clausen, respectively (Hara et al., 2006; Zahner et al., 2011). *Atg5$^{+/-}$* mice were generated at the IBMC (Arnold et al., 2016). [*Atg5$^{+/-}$* ; *Cd207-cre*] were obtained from a first cross between *Cd207-cre* and *Atg5$^{+/-}$*, then bred to *Atg5$^{flox/flox}$* to obtain [*Atg5$^{flox/-}$* ; *Cd207-cre*] (*Atg5^{ΔCd207}*) and littermates [*Atg5$^{flox/+}$* ; *Cd207-cre*] (*Atg5$^{WT/Δ}$*) and [*Atg5$^{flox/+}$*] (*Atg5^{WT}*). Mice were genotyped for their *Atg5* allele and the *Cd207-cre* transgene as previously described (Arnold et al., 2016; Zahner et al., 2011). All mice were bred and maintained in accordance with guidelines of the local institutional Animal Care and Use Committee (CREMEAS).

Antibodies and reagents for flow cytometry and immunofluorescence microscopy

Antibody stainings for flow cytometry or immunofluorescent microscopy were performed in SE buffer (Fetal Calf Serum 2%, EDTA 2.5mM). All reagents and antibodies are listed in **Table 1.**

Cell preparation and culture

Lymph nodes: Brachial and inguinal lymph nodes were digested for 1h at 37°C under shaking in R2 buffer (RPMI-1640 medium containing L-glutamine (Lonza) plus 2% fetal calf serum (Dutscher)) supplemented with 50µg/mL DNAse and 10µg/mL collagenase D (Roche).

Digestion of back skin epidermis (electron microscopy, LC proportions, caspase-3 activation, proliferation assays): Back skin was incubated with 0.5% Trypsin (VWR) for 45min at 37°C. After removal of the dermis, the epidermis was teased apart with forceps, followed by 15min of gentle shaking on a rotating wheel. Where indicated, CD11b$^+$ LCs were enriched by magnetic bead separation (Miltenyi-Biotec).

Ear skin digestion (skin DC subsets, quantification of immune infiltrates): Ear skin were cut into small pieces, digested in R2 buffer containing 0.15mg/ml LiberaseTM and 0.12mg/ml DNAse (Roche) for 45min at 37°C and filtered through 100µm cell strainers.

Epidermal crawl-out assay (Bodipy C16 and glucose uptake, in vitro treatment with inhibitors, Seahorse assay): Back skin was incubated overnight at 4°C in R2 buffer, containing 1mg/mL dispase II (Roche). The separated epidermis was then laid upon cell culture medium (RPMI medium supplemented with 10% fetal calf serum, 50mM β-Mercaptoethanol, (Gibco), 1% Gentamicin (Gibco), and 10mM HEPES (Lonza)) in a Petri dish for 24h at 37°C, allowing emigration of LCs.

Bone marrow-derived DCs: Femurs and tibias were collected from C57BL/6 mice. Bone marrow was flushed out, red blood cells lysed, filtered and cultured for 7 days in complete RPMI medium (RPMI-1640 medium containing L-glutamine plus 10% fetal calf serum) containing 20ng/mL recombinant GM-CSF (Peprotech).

Induction of cutaneous inflammation

For each mouse, one ear was injected intradermally with 25µL of 100µg/mL alum hydroxide (Roche), and the contralateral ear was left untreated. 4h later, whole skin was digested and cell suspensions were monitored by flow cytometry for $CD45^+$ $CD3^-$ $CD11b^+$ $Gr1^+$ $Ly6G^+$ neutrophils and $CD45^+$ $CD3^-$ $CD11b^+$ $Gr1^+$ $Ly6G^-$ monocytes.

Electron microscopy

Epidermal cell suspensions (freshly isolated or cultured for 3 days) were processed for electron microscopy essentially as described (Cavinato et al., 2017). Briefly, after pre-enrichment on bovine serum albumin density gradient, cells were washed and fixed using Karnovsky's formaldehyde-glutaraldehyde fixative for 1h at room temperature. Specimens were post-fixed in aqueous 3% osmium tetroxide and contrasted with 0.5% veronal-buffered uranyl acetate. Dehydration of samples was done in graded series of ethanol concentrations, followed by embedding in Epon 812 resin. Ultrathin sections were mounted on nickel grids, contrasted with lead citrate and examined by transmission electron microscopy (Phillips EM 400; Fei Company Electron Optics, Eindhoven, The Netherlands) at an operating voltage of 80kV. LCs were identified within epidermal cell suspensions by their electron-lucent cytoplasm, the absence of keratin tonofilament bundles, the presence of cytoplasmic processes (dendrites) and their ultrastructural hallmarks, the Birbeck granules.

Autophagy flux assessment by flow cytometry.

Measurements of autophagy fluxes were carried out using the Guava Autophagy LC3 Antibody-based Detection Kit (Luminex). LCs isolated through epidermal crawl-outs were cultured 18h at 37°C with or without the lysosome inhibitor provided with the kit (60 µM hydroxychloroquine). After labelling by FVD450, cells were stained for CD45, I-A/I-E, and TCRγ/δ. Cells were permeabilized with 0.05% saponin (Merck Millipore) to wash out the cytosolic LC3-I, then membrane-associated LC3 (LC3-II) was preferentially stained with anti-LC3 FITC (clone 4E12). Flow cytometry analysis allowed to calculate autophagy fluxes, dividing the LC3-FITC mean fluorescence intensities of treated cells by that of untreated cells.

Glucose uptake

Cells obtained by crawl-out were glucose-starved for 24h in PBS (Lonza) supplemented with 0.5% fetal calf serum for 8 hours. Cells were then incubated for 30min at 37°C with 150µM of 2-[N-(7-nitrobenz-2-oxa-1,3-diazol-4-yl) amino]-2-deoxy-D-glucose (ThermoFisher).

Pharmacological inhibitions

Cells obtained by crawl-out were incubated for 24h at 37°C with the phosphatidylinositol-3-kinase inhibitor wortmannin **or the** carnitine palmitoyltransferase-1 inhibitor etomoxir (both from **Sigma-Aldrich),** at 10 and 200µM respectively.

5-bromo-2'-deoxyuridine incorporation

1mg of 5-bromo-2'-deoxyuridine (BrdU; Sigma) was administered by intraperitoneal injection 72 hours prior to analysis. Drinking water also contained 0.8mg/mL BrdU. Following staining of surface markers CD45, I-A/I-E and TCRγδ, epidermal single-cell suspensions were fixed with Cytofix/Cytoperm buffer (BD Biosciences) and permeabilized with permeabilization buffer (BD

Biosciences). DNA was then denatured with a DNAse solution (100µg/mL, BD Biosciences) to improve the accessibility of the incorporated BrdU to the detection antibody.

Quantitative real-time RT-PCR analysis

RNA was extracted from cells sorted from lymph nodes on a FACS Aria cell sorter (BD Biosciences) with RNeasy microKit (Qiagen). cDNA was obtained with Maxima Reverse Transcriptase Kit (ThermoFisher) using a T100 Thermal cycler (Biorad). Quantitative real-time PCR was performed on cDNA using Taqman preAmp MasterMix and Taqman Universal Mastermix (ThermoFisher) and Assays-on-Demand probes (*Gapdh*: Mm03302249_g1; *Atg5: Mm00504340_m1*). Each sample was amplified in triplicate in a StepOnePlus real-time PCR system (Applied Biosystems). mRNA levels were calculated with the StepOne v2.1 software (Applied Biosystems), using the comparative cycle threshold method, and normalized to the mean expression of *Gapdh* housekeeping gene.

Immunofluorescence microscopy of epidermal sheets

Ear epidermis was separated from the dermis by ammonium thiocyanate digestion (0.15M) for 20min at 37°C. Alternatively, for optimal preservation of neuronal networks, epidermal sheets were separated after 10mM EDTA diluted in PBS for 1h. Epidermis was then fixed by incubation in PBS 4% PFA or in glacial acetone for 15min at 4°C followed by incubation with PBS 5% BSA 0.1% Triton. Primary antibodies were incubated overnight at 4°C. After fixation, epidermal sheets were washed four times in blocking buffer consisting in 5% BSA in PBS for 15 minutes each time at room temperature. Sheets were then incubated overnight at 4°C with the primary antibodies: anti-β3-tubulin and AF647 anti-CD207 diluted in blocking buffer. After washing the sheets as described above, they were incubated with a solution of goat anti-mouse AF594, and 4',6-diamidino-2-phenylindole (DAPI) in blocking buffer for 1h at room temperature. After additional washings, epidermal sheets were mounted in Fluoromount-G mounting medium (ThermoFisher) and observed under a confocal microscope (Yokogawa Spinning Disk, Zeiss). Whole-mount epidermal images were processed using the open-source software FIJI to measure the total analysed area for each sample and to quantify the mean fluorescence intensity.

Immunofluorescence microscopy of epidermal cell suspensions

Cell suspensions were deposited on Lab-Tek chamber slides (Thermo Scientific Nunc) previously coated with a poly-L-Lysine solution (Sigma-Aldrich) diluted in ultra-pure water at 0.02% (v/v) to enhance cellular adhesion. Epidermal cells were then incubated with Mitotracker, Mitosox, ER-tracker, Bodipy or Bodipy-C16 according to the manufacturer's instructions (Invitrogen), before fixation using 2% PFA in PBS for 15min at RT. DAPI was incubated 15min at RT. Tissues were mounted and observed under a confocal microscope (Yokogawa Spinning Disk, Zeiss).

RNA sequencing

Total RNA was isolated from 10^5 sorted LCs with the RNeasy Mini Kit (Qiagen). RNA integrity was evaluated on an Agilent Bioanalyzer 2100 (Agilent Technologies). Total RNA Sequencing libraries were prepared with SMARTer® Stranded Total RNA-Seq Kit v2 - Pico Input Mammalian

(TaKaRa) according to the manufacturer's protocol. Briefly, random priming was used for first strand synthesis and ribosomal cDNA has been cleaved by ZapR v2 in the presence of mammalian R-probes V2. Libraries were pooled and sequenced (paired-end 2*75bp) on a NextSeq500 using the NextSeq 500/550 High Output Kit v2 according to the manufacturer's instructions (Illumina). For analysis, quality control of each sample was carried out and assessed with the NGS Core Tools FastQC (http://www.bioinformatics.babraham.ac.uk/projects/fastqc/). Sequence reads were mapped on the GRCm38 reference genome using STAR (Dobin et al., 2013) and unmapped reads were remapped with Bowtie2 (Langmead and Salzberg, 2012) using a very sensitive local option to optimize the alignment. The total mapped reads were finally available in BAM (Binary Alignment Map) format for raw read counts extraction. Read counts were found by the HTseq-count tool of the Python package HTSeq (Anders et al., 2015) with default parameters to generate an abundance matrix. At last, differential analyses were performed using the DEseq2 (Love et al., 2014) package of the Bioconductor framework. Differentially expressed genes between $Atg5^{\Delta Cd207}$ and $Atg5^{WT}$ were selected based on the combination of adjusted p-value < 0.05 and FDR < 0.1. Pathway enrichment analysis was performed using Metascape (https://metascape.org) (Zhou et al., 2019).

Metabolic parameter quantitation by extracellular flux assay

$CD45^+$ $MHCII^+$ $CD207^+$ $CD103^-$ $TCR\gamma\delta^-$ LCs were sorted from epidermal crawl-out suspensions on a FACSFusion cell sorter (Becton-Dickinson). Purified LCs or BMDCs (2.10^5 cells/well) were seeded in Seahorse XF96 culture plate coated with poly-lysine (Sigma). After overnight culture, a Mitochondrial Stress Test was performed. In this assay, culture wells are injected sequentially with different inhibitors of the mitochondrial respiration. Energy production resulting from mitochondrial respiration was determined after each injection by measuring oxygen consumption rates (OCR, pmoles/min) on a Seahorse XF96 according to the manufacturer's instructions (Agilent). Oligomycin (OM) injection allowed calculating the oxygen consumption used for mitochondrial ATP synthesis. Carbonyl cyanide 4-(trifluoromethoxy)phenylhydrazone (FCCP) uncoupled mitochondrial respiration, allowing to calculate maximal respiration and spare respiratory capacity. Finally, rotenone (ROT) and antimycin A (AA) blocked mitochondrial complex I and III to determine the non-mitochondrial oxygen consumption. The following metabolic parameters were calculated:

ATP production = $OCR_{baseline} - OCR_{OM}$

Maximum respiration = $OCR_{FCCP} - OCR_{AA+ROT}$

Spare respiratory capacity (SRC) = $OCR_{FCCP} - OCR_{baseline}$

Lipid peroxidation assay

Upon enrichment in $CD11b^+$ epidermal cells using magnetic bead separation (Miltenyi-Biotec), at least 50 000 cells were seeded and incubated for 10min at 37ºC with 2mM Bodipy-C11 (581/591) (4,4-difluoro-5,7-dimethyl-4-bora-3a,4a-diaza-s-indacene-3-undecanoic acid; Invitrogen) in PBS. Cells were then resuspended in SE buffer and incubated with the following antibodies: CD3e-PerCP-Cy5.5, MHC-II-AF700 and CD45-APC-Cy7. Upon gating on $CD45^+$ CD3-

MHCII^{+} cells, the fluorescence of Bodipy-C11 was collected from the FITC channel on a Gallios cytometer (Beckman-Coulter).

Quantification of the density of epidermal nerve endings

The open-source software iLastik was used to segmentate images of whole-mount epidermal sheets stained for β3-tubulin and CD207, using machine learning to differentiate background from b3-tubulin signal. Images were then processed using the open-source software FIJI to measure the total area of each scan, as well as the area that was determined positive for b3-tubulin.

Statistical analyses

Statistical significance was calculated with the indicated tests using Prism software (GraphPad, versions 6-9). All data were presented as mean ± standard error of the mean (SEM). P-values < 0.05 were considered statistically significant (*, $p<0.05$, **, $p<0.01$, ***, $p<0.001$, ****,$p<0.0001$).

AUTHOR CONTRIBUTIONS

F.A, F.G. and V.F. designed the research.

N.R. contributed electron microscopy images.

B.E.C. , E.L.G. and T.H. contributed essential reagents and critically reviewed the paper

F.A, D.B., W.B., R.S.-C., Q.F., L.F., R.F., F.G. and V.F. performed the experiments.

O.G. and H.P. helped design and analyze the metabolic measurement assays

R.C., A.M., S.B. and B.V. designed and analyzed the RNA sequencing assay

F.A, W.B., R.S.-C, J.-D.F., F.G. and V.F. analyzed the data.

F.A, C.G.M., F.G. and V.F. wrote the paper.

Bibliography

Agmon, E., J. Solon, P. Bassereau, and B.R. Stockwell. 2018. Modeling the effects of lipid peroxidation during ferroptosis on membrane properties. *Sci Rep*. 8:5155. doi:10.1038/s41598-018-23408-0.

Alissafi, T., A. Banos, L. Boon, T. Sparwasser, A. Ghigo, K. Wing, D. Vassilopoulos, D. Boumpas, T. Chavakis, K. Cadwell, and P. Verginis. 2017. Tregs restrain dendritic cell autophagy to ameliorate autoimmunity. *J Clin.Invest*. 127:2789–2804. doi:10.1172/JCI92079.

Anders, S., P.T. Pyl, and W. Huber. 2015. HTSeq--a Python framework to work with high-throughput sequencing data. *Bioinformatics*. 31:166–169. doi:10.1093/bioinformatics/btu638.

Anding, A.L., and E.H. Baehrecke. 2017. Cleaning House: Selective Autophagy of Organelles. *Dev.Cell*. 41:10–22. doi:10.1016/j.devcel.2017.02.016.

Arbogast, F., J. Arnold, P. Hammann, L. Kuhn, J. Chicher, D. Murera, J. Weishaar, S. Muller, J.D. Fauny, and F. Gros. 2018. ATG5 is required for B cell polarization and presentation of particulate antigens. *Autophagy*. 1–15. doi:10.1080/15548627.2018.1516327.

Arnold, J., D. Murera, F. Arbogast, J.D. Fauny, S. Muller, and F. Gros. 2016. Autophagy is dispensable for B-cell development but essential for humoral autoimmune responses. *Cell Death.Differ*. 23:853–864. doi:10.1038/cdd.2015.149.

Bah, A., and I. Vergne. 2017. Macrophage Autophagy and Bacterial Infections. *Front Immunol*. 8:1483. doi:10.3389/fimmu.2017.01483.

Bedogni, B., S.M. Welford, D.S. Cassarino, B.J. Nickoloff, A.J. Giaccia, and M.B. Powell. 2005. The hypoxic microenvironment of the skin contributes to Akt-mediated melanocyte transformation. *Cancer Cell*. 8:443–454. doi:10.1016/j.ccr.2005.11.005.

Bedoui, S., P.G. Whitney, J. Waithman, L. Eidsmo, L. Wakim, I. Caminschi, R.S. Allan, M. Wojtasiak, K. Shortman, F.R. Carbone, A.G. Brooks, and W.R. Heath. 2009. Cross-presentation of viral and self antigens by skin-derived CD103+ dendritic cells. *Nat.Immunol*. 10:488–495.

Bennett, C.L., E. van Rijn, S. Jung, K. Inaba, R.M. Steinman, M.L. Kapsenberg, and B.E. Clausen. 2005. Inducible ablation of mouse Langerhans cells diminishes but fails to abrogate contact hypersensitivity. *J.Cell.Biol*. 169:569–576.

Bobr, A., B.Z. Igyarto, K.M. Haley, M.O. Li, R.A. Flavell, and D.H. Kaplan. 2012. Autocrine/paracrine TGF-beta1 inhibits Langerhans cell migration. *Proc.Natl.Acad.Sci.U.S.A*. 109:10492–10497. doi:10.1073/pnas.1119178109.

Cavinato, M., R. Koziel, N. Romani, R. Weinmüllner, B. Jenewein, M. Hermann, S. Dubrac, G. Ratzinger, J. Grillari, M. Schmuth, and P. Jansen-Dürr. 2017. UVB-Induced Senescence of Human Dermal Fibroblasts Involves Impairment of Proteasome and Enhanced Autophagic Activity. *J Gerontol A Biol Sci Med Sci*. 72:632–639. doi:10.1093/gerona/glw150.

Chorro, L., A. Sarde, M. Li, K.J. Woollard, P. Chambon, B. Malissen, A. Kissenpfennig, J.B. Barbaroux, R. Groves, and F. Geissmann. 2009. Langerhans cell (LC) proliferation mediates neonatal development, homeostasis, and inflammation-associated expansion of the epidermal LC network. *J Exp Med*. 206:3089–3100. doi:10.1084/jem.20091586.

Clarke, A.J., T. Riffelmacher, D. Braas, R.J. Cornall, and A.K. Simon. 2018. B1a B cells require autophagy for metabolic homeostasis and self-renewal. *J Exp.Med.* 215:399–413. doi:10.1084/jem.20170771.

Clarke, A.J., and A.K. Simon. 2018. Autophagy in the renewal, differentiation and homeostasis of immune cells. *Nat.Rev.Immunol.* doi:10.1038/s41577-018-0095-2.

Cloherty, A.P.M., N.H. van Teijlingen, T.-J.T.H.D. Eisden, J.L. van Hamme, A.G. Rader, T.B.H. Geijtenbeek, R.R.C.E. Schreurs, and C.M.S. Ribeiro. 2021. Autophagy-enhancing drugs limit mucosal HIV-1 acquisition and suppress viral replication ex vivo. *Sci Rep*. 11:4767. doi:10.1038/s41598-021-84081-4.

Cubillos-Ruiz, J.R., P.C. Silberman, M.R. Rutkowski, S. Chopra, A. Perales-Puchalt, M. Song, S. Zhang, S.E. Bettigole, D. Gupta, K. Holcomb, L.H. Ellenson, T. Caputo, A.-H. Lee, J.R. Conejo-Garcia, and L.H. Glimcher. 2015. ER Stress Sensor XBP1 Controls Anti-tumor Immunity by Disrupting Dendritic Cell Homeostasis. *Cell*. 161:1527–1538. doi:10.1016/j.cell.2015.05.025.

Dang, A.T., R.M. Teles, P.T. Liu, A. Choi, A. Legaspi, E.N. Sarno, M.T. Ochoa, K. Parvatiyar, G. Cheng, M. Gilliet, B.R. Bloom, and R.L. Modlin. 2019. Autophagy links antimicrobial activity with antigen presentation in Langerhans cells. *JCI Insight*. 4. doi:10.1172/jci.insight.126955.

Dobin, A., C.A. Davis, F. Schlesinger, J. Drenkow, C. Zaleski, S. Jha, P. Batut, M. Chaisson, and T.R. Gingeras. 2013. STAR: ultrafast universal RNA-seq aligner. *Bioinformatics*. 29:15–21. doi:10.1093/bioinformatics/bts635.

Doebel, T., B. Voisin, and K. Nagao. 2017. Langerhans Cells - The Macrophage in Dendritic Cell Clothing. *Trends Immunol*. 38:817–828. doi:10.1016/j.it.2017.06.008.

Doss, A.L.N., and P.G. Smith. 2014. Langerhans cells regulate cutaneous innervation density and mechanical sensitivity in mouse footpad. *Neurosci Lett*. 578:55–60. doi:10.1016/j.neulet.2014.06.036.

Fayngerts, S.A., J. Wu, C.L. Oxley, X. Liu, A. Vourekas, T. Cathopoulis, Z. Wang, J. Cui, S. Liu, H. Sun, M.A. Lemmon, L. Zhang, Y. Shi, and Y.H. Chen. 2014. TIPE3 is the transfer protein of lipid second messengers that promote cancer. *Cancer Cell*. 26:465–478. doi:10.1016/j.ccr.2014.07.025.

Flacher, V., C.H. Tripp, D.G. Mairhofer, R.M. Steinman, P. Stoitzner, J. Idoyaga, and N. Romani. 2014. Murine Langerin+ dermal dendritic cells prime CD8+ T cells while Langerhans cells induce cross-tolerance. *EMBO Mol Med*. 6:1191–1204. doi:10.15252/emmm.201303283.

Galluzzi, L., F. Pietrocola, B. Levine, and G. Kroemer. 2014. Metabolic control of autophagy. *Cell*. 159:1263–1276. doi:10.1016/j.cell.2014.11.006.

Gao, M., X. Huang, B.-L. Song, and H. Yang. 2019. The biogenesis of lipid droplets: Lipids take center stage. *Prog Lipid Res*. 75:100989. doi:10.1016/j.plipres.2019.100989.

Ghigo, C., I. Mondor, A. Jorquera, J. Nowak, S. Wienert, S.P. Zahner, B.E. Clausen, H. Luche, B. Malissen, F. Klauschen, and M. Bajenoff. 2013. Multicolor fate mapping of Langerhans cell homeostasis. *J Exp Med.* 210:1657–1664. doi:10.1084/jem.20130403.

Ghislat, G., and T. Lawrence. 2018. Autophagy in dendritic cells. *Cell Mol.Immunol.* 15:944–952. doi:10.1038/cmi.2018.2.

Grootjans, J., A. Kaser, R.J. Kaufman, and R.S. Blumberg. 2016. The unfolded protein response in immunity and inflammation. *Nat Rev Immunol*. 16:469–484. doi:10.1038/nri.2016.62.

Hara, T., K. Nakamura, M. Matsui, A. Yamamoto, Y. Nakahara, R. Suzuki-Migishima, M. Yokoyama, K. Mishima, I. Saito, H. Okano, and N. Mizushima. 2006. Suppression of basal autophagy in neural cells causes neurodegenerative disease in mice. *Nature*. 441:885–889. doi:10.1038/nature04724.

Heckmann, B.L., and D.R. Green. 2019. LC3-associated phagocytosis at a glance. *J Cell Sci*. 132. doi:10.1242/jcs.222984.

Henri, S., L.F. Poulin, S. Tamoutounour, L. Ardouin, M. Guilliams, B. de Bovis, E. Devilard, C. Viret, H. Azukizawa, A. Kissenpfennig, and B. Malissen. 2010. CD207+ CD103+ dermal dendritic cells cross-present keratinocyte-derived antigens irrespective of the presence of Langerhans cells. *J.Exp.Med.* 207:189–206.

Herzig, S., and R.J. Shaw. 2018. AMPK: guardian of metabolism and mitochondrial homeostasis. *Nat Rev Mol Cell Biol*. 19:121–135. doi:10.1038/nrm.2017.95.

Hoeffel, G., Y. Wang, M. Greter, P. See, P. Teo, B. Malleret, M. Leboeuf, D. Low, G. Oller, F. Almeida, S.H. Choy, M. Grisotto, L. Renia, S.J. Conway, E.R. Stanley, J.K. Chan, L.G. Ng, I.M. Samokhvalov, M. Merad, and F. Ginhoux. 2012. Adult Langerhans cells derive predominantly from embryonic fetal liver monocytes with a minor contribution of yolk sac-derived macrophages. *J Exp Med.* 209:1167–1181. doi:10.1084/jem.20120340.

Igyarto, B.Z., K. Haley, D. Ortner, A. Bobr, M. Gerami-Nejad, B.T. Edelson, S.M. Zurawski, B. Malissen, G. Zurawski, J. Berman, and D.H. Kaplan. 2011. Skin-resident murine dendritic cell subsets promote distinct and opposing antigen-specific T helper cell responses. *Immunity.* 35:260–272. doi:10.1016/j.immuni.2011.06.005.

Kamath, A.T., S. Henri, F. Battye, D.F. Tough, and K. Shortman. 2002. Developmental kinetics and lifespan of dendritic cells in mouse lymphoid organs. *Blood*. 100:1734–1741.

Kaplan, D.H. 2017. Ontogeny and function of murine epidermal Langerhans cells. *Nat.Immunol.* 18:1068–1075. doi:10.1038/ni.3815.

Kaplan, D.H., M.O. Li, M.C. Jenison, W.D. Shlomchik, R.A. Flavell, and M.J. Shlomchik. 2007. Autocrine/paracrine TGFbeta1 is required for the development of epidermal Langerhans cells. *J.Exp.Med.* 204:2545–2552.

Kashem, S.W., B.Z. Igyarto, M. Gerami-Nejad, Y. Kumamoto, J. Mohammed, E. Jarrett, R.A. Drummond, S.M. Zurawski, G. Zurawski, J. Berman, A. Iwasaki, G.D. Brown, and D.H. Kaplan. 2015. Candida albicans Morphology and Dendritic Cell Subsets Determine T Helper Cell Differentiation. *Immunity.* 42:356–366. doi:10.1016/j.immuni.2015.01.008.

Kel, J.M., M.J.H. Girard-Madoux, B. Reizis, and B.E. Clausen. 2010. TGF-beta is required to maintain the pool of immature Langerhans cells in the epidermis. *J Immunol*. 185:3248–3255. doi:10.4049/jimmunol.1000981.

Kellersch, B., and T. Brocker. 2013. Langerhans cell homeostasis in mice is dependent on mTORC1 but not mTORC2 function. *Blood*. 121:298–307. doi:10.1182/blood-2012-06-439786.

Kim, S.J., G.H. Syed, M. Khan, W.W. Chiu, M.A. Sohail, R.G. Gish, and A. Siddiqui. 2014. Hepatitis C virus triggers mitochondrial fission and attenuates apoptosis to promote viral persistence. *Proc.Natl.Acad.Sci.U.S.A*. 111:6413–6418. doi:10.1073/pnas.1321114111.

Kolter, J., R. Feuerstein, P. Zeis, N. Hagemeyer, N. Paterson, P. d'Errico, S. Baasch, L. Amann, T. Masuda, A. Losslein, K. Gharun, M. Meyer-Luehmann, C. Waskow, C.W. Franzke, D. Grun, T. Lammermann, M. Prinz, and P. Henneke. 2019. A Subset of Skin Macrophages Contributes to the Surveillance and Regeneration of Local Nerves. *Immunity.* 50:1482–1497. doi:10.1016/j.immuni.2019.05.009.

Kounakis, K., M. Chaniotakis, M. Markaki, and N. Tavernarakis. 2019. Emerging Roles of Lipophagy in Health and Disease. *Front Cell Dev Biol*. 7:185. doi:10.3389/fcell.2019.00185.

Langmead, B., and S.L. Salzberg. 2012. Fast gapped-read alignment with Bowtie 2. *Nat Methods*. 9:357–359. doi:10.1038/nmeth.1923.

Lee, H.K., L.M. Mattei, B.E. Steinberg, P. Alberts, Y.H. Lee, A. Chervonsky, N. Mizushima, S. Grinstein, and A. Iwasaki. 2010. In vivo requirement for Atg5 in antigen presentation by dendritic cells. *Immunity.* 32:227–239.

Liang, J., S.H. Shao, Z.-X. Xu, B. Hennessy, Z. Ding, M. Larrea, S. Kondo, D.J. Dumont, J.U. Gutterman, C.L. Walker, J.M. Slingerland, and G.B. Mills. 2007. The energy sensing LKB1–AMPK pathway regulates p27kip1 phosphorylation mediating the decision to enter autophagy or apoptosis. *Nat Cell Biol*. 9:218–224. doi:10.1038/ncb1537.

Love, M.I., W. Huber, and S. Anders. 2014. Moderated estimation of fold change and dispersion for RNA-seq data with DESeq2. *Genome Biol*. 15:550. doi:10.1186/s13059-014-0550-8.

Merad, M., M.G. Manz, H. Karsunky, A. Wagers, W. Peters, I. Charo, I.L. Weissman, J.G. Cyster, and E.G. Engleman. 2002. Langerhans cells renew in the skin throughout life under steady-state conditions. *Nat.Immunol.* 3:1135–1141.

Mintern, J.D., C. Macri, W.J. Chin, S.E. Panozza, E. Segura, N.L. Patterson, P. Zeller, D. Bourges, S. Bedoui, P.J. McMillan, A. Idris, C.J. Nowell, A. Brown, K.J. Radford, A.P. Johnston, and J.A. Villadangos. 2015. Differential use of autophagy by primary dendritic cells specialized in cross-presentation. *Autophagy.* 11:906–917. doi:10.1080/15548627.2015.1045178.

Müller, G., C. Lübow, and G. Weindl. 2020. Lysosomotropic beta blockers induce oxidative stress and IL23A production in Langerhans cells. *Autophagy*. 16:1380–1395. doi:10.1080/15548627.2019.1686728.

Munz, C. 2015. Of LAP, CUPS, and DRibbles - Unconventional Use of Autophagy Proteins for MHC Restricted Antigen Presentation. *Front Immunol*. 6:200. doi:10.3389/fimmu.2015.00200.

Murera, D., F. Arbogast, J. Arnold, D. Bouis, S. Muller, and F. Gros. 2018. CD4 T cell autophagy is integral to memory maintenance. *Sci.Rep.* 8:5951. doi:10.1038/s41598-018-23993-0.

Oh, D.S., and H.K. Lee. 2019. Autophagy protein ATG5 regulates CD36 expression and anti-tumor MHC class II antigen presentation in dendritic cells. *Autophagy*. 15:2091–2106. doi:10.1080/15548627.2019.1596493.

Parekh, V.V., S.K. Pabbisetty, L. Wu, E. Sebzda, J. Martinez, J. Zhang, and K.L. Van. 2017. Autophagy-related protein Vps34 controls the homeostasis and function of antigen cross-presenting CD8alpha(+) dendritic cells. *Proc.Natl.Acad.Sci.U.S.A*. 114:E6371–E6380. doi:10.1073/pnas.1706504114.

Pengo, N., M. Scolari, L. Oliva, E. Milan, F. Mainoldi, A. Raimondi, C. Fagioli, A. Merlini, E. Mariani, E. Pasqualetto, U. Orfanelli, M. Ponzoni, R. Sitia, S. Casola, and S. Cenci. 2013. Plasma cells require autophagy for sustainable immunoglobulin production. *Nat Immunol*. 14:298–305. doi:10.1038/ni.2524.

Pierobon, D., F. Raggi, I. Cambieri, S. Pelassa, S. Occhipinti, P. Cappello, F. Novelli, T. Musso, A. Eva, C. Castagnoli, L. Varesio, M. Giovarelli, and M.C. Bosco. 2016. Regulation of Langerhans cell functions in a hypoxic environment. *J Mol.Med.(Berl)*. 94:943–955. doi:10.1007/s00109-016-1400-9.

Price, J.G., J. Idoyaga, H. Salmon, B. Hogstad, C.L. Bigarella, S. Ghaffari, M. Leboeuf, and M. Merad. 2015. CDKN1A regulates Langerhans cell survival and promotes Treg cell generation upon exposure to ionizing irradiation. *Nat.Immunol.* 16:1060–1068. doi:10.1038/ni.3270.

Ribeiro, C.M., R. Sarrami-Forooshani, L.C. Setiawan, E.M. Zijlstra-Willems, J.L. van Hamme, W. Tigchelaar, N.N. Van der Wel, N.A. Kootstra, S.I. Gringhuis, and T.B. Geijtenbeek. 2016. Receptor usage dictates HIV-1 restriction by human TRIM5alpha in dendritic cell subsets. *Nature*. 540:448–452. doi:10.1038/nature20567.

Riffelmacher, T., A. Clarke, F.C. Richter, A. Stranks, S. Pandey, S. Danielli, P. Hublitz, Z. Yu, E. Johnson, T. Schwerd, J. McCullagh, H. Uhlig, S.E.W. Jacobsen, and A.K. Simon. 2017. Autophagy-Dependent Generation of Free Fatty Acids Is Critical for Normal Neutrophil Differentiation. *Immunity*. 47:466-480.e5. doi:10.1016/j.immuni.2017.08.005.

Said, A., S. Bock, T. Lajqi, G. Müller, and G. Weindl. 2014. Chloroquine promotes IL-17 production by CD4+ T cells via p38-dependent IL-23 release by monocyte-derived Langerhans-like cells. *J Immunol*. 193:6135–6143. doi:10.4049/jimmunol.1303276.

Schuler, G., and R.M. Steinman. 1985. Murine epidermal Langerhans cells mature into potent immunostimulatory dendritic cells in vitro. *J.Exp.Med.* 161:526–546.

Sil, P., J. Suwanpradid, G. Muse, A. Gruzdev, L. Liu, D.L. Corcoran, C.J. Willson, K. Janardhan, S. Grimm, P. Myers, L.M. Degraff, A.S. MacLeod, and J. Martinez. 2020. Noncanonical autophagy in dermal dendritic cells mediates immunosuppressive effects of UV exposure. *J Allergy Clin Immunol*. 145:1389–1405. doi:10.1016/j.jaci.2019.11.041.

Singh, T.P., H.H. Zhang, I. Borek, P. Wolf, M.N. Hedrick, S.P. Singh, B.L. Kelsall, B.E. Clausen, and J.M. Farber. 2016. Monocyte-derived inflammatory Langerhans cells and dermal dendritic cells mediate psoriasis-like inflammation. *Nat Commun*. 7:13581. doi:10.1038/ncomms13581.

Song, S., J. Tan, Y. Miao, and Q. Zhang. 2018. Crosstalk of ER stress-mediated autophagy and ER-phagy: Involvement of UPR and the core autophagy machinery. *J Cell Physiol*. 233:3867–3874. doi:10.1002/jcp.26137.

Sparber, F., J.M. Scheffler, N. Amberg, C.H. Tripp, V. Heib, M. Hermann, S.P. Zahner, B.E. Clausen, B. Reizis, L.A. Huber, P. Stoitzner, and N. Romani. 2014. The late endosomal

adaptor molecule p14 (LAMTOR2) represents a novel regulator of Langerhans cell homeostasis. *Blood*. 123:217–227. doi:10.1182/blood-2013-08-518555.

Sparber, F., C.H. Tripp, K. Komenda, J.M. Scheffler, B.E. Clausen, L.A. Huber, N. Romani, and P. Stoitzner. 2015. The late endosomal adaptor molecule p14 (LAMTOR2) regulates TGFbeta1-mediated homeostasis of Langerhans cells. *J Invest Dermatol.* 135:119–129. doi:10.1038/jid.2014.324.

Stockwell, B.R. 2022. Ferroptosis turns 10: Emerging mechanisms, physiological functions, and therapeutic applications. *Cell*. 185:2401–2421. doi:10.1016/j.cell.2022.06.003.

Su, Q., A. Bouteau, J. Cardenas, B. Uthra, Y. Wang, C. Smitherman, J. Gu, and B.Z. Igyártó. 2020. Brief communication: Long-term absence of Langerhans cells alters the gene expression profile of keratinocytes and dendritic epidermal T cells. *PLoS One*. 15:e0223397. doi:10.1371/journal.pone.0223397.

Takahama, M., S. Akira, and T. Saitoh. 2018. Autophagy limits activation of the inflammasomes. *Immunol Rev*. 281:62–73. doi:10.1111/imr.12613.

Tavernier, S.J., F. Osorio, L. Vandersarren, J. Vetters, N. Vanlangenakker, I.G. Van, K. Vergote, R.R. De, E. Parthoens, L. van de Laar, T. Iwawaki, J.R. Del Valle, C.C. Hu, B.N. Lambrecht, and S. Janssens. 2017. Regulated IRE1-dependent mRNA decay sets the threshold for dendritic cell survival. *Nat.Cell Biol.* 19:698–710. doi:10.1038/ncb3518.

Tripp, C.H., S. Chang-Rodriguez, P. Stoitzner, S. Holzmann, H. Stössel, P. Douillard, S. Saeland, F. Koch, A. Elbe-Bürger, and N. Romani. 2004. Ontogeny of Langerin/CD207 expression in the epidermis of mice. *J.Invest.Dermatol.* 122:670–672.

Valecka, J., C.R. Almeida, B. Su, P. Pierre, and E. Gatti. 2018. Autophagy and MHC-restricted antigen presentation. *Mol Immunol*. 99:163–170. doi:10.1016/j.molimm.2018.05.009.

Velázquez, A.P., T. Tatsuta, R. Ghillebert, I. Drescher, and M. Graef. 2016. Lipid droplet-mediated ER homeostasis regulates autophagy and cell survival during starvation. *J Cell Biol*. 212:621–631. doi:10.1083/jcb.201508102.

Voisin, B., D. Chartoire, C. Devouassoux, C. Kowalczyk-Quintas, F. Clauss, F. Lezot, P. Schneider, V. Flacher, and C.G. Mueller. 2019. The hair cycle underlies regulation of Langerhans cell renewal. *bioRxiv*. 832774. doi:10.1101/832774.

Weindel, C.G., L.J. Richey, A.J. Mehta, M. Shah, and B.T. Huber. 2017. Autophagy in Dendritic Cells and B Cells Is Critical for the Inflammatory State of TLR7-Mediated Autoimmunity. *J Immunol*. 198:1081–1092. doi:10.4049/jimmunol.1601307.

Wu, M.-Y., and J.-H. Lu. 2019. Autophagy and Macrophage Functions: Inflammatory Response and Phagocytosis. *Cells*. 9:E70. doi:10.3390/cells9010070.

Xia, H., S. Li, X. Li, W. Wang, Y. Bian, S. Wei, S. Grove, W. Wang, L. Vatan, J.R. Liu, K. McLean, R. Rattan, A. Munkarah, J.-L. Guan, I. Kryczek, and W. Zou. 2020. Autophagic adaptation to oxidative stress alters peritoneal residential macrophage survival and ovarian cancer metastasis. *JCI Insight*. 5:141115. doi:10.1172/jci.insight.141115.

Xu, X., K. Araki, S. Li, J.H. Han, L. Ye, W.G. Tan, B.T. Konieczny, M.W. Bruinsma, J. Martinez, E.L. Pearce, D.R. Green, D.P. Jones, H.W. Virgin, and R. Ahmed. 2014. Autophagy is essential for

effector CD8(+) T cell survival and memory formation. *Nat Immunol*. 15:1152–61. doi:10.1038/ni.3025.

Zahner, S.P., J.M. Kel, C.A. Martina, I. Brouwers-Haspels, M.A. van Roon, and B.E. Clausen. 2011. Conditional deletion of TGF-betaR1 using Langerin-Cre mice results in Langerhans cell deficiency and reduced contact hypersensitivity. *J.Immunol.* 187:5069–5076.

Zhang, S., T.N. Edwards, V.K. Chaudhri, J. Wu, J.A. Cohen, T. Hirai, N. Rittenhouse, E.G. Schmitz, P.Y. Zhou, B.D. McNeil, Y. Yang, H.R. Koerber, T.L. Sumpter, A.C. Poholek, B.M. Davis, K.M. Albers, H. Singh, and D.H. Kaplan. 2021. Nonpeptidergic neurons suppress mast cells via glutamate to maintain skin homeostasis. *Cell*. 184:2151-2166.e16. doi:10.1016/j.cell.2021.03.002.

Zhang, X., X. Li, Y. Wang, Y. Chen, Y. Hu, C. Guo, Z. Yu, P. Xu, Y. Ding, Q.-S. Mi, J. Wu, J. Gu, and Y. Shi. 2022. Abnormal lipid metabolism in epidermal Langerhans cells mediates psoriasis-like dermatitis. *JCI Insight*. 7:e150223. doi:10.1172/jci.insight.150223.

Zhou, Y., B. Zhou, L. Pache, M. Chang, A.H. Khodabakhshi, O. Tanaseichuk, C. Benner, and S.K. Chanda. 2019. Metascape provides a biologist-oriented resource for the analysis of systems-level datasets. *Nat Commun*. 10:1523. doi:10.1038/s41467-019-09234-6.

Figure legends

Figure 1: ATG5 deficiency in Langerhans cells disrupts autophagosomes and depletes their epidermal network. (A) Representative immunofluorescent stainings of MAP1LC3B (LC3) on LCs obtained by *in vitro* emigration from epidermal sheets of $Atg5^{WT}$ **(Supplementary Video SV1)** and $Atg5^{\Delta Cd207}$ **(Supplementary Video SV2)** mice. Scale bars: 10µm. **(B)** Representative histogram plot of LC3β staining and quantification of mean fluorescence intensity for LCs of 3-week-old $Atg5^{WT}$ and $Atg5^{\Delta Cd207}$ mice, treated or not with the lysosomal acidification inhibitor chloroquine. Autophagy flux was calculated as a ratio between mean fluorescence intensity for LC3β in treated and untreated cells. Data are presented as mean ±SEM, with each point corresponding to one individual mouse. Statistical analysis was performed using Mann-Whitney U test (***, p<0.001). **(C)** Representative dot plots (pre-gated on live CD45$^+$ cells) for the identification of MHCII$^+$ TCRγδ$^-$ Langerhans cells (LCs; all CD207$^+$) and MHCII$^-$ TCRγδ$^+$ dendritic epidermal T Cells (DETCs) in freshly digested back skin epidermal suspension of 6-month-old $Atg5^{WT}$ and $Atg5^{\Delta Cd207}$ mice. **(D)** Comparison over time of the percentage of LCs among live CD45$^+$ epidermal cells for control ($Atg5^{WT}$ and $Atg5^{WT/\Delta}$) and $Atg5^{\Delta Cd207}$ mice. Data are presented as mean ±SEM, with each point corresponding to n≥4 mice per time-point. Statistical analysis was performed using two-way ANOVA followed by Tukey's multiple comparison test. Only significant differences between $Atg5^{WT}$ and $Atg5^{\Delta Cd207}$ mice are shown (****, p<0.0001). **(E)** Percentage of LCs among live CD45$^+$ cells in freshly digested back skin epidermis of 10-20 week-old $Atg7^{WT}$ and $Atg7^{\Delta Cd207}$ mice. Data are presented as mean ±SEM, with each point corresponding to one individual mouse. Statistical analysis was performed using Mann-Whitney U test (***, p<0.001). **(F)** Representative immunofluorescent staining of CD207 on epidermal sheets of ear skin from 3-week (upper panels) and 6-month-old (lower panels) $Atg5^{WT}$ and $Atg5^{\Delta Cd207}$ mice. Scale bars: 100µm. **(G)** Percentages of epidermal LCs expressing the proliferation markers 5-bromo-2'-deoxyuridine (BrdU) and Ki-67 for 4-week (upper panels) and 6-month-old (lower panels) $Atg5^{WT}$ and $Atg5^{\Delta Cd207}$ mice. Data are presented as mean ±SEM, with each point corresponding to one individual mouse. Statistical analysis was performed using Mann-Whitney U test (**, p<0.01; ns, p>0.05).

Figure 2: ATG5-deficient LCs undergo apoptosis. (A) CD86 and **(B)** MHC-II mean fluorescence intensity for epidermal LCs of control ($Atg5^{WT}$ and $Atg5^{WT/\Delta}$) and $Atg5^{\Delta Cd207}$ mice. Data are presented as mean ±SEM, with each point corresponding to one individual mouse. Statistical analysis was performed using Kruskal-Wallis one-way ANOVA followed by Dunn's multiple comparison test (ns, p>0.05). **(C)** Percentages and **(D)** absolute numbers of LCs, cDC1 and CD207$^-$ DCs in freshly digested skin draining lymph nodes of control ($Atg5^{WT}$ and $Atg5^{WT/\Delta}$) and $Atg5^{\Delta Cd207}$ mice. Data are presented as mean ±SEM, with each point corresponding to one individual mouse. Statistical analysis was performed using Mann-Whitney U test (*, p<0.05; ns, p>0.05). **(E)** Percentage of cells with activated caspase-3 in LCs of freshly digested back skin epidermis (left panel) and LCs, cDC1 and CD207- dermal DCs of skin-draining lymph nodes (right panel) for control ($Atg5^{WT}$ and $Atg5^{WT/\Delta}$) and $Atg5^{\Delta Cd207}$ mice. Data are presented as mean ±SEM, with each point corresponding to one individual mouse. Statistical analysis was

performed using Kruskal-Wallis one-way ANOVA followed by Dunn's multiple comparison test (*, p<0.05; **, p<0.01; ns, p>0.05).

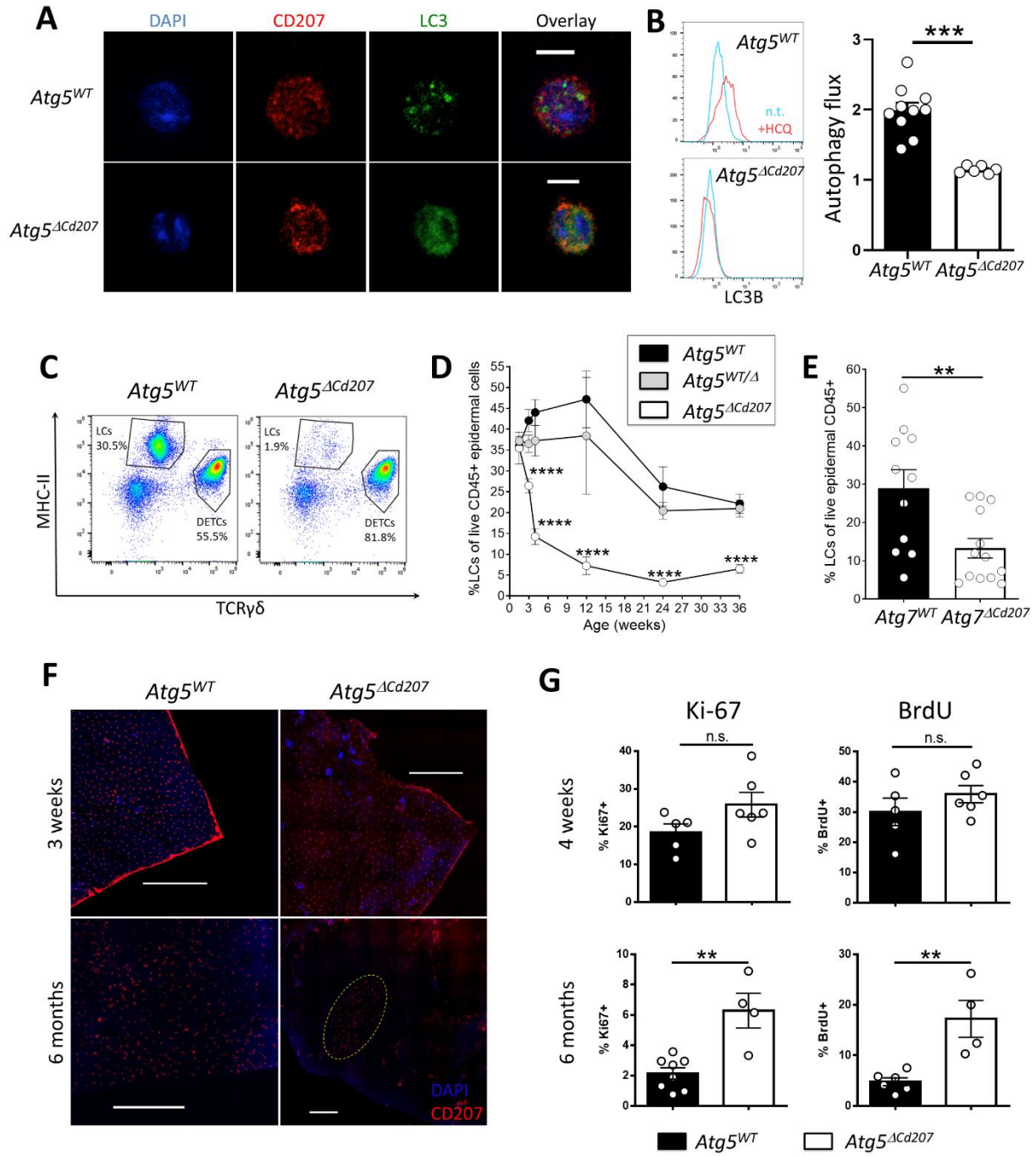**Figure 3: Impaired autophagy increases the lipid storage compartments of Langerhans cells.** **(A)** Differentially expressed transcripts related to lipid metabolism in $Atg5^{WT}$ vs. $Atg5^{\Delta Cd207}$ LCs. **(B-D)** Flow cytometry quantification of the Bodipy mean fluorescence intensity in epidermal LCs obtained from C57BL/6 mice then treated with **(B)** etomoxir or **(C)** wortmannin, or **(D)** from control ($Atg5^{WT}$ and $Atg5^{WT/\Delta}$) and $Atg5^{\Delta Cd207}$ mice. Data are presented as mean ±SEM, with each point corresponding to one individual mouse. Statistical analysis was performed using Kruskal-Wallis one-way ANOVA followed by Dunn's multiple comparison test (*, p<0.05; **, p<0.01; ns, p>0.05). **(E-F)** Representative immunofluorescent stainings of CD207$^+$ epidermal LCs obtained from $Atg5^{WT}$ (upper panels) and $Atg5^{\Delta Cd207}$ (lower panels) mice and stained with Bodipy **(E and Supplementary Videos SV5 and SV6)** or anti-Perilipin-1 antibody **(F)**. Scale bars: 10µm.

Figure 4: Impaired lipid metabolism leads ATG5-deficient LCs to ferroptosis. (A-E) Flow cytometry quantification of mean intensity of fluorescence for **(A)** Phosphorylated AMPK, **(B)** GLUT1, **(C)** 2-NDBG uptake, **(D)** CD36 and **(E)** Bodipy C16 uptake in epidermal LCs obtained from control ($Atg5^{WT}$ and $Atg5^{WT/\Delta}$) and $Atg5^{\Delta Cd207}$ mice. Data are presented as mean ±SEM, with each point corresponding to one individual mouse. Statistical analysis was performed using Kruskal-Wallis one-way ANOVA followed by Dunn's multiple comparison test (*, p<0.05; **, p<0.01; ns, p>0.05). **(F)** Epidermal LCs sorted from $Atg5^{WT}$ or $Atg5^{\Delta Cd207}$ mice and BMDCs from C57BL/6 mice were sequentially exposed to Oligomycin (OM), Carbonyl cyanide 4-(trifluoromethoxy)phenylhydrazone (FCCP), rotenone (ROT) and antimycin A (AA), and oxygen consumption rates (OCR) were measured by a Seahorse XF96 analyzer throughout the experiment. Data are from one representative experiment out of three. **(G)** ATP production (OCR$_{baseline}$ – OCR$_{OM}$), maximum respiration (Max; OCR$_{FCCP}$ – OCR$_{AA+ROT}$) and spare respiratory capacity (SRC; OCR$_{FCCP}$ – OCR$_{baseline}$) were calculated from the OCR curves Data are presented as mean ±SEM, with each point corresponding to a pool of individual mice. Statistical analysis was performed using two-way ANOVA followed by Šídák's multiple comparisons test (*, p<0.05; ***, p<0.001; ns, p>0.05). **(H)** Differentially expressed transcripts related to mitochondrial function in Atg5^{WT} vs. Atg5$^{\Delta Cd207}$ LCs. **(I)** Mitochondrial load for epidermal LCs of $Atg5^{WT}$, $Atg5^{WT/\Delta}$ and $Atg5^{\Delta Cd207}$ mice, as measured by mean fluorescence intensity of Mitotracker Green staining. Data are presented as mean ±SEM, with each point corresponding to one individual mouse. Statistical analysis was performed using Kruskal-Wallis one-way ANOVA followed by Dunn's multiple comparison test (*, p<0.05; **, p<0.01; ns, p>0.05). **(J)** Differentially expressed transcripts related to ferroptosis in Atg5^{WT} vs. Atg5$^{\Delta Cd207}$ LCs. **(K)** Quantification of lipid peroxidation for epidermal LCs of control ($Atg5^{WT}$ and $Atg5^{WT/\Delta}$) and $Atg5^{\Delta Cd207}$ mice, as measured by mean fluorescence intensity of Bodipy-C11. Data are presented as mean ±SEM, with each point corresponding to one individual mouse. Statistical analysis was performed using Kruskal-Wallis one-way ANOVA followed by Dunn's multiple comparison test (*, p<0.05; ns, p>0.05).

Figure 5: Langerhans cells under metabolic stress have impaired tissue homeostasis function. (A) Differentially expressed genes in $Atg5^{WT}$ vs. $Atg5^{\Delta Cd207}$ LCs: transcripts related to immune function. **(B)** One ear of $Atg5^{WT}$ or $Atg5^{\Delta Cd207}$ mice was injected intradermally with 2.5µg alum hydroxide and the contralateral ear was left untreated. 4h later, whole skin was digested and cell suspensions were monitored by flow cytometry for $CD45^+$ $CD3^-$ $CD11b^+$ $Gr1^+$ $Ly6G^+$ neutrophils and $CD45^+$ $CD3^-$ $CD11b^+$ $Gr1^{low}$ $Ly6G^-$ monocytes. **(C,D)** Percentage of neutrophils **(C)** and monocytes **(D)** among live $CD45^+$ cells. Data are presented as mean ±SEM, with each point corresponding to one individual mouse. Statistical analysis was performed using Mann-Whitney U tests for unpaired comparison between mice, and Wilcoxon tests for paired comparison of alum-treated vs. untreated ears (*, $p<0.05$; **, $p<0.01$; ***, $p<0.001$; ns, $p>0.05$). **(E)** Differentially expressed genes in $Atg5^{WT}$ vs. $Atg5^{\Delta Cd207}$ LCs: transcripts related to neuronal interactions. **(F)** Representative immunofluorescence microscopy image of epidermal sheets obtained from ears of $Atg5^{WT}$ and $Atg5^{\Delta Cd207}$ mice and stained with antibodies against β3-tubulin (neurons) and CD207 (LCs). Scale bar: 50µm. Quantification in $Atg5^{WT}$, $Atg5^{WT/-}$ and $Atg5^{\Delta Cd207}$ mice: **(G)** Number of $CD207^+$ LCs per mm². **(H)** Relative area of β3-tubulin staining. Data are presented as mean ±SEM, with each point corresponding to one field of view (n=3 mice per condition). Statistical analysis was performed using Kruskal-Wallis one-way ANOVA followed by Dunn's multiple comparison test (**, $p<0.01$; ****, $p<0.0001$; ns, $p>0.05$).
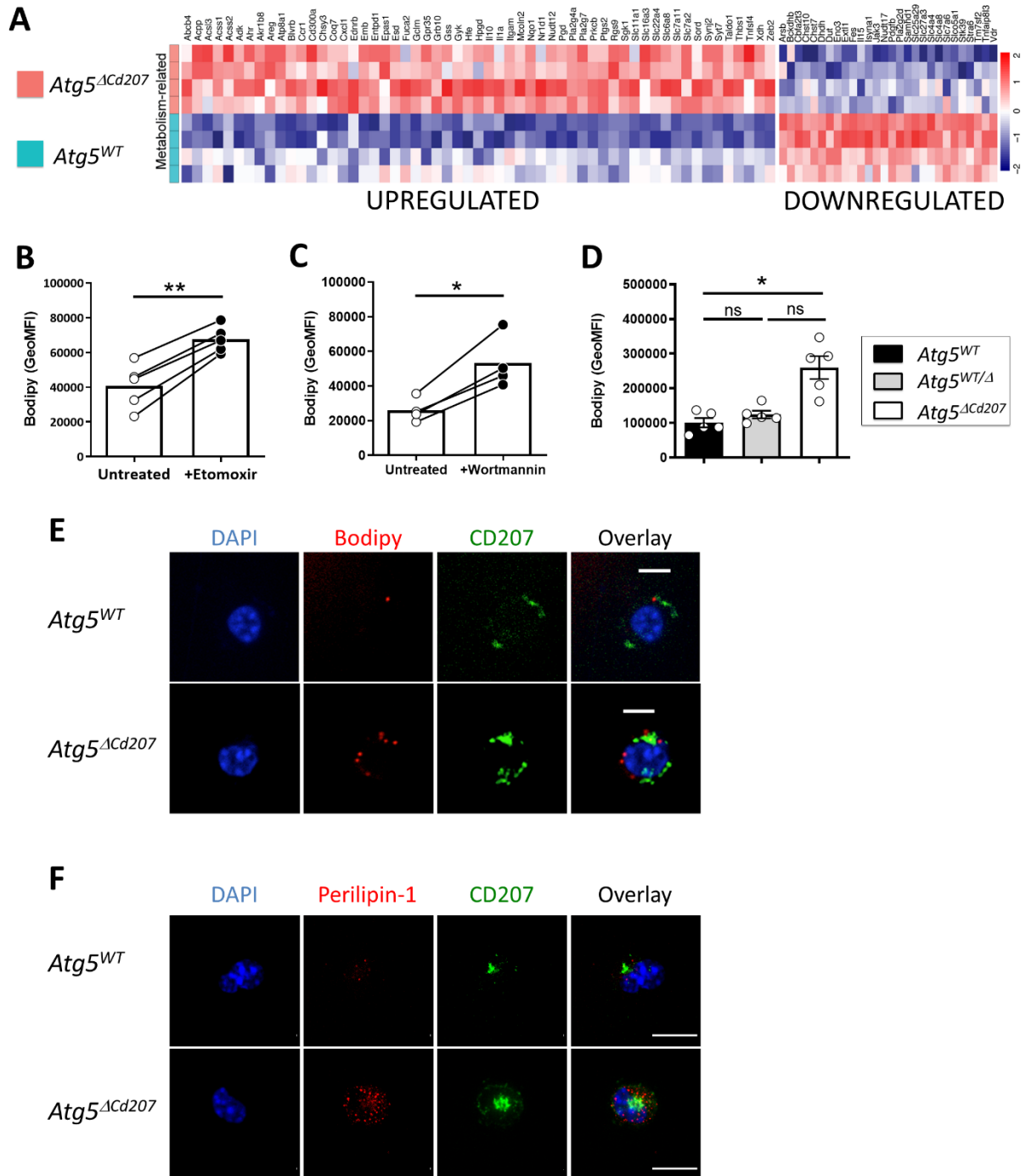
Figure 1: ATG5 deficiency in Langerhans cells disrupts autophagosomes and depletes their epidermal network.

Figure 2: ATG5-deficient LCs are more prone to apoptosis.
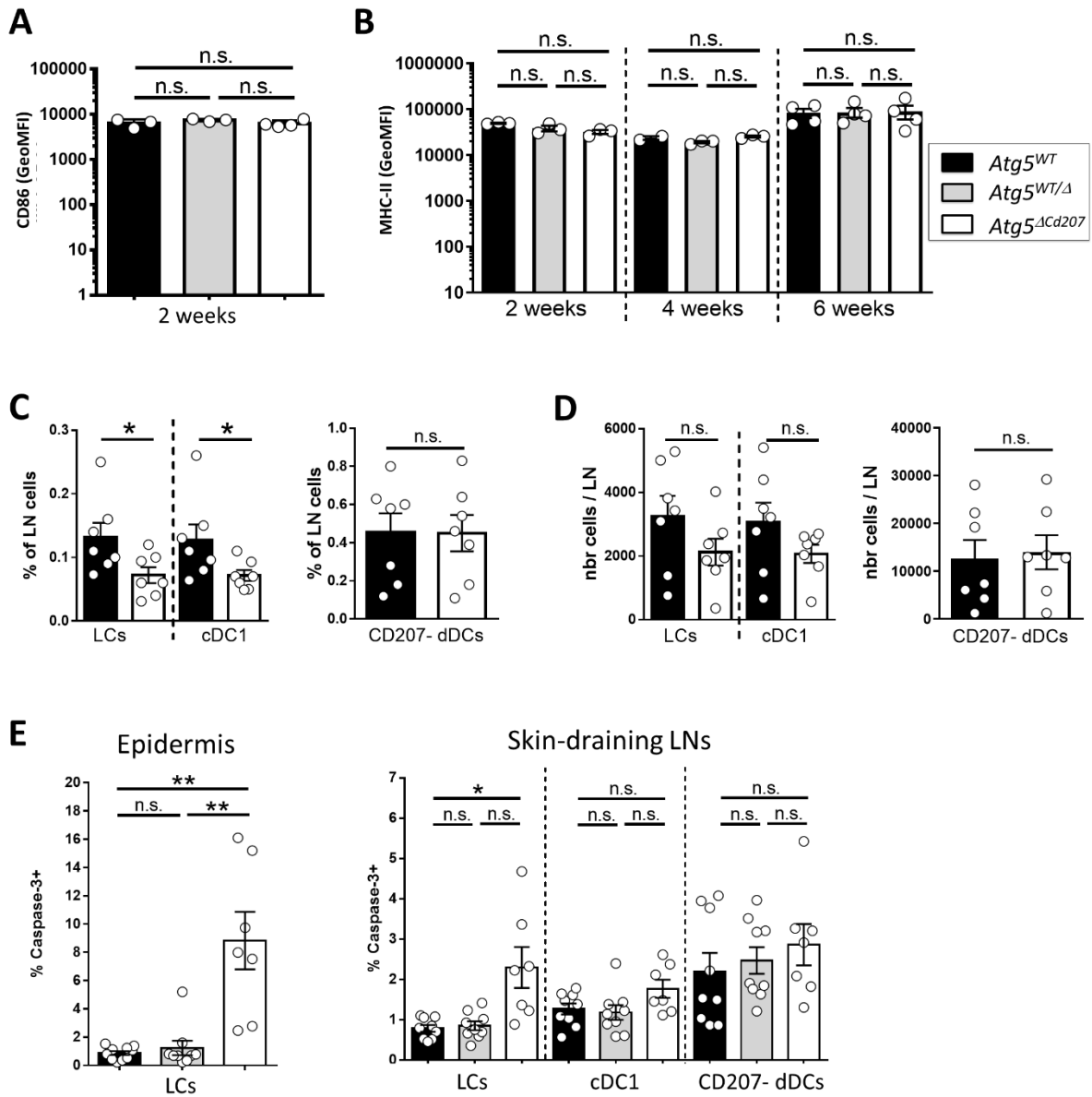
Figure 3: Impaired autophagy increases the lipid storage compartments of Langerhans cells.

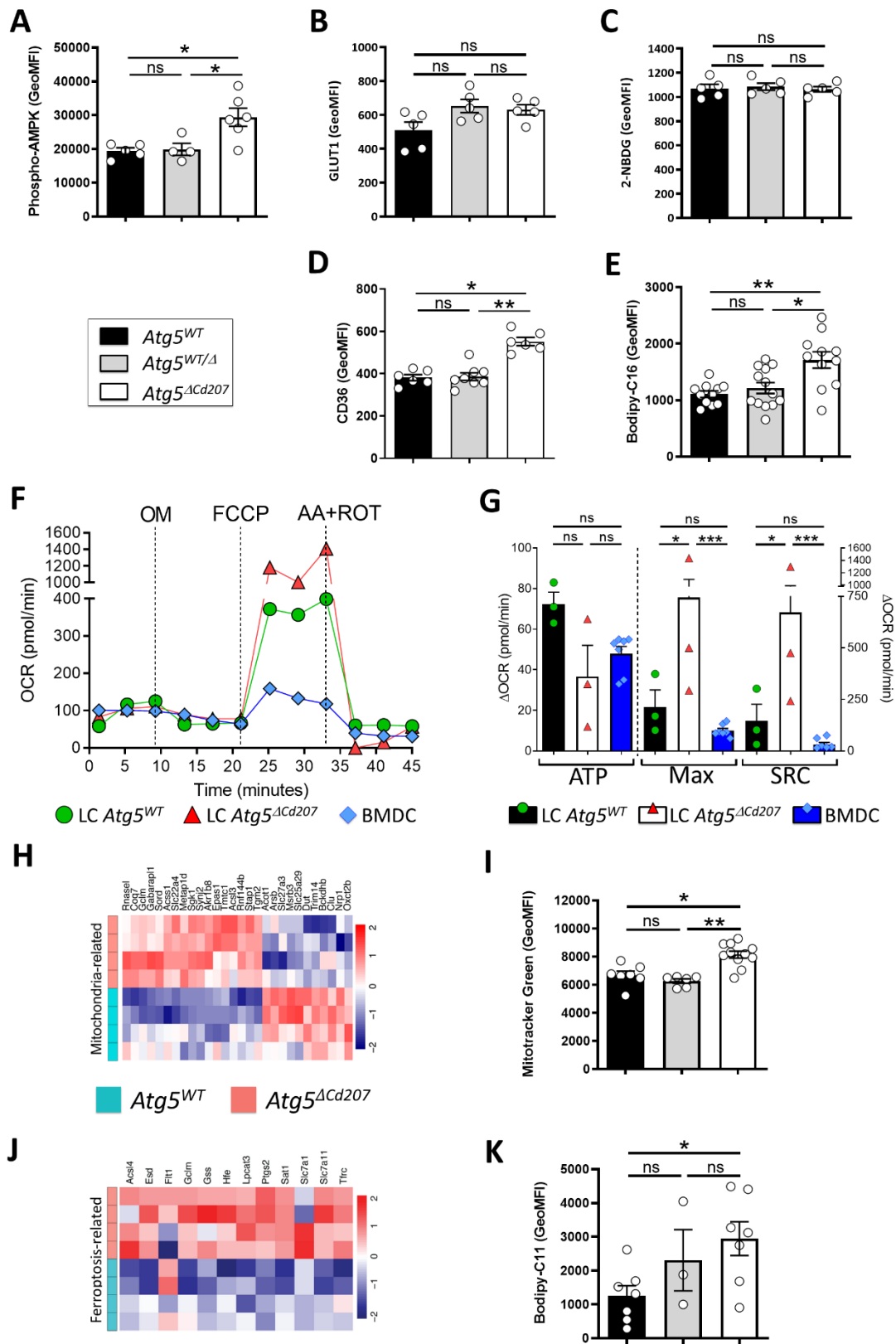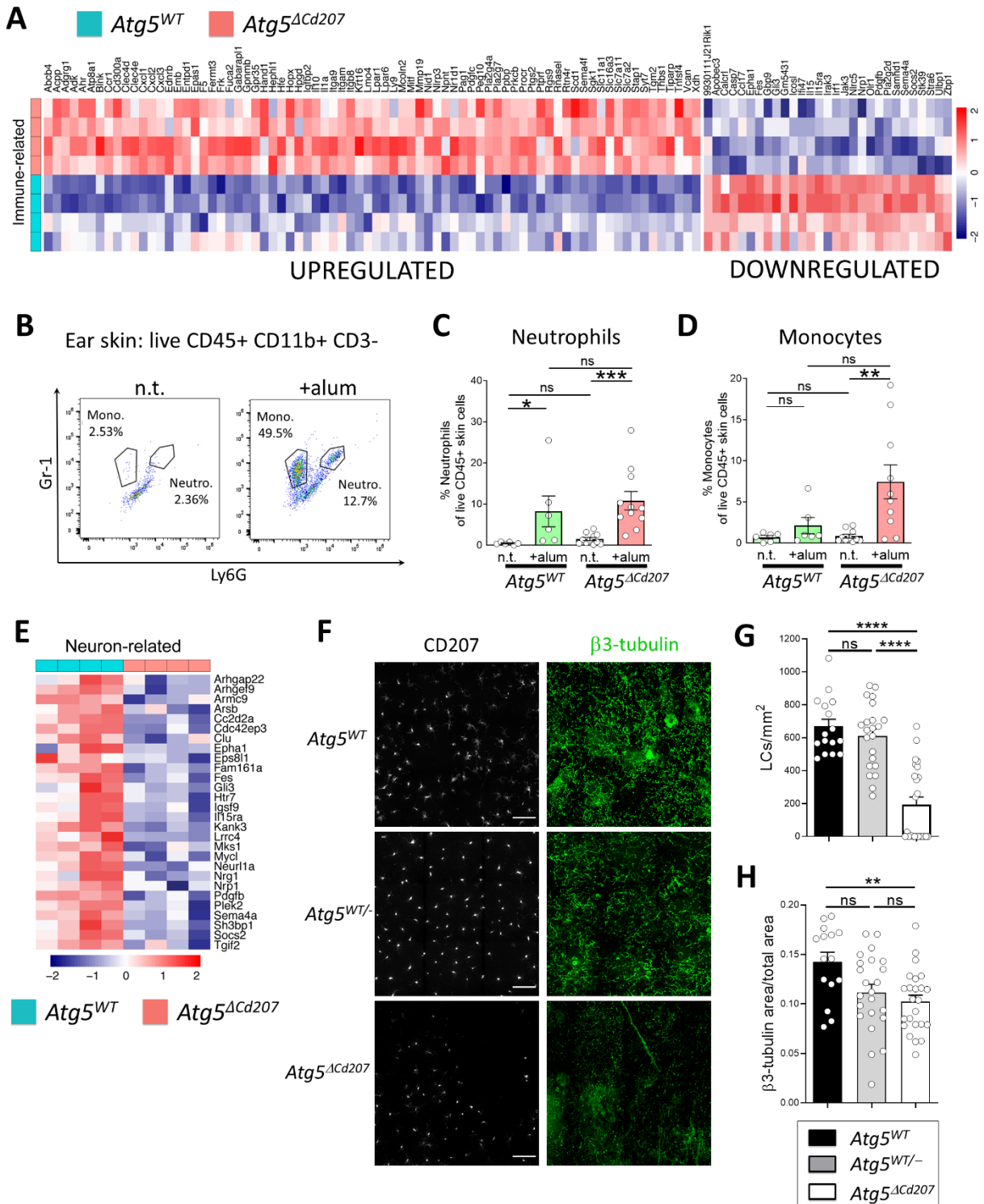# Figure 4: Impaired lipid metabolism leads ATG5-deficient LCs to ferroptosis

Fig 5 LCs under metabolic stress have impaired tissue homeostasis function

A *Atg5^WT* *Atg5^ΔCd207*

UPREGULATED   DOWNREGULATED

B Ear skin: live CD45+ CD11b+ CD3-

n.t.   +alum

C Neutrophils

D Monocytes

E Neuron-related

F CD207   β3-tubulin

G

H

Supplementary figures

Figure S1: Autophagosomes are detectable in murine Langerhans cells. (A) Transmission electron microscopy of LCs in a bulk epidermal cell suspension freshly isolated from C57BL/6 mice (far right panel) or cultured for 3 days. The inset image highlights a Birbeck granule (arrow). **(B)** Close-up micrographs of autophagic structures corresponding to the boxes in the low power overview micrographs. 1 and 3 appear to be limiting membranes of incipient autophagy; 2 and 4 show double membrane-limited autophagosomes. Scale bars: 1µm (A); 500nm (B).

Figure S2: *Atg5* is efficiently deleted in Langerhans cells and dermal cDC1 of *Atg5^{ΔCd207}* mice. (A) Representative electrophoresis of genotyping PCR. Left panel: floxed, wild-type (WT) and exon 3-deleted (KO) alleles of *Atg5*. Right panel: wild-type and *Cre* knock-in alleles of *Cd207*. **(B)** *Atg5* mRNA expression in sorted epidermal CD45+ MHCII+ TCRγδ⁻ LCs from control (*Atg5^{WT}* and *Atg5^{WT/Δ}*) and *Atg5^{ΔCd207}* mice. Fold changes were calculated relative to mRNA expression in LCs of *Atg5^{WT}* control mice. Data are presented as mean ±SEM, with each point corresponding to one individual mouse. Statistical analysis was performed using Kruskal-Wallis one-way ANOVA followed by Dunn's multiple comparison test (*, p<0.05; ns, p>0.05). **(C)** Gating strategy used to sort lymph nodes MHC-II⁺ CD207- FSA high dermal DCs (dDCs), MHC-II⁺ CD207⁺ CD103⁻ LCs (LCs) and MHC-II⁺ CD207⁺ CD103⁺ cDC1 (CD103⁺). Red dots in the top panel depict backgating of CD207⁺ LCs/cDC1. **(D)** *Atg5* mRNA expression in LCs, cDC1 and CD207- dDCs sorted from pooled lymph node cell suspensions of at least 3 control (*Atg5^{WT}* and *Atg5^{WT/Δ}*) or *Atg5^{ΔCd207}* mice. Fold changes were calculated relative to mRNA expression in cells of *Atg5^{WT}* control mice. ND, not detectable.

Figure S3: ATG5-deficient LCs have functional lysosomes. Representative half-set overlay of LysoTracker-Red (left panel) and LysoSensor (right panel) stainings and comparison of the ratio of mean fluorescence intensities of each marker for epidermal LCs of control (*Atg5^{WT}* and *Atg5^{WT/Δ}*) and *Atg5^{ΔCd207}* mice. Data are presented as mean ±SEM, with each point corresponding to one individual mouse. Statistical analysis was performed using Kruskal-Wallis one-way ANOVA followed by Dunn's multiple comparison test (ns, p>0.05).

Figure S4: Rubicon deficiency does not alter the Langerhans cell network. (A) Percentage of CD45⁺ MHCII⁺ CD207⁺ LCs among live CD45⁺ cells obtained from fresh epidermal cell suspensions. Data are presented as mean ±SEM, with each point corresponding to one individual mouse. Statistical analysis was performed using Mann-Whitney U test (ns, p > 0.05). **(B)** Representative immunofluorescence staining of CD207⁺ LCs in ear epidermal sheets of 2-month old mice. Scale bar = 50µm.

Figure S5: ATG5 deficiency does not affect cDC1 homeostasis. (A) Representative dot plots for the identification of CD207⁺ CD11b⁺ LCs, CD207⁺ CD11b⁻ cDC1, CD207⁻ CD11b⁺ cDC2/macrophages and CD207⁻ CD11b⁻ (DN, double-negative) DCs among live CD45⁺ lineage-CD11c⁺ MHCII⁺ skin DCs in whole skin cell suspensions from *Atg5^{WT}* and *Atg5^{ΔCd207}* mice (lineage markers: B220, NK1.1, Ly6G and CD3). **(B)** Percentages of LCs and cDC1 among skin DCs. Data are presented as mean ±SEM, with each point corresponding to one individual

mouse. Statistical analysis was performed using Kruskal-Wallis one-way ANOVA followed by Dunn's multiple comparison test (*, p<0.05; ns, p>0.05).

Figure S6: ATG5 deficient LCs present ER swelling but no unfolded protein response. (A) Mean fluorescence intensity for ER-tracker on epidermal LCs treated or not with Wortmannin. Data are presented as mean ±SEM, with each point corresponding to one individual mouse. Statistical analysis was performed using Mann-Whitney U test (*, p<0.05). **(B)** Representative half-set overlay (left panel) and mean fluorescence intensity (right panel) of ER-tracker in epidermal LCs of control ($Atg5^{WT}$ and $Atg5^{WT/\Delta}$) and $Atg5^{\Delta Cd207}$ mice. Data are presented as mean ±SEM, with each point corresponding to one individual mouse. Statistical analysis was performed using Kruskal-Wallis one-way ANOVA followed by Dunn's multiple comparison test (**, p<0.01). **(C)** Representative immunofluorescent stainings of the endoplasmic reticulum using the ER-tracker dye on epidermal LCs of $Atg5^{WT}$ **(Supplementary Video SV3)** and $Atg5^{\Delta Cd207}$ **(Supplementary Video SV4)** mice. Scale bar: 10µm **(D)** Expression of $Ern1$, total and spliced $Xbp1$, and $Ddit3$ mRNAs, in epidermal LCs of control ($Atg5^{WT}$ and $Atg5^{WT/\Delta}$) and $Atg5^{\Delta Cd207}$ mice. Fold changes were calculated relative to mRNA expression in cells of $Atg5^{WT}$ control mice. Data are presented as mean ±SEM, with each point corresponding to one individual mouse. Statistical analysis was performed using Kruskal-Wallis one-way ANOVA followed by Dunn's multiple comparison test (ns, p>0.05).

Figure S7: Lack of autophagy alters the transcriptome of Langerhans cells. (A) Visualization of the exon 3 region of $Atg5$ gene from RNA-seq of sorted LCs of indicated mouse genotype using integrative Genomic Viewer tool. **(B)** Principal component analysis of RNA-seq transcriptome analysis from sorted LCs of $Atg5^{WT}$ and A$tg5^{\Delta Cd207}$ mice. **(C)** Heatmap showing the differentially expressed genes (FDR<0.1, Absolute Log2 Fold Change value > 1, p-value<0.05) between LCs of indicated mouse genotypes **(D)** Volcano plot showing the differential expression of genes between LCs of indicated mouse genotypes. Gene names refer to the top 20 up and downregulated genes, based on the following combinations of p-value and fold-change criteria: blue dots: p-value<0.05 with no cutoff on Absolute Log2 Fold Change; red dots: p-value<0.05 and Absolute Log2 Fold Change value > 1. **(E)** Metascape pathway analysis of genes significantly upregulated or downregulated in $Atg5^{\Delta Cd207}$ LCs.

Figure S8: ATG5-deficient LCs do not display defects in mitochondrial function. (A) Representative dot plot of Mitotracker Green and Deep-Red staining and comparison of Mitotracker Deep-Red mean fluorescence intensity of epidermal LCs obtained from control ($Atg5^{WT}$ and $Atg5^{WT/\Delta}$) and $Atg5^{\Delta Cd207}$ mice. **(B)** Representative dot plot of Mitosox Red staining and comparison of Mitosox^{high} percentage of epidermal LCs obtained from control ($Atg5^{WT}$ and $Atg5^{WT/\Delta}$) and $Atg5^{\Delta Cd207}$ mice. Data are presented as mean ±SEM, with each point corresponding to one individual mouse. Statistical analysis was performed using Kruskal-Wallis one-way ANOVA followed by Dunn's multiple comparison test (ns, p>0.05).

Figure S9: Correlation of epidermal nerve and Langerhans cell densities is lost in $Atg5^{\Delta Cd207}$ mice. Based on epidermal sheet stainings (Figure 7F-H), the number of CD207$^+$ LCs per mm²

(X axis) was plotted against the relative areas for β3-tubulin$^+$ nerves (Y axis). Linear regressions and R² values were calculated for *Atg5^{WT}*, *Atg5$^{WT/-}$* and *Atg5^{ΔCd207}* mice.

Supplementary videos

https://www.biorxiv.org/content/10.1101/2022.09.16.507799v1.supplementary-material

Supplementary Video SV1: Autophagosome staining of *Atg5^{WT}* LCs. LC3: green; CD207: red.

Supplementary Video SV2: Endoplasmic reticulum staining of *Atg5^{ΔCd207}* LCs. LC3: green; CD207: red.

Supplementary Video SV3: Endoplasmic reticulum staining of *Atg5^{WT}* LCs. CD207: green; ER-tracker: red.
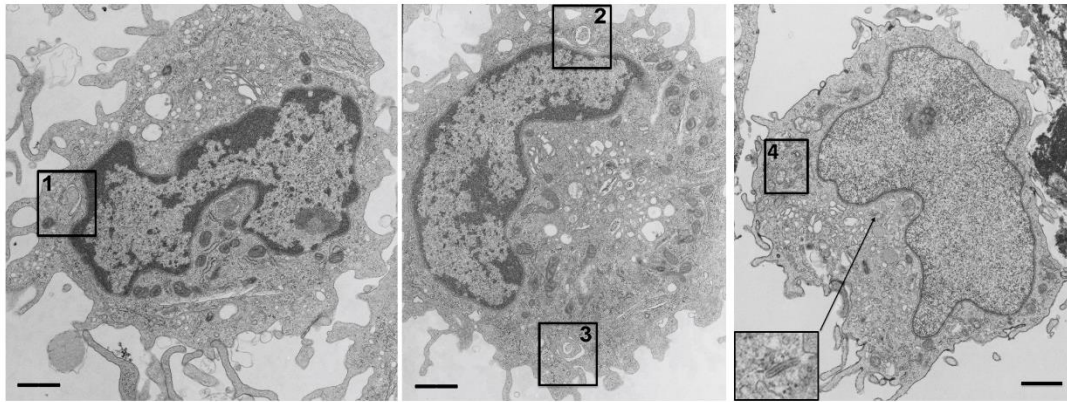
Supplementary Video SV4: Endoplasmic reticulum staining of *Atg5^{ΔCd207}* LCs. CD207: green; ER-tracker: red.

Supplementary Video SV5: Lipid droplets of *Atg5^{WT}* LCs. CD207: green; Bodipy: red.
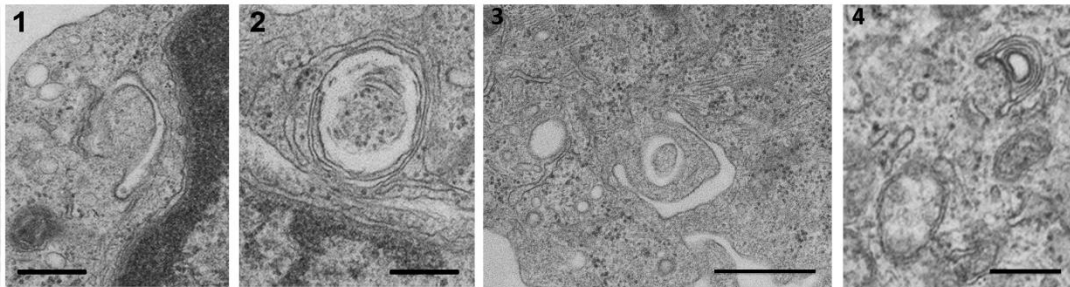
Supplementary Video SV6: Lipid droplets of *Atg5^{ΔCd207}* LCs. CD207: green; Bodipy: red.

Figure S1. Autophagosomes are detectable in murine Langerhans cells.

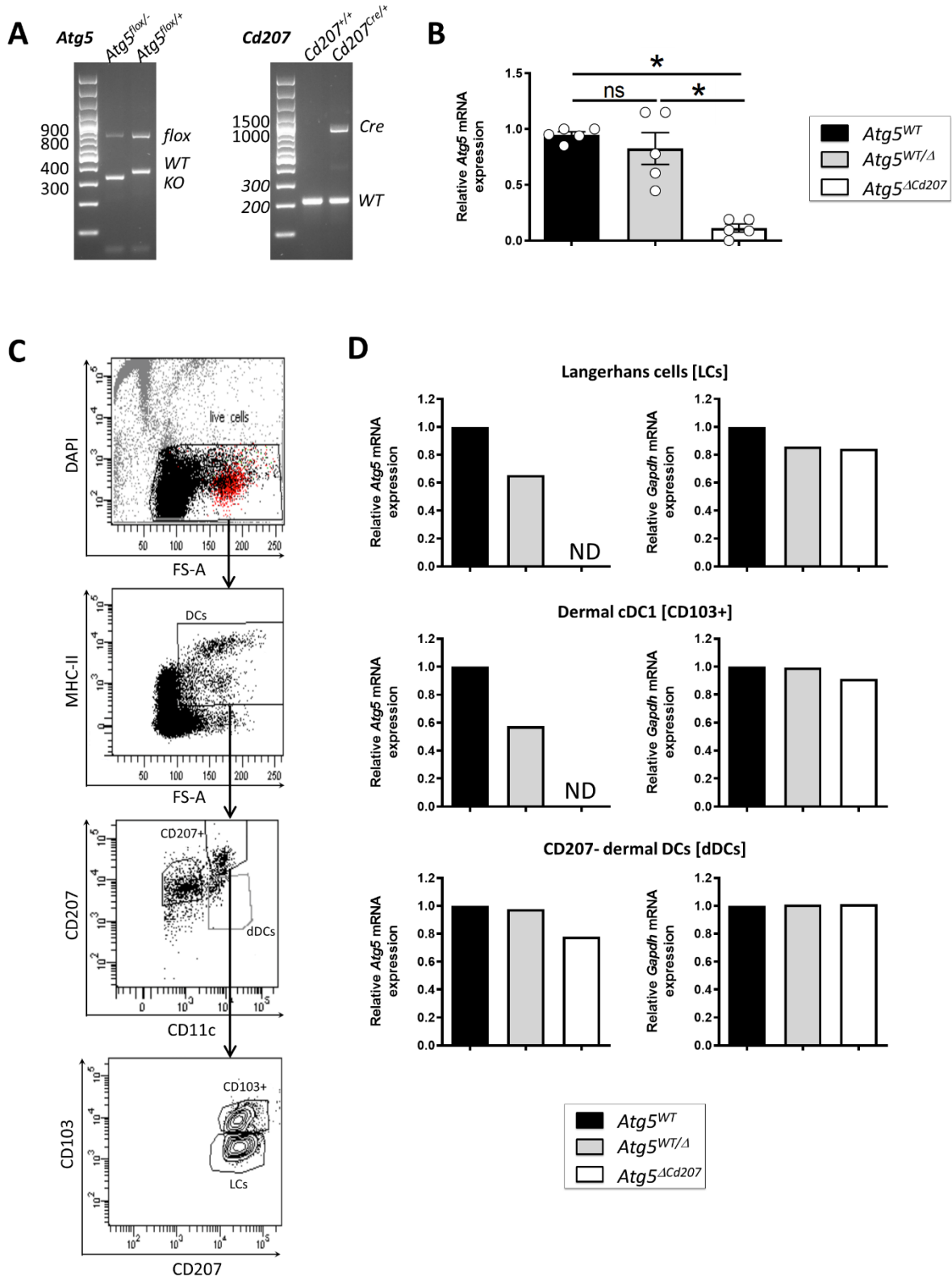# Figure S2: *Atg5* is efficiently deleted in Langerhans cells and dermal cDC1 of *Atg5^{ΔCd207}* mice

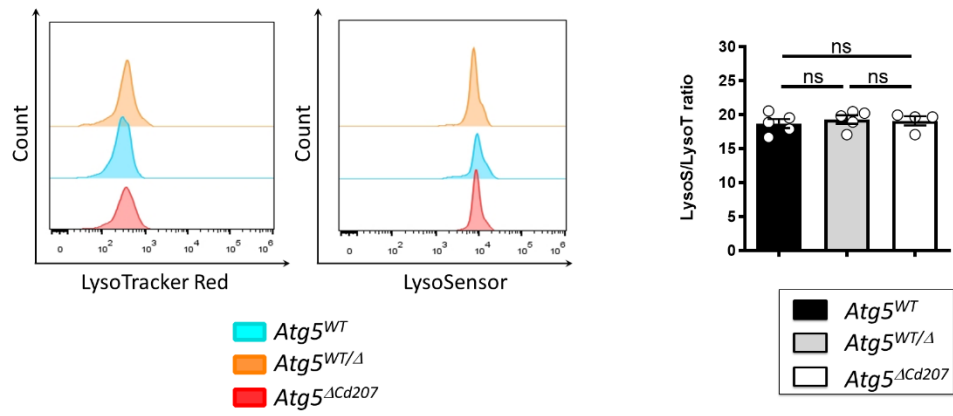**Figure S3: ATG5-deficient LCs have functional lysosomes.**

Count

LysoTracker Red

Count

LysoSensor

$Atg5^{WT}$
$Atg5^{WT/\Delta}$
$Atg5^{\Delta Cd207}$

LysoS/LysoT ratio

ns
ns
ns

30
25
20
15
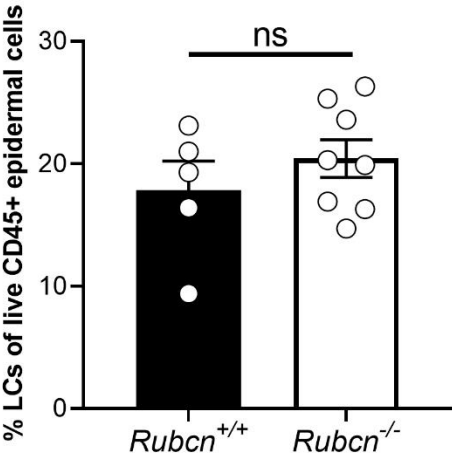10
5
0

$Atg5^{WT}$
$Atg5^{WT/\Delta}$
$Atg5^{\Delta Cd207}$

Figure S4: Rubicon deficiency does not alter the Langerhans cell network

Figure S5: ATG5 deficiency does not affect cDC1 homeostasis.

A

Skin DCs (Lin- CD11c+ MHCII+)

Atg5^{WT}   *Atg5^{ΔCd207}*

B
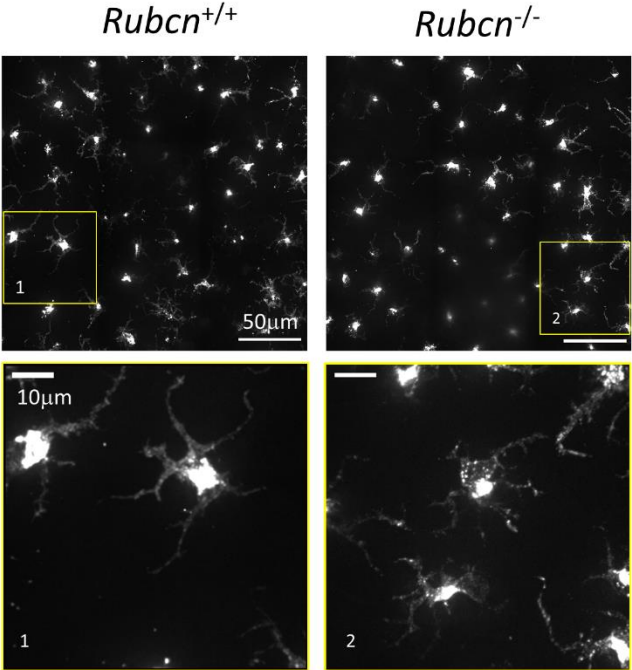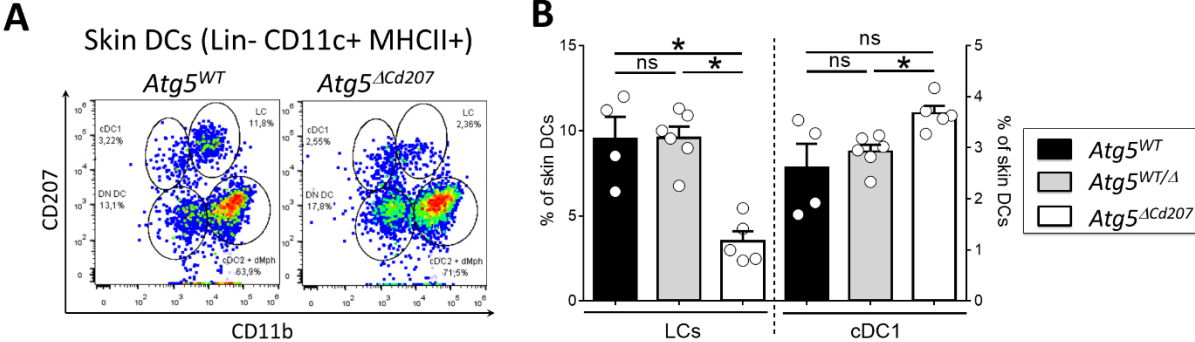
Figure S6: ATG5 deficient LCs present ER swelling but no unfolded protein response.
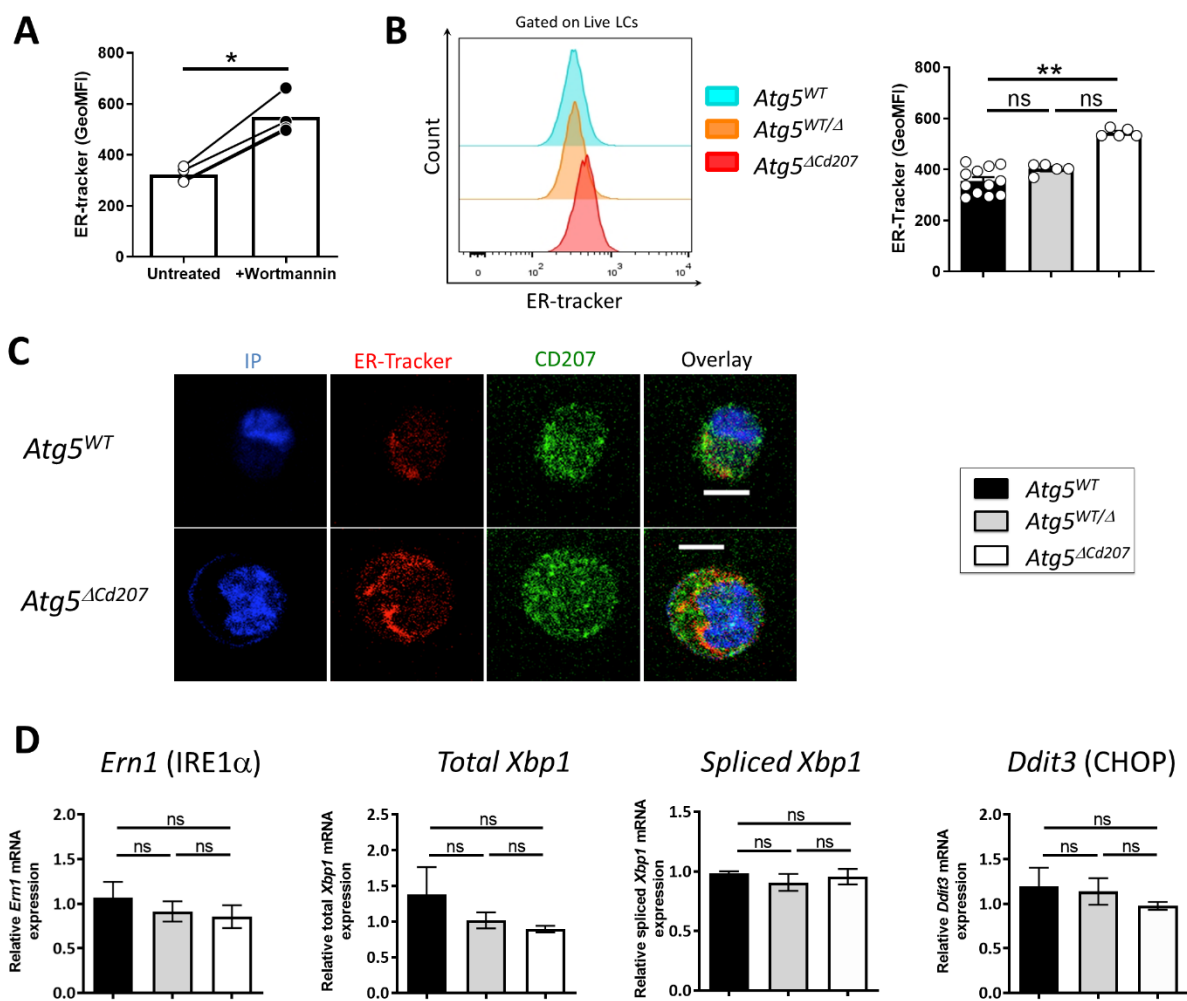
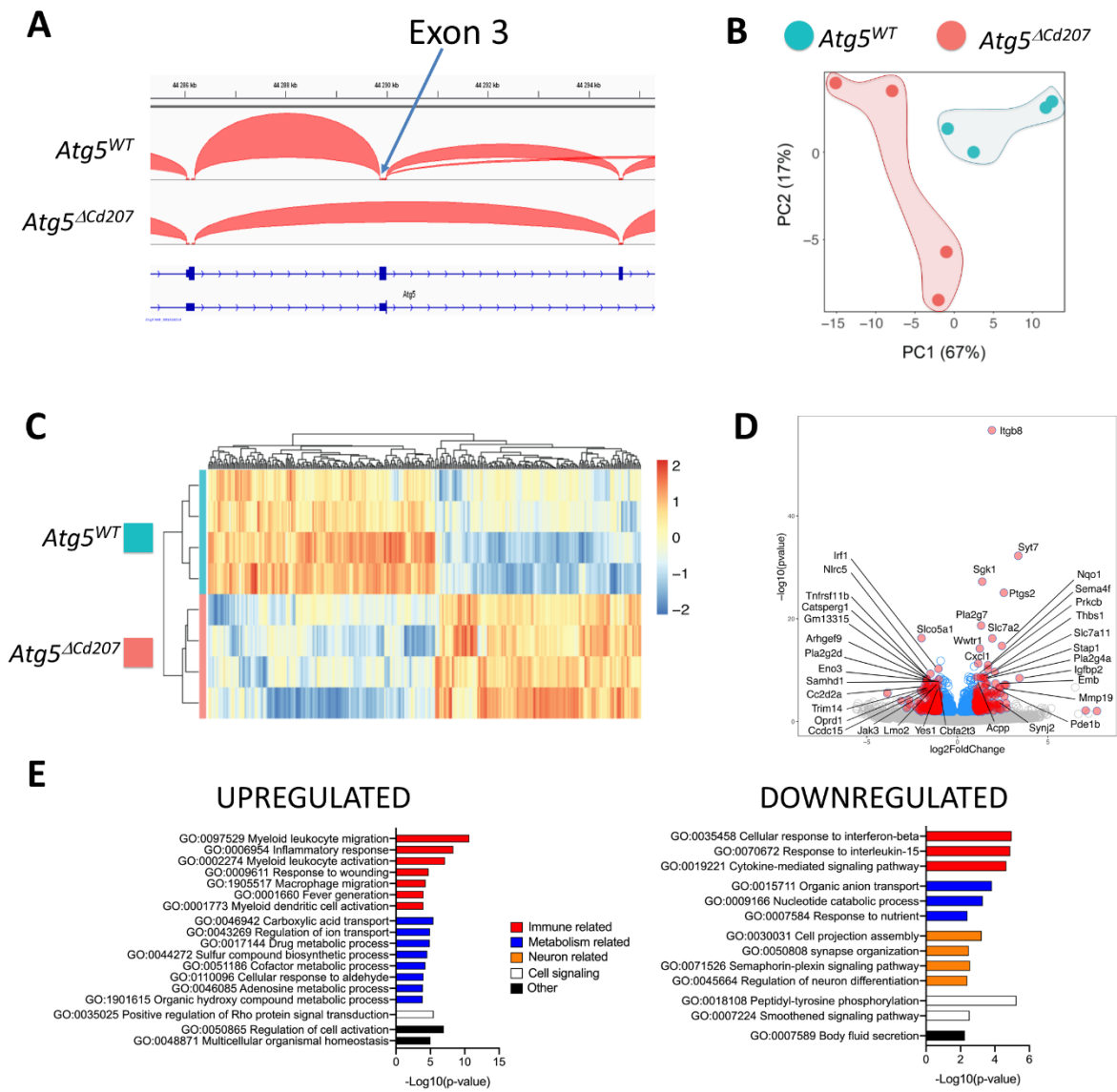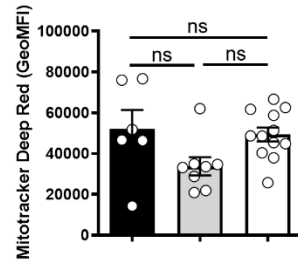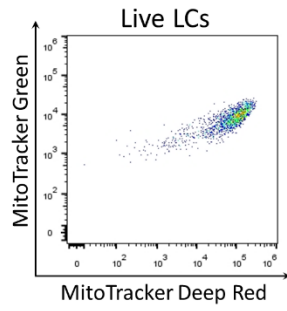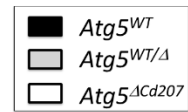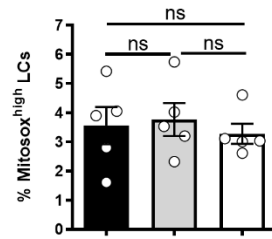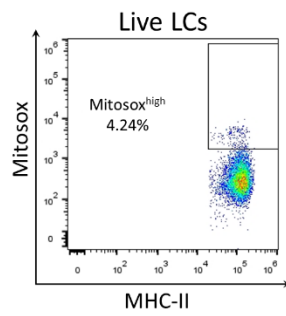**Figure S7: Lack of autophagy alters the transcriptome of Langerhans cells**

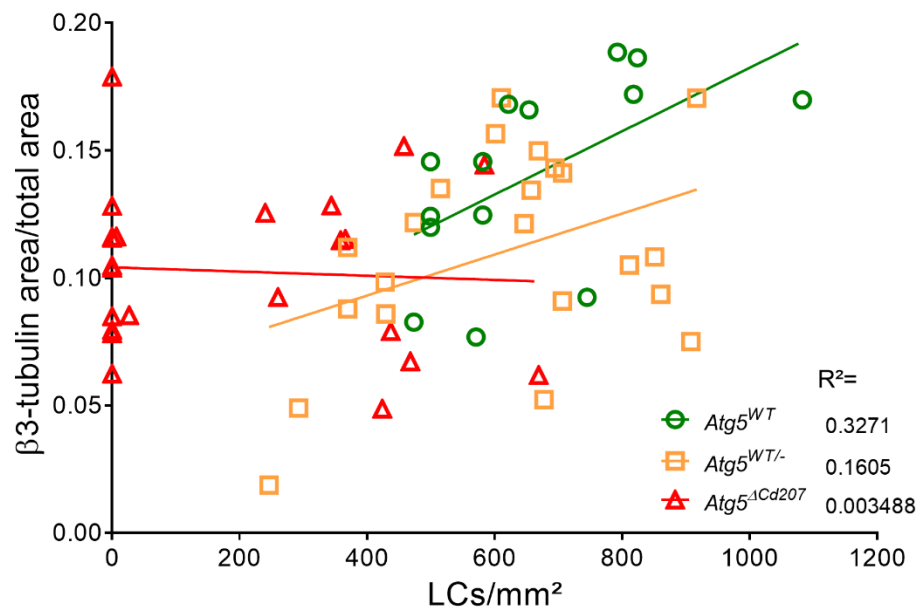**Figure S8: ATG5-deficient LCs do not display defects in mitochondrial function.**

Figure S9: Correlation of epidermal nerve and Langerhans cell densities is lost in *Atg5^{ΔCd207}* mice.

Annex 2 :

Manuscript in preparation

The hair cycle underlies regulation of Langerhans cell renewal.

Context

Langerhans cells (LCs) are the immune sentinels of the epidermis, including the pilosebaceous unit. Part of them is associated with the hair follicle or next to the sebaceous glands. Moreover, the density of LCs varies across skin areas, which primarily differ from each other by the density and type of hair. During his PhD thesis with Dr. Christopher Mueller, Benjamin Voisin worked with Dr. Vincent Flacher to determine whether hair follicle renewal exerts an influence on LCs. He found that the periods of hair growth coincided with intense proliferative activity of LCs. Further experiments and in vitro blocking with an antagonist antibody identified the cytokine IL-34 as a key factor to promote LC proliferation during the anagen phase.

These findings were reported in a manuscript that was made available in 2019 through the online repository bioRxiv and provided thereafter. This manuscript was unsuccessfully submitted to different journals, and the comments of reviewers consistently suggested to generate a mouse strain with inducible, hair follicle-specific genetic deletion. In recent years, Dr. Flacher has developed two mouse models based on CRE-ER^{T2} expression controlled by the *Lgr5* or *Sox9* promoters, which are specific of different stem cell populations that respectively give rise to the lower and upper parts of the hair follicle. Dr. Flacher allowed me to handle the quantification of LC proliferation according to hair follicle cycling in the *Sox9-CreERT2 Il34$^{fl/fl}$* model. Analyses of these experiments are still ongoing under the supervision of Dr. Voisin, now a postdoctoral fellow in the team, and they could not be reported yet in the present manucript. However, my significant contribution granted me a position as the second author in the revised version which is under preparation.

The hair cycle underlies regulation of Langerhans cell renewal.

Benjamin Voisin[1], Wacym Boufenghour[1], Dimitri Chartoire[1], Caroline Devouassoux[1], Christine Kowalczyk-Quintas[2], François Clauss[3], Frédéric Lezot[4], Pascal Schneider[2], Vincent Flacher[1]* and Christopher G. Mueller[1]*#

1 Laboratory CNRS I²CT/UPR3572 Immunology, Immunopathology and Therapeutic Chemistry, Strasbourg Drug Discovery and Development Institute (IMS), Institut de Biologie Moléculaire et Cellulaire, Strasbourg, France.

2 Department of Biochemistry, University of Lausanne, Epalinges, Switzerland.

3 INSERM UMR1109 Osteoarticular and Dental Regenerative Nanomedicine, Faculté de Chirurgie Dentaire, Pôle de Médecine et de Chirurgie Bucco-Dentaires, Strasbourg, France.

4 UFR Médecine et Techniques Médicales, Pôle Os - Articulations - Chirurgie Plastique, Nantes, France

*V. Flacher and C.G. Mueller contributed equally to this paper

#Correspondence: Dr. Christopher G. Mueller: c.mueller@ibmc-cnrs.unistra.fr

Condensed title: Hair cycle regulates Langerhans cell homeostasis

ABSTRACT

In the epidermis, Langerhans cells (LCs) provide an essential link between the innate and adaptive immune systems. They self-renew in situ and continuously transport antigen from skin to lymph node (LN) T cells in the steady state. The cyclic renewal of hair follicles (HF) causes profound alterations in the cutaneous microenvironment, however little is known about its impact on LC homeostasis. Here we show that mouse LCs developed normally in the absence of hair but perceived critical transition periods in the hair cycle. LCs underwent a proliferation burst during the HF growth phase (anagen). Reinitiation or abolishment of anagen as well as loss of the HF had direct consequences on LC self-renewal. Because dividing LCs were found close to the anagen HF, we searched for the proliferative signal within this structure and identified increased *Il34* expression by HF stem cells and their progeny. Inhibition of the IL-34 receptor CSF-1R at the onset of anagen completely and specifically blocked LC proliferation. Altogether, our findings demonstrate that the hair cycle directly oversees LC self-renewal and migration.

INTRODUCTION

Organized in a dense network within the epidermis, Langerhans cells (LCs) are the outermost sentinels of the skin immune system **(Kaplan, 2017;Doebel *et al.*, 2017)**. Their location allows them to efficiently collect antigens from keratinocytes, commensal or pathogenic microorganisms, or topically-applied chemicals. When activated by environmental danger signals, LCs migrate into skin-draining LNs where they present antigens to T cells. In the steady state, the traffic occurs continuously but at a lower frequency. LCs that reach LNs without prior exposure to danger signals are thought to contribute to immune tolerance **(Steinman and Nussenzweig, 2002;Flacher *et al.*, 2014;Idoyaga *et al.*, 2013;Seneschal *et al.*, 2012)**. Recently, molecular mechanisms governing this spontaneous emigration have been revealed **(Bobr *et al.*, 2012;Zahner *et al.*, 2011)**, although further investigations on their initiation are still needed.

Development of the LC network requires precursors derived from the yolk sac or the fetal liver and recruited into the embryonic skin **(Hoeffel *et al.*, 2012;Schulz *et al.*, 2012)**. Shortly after birth, these precursors differentiate into *bona fide* LCs and undergo intense but transient proliferation to take up residence in the newly formed epithelium **(Chorro *et al.*, 2009)**. In adult mice, the integrity of the network is maintained by a low-rate self-renewal **(Giacometti and Montagna, 1967;Czernielewski *et al.*, 1985;Merad *et al.*, 2002)**, likely originating from a specialized LC subset endowed with a higher proliferative capacity **(Ghigo *et al.*, 2013).** This unique homeostatic maintenance of LCs together with their constant traffic to the draining LNs raises important questions regarding the existence of local and/or temporal control mechanisms.

The hair follicle (HF) is a complex multilayered formation that extends from the epidermis deep into the dermis, and integrates sebaceous glands **(Schneider *et al.*, 2009;Hsu *et al.*, 2014)**. It protects mammals against extreme temperatures, UV light or physical trauma. However, at the same time, the HF provides a niche for microorganisms that can challenge the immune system **(Polak-Witka *et al.*, 2019)**. HF morphogenesis draws its origins from the interaction between the embryonic ectoderm and the underlying mesoderm and is completed two weeks after birth **(Schneider *et al.*, 2009)**. A key feature of HF is its cyclic renewal, which allows for the replacement of damaged hair shaft and seasonal adjustments to the fur coat. The cycle is subdivided in three main stages: growth (anagen), regression (catagen) and resting (telogen) **(Schneider *et al.*, 2009)**. These phases are under the control of complex regulatory mechanism entailing periodic activation and quiescence of HF-associated stem cells **(Hsu *et al.*, 2014)**. The first cycle is synchronized for most HFs until the second telogen. Later on, HFs are uncoupled and their renewal occurs with variable kinetics within different areas of the skin **(Hodgson *et al.*, 2014;Plikus *et al.*, 2011)**. It has been recognized that the hair cycle impinges on skin physiology a number of important changes **(Stenn and Paus, 2001)**. By using HF synchronization mouse models, studies have demonstrated variations in the number or activation of perifollicular macrophages, dendritic epidermal T cells (DETCs) and mast cells **(Castellana *et al.*, 2014;Paus *et al.*, 1998;Westgate *et al.*, 1991;Hashizume *et al.*, 1994;Kumamoto *et al.*, 2003)**. It has been known for a long time that LCs associate with the HF **(Breathnach, 1963;Moresi and Horn, 1997;Christoph *et al.*, 2000)**, particularly in the non-cycling distal portion and the nearby sebaceous glands **(Haid *et al.*, 2015)** that is most exposed to trauma and infection. When acute, inflammation-induced LC emigration requires the recruitment and differentiation of precursors to replenish the network **(Katz *et al.*, 1979;Ginhoux *et al.*, 2006),** HFs have been depicted as a portal to blood-derived precursors **(Nagao *et al.*, 2012)** and as a niche for keratinocytes that support TGF-Ⓑ-driven differentiation **(Mohammed *et al.*, 2016)**. Finally, deciphering the immunosurveillance of HFs is particularly important because they have been proposed as a privileged route of entry of bioactive molecules **(Knorr *et al.*, 2009)**.

In spite of these elements, the effect of the periodic activation of hair renewal and regression on LC biology remains unknown. By establishing temporal associations with the synchronized hair cycle or by

its physical and genetic manipulation, we present evidence that the hair cycle regulates LC self-renewal by CSF-1R engagement. These findings show that the dynamic changes in skin physiology elicited by the hair cycle can have a major impact on the cutaneous immune system.

MATERIAL AND METHODS

Mice. Mice were housed in specific-pathogen free conditions facilities at the Institut de Biologie Moléculaire et Cellulaire (Strasbourg, France) and at the Faculté de Biologie et Médecine de Lausanne (Lausanne, Switzerland). Il34tm1a mice were provided by Dr. Frédéric Lezot (Nantes, France). OT-II mice were purchased from Charles River Laboratories (L'Arbresle, France). All experiments were carried out in conformity to the French and Swiss animal bioethics legislation. $Rankl^{-/-}$ **(Duheron *et al.*, 2011)** and EDA-deficient *Tabby* **(Gaide and Schneider, 2003)** mice have been previously described. Due to gender-related hair growth kinetics, experimental procedures were performed on male mice only.

Antibodies and reagents. Anti-Ki67-PerCP-Cy5.5 (clone B56), anti-CD103-PE (M290), anti-CD45-APC (30-F11), anti-CD4-PerCP-Cy5.5 (RM4-5) and anti-CD8α-APC (53-6.7) antibodies were purchased from BD Biosciences (Franklin Lakes, NJ). Anti-TCRγ/δ-PE (GL3) and anti-Ia/Ie -APC or −PerCP-Cy5.5 (M5/114.15.2) antibodies were purchased from BioLegend (San Diego, CA). Anti-CD11c-PerCP-Cy5.5 (N418), anti-CD45.1-APC or -PerCP-Cy5.5 (A20) and anti-CD4-PE (GK1.5) antibodies were purchased from eBioscience (San Diego, CA). Anti-CD45-PE-Cy7 (I3/2.3) antibody was purchased from Cell LAB (Beckman-Coulter, Brea, CA). Anti-Langerin-AlexaFluor (AF) 488 or −AF647 (929F3.01) antibodies were purchased from Dendritics (Lyon, France). Anti-EpCAM (G8.8) antibody was purchased from Abcam (Cambridge, UK).

BrdU incorporation. Mice were intra-peritoneally injected with 1mg BrdU (Sigma-Aldrich, St-Louis, MO) in saline per 20-g body weight on the first experimental day. Drinking water was supplemented with 0.8 mg/mL BrdU for 3 or 4 days depending on the experimental settings. Mice were then sacrificed and back skins were collected.

Skin depilation. Adult mice (>90 days old) were anesthetized by intra-peritoneal injection of 100µg/g body weight of Ketamine mixed with 10µg/g body weight of xylazine. The hair of the back skin was trimmed by an electric razor before removal with cold wax (Klorane).

CSF-1R blocking in vivo. Mice were anesthetized by isoflurane inhalation and received on the first experimentation day 0.5mg of anti-CSF-1R blocking antibody AFS98 **(Fend *et al.*, 2013;Sudo *et al.*, 1995;Greter *et al.*, 2012)**, kindly provided by Dr. Hélène Haegel (Transgene SAS, Strasbourg) or rat IgG2a isotype control (2A3, BioXcell, West Lebanon, NH) by sub-cutaneous injections. Each following day mice were similarly injected with 0.25mg of blocking or isotype control antibodies until sacrifice.

Reversion of hairless tail phenotype in EDA-deficient (*Tabby*) mice. Briefly, hair follicle deficiency in the tail of *Tabby* mice was reverted by intravenous injection of 100µg anti-EDAR agonist antibody (clone EDAR3) into pregnant mice at E14 of gestation **(Kowalczyk *et al.*, 2011)**.

Skin cell suspensions. Back or tail skins were taken at precise timings corresponding to HF morphogenesis (d5 and d14), catagen/telogen (d20 and d45), anagen (d27 and d35) or unsynchronized (d90) phases, as previously described **(Lin *et al.*, 2009)**. For epidermal cell isolation, the hypodermis was mechanically removed from tail and back skins with a razor. Then skins were incubated, dermal side down, in RPMI medium (Lonza) supplemented with 2% FCS and 1mg/mL dispase II (Roche) overnight at 4°C. Epidermis was removed from the dermis and incubated at 37°C in trypsin solution (TrypLE Select, Life Technologies) for 45 minutes. Cells were liberated by gentle shaking, filtered through 100µm and 40µm cell strainers (BD) to remove epidermal fragments and hair, and washed in saline supplemented in 2% FCS and 0.2mM EDTA (SE buffer).

Flow cytometry. To label viable cells and block Fc receptors, cell suspensions were pre-incubated for 20 minutes at 4°C with Fixable Viability Dye eFluor780 (eBioscience) and 2µg/mL of anti-CD16/CD32 antibody (clone 2.4G2, BD). Surface staining was done with 1µg/mL of appropriate antibodies diluted

in SE buffer for 15 minutes at 4°C and washed twice. For intracellular staining, cells were fixed and permeabilized for 20 minutes at 4°C (Cytofix/Cytoperm buffer, BD), washed and labeled with 1µg/mL appropriate antibodies for 20 minutes at 4°C. BrdU and Ki-67 detection with Flow BrdU or Ki-67 detection kit (BD Pharmingen) were performed according to the manufacturer's protocol. Flow cytometry acquisitions were performed with a FACS Gallios™ system (Beckman Coulter) and data was analyzed with Flowjo software (TreeStar, Ashland, OR).

Epidermal sheet preparation and labeling. Tail skin epidermis from C57Bl/6, *Tabby* or control mice were isolated from dermis by dispase II treatment as described above. Epidermal sheets were fixed with cold acetone on ice for 20min. Sheets were then washed in TRIS-buffered saline (TBS) and non-specifics sites were blocked in TBS supplemented with 5% donkey serum for 1 hour at room temperature. Tissues were then incubated with 1µg/mL anti-Langerin-AF488 or 1µg/mL uncoupled anti-Ia antibody (2G9, BD) for 3 hours at room temperature. After washing, sheets were incubated with 0.5µg/mL A555-coupled donkey anti-rat antibody for 1 hour at room temperature. DAPI staining was then realized for 15 minutes at room temperature. Stained tissues were mounted in medium from Dako (Glostrup, Denmark). Images were acquired on a widefield fluorescence microscopy (Axiovert 200M, Zeiss, Iena, Germany) with a 10x or 20x objective (EC Plan-Neofluar, NA: 1.3).

Histochemistry and image acquisition. Collected samples comprised pieces of juvenile back skin (d27), depilated skin (d+7) and dermis (d27) isolated from epidermis by dispase II treatment, as described above. Samples were fixed in 4% paraformaldehyde for 48 hours at 4°C. Tissues were then included in paraffin. Briefly, the inclusion protocol consisted of a 3 hour incubation in 70% ethanol, 4 hours in 95% ethanol, 16 hours in 100% ethanol, 24 hours in butanol before 48 hours inclusion in paraffin. Tissue was sectioned (8µm) with a microtome (RM2235, Leica, Wetzlar, Germany) and heated overnight at 58°C. Deparaffinization steps comprised incubations in 100% Toluene, 100% ethanol, 95% ethanol, and distilled water.

Sections obtained from depilated skins and skin from mice treated with anti-CSF-1R blocking antibody or control isotype were colored with hematoxylin and eosin. Sections of mouse skin (d27) treated or not with dispase II were colored in Masson's trichrome.

For immunolabeling, juvenile back skin slices were first deparafinized, followed by a demasking step in boiling 10mM EDTA for 30 minutes. Non-specific sites were blocked in TBS supplemented with 5% donkey serum for 1 hour at room temperature. Tissues were then incubated with 1µg/mL anti-Langerin (M200, Santa Cruz, Dallas, TX) and 20µg/mL anti-Ki67 (TEC-3, Dako) antibodies diluted in TBS with 2% donkey serum for 3 hours at room temperature. After 2 washes in saline, sections were incubated with 0.5µg/mL donkey anti-mouse AF488-coupled secondary antibody (Life Technologies) and 0.5µg/mL donkey anti-rat Cy3-coupled secondary antibody (Jackson ImmunoResearch, West Grove, PA) for 1 hour at room temperature. Tissues were then washed three times and labeled with DAPI for 15 minutes at room temperature before mounting in Dako medium. Z-stack acquisitions were performed with the Axio observer Z1 microscope (Zeiss) equipped with a LSM700 confocal head (Oil-objective 40x, EC Plan-Neofluar, NA: 1.30). Compilations and analysis were realized with Image J software (Macbiophotonics, NIH). For statistics, at least 50 hair follicles were analyzed.

LacZ stainings. Sections (12µm) of $Il34^{tm1a}$ and $Il34^{wt}$ epidermis embedded in OCT were cut using Cryostat Leica CM3050S. Slices were fixed with PFA 1% 5min, rinced with PBS 1x and incubated in Xgal (5-bromo-4-chloro-3-indolyl-beta-D-galactopyranoside) solution overnight at 37°C. Sections were rinced with PBS 1x, left to dry and mounted with EUKITT® medium.

Cyclosporin A treatment. C57BL/6 mice were shaved (d-4), then injected subcutaneously with 50µL saline or cyclosporin A (Sandimmun; Novartis) diluted at 50mg/kg into each flank. Injections were repeated at d-2 and d0. At d5, d11 and d17, mice were treated with BrdU as described above. Three days later, epidermal suspensions were generated from back skin and LCs were tested for BrdU incorporation by flow cytometry.

FACS sorting, RNA extraction and quantitative RT-PCR. Isolated epidermal cells from telogen (d20) or anagen (d27) skin were sorted on a FACSAria II (BD) on the basis of their Sca-1, CD34 and CD49f profile expression. Sorted cells (>95% purity upon post-sort verification) were lysed in RLT buffer (Qiagen, Venlo, The Netherlands). RNA was extracted with RNeasy Micro kits (Qiagen), and cDNA was synthesized with oligo(dT)15 primers and the Thermo Scientific Maxima First Strand cDNA Synthesis Kit. Quantitative PCR was performed using Thermo Scientific Luminaris Color HiGreen qPCR Master Mix and ran on a Stratagene MX4000 thermal cycler. Gene-specific primers are listed in Table S1. CT values of target genes were normalized to GAPDH, HPRT and β-actin. The expression factor was calculated by using the Relative Expression Software Toll (REST, http://mmm.gene-quantification.de/rest.html).

RESULTS

The Langerhans cell network develops in the absence of hair follicles

The development of the LC network coincides with HF formation between embryonic day 14.5 and post-natal day 15 (**Schulz *et al.*, 2012;Schmidt-Ullrich and Paus, 2005**), and immunofluorescence staining of hairy (tail skin) epidermal sheets revealed a close association between LCs and the HF infundibulum (**Fig. 1A**). In light of this spatiotemporal relationship between LCs and HFs, we first asked whether formation of the LC network is dependent on HF morphogenesis. Among the different mouse models lacking hair, mice deficient for epithelial morphogen ectodysplasin-A (EDA), a TNF-family member, or its receptor are particularly relevant because they display an embryonic deficiency in HFs (**Gruneberg, 1971;Headon and Overbeek, 1999**). The *Tabby* mouse is a natural mutant of EDA and is completely devoid of HFs on the tail and behind the ears because of a complete lack of morphogenesis (**Mikkola, 2008**). Immunofluorescence staining for MHC-II in hairless tail epidermis of *Tabby* mice revealed the presence of a LC network comparable to that of wild-type mice. (**Fig. 1B**). Therefore, HF morphogenesis is dispensable for LC development and residence in the epithelium.

A Langerhans cell proliferation burst occurs concomitantly with the anagen hair cycle phase

To assess the impact of the hair cycle on LC renewal we took advantage of the synchronized first postnatal hair cycle of mouse back skin (**Fig. 2A**) (**Schneider *et al.*, 2009**). At critical time points of the cycle, back skin was processed with dispase II to allow a clean separation of the whole epidermo-pilosebaceous unit from the dermis (**Fig. S1**) (**Gilliam *et al.*, 1998**). LCs were then liberated by trypsin digestion and expression of the Ki-67 cell division marker determined by flow cytometry (**Fig. 2B, C**). As expected (**Chorro *et al.*, 2009**), LC proliferation was high at d5 and then declined. Strikingly, we found a reactivation of LC proliferation (22 ± 4.6%) concomitant with early anagen (d27) before the proportion of Ki-67^{+} LCs returned to the low levels of adults (d90). Maximal bromodeoxyuridine (BrdU) incorporation into anagen LCs confirmed the high proliferation rate at this phase of the hair cycle (**Fig. 2D, E**). However, no such anagen-associated increase was observed for dendritic epidermal T cells (DETCs) (**Fig. S2**). Thus, the anagen phase of the natural hair cycle is associated with a high rate of LC proliferation.

Hair cycle manipulation modifies Langerhans cell proliferation

To further establish a direct relationship between LC proliferation and the growth phase of the hair cycle, we next tested whether physical and genetic manipulations of the cycle would affect LC turnover. Hair shaft removal provoked by depilation triggers synchronized hair growth in adults (**Fig. 3A**) (**Chase, 1954;Paus *et al.*, 1990**). We measured LC proliferation in this model at different time points and observed a peak at early induced anagen (d+7) (**Fig. 3B**).

A well-described side effect of cyclosporin A (CsA), a widely prescribed immunosuppressant drug, is the enhancement of hair growth **(Paus *et al.*, 1998)**. We followed LC proliferation in mice shaved then injected subcutaneously with CsA **(Fig. S3A)**. As expected, the back fur grew back faster in CsA-treated mice **(Fig. S3B)**. In line with this, the rate of BrdU+ LCs was increased 5-11 days after the CsA treatment **(Fig. S3C)**.

Next, we investigated mice deficient for TNF-family member RANKL/TNFSF11, which are unable to transit into anagen **(Duheron *et al.*, 2011)**. Although LCs retained a normal capacity to proliferate shortly after birth (d14), the anagen proliferation burst observed in control mice (d27) was missing in *Rankl*⁻/⁻ mice **(Fig. 3C, D)**. Finally, we made use of the *Tabby* mice that lack tail HFs. At d35 when tail hair undergoes anagen **(Hodgson *et al.*, 2014)**, LC division was measured in *Tabby* mice and compared with *Tabby* mice rescued by embryonic administration of agonist anti-EDAR antibody **(Kowalczyk *et al.*, 2011)**. At the expected time for anagen, tail LC proliferation of *Tabby* mice was clearly reduced in comparison to rescued mice **(Fig. 3E, F)**. Taken together, these findings demonstrate that anagen is directly associated with a high LC proliferation rate.

Dividing Langerhans cells are physically associated with the hair follicle

To investigate the spatial relationship between proliferating LCs and cycling HFs, we labelled anagen skin cross-sections for Langerin and Ki-67. Similar to the epidermal sheet overview shown in **Figure 1A** and in line with previous findings **(Breathnach, 1963;Moresi and Horn, 1997;Christoph *et al.*, 2000)**, LCs were found in both the interfollicular areas and the upper portion of the HF **(Fig. 4A)**. The number of Ki-67⁺ LCs was determined in the interfollicular section (blue outline) and the HF (yellow outline). We found that the large majority of LCs undergoing cell division resided in or close to the HF (**Fig. 4B**). This finding suggests that the anagen HF conveys LC proliferation signals.

Anagen-associated Langerhans cell proliferation relies on CSF-1R signaling

The cytokine IL-34 is expressed by epithelial cells and plays a critical role in the maintenance of the LC network **(Greter *et al.*, 2012;Wang *et al.*, 2012)**. Because CSF-1R is the high-affinity receptor for IL-34 **(Lin *et al.*, 2008)**, and previous reports have confirmed identical effects of CSF-1R blocking and deficiency in IL-34 **(Greter *et al.*, 2012)**, we assessed the functional relevance of CSF-1R signaling on LC renewal. Therefore, we administered antagonistic anti-CSF-1R antibody to mice at the onset of anagen and for 3 days, together with BrdU (**Fig. 5A**). This regimen was sufficient to impair CSF-1R signaling, as shown by a strong reduction of monocytes in peripheral blood (**Fig. S4A**) **(Greter *et al.*, 2012)** without disturbing transition into anagen (**Fig. S4B**). Although the treatment did not decrease the overall percentage of LCs in the epidermis **(Fig. S4C)**, CSF-1R blocking led to a substantial repression of LC proliferation (**Fig. 5B, C**). In contrast, the cell division of DETCs (**Fig. S4D, E**) and keratinocytes (**Fig. S4D, F**) remained unchanged. This suggests that CSF-1R signaling is implicated in LC proliferation during the hair cycle growth phase.

IL-34 is expressed by anagen-activated hair follicle stem cells

Since CSF-1R blocking affected LC proliferation in anagen, we addressed the question of whether the HF produces IL-34. Using *Il34*^tm1a mice that express the *LacZ* gene under control of the *Il34* promoter **(Greter *et al.*, 2012;Wang *et al.*, 2012)**, we observed β-galactosidase activity in the interfollicular epidermis and in the upper part of the HF, corresponding to the infundibulum **(Fig. 6A)**. No obvious difference could be visualized when comparing HF in anagen vs. telogen.

To extend this observation, we sorted the different epithelial cell types of anagen and telogen HFs (**Fig. 6B, C**) **(Jensen *et al.*, 2008;Nagao *et al.*, 2012)** and measured *Il34* transcriptional activity in each subset (**Fig. 5C**). Among non-hematopoietic (CD45^neg) cells, we first distinguished Sca-1⁺ CD34⁻ interfollicular and infundibulum keratinocytes. For this subset, there was no difference in *Il34* mRNA synthesis between the two phases, similarly to our observations in the IL-34tm1a model (**Fig. 6D**). The Sca-1⁻ CD34⁻ cycling portion of the HF showed an increase in *Il34* mRNA during anagen. An even greater

induction of *Il34* expression was noted for the CD34$^+$ CD49f$^-$ stem cells of the bulge area, a cell subset which in addition is amplified during anagen (44 ± 5 % in telogen versus 77 ± 1.5 % in anagen) (**Fig. 6C**). Thus, although this could not be visualized in *Il34*^{tm1a} mice, HF-associated suprabasal stem cells or their progeny might contribute to a localized increase in IL-34 production during hair growth.

DISCUSSION

The immune sentinel function of LCs implies a fine regulation of their epidermal network. This most likely depends on matching their in situ proliferation with their rate of migration to LNs. Although the cyclic renewal of HF has recognized effects on skin physiology, its impact on LCs had so far not been addressed. In this study, we present evidence that the hair cycle exerts a strong influence on LC self-renewal.

By comparing the rate of cell division between postnatal LC development, the different phases of the hair cycle and adult resting skin, we uncovered a strikingly high level of LC renewal during the first synchronized anagen phase. More precisely, it occurred at early anagen, when the HF is in its maximal activity. Mutants that fail to transit into anagen (*Rankl*$^{-/-}$) or that are devoid of HFs (*Tabby*) lacked this proliferation burst. However, DETCs, a specialized subset of epithelial gamma/delta T cells also residing in the epidermis and capable of self-renewal **(Honjo *et al.*, 1990;Sumaria *et al.*, 2011)**, were unresponsive to natural anagen. These findings demonstrate a direct and specific relationship between the hair cycle and LC self-renewal. Moreover, LCs underwent increased cell division in response to synchronized anagen in the adult. Depilation is a well-established model to reinitiate hair growth in the adult, when otherwise the hair cycle occurs in a stochastic fashion **(Paus *et al.*, 1998;Plikus *et al.*, 2011)**. Although it is difficult to totally rule out some degree of inflammation in this model, it should be noted that anagen-associated LC proliferation occurs one week after depilation, i.e. after the acute inflammatory response. It is therefore probable that the hair cycle also affects LC renewal in the unsynchronized animal, although such measures are offset by the simultaneous occurrence of catagen, telogen and anagen phases in different body areas **(Hodgson *et al.*, 2014)**.

CSF-1R is the high affinity receptor for cytokines CSF-1/M-CSF and IL-34 **(Lin *et al.*, 2008)**. A number of elements incited us to ask whether the CSF-1R / IL-34 axis plays a functionally important role in anagen LC proliferation. First, the expression of CSF-1R is critical for LC development **(Ginhoux *et al.*, 2006)**. Secondly, only the deletion of *Il34*, but not *Csf1*, results in the absence of LCs **(Wang *et al.*, 2012;Greter *et al.*, 2012)**. Finally, previous findings on human monocytes support the importance of CSF-1R in cell division **(Clanchy *et al.*, 2006;Lin *et al.*, 2008)**. We therefore tested the role of CSF-1R in anagen LC renewal. Detailed analyses of *Il34*^{tm1a} mouse skin showed the presence of *Il34* expression within HFs. The use of antagonistic antibody against CSF-1R **(Greter *et al.*, 2012)** allowed for precisely timed CSF-1R inhibition, thereby restricting the blocking effects to the anagen phase without interfering with development of the LC network (Wang, Greter). This approach revealed the importance of CSF-1R signaling for LC proliferation during anagen. The unresponsiveness of keratinocytes and DETCs to the blocking antibody strongly suggests that CSF-1R blocking has no effect on the other epidermal cell types.

The lack of a role for CSF-1 in LC development and homeostasis **(Ginhoux *et al.*, 2006)**, the higher affinity of IL-34 for CSF-1R **(Lin *et al.*, 2008)**, and the demonstration that CSF-1 is not expressed by murine epidermal cells (http://biogps.org/#goto=genereport&id=12977) **(Greter *et al.*, 2012)** strongly supports that IL-34 is the CSF-1R ligand responsible for LC proliferation. However, our experiments do not formally exclude a contribution of CSF-1, which has been suggested in the context of cutaneous inflammation **(Wang *et al.*, 2016)**. Despite our efforts, we did not succeed in reliably estimating the local concentration of IL-34 protein with commercially available ELISA kits. Although the *LacZ* reporter system did not reveal any clear difference of *Il34* promoter activity between anagen and telogen HFs, *Il34* transcription determined by RT-qPCR clearly increased in anagen in the stem cell compartment of

the so-called bulge. This region lies just below the constant portion of the HF where reside those LCs that undergo most cell division during anagen. In this context, it can be noted that, in a model of human skin activation by UV, the majority of dividing LCs also localized to the distal part of the HF **(Gilliam *et al.*, 1998)**. It was not possible to further dissect the infundibulum from the epidermis because of lack of cell-specific markers.

Previous studies in the context of inflammation suggest that LC renewal and migration to LNs are intrinsically linked **(Katz *et al.*, 1979;Ginhoux *et al.*, 2006)**. Our attempts to evaluate LC density at catagen and anagen proved unreliable because the interference of the numerous HF in back skin precluded a clear LC visualization. In addition, the result would have been questionable in the context of a rapidly growing juvenile mouse. Yet, the previous finding that *Rankl*$^{-/-}$ mice display a reduced LC density comes in support of the idea that anagen is required to positively adjust the network density **(Barbaroux *et al.*, 2008)**.

Altogether, our study highlights a novel link between the hair cycle and LC homeostasis in steady-state conditions. The demonstration that LC self-renewal is regulated by the hair cycle should incite further investigations into factors released by this ectodermal appendage on the skin immune system.

ACKNOWLEDGEMENTS

BIBLIOGRAPHY

Barbaroux J.B., M. Beleut, C. Brisken, C.G. Mueller, R.W. Groves. 2008. Epidermal receptor activator of NF-kappaB ligand controls Langerhans cells numbers and proliferation. *J. Immunol.* 181:1103-1108.

Bobr A., B.Z. Igyarto, K.M. Haley, M.O. Li, R.A. Flavell, D.H. Kaplan. 2012. Autocrine/paracrine TGF-beta1 inhibits Langerhans cell migration. *Proc. Natl. Acad. Sci. U. S. A* 109:10492-10497. **http://dx.doi.org/10.1073/pnas.1119178109**

Breathnach A.S. 1963. The distribution of Langerhans cells within the human hair follicle, and some observations on its staining properties with gold chloride. *J Anat.* 97:73-80.

Castellana D., R. Paus, M. Perez-Moreno. 2014. Macrophages contribute to the cyclic activation of adult hair follicle stem cells. *PLoS. Biol.* 12:e1002002. **http://dx.doi.org/10.1371/journal.pbio.1002002** [doi];PBIOLOGY-D-14-01467 [pii]

Chase H. 1954. Growth of the hair. *Physiol Rev.* 34:113-126. **http://dx.doi.org/10.1152/physrev.1954.34.1.113** [doi]

Chorro L., A. Sarde, M. Li, K.J. Woollard, P. Chambon, B. Malissen, A. Kissenpfennig, J.B. Barbaroux, R. Groves, F. Geissmann. 2009. Langerhans cell (LC) proliferation mediates neonatal development, homeostasis, and inflammation-associated expansion of the epidermal LC network. *J Exp Med.* 206:3089-3100. **http://dx.doi.org/10.1084/jem.20091586**

Christoph T., S. Muller-Rover, H. Audring, D.J. Tobin, B. Hermes, G. Cotsarelis, R. Ruckert, R. Paus. 2000. The human hair follicle immune system: cellular composition and immune privilege. *Br. J Dermatol.* 142:862-873.

Clanchy F.I., A.C. Holloway, R. Lari, P.U. Cameron, J.A. Hamilton. 2006. Detection and properties of the human proliferative monocyte subpopulation. *J Leukoc. Biol.* 79:757-766. **http://dx.doi.org/10.1189/jlb.0905522**

Czernielewski J., P. Vaigot, M. Prunieras. 1985. Epidermal Langerhans cells - a cycling cell population. *J. Invest. Dermatol.* 84:424-426.

Doebel T., B. Voisin, K. Nagao. 2017. Langerhans Cells - The Macrophage in Dendritic Cell Clothing. *Trends Immunol.* 38:817-828. **http://dx.doi.org/S1471-4906(17)30123-0** [pii];10.1016/j.it.2017.06.008 [doi]

Duheron V., E. Hess, M. Duval, M. Decossas, B. Castaneda, J.E. Klopper, L. Amoasii, J.B. Barbaroux, I.R. Williams, H. Yagita, J. Penninger, Y. Choi, F. Lezot, R. Groves, R. Paus, C.G. Mueller. 2011. Receptor activator of NF-kappaB (RANK) stimulates the proliferation of epithelial cells of the epidermo-pilosebaceous unit. *Proc. Natl. Acad. Sci. U. S. A* 108:5342-5347. **http://dx.doi.org/10.1073/pnas.1013054108**

Fend L., N. Accart, J. Kintz, S. Cochin, C. Reymann, P.F. Le, J.B. Marchand, T. Menguy, P. Slos, R. Rooke, S. Fournel, J.Y. Bonnefoy, X. Preville, H. Haegel. 2013. Therapeutic effects of anti-CD115 monoclonal antibody in mouse cancer models through dual inhibition of tumor-associated macrophages and osteoclasts. *PLoS. One.* 8:e73310. **http://dx.doi.org/10.1371/journal.pone.0073310**

Flacher V., C.H. Tripp, D.G. Mairhofer, R.M. Steinman, P. Stoitzner, J. Idoyaga, N. Romani. 2014. Murine Langerin+ dermal dendritic cells prime CD8+ T cells while Langerhans cells induce cross-tolerance. *EMBO Mol. Med.* 6:1191-1204. **http://dx.doi.org/10.15252/emmm.201303283**

Gaide O., P. Schneider. 2003. Permanent correction of an inherited ectodermal dysplasia with recombinant EDA. *Nat. Med.* 9:614-618. **http://dx.doi.org/10.1038/nm861**

Ghigo C., I. Mondor, A. Jorquera, J. Nowak, S. Wienert, S.P. Zahner, B.E. Clausen, H. Luche, B. Malissen, F. Klauschen, M. Bajenoff. 2013. Multicolor fate mapping of Langerhans cell homeostasis. *J Exp Med.* 210:1657-1664. **http://dx.doi.org/10.1084/jem.20130403**

Giacometti L., W. Montagna. 1967. Langerhans cells: uptake of tritiated thymidine. *Science* 157:439-440.

Gilliam A.C., I.B. Kremer, Y. Yoshida, S.R. Stevens, E. Tootell, M.B.M. Teunissen, C. Hammerberg, K.D. Cooper. 1998. The human hair follicle: A reservoir of CD40^{+} B7-deficient Langerhans cells that repopulate epidermis after UVB exposure. *J. Invest. Dermatol.* 110:422-427.

Ginhoux F., F. Tacke, V. Angeli, M. Bogunovic, M. Loubeau, X.M. Dai, E.R. Stanley, G.J. Randolph, M. Merad. 2006. Langerhans cells arise from monocytes in vivo. *Nat. Immunol.* 7:265-273.

Greter M., I. Lelios, P. Pelczar, G. Hoeffel, J. Price, M. Leboeuf, T.M. Kundig, K. Frei, F. Ginhoux, M. Merad, B. Becher. 2012. Stroma-derived interleukin-34 controls the development and maintenance of langerhans cells and the maintenance of microglia. *Immunity.* 37:1050-1060.

Gruneberg H. 1971. The tabby syndrome in the mouse. *Proc. R. Soc. Lond B Biol. Sci.* 179:139-156.

Haid B., D.E. Schlogl, M. Hermann, C.H. Tripp, P. Stoitzner, N. Romani, V. Flacher. 2015. Langerhans cells in the sebaceous gland of the murine skin. *Exp Dermatol.* **http://dx.doi.org/10.1111/exd.12803** [doi]

Hashizume H., Y. Tokura, M. Takigawa. 1994. Increased number of dendritic epidermal T cells associated with induced anagen phase of hair cycles. *J Dermatol. Sci.* 8:119-124.

Headon D.J., P.A. Overbeek. 1999. Involvement of a novel Tnf receptor homologue in hair follicle induction. *Nat. Genet.* 22:370-374. **http://dx.doi.org/10.1038/11943**

Hodgson S.S., Z. Neufeld, R.M. Villani, E. Roy, K. Khosrotehrani. 2014. Transgenic flash mice for in vivo quantitative monitoring of canonical Wnt signaling to track hair follicle cycle dynamics. *J Invest Dermatol.* 134:1519-1526. **http://dx.doi.org/10.1038/jid.2014.92**

Hoeffel G., Y. Wang, M. Greter, P. See, P. Teo, B. Malleret, M. Leboeuf, D. Low, G. Oller, F. Almeida, S.H. Choy, M. Grisotto, L. Renia, S.J. Conway, E.R. Stanley, J.K. Chan, L.G. Ng, I.M. Samokhvalov, M. Merad, F. Ginhoux. 2012. Adult Langerhans cells derive predominantly from embryonic fetal liver monocytes with a minor contribution of yolk sac-derived macrophages. *J Exp Med.* 209:1167-1181. **http://dx.doi.org/10.1084/jem.20120340**

Honjo M., A. Elbe, G. Steiner, I. Assmann, K. Wolff, G. Stingl. 1990. Thymus-independent generation of Thy-1$^+$ epidermal cells from a pool of Thy-1$^-$ bone marrow precursors. *J. Invest. Dermatol.* 95:562-567.

Hsu Y.C., L. Li, E. Fuchs. 2014. Emerging interactions between skin stem cells and their niches. *Nat. Med.* 20:847-856. **http://dx.doi.org/10.1038/nm.3643**

Idoyaga J., C. Fiorese, L. Zbytnuik, A. Lubkin, J. Miller, B. Malissen, D. Mucida, M. Merad, R.M. Steinman. 2013. Specialized role of migratory dendritic cells in peripheral tolerance induction. *J Clin. Invest* 123:844-854. **http://dx.doi.org/10.1172/JCI65260**

Jensen U.B., X. Yan, C. Triel, S.H. Woo, R. Christensen, D.M. Owens. 2008. A distinct population of clonogenic and multipotent murine follicular keratinocytes residing in the upper isthmus. *J Cell Sci.* 121:609-617. **http://dx.doi.org/10.1242/jcs.025502**

Kaplan D.H. 2017. Ontogeny and function of murine epidermal Langerhans cells. *Nat. Immunol.* 18:1068-1075. **http://dx.doi.org/ni.3815** [pii];10.1038/ni.3815 [doi]

Katz S.I., K. Tamaki, D.H. Sachs. 1979. Epidermal Langerhans cells are derived from cells originating in bone marrow. *Nature* 282:324-326.

Knorr F., J. Lademann, A. Patzelt, W. Sterry, U. Blume-Peytavi, A. Vogt. 2009. Follicular transport route--research progress and future perspectives. *Eur. J Pharm. Biopharm.* 71:173-180. **http://dx.doi.org/10.1016/j.ejpb.2008.11.001**

Kowalczyk C., N. Dunkel, L. Willen, M.L. Casal, E.A. Mauldin, O. Gaide, A. Tardivel, G. Badic, A.L. Etter, M. Favre, D.M. Jefferson, D.J. Headon, S. Demotz, P. Schneider. 2011. Molecular and therapeutic characterization of anti-ectodysplasin A receptor (EDAR) agonist monoclonal antibodies. *J Biol. Chem.* 286:30769-30779. **http://dx.doi.org/10.1074/jbc.M111.267997**

Kumamoto T., D. Shalhevet, H. Matsue, M.E. Mummert, B.R. Ward, J.V. Jester, A. Takashima. 2003. Hair follicles serve as local reservoirs of skin mast cell precursors. *Blood* 102:1654-1660. **http://dx.doi.org/10.1182/blood-2003-02-0449**

Lin H., E. Lee, K. Hestir, C. Leo, M. Huang, E. Bosch, R. Halenbeck, G. Wu, A. Zhou, D. Behrens, D. Hollenbaugh, T. Linnemann, M. Qin, J. Wong, K. Chu, S.K. Doberstein, L.T. Williams. 2008. Discovery of a cytokine and its receptor by functional screening of the extracellular proteome. *Science* 320:807-811. **http://dx.doi.org/10.1126/science.1154370**

Lin K.K., V. Kumar, M. Geyfman, D. Chudova, A.T. Ihler, P. Smyth, R. Paus, J.S. Takahashi, B. Andersen. 2009. Circadian clock genes contribute to the regulation of hair follicle cycling. *PLoS. Genet.* 5:e1000573. **http://dx.doi.org/10.1371/journal.pgen.1000573**

Merad M., M.G. Manz, H. Karsunky, A. Wagers, W. Peters, I. Charo, I.L. Weissman, J.G. Cyster, E.G. Engleman. 2002. Langerhans cells renew in the skin throughout life under steady-state conditions. *Nat. Immunol.* 3:1135-1141.

Mikkola M.L. 2008. TNF superfamily in skin appendage development. *Cytokine Growth Factor Rev.* 19:219-230. **http://dx.doi.org/10.1016/j.cytogfr.2008.04.008**

Mohammed J., L.K. Beura, A. Bobr, B. Astry, B. Chicoine, S.W. Kashem, N.E. Welty, B.Z. Igyarto, S. Wijeyesinghe, E.A. Thompson, C. Matte, L. Bartholin, A. Kaplan, D. Sheppard, A.G. Bridges, W.D. Shlomchik, D. Masopust, D.H. Kaplan. 2016. Stromal cells control the epithelial residence of DCs and memory T cells by regulated activation of TGF-beta. *Nat. Immunol.* 17:414-421. **http://dx.doi.org/ni.3396** [pii];10.1038/ni.3396 [doi]

Moresi J.M., T.D. Horn. 1997. Distribution of Langerhans cells in human hair follicle. *J. Cutan. Pathol.* 24:636-640.

Nagao K., T. Kobayashi, K. Moro, M. Ohyama, T. Adachi, D.Y. Kitashima, S. Ueha, K. Horiuchi, H. Tanizaki, K. Kabashima, A. Kubo, Y.H. Cho, B.E. Clausen, K. Matsushima, M. Suematsu, G.C. Furtado, S.A. Lira, J.M. Farber, M.C. Udey, M. Amagai. 2012. Stress-induced production of chemokines by hair follicles regulates the trafficking of dendritic cells in skin. *Nat. Immunol.* 13:744-752. **http://dx.doi.org/10.1038/ni.2353**

Paus R., K.S. Stenn, R.E. Link. 1990. Telogen skin contains an inhibitor of hair growth. *Br. J. Dermatol.* 122:777-784.

Paus R., d. van, V, S. Eichmuller, T. Kopp, E. Hagen, S. Muller-Rover, U. Hofmann. 1998. Generation and cyclic remodeling of the hair follicle immune system in mice. *J Invest Dermatol.* 111:7-18. **http://dx.doi.org/10.1046/j.1523-1747.1998.00243.x**

Plikus M.V., R.E. Baker, C.C. Chen, C. Fare, D. de la Cruz, T. Andl, P.K. Maini, S.E. Millar, R. Widelitz, C.M. Chuong. 2011. Self-organizing and stochastic behaviors during the regeneration of hair stem cells. *Science* 332:586-589. **http://dx.doi.org/10.1126/science.1201647**

Polak-Witka K., L. Rudnicka, U. Blume-Peytavi, A. Vogt. 2019. The role of the microbiome in scalp hair follicle biology and disease. *Exp Dermatol.* **http://dx.doi.org/10.1111/exd.13935** [doi]

Schmidt-Ullrich R., R. Paus. 2005. Molecular principles of hair follicle induction and morphogenesis. *BioEssays* 27:247-261. **http://dx.doi.org/10.1002/bies.20184**

Schneider M.R., R. Schmidt-Ullrich, R. Paus. 2009. The hair follicle as a dynamic miniorgan. *Curr. Biol.* 19:R132-R142. **http://dx.doi.org/10.1016/j.cub.2008.12.005**

Schulz C., P.E. Gomez, L. Chorro, H. Szabo-Rogers, N. Cagnard, K. Kierdorf, M. Prinz, B. Wu, S.E. Jacobsen, J.W. Pollard, J. Frampton, K.J. Liu, F. Geissmann. 2012. A lineage of myeloid cells independent of Myb and hematopoietic stem cells. *Science* 336:86-90. **http://dx.doi.org/10.1126/science.1219179**

Seneschal J., R.A. Clark, A. Gehad, C.M. Baecher-Allan, T.S. Kupper. 2012. Human epidermal Langerhans cells maintain immune homeostasis in skin by activating skin resident regulatory T cells. *Immunity.* 36:873-884. **http://dx.doi.org/10.1016/j.immuni.2012.03.018**

Steinman R.M., M.C. Nussenzweig. 2002. Avoiding horror autotoxicus: The importance of dendritic cells in peripheral T cell tolerance. *Proc. Natl. Acad. Sci. U. S. A* 99:351-358.

Stenn K.S., R. Paus. 2001. Controls of hair follicle cycling. *Physiol Rev.* 81:449-494.

Sudo T., S. Nishikawa, M. Ogawa, H. Kataoka, N. Ohno, A. Izawa, S. Hayashi, S. Nishikawa. 1995. Functional hierarchy of c-kit and c-fms in intramarrow production of CFU-M. *Oncogene* 11:2469-2476.

Sumaria N., B. Roediger, L.G. Ng, J. Qin, R. Pinto, L.L. Cavanagh, E. Shklovskaya, G.B. Fazekas de St, J.A. Triccas, W. Weninger. 2011. Cutaneous immunosurveillance by self-renewing dermal gammadelta T cells. *J Exp Med.* 208:505-518. **http://dx.doi.org/10.1084/jem.20101824**

Wang Y., M. Bugatti, T.K. Ulland, W. Vermi, S. Gilfillan, M. Colonna. 2016. Nonredundant roles of keratinocyte-derived IL-34 and neutrophil-derived CSF1 in Langerhans cell renewal in the steady state and during inflammation. *Eur. J Immunol.* 46:552-559. **http://dx.doi.org/10.1002/eji.201545917** [doi]

Wang Y., K.J. Szretter, W. Vermi, S. Gilfillan, C. Rossini, M. Cella, A.D. Barrow, M.S. Diamond, M. Colonna. 2012. IL-34 is a tissue-restricted ligand of CSF1R required for the development of Langerhans cells and microglia. *Nat. Immunol.* 13:753-760. **http://dx.doi.org/10.1038/ni.2360**

Westgate G.E., R.I. Craggs, W.T. Gibson. 1991. Immune privilege in hair growth. *J Invest Dermatol.* 97:417-420.

Zahner S.P., J.M. Kel, C.A. Martina, I. Brouwers-Haspels, M.A. van Roon, B.E. Clausen. 2011. Conditional deletion of TGF-betaR1 using Langerin-Cre mice results in Langerhans cell deficiency and reduced contact hypersensitivity. *J. Immunol.* 187:5069-5076.

FIGURE LEGENDS

Figure 1: Langerhans cell network formation is independent of hair follicle morphogenesis. (A) Epidermal sheets comprising complete HFs from C57BL/6 tail skin were stained for Langerin (red) and DAPI (blue). The image shows LCs in an epidermal network that comprises the upper HF (infundibulum, outlined by a bracket). The arrow points to a sebaceous gland. Scale bar: 100μm. **(B)** Epidermal sheets obtained from tail skin of hairless (*Tabby*) or wild-type littermate control mice were stained for MHC class II (red) and DAPI (blue). Scale bar: 100μm.

Figure 2: Langerhans cell renewal increases during anagen. (A) Schematic representation of the timing of HF morphogenesis and the natural synchronized hair cycle in the back skin of C57BL/6 mice. **(B)** Epidermal cell suspensions from back skin at different hair cycle phases were analyzed by flow cytometry. Langerin$^+$ LCs were gated and their intracellular expression of Ki-67 protein was analyzed. Iso: Ki-67 isotype control antibody labeling performed on d27 mouse skin. **(C)** Percentages of Ki-67$^+$ cells among LCs at different time points. Each data point corresponds to one mouse. Data is pooled from 2 independent experiments (d5: n=6, d14: n=12, d20: n=6, d27: n=12, d35: n=5, d45: n=5, d90: n=5). **(D)** Mice were fed or not (control) with BrdU for 4 days. BrdU incorporation into LCs was determined by flow cytometry at the indicated days. **(E)** Percentages of BrdU$^+$ cells among LCs at different time points. Each data point corresponds to one mouse. Data is pooled from 2 independent experiments (d20: n=6, d27: n=7, d35: n=6, d45: n=6). Bars correspond to mean values. In **(D)** and **(E)**, the arrows indicate the age taken as a reference for statistical analysis (Student's *t*-test, *p<0.05, ** p<0.01, *** p<0.001)

Figure 3: HF cycle manipulation affects the proliferative burst of Langerhans cells. (A) Representative image depicting HFs in anagen (arrows) 7 days after depilation. **(B)** Percentages of Ki-67$^+$ cells among LCs in resting phase (d-1), induced anagen (d+2, d+7, d+13) and catagen/telogen (d+18). Data were obtained by flow cytometry on isolated epidermal cells from 2 independent experiments (d-1: n=6, d+2: n=7, d+7: n=9, d+13: n=3, d+18: n=3). In panel B, the arrow indicates the time point taken as a reference for statistical analysis. **(C)** Representative dot plots showing BrdU$^+$ and Ki-67$^+$ cells among Langerin$^+$ LCs in *Rankl$^{+/-}$* (normal hair cycle) and in *Rankl$^{-/-}$* skin (no transition into anagen) at the expected time point for anagen (d27). **(D)** Percentages of Ki-67$^+$ cells among LCs in *Rankl$^{+/-}$* and *Rankl$^{-/-}$* mice during morphogenesis (day 14) (n=7 and n=5, respectively) and at the expected time point for anagen (d27; n=5 and n=5, respectively). Each data point corresponds to one mouse. **(E)** Langerin$^+$ LCs from tail skin were analyzed for Ki-67 expression in *Tabby* mice rescued by anti-EDAR agonist antibody injection and untreated, hairless *Tabby* mice. **(F)** Percentage of Ki-67$^+$ cells among LCs. Each data point corresponds to one mouse. Data is pooled from 2 independent experiments (n=8 in each group). Bars correspond to mean values. In panels B, D and F, statistical analysis was performed using Student's *t*-test (** p<0.01, *** p<0.001).

Figure 4: Proliferating Langerhans cells are localized close to the hair follicle. (A) Transversal sections of back skin with HFs in anagen were labeled with anti-Langerin (green) and anti-Ki-67 (red) antibodies, counterstained with DAPI (blue) and visualized by confocal microscopy. Two distinct areas were discriminated for analysis: interfollicular epidermis (dashed blue line) and HF (dashed yellow lines). Red arrows indicate Ki-67$^+$ epidermal keratinocytes, green arrow indicates LCs and red/green arrows indicate Ki-67$^+$ LCs. Pictures are optical slices from Z-stack acquisitions. Scale bar: 50μm. **(B)** Percentages of Ki-67$^+$ proliferating LCs within the HF and the interfollicular epidermis. The data is compiled from a total of 50 HFs analyzed from 3 different mice. Statistical analysis was performed using Student's *t*-test (*** p<0.001).

Figure 5: Signaling of IL-34 receptor CSF-1R is required for the anagen-driven Langerhans cell proliferation. (A) Schematic representation of the experimental procedure. At the onset of anagen (d24), the mice received a subcutaneous (s.c.) injection of anti-CSF-1R blocking antibody together with

BrdU (intraperitoneal [I.P.] and in drinking water). Anti-CSF-1R injections were repeated every other day until sacrifice. **(B)** The percentage of proliferating Langerin⁺ LCs was assessed by Ki-67 expression and BrdU incorporation in mice having received isotype control or anti-CSF-1R blocking antibody. **(C)** Bar graphs show the compiled percentages of Ki-67⁺ or BrdU⁺ cells among LCs for each individual mouse from two independent experiments (BrdU: Iso n=4, CSF-1R n=5; Ki-67: Iso n=6, CSF-1R n=7). Statistical analysis was performed using the Student's *t*-test (** p<0.01, *** p<0.001).

Figure 6: *Il34* expression increases in hair follicle stem cells in anagen. (A) Back skin sections (thickness: 16μm) mice were obtained from wild-type (i, iii) or *Il34^{tm1a}* (ii, iv) mice during telogen (d21) and anagen (d28) phase. Blue X-gal staining (arrows) depicts areas with LacZ activity. Sections where observed with 200x magnification. IFE: interfollicular epidermis, IFD: Infundibulum, SG: Sebaceous Gland, **(B)** Schematic representation of HF epithelial cell subsets expressing specific marker combinations. The infundibulum and the interfollicular epidermal cells (pink) express Sca-1. Stem cells (SCs) in the bulge are characterized by CD34 expression. As opposed to suprabasal SCs (green), basal SCs (purple) carry CD49f/⍰6 integrin. Epithelial cells of the distal HF (blue) lack both Sca-1 and CD34. **(C)** Flow cytometry profile of the CD45^{neg} epithelial cells with color-coded gates corresponding to the subsets defined in panel A. Representative percentages of bulge SCs in telogen and anagen are shown. **(D)** *Il34* mRNA expression by sorted epithelial cell subsets both in telogen or anagen was measured by quantitative RT-PCR and normalized to three housekeeping genes. Bar graphs show the mean -/+ SEM of 3 different mice, expressed as a percentage of telogen epidermal cells. Statistical analysis was performed using the Mann-Whitney test (* p<0.05).
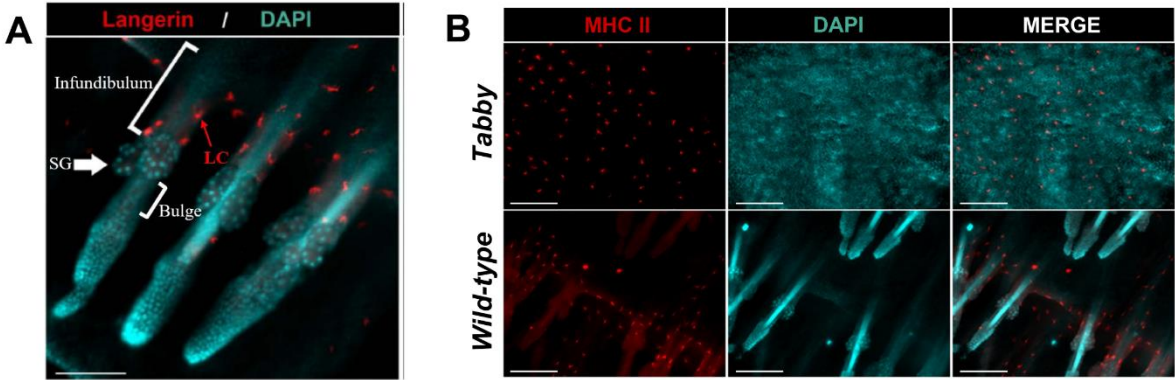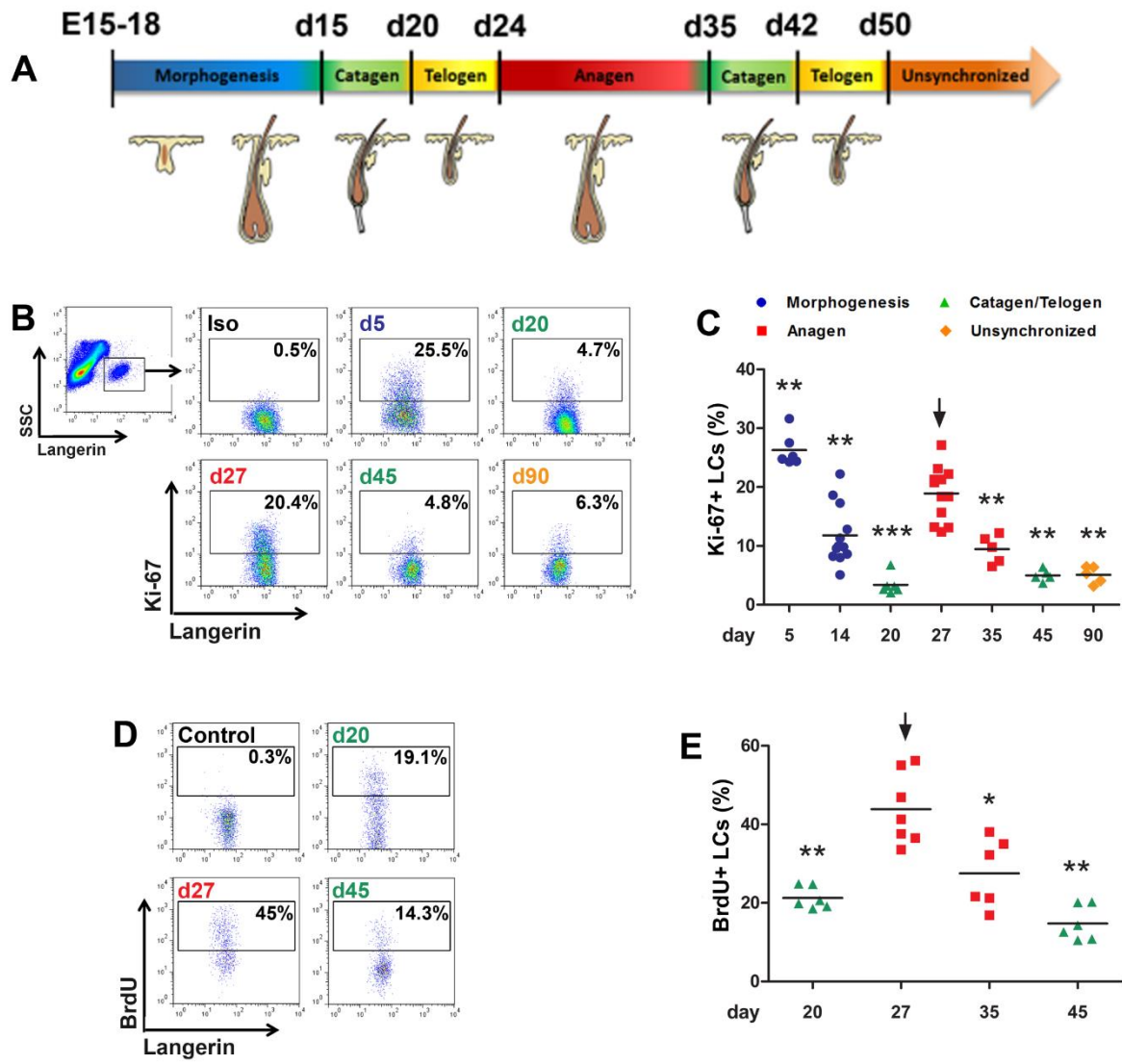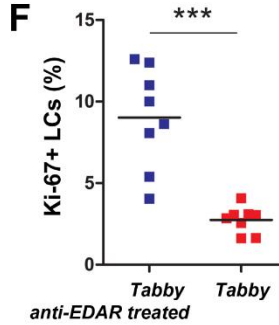
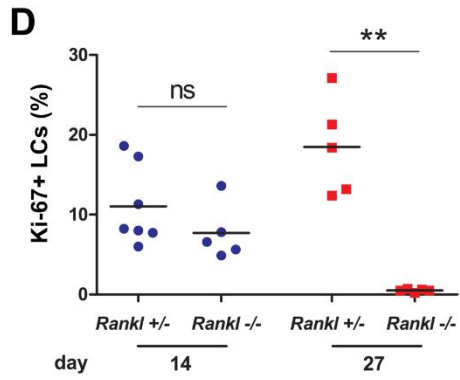Figure 1

Figure 2

A Day +7

B

Ki-67+ LCs (%)

day   -1   +2   +7   +13   +18

depilation

Induced Anagen   Catagen Telogen

C Day 27

BrdU

Rankl+/- 37%   Rankl-/- 4%

Ki-67

Rankl+/- 27%   Rankl-/- 0.5%

Langerin

D

Ki-67+ LCs (%)

ns   **

Rankl +/-   Rankl -/-   Rankl +/-   Rankl -/-

day   14   27

E

Ki-67

Tabby anti-EDAR treated 10%   Tabby 3%

Langerin

F

Ki-67+ LCs (%)

***

Tabby anti-EDAR treated   Tabby

Figure 3

A

Ki-67
Langerin

DAPI

Interfollicular
epidermis

Dermis

HF   HF

DAPI

B

Ki-67+ LCs (%)

***

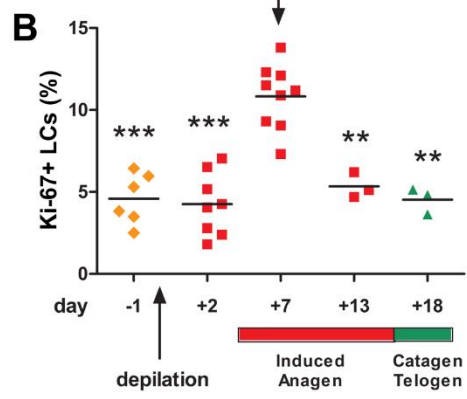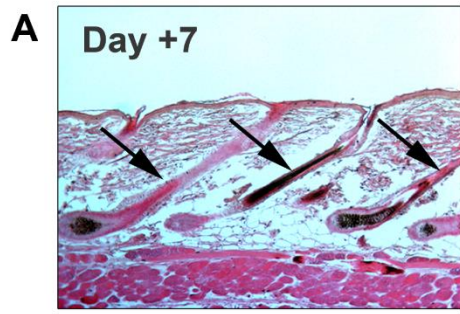Interfollicular   Hair follicle
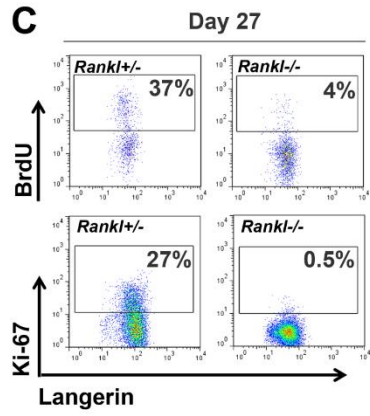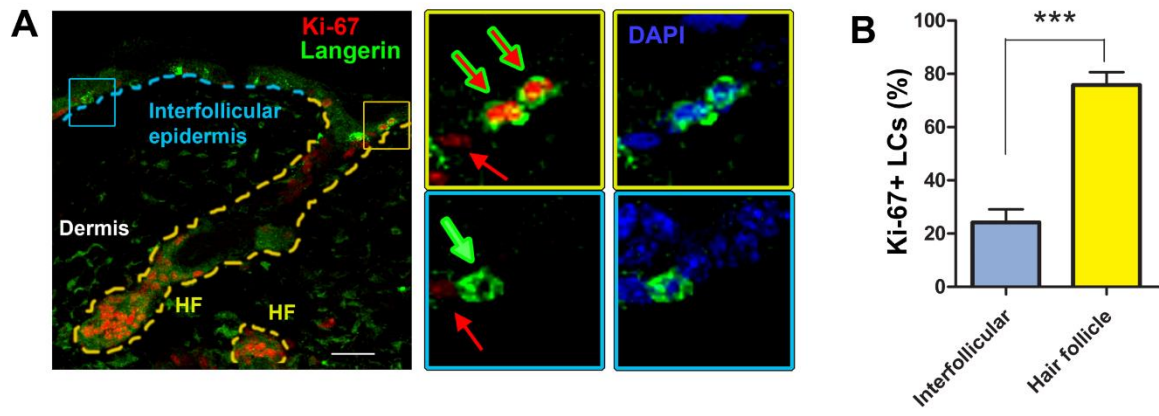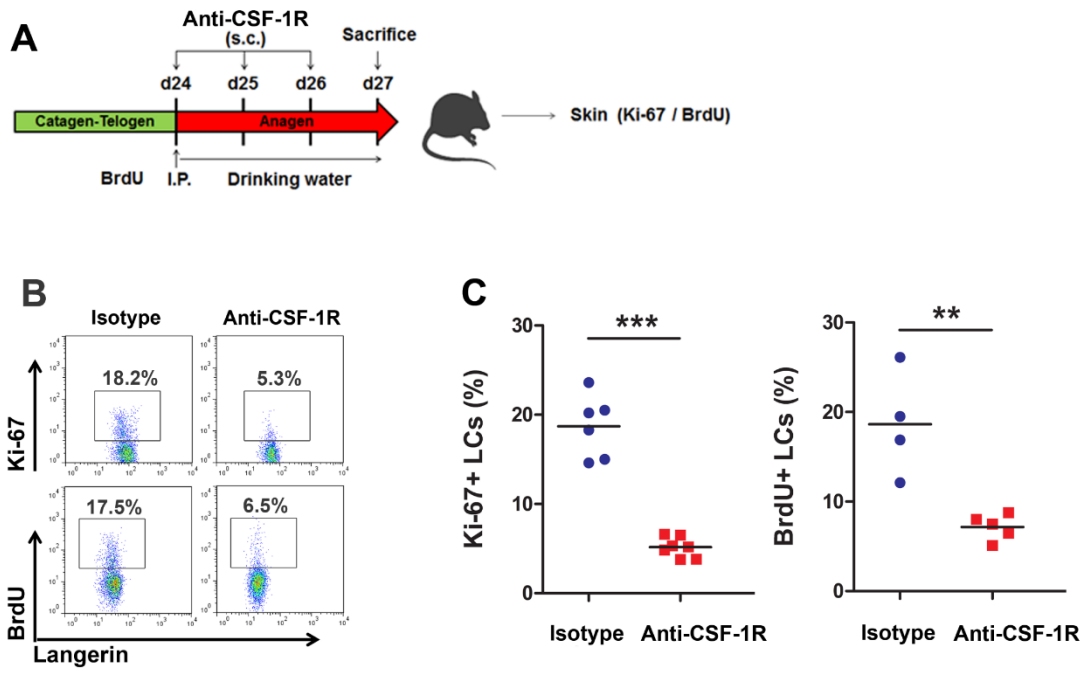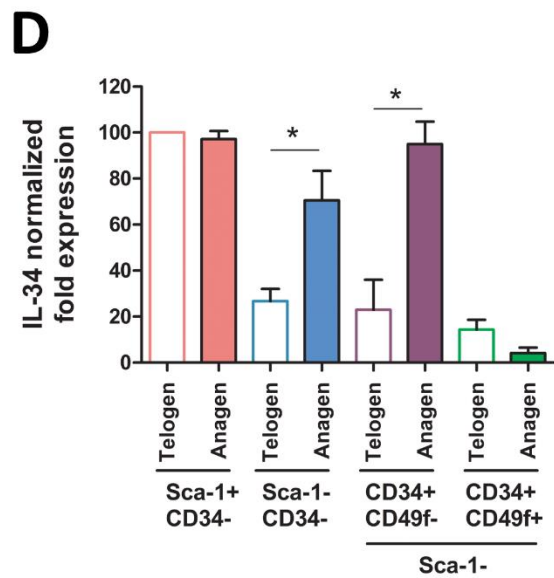
Figure 4

Figure 5

Figure 6

ONLINE SUPPLEMENTAL MATERIAL

Figure S1: Dispase II efficiently isolates the epidermis together with hair follicles. Anagen back skin was treated (right panel) or not (left panel) with dispase II by floating skin onto culture medium containing the enzyme overnight at 4°C. Separation of epidermis from dermis was performed on treated skin, which was then fixed and included in paraffin. Transversal sections were colored in Masson's trichrome. Filled red arrow indicates the epidermis in untreated skin while empty red arrow shows its absence after dispase II treatment. Scale bar: 100μm.

Figure S2: Proliferation of dendritic epidermal T cells does not depend on the natural hair cycle. (A) Mice were fed or not (control) with BrdU for 4 days and its incorporation into DETCs (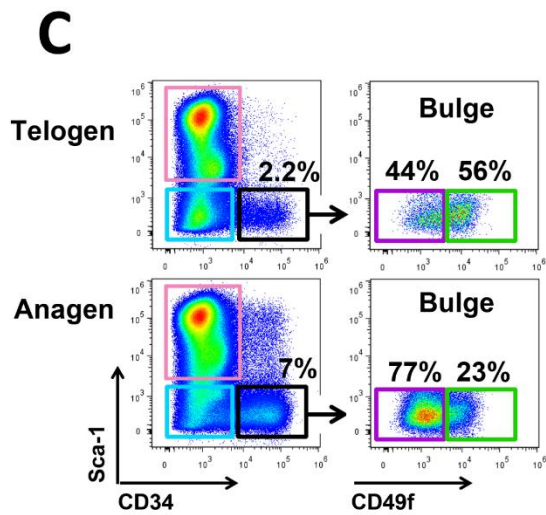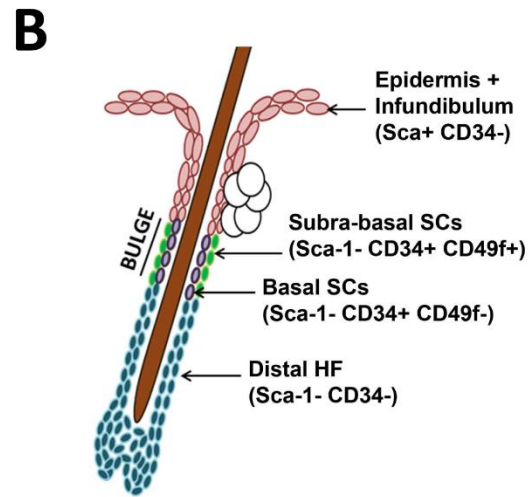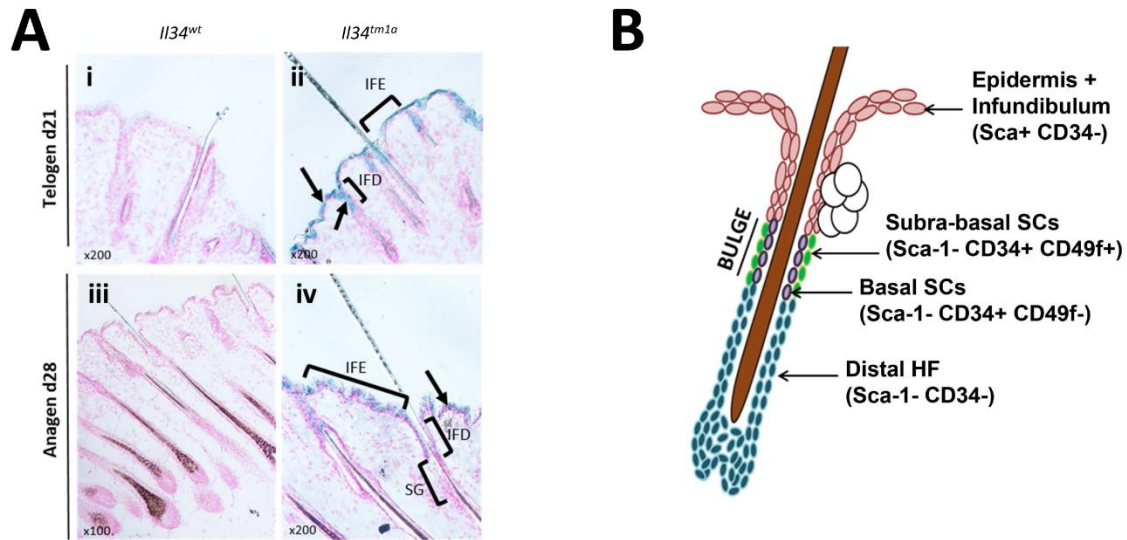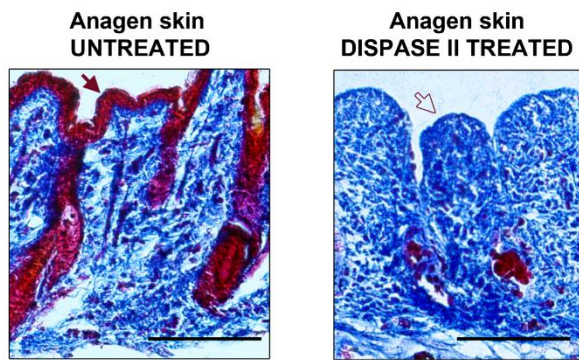TCRɣδ$^+$) was measured by flow cytometry at the indicated days. **(B)** Percentages of BrdU$^+$ cells among DETCs. Data is pooled from 2 distinct experiments (d21: n=7, d28: n=7, d35: n=12, d45: n=6). Bars represent mean values. The arrow indicates the age taken as a reference for statistical analysis (Student's t-test, *** p<0.001).

Figure S3: Cyclosporin A promotes hair growth and LC proliferation. Mice were shaved at d-4 and treated with cyclosporin A (CsA) at d-4, d-2, d-0. **(A)** Representative pictures of the back skin at d11 and d17 for untreated and CsA-treated mice. **(B)** BrdU incorporation in epidermal LCs 5, 11 or 17 days after CsA treatment.

Figure S4: Transient blocking of CSF-1R does not affect the hair cycle nor the proliferation of keratinocytes or dendritic epidermal T cells. Mice received subcutaneous injections of anti-CSF-1R or isotype control (control) from day 24 to day 27. **(A)** Blood was collected at day 27 to assess the efficiency of CSF-1R blocking by the loss of monocytes (CD11b$^+$ GR-1$^+$ Ly6G-) in injected mice as compared to control. **(B)** Entry into anagen in treated or control mice skin at day 27 was determined by hematoxilin eosin colorization of back skin slices. **(C)** Percentage of LCs (Langerin+) was determined in epidermal suspension of treated (n=4) or control mice (n=6) skin. Data were obtained from 2 distinct experiments for each group. **(D)** Proliferation of DETC (TCRɣδ+ cells) and keratinocytes (Langerin- TCRɣδ-) was analyzed by the expression of Ki-67 in skin epidermal suspension of anti-CSF-1R or isotype treated mice. Iso-Ki-67: Isotype control of Ki-67 antibody. **(E)** and **(F)** Graphs show the compilation of flow cytometry results obtained from panel D (n=4 for each group). Data were obtained from 2 distinct experiments for each group. Statistical analysis was performed using the Student's t-test (ns: non significant).

Anagen skin UNTREATED

Anagen skin DISPASE II TREATED

Figure S1

Figure S2

A

Shave, then:

d-4 d-2 d0 CsA   d5   d11   d17

| Unsynchronized | Anagen | Catagen | Telogen |

B

	n.t.	CsA
d11		
d17		

C
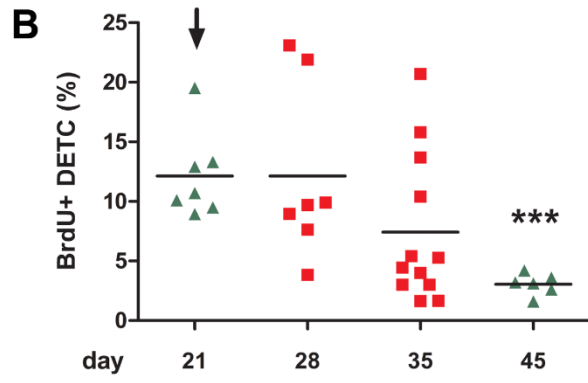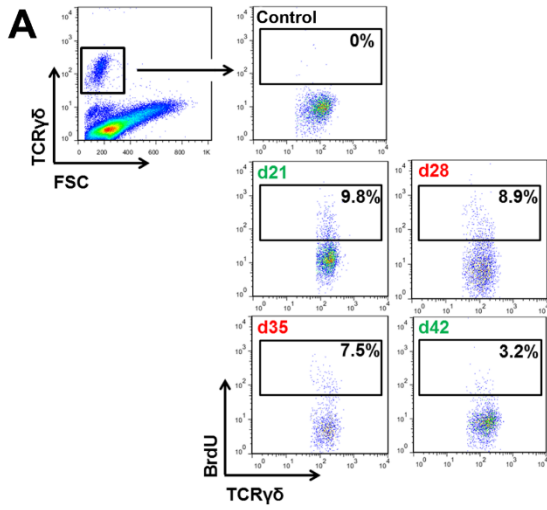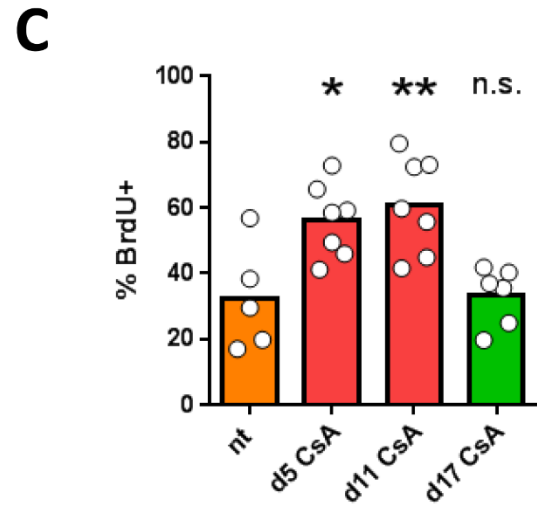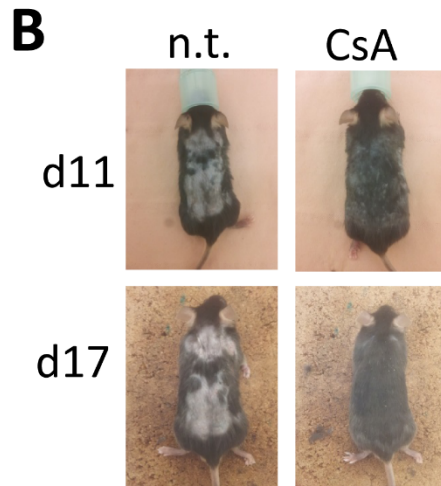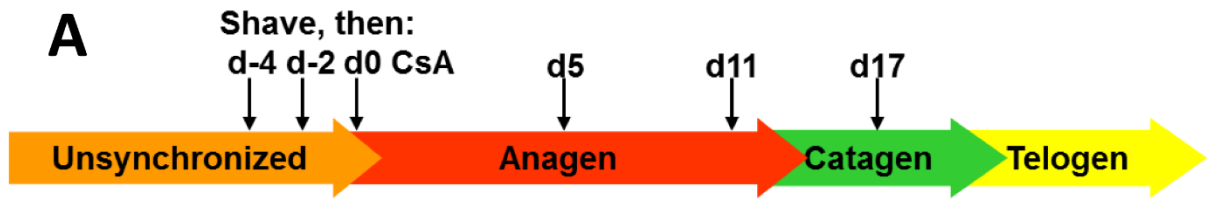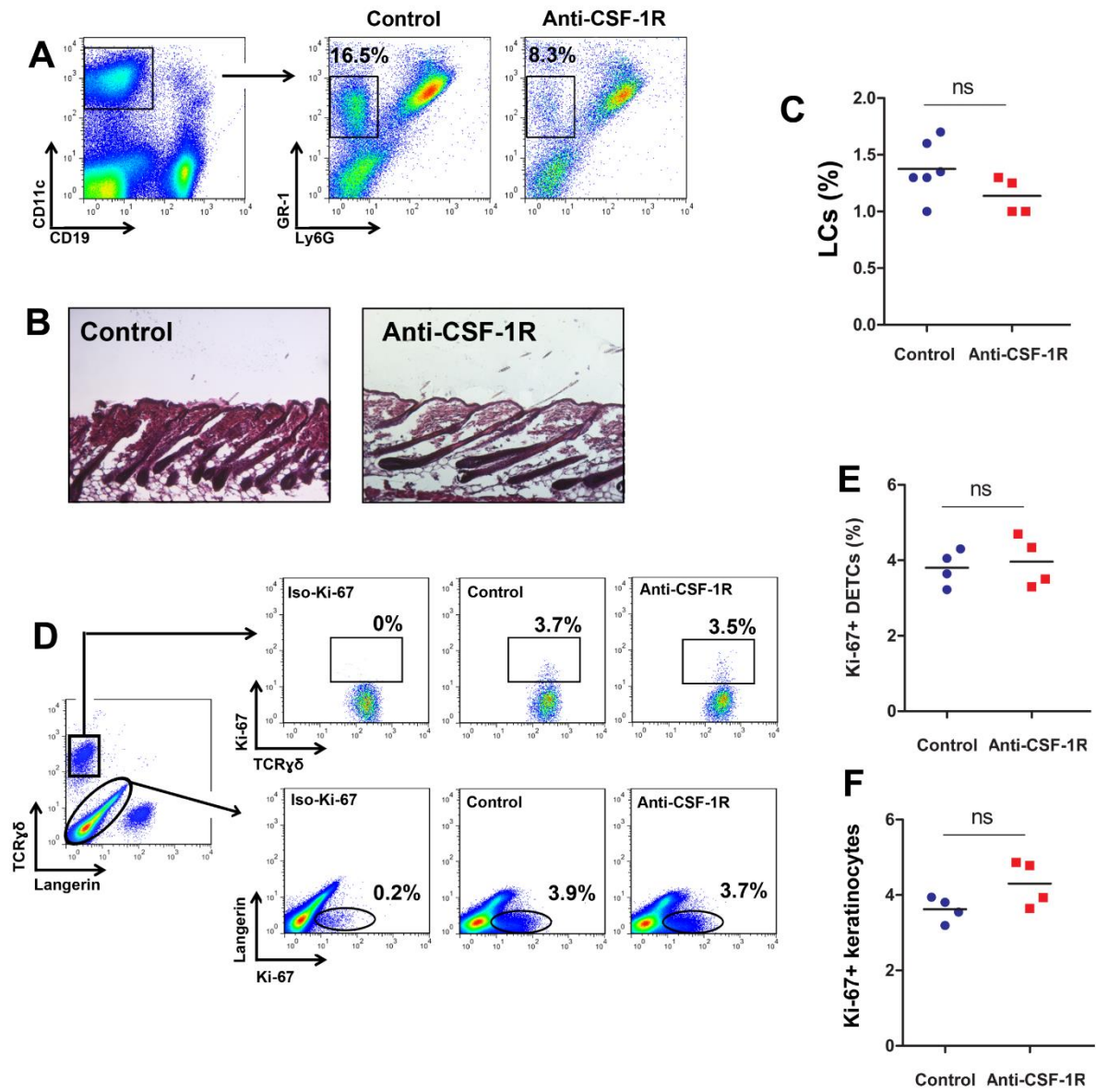
Figure S3

Figure S4

Primer	Sequence (5' to 3')
GAPDH	Forward: tgacgtgccgctggagaaa
	Reverse: agtgtagcccaagatgcccttcag
HPRT	Forward: cttgctggtgaaaaggacctct
	Reverse: aagtactcattatagtcaagggca
β-actin	Forward: atgagctgcctgacggccaggtcatc
	Reverse: tggtaccaccagacagcactgtgtt
IL-34	Forward: ggacacacttctggggaca
	Reverse: ccaaagccacgtcaagtagg

Supplementary Table 1

INTRODUCTION

1. La peau

La peau humaine (Figure 1a) est un large épithélium pluristratifié et kératinisé, d'environ deux mètres carrés de surface et d'épaisseur variable, recouvrant la quasi-totalité du corps. La peau se développe à partir de trois semaines après la fécondation, au moment de la gastrulation, où l'ectoderme donnera l'épiderme et la mésoderme le derme et l'hypoderme sous-jacents.

L'épiderme (Figure 1b), dans son rôle premier de barrière physique envers les agressions externes, présente une épaisse couche superficielle imperméable et solidaire de kératinocytes morts : la **couche cornée**. Ces **kératinocytes**, poussés vers l'extérieur par les divisions répétées des cellules souches de la **couche basale**, auront traversé la hauteur de l'épiderme avant de finir à la surface. Au cours de leur périple au travers des **couches épineuse et granuleuse**, les kératinocytes se différencient progressivement : corps cellulaire plus aplati, renforcement des jonctions cellule-cellule (Figure 2), intégration de la mélanine produite par les **mélanocytes**, expression de **cornéodesmosomes** puis une ultime différenciation en surface afin de sanctuariser notre corps face aux menaces externes. Cette différenciation est étayée par un spectre de filaments intermédiaires produits différentiellement dans le temps : Les cellules basales expriment davantage de **Kératines** 5 et 14, perdues progressivement au profit des Kératines 10, 2 et de la Filaggrine. Ce processus de renouvellement tissulaire prend entre 40 et 60 jours.

La couche basale de l'épiderme repose sur une **membrane basale**, produite par les kératinocytes basaux sur laquelle ils s'ancrent solidement au moyen **d'intégrines β4/α6** contactant la laminine et le collagène IV de la membrane basale (Figure 2). C'est cette fine lame de contact qui assure la jonction entre l'épiderme et le derme, vaste tissu fibreux relativement pauvre en cellules. Le **derme** est principalement colonisé par les fibroblastes, mais aussi les cellules immunitaires résidentes. Il assure une fonction de soutien structurel, par sa riche matrice extracellulaire assurant robustesse et élasticité, mais aussi un soutien nutritionnel lié au passage de nombreux vaisseaux sanguins et enfin fonctionnel pour ce qui concerne l'immunité et la fonction sensorielle, le derme étant parcouru de nombreuses terminaisons nerveuses.

La peau est également la résidence de micro-organismes commensaux : le **microbiote**. Majoritairement représentés par le règne *Bacteria*, à savoir les espèces *Propionibacterium sp., Staphylococcus* et *Corynebacterium*, le microbiote joue un rôle primordial dans la défense et la physiologie de la peau. En effet, ils entrent en compétition avec de potentiels pathogènes contractés à l'extérieur, et produisent des molécules importantes, comme par exemple l'acide propionique aux propriétés bactériostatiques, immunorégulatrices et promouvant la réparation tissulaire.

2. L'unité pilosébacée, un organe dans un organe

Une caractéristique commune au clade des mammifères est la présence de poils à la surface de leur peau. Ces poils sont produits par le **follicule pileux**, une structure enchâssée dans la peau présentant une organisation mixte, avec des couches concentriques épithéliales et une base mésenchymateuse qui en assure le soutien et la nutrition : **la papille dermique**.

Le développement embryonnaire du poil (Figure 3), en trois phases, fait donc intervenir l'ectoderme et le mésoderme. L'initiation débute par l'**induction** d'une placode ectodermique guidée par des signaux des cellules du mésoderme sous-jacentes. Parmi ces signaux, Wnt/β-caténine (Figure 4) et EDAR y jouent un rôle important, tandis que la voie BMP inhibe la formation d'une placode. S'ensuit une phase d'**organogénèse**, où les fibroblastes du mésoderme se condensent et organisent la prolifération de la placode, notamment par la production de **Sonic Hedgehog (SHH)**. Les cellules de la placode prolifèrent rapidement, poussant vers l'intérieur de la peau embryonnaire, et entraînant la future papille dermique avec eux. Ce mouvement produit un gradient de SHH et aboutit à la formation du **germe folliculaire.** Finalement, les kératinocytes du germe cessent de proliférer et se différencient suivant leur position, formant *in fine* des couches épithéliales concentriques : les gaines racinaires interne et externe.

Le follicule pileux mature se structure en quatre grands segments (Figure 6), de la surface vers sa base : **L'infundibulum, l'isthme, le renflement et la région variable**. Le renflement renferme des cellules souches nécessaires au maintien du cycle folliculaire. La région variable fluctue en taille avec le cycle, et permet la croissance du poil par la prolifération des kératinocytes de la matrice, située à sa base. Le follicule est aussi très souvent accompagné d'une ou plusieurs **glandes sébacées**, qui produisent le **sébum** et le déversent dans le canal folliculaire, au niveau de l'infundibulum. Le sébum est un produit lipophile important pour la lubrification de la peau, du poil et la régulation du microbiote en surface.

Le poil est un organe dynamique, qui évolue selon un cycle bien défini (Figure 7), en trois grandes phases : **L'anagène**, la phase d'élongation du poil et celle où le follicule est le plus développé. Les divisions cellulaires à la base du poil, dans le bulbe, au niveau de la matrice, alimentent cette croissance pileuse. L'anagène peut perdurer pendant de longues périodes, plusieurs années chez l'Homme, plusieurs semaines chez la souris. Cependant, les deux premières anagènes chez la souris sont relativement courtes et synchronisées, la première se manifestant 2 semaines après la naissance, et est immédiatement suivie d'un second cycle de même durée. L'anagène est suivie par la **catagène**, une phase d'involution où la région variable du follicule se réduit progressivement, le poil ne poussant plus. Cette phase très courte se conclut et laisse place au **télogène**, une phase de quiescence qui prépare le prochain cycle. La région variable a quasiment disparu, faisant remonter la papille dermique au niveau du renflement, qui, à son contact, initie la prolifération de ses cellules souches et le démarrage d'un nouveau cycle folliculaire.

Le follicule pileux arbore également un microbiote, proche de celui de la peau, mais avec quelques différences : les conditions anoxiques du canal folliculaire et sa protection naturelle

contre les éléments extérieurs favorisent la pousse de *Burkholderia sp.* et offrent un habitat favorable aux mites de la famille *Demodex*.

Le follicule pileux a de nombreux rôles notamment chez les mammifères qui en sont recouvert, dans la protection contre le froid, les parasites cutanés, les rayons UV et les attaques physiques. L'Homme aura perdu secondairement ces fonctions, mais gagné une endurance à l'effort accrue grâce à la sudation, quasi inexistante chez les autres mammifères, sauf le cheval. Une fonction du poil restée commune aux hommes et autres animaux est la perception de leur environnement, car le follicule pileux agit comme un mécanorécepteur, capable de transmettre les vibrations et les contacts, parfois très finement dans des organes spécialisés comme les vibrisses de la souris.

3. Immunité de la peau, un délicat équilibre

La peau est avant tout un organe de défense, à la fois physiquement par l'effet barrière de la couche cornée, mais aussi par l'accueil des acteurs du système immunitaire (Figure 8). Les **macrophages** résident dans le derme, et sont quiescents et immobiles au repos, mais leur activité peut être stimulée, notamment par la détection de signaux de danger. Ce sont des phagocytes professionnels, capables de capter, ingérer et détruire les micro-organismes ayant envahi le tissu. Les macrophages produisent également des **cytokines pro-inflammatoires** comme l'IL-1β, TNF-α ou IL-6 dans le but d'éveiller l'organisme à la menace détectée, en activant les défenses innées présentes dans toute sorte de cellule de leur environnement, et en permettant le recrutement de cellules immunitaires supplémentaires par la vasodilatation et la chemoattraction, notamment par le renfort de neutrophiles attirés par IL-8/CXCL8. Les **polynucléaires neutrophiles** ne sont pas ou peu présents dans la peau au repos, mais l'infiltrent en masse lors des réponses inflammatoires. De petite taille et de forme ronde, au noyau polylobé, les neutrophiles agissent au contact par phagocytose, dégranulation d'enzymes bactéricides ou encore par les Neutrophile Extracellular Traps (NETs). **La NETose** consiste en l'expulsion de chromatine, dont les propriétés liées aux histones la rendent intrinsèquement bactéricide, et permet à la fois l'immobilisation et la destruction des intrus.

Autre élément important de l'immunité innée, les **cellules dendritiques** habitent la peau et permettent l'activation des réponses adaptatives, portées à la fois par les **lymphocytes T** à mémoire résidant dans la peau et ceux regroupés dans les ganglions lymphatiques, incluant les **lymphocytes B**. Les cellules dendritiques sont capables, par phagocytose, d'internaliser et découper les microorganismes en antigènes, qui seront ensuite présentés en surface par le biais des molécules du **CMH de type I (présentation croisée) ou II**. L'association des CMH-I ou CMH-II avec un antigène est reconnue par le **TCR** des lymphocytes T CD8+ ou CD4+, respectivement Cela déclenche leur activation, leur prolifération et leur différenciation, orientée par les cytokines produites par la cellule dendritique présentatrice.

Tandis que les lymphocytes **T CD8+ cytotoxiques** jouent un rôle direct dans la destruction des cellules infectées, les **T CD4+ auxiliaires** sont capables d'orienter la réponse immunitaire en stimulant les autres cellules immunitaires, comme les macrophages ou encore les

lymphocytes B. Les B sont spécialisés dans la production **d'anticorps**, protéines d'appoint capables de fixer et neutraliser leurs cibles en les marquant pour leur élimination par phagocytose ou par l'action du complément. Bien que des anticorps de toutes classes entrent dans la peau, on n'y retrouve en général pas de lymphocytes B, qui sécrètent ces anticorps depuis des organes lymphoïdes secondaires.

4. L'Hidradénite Suppurée

Maladie anciennement décrite mais toujours mal comprise, l'hidradénite suppurée (HS) était anciennement appelée **maladie de Verneuil**, du nom de Aristide Verneuil, chirurgien français ayant décrit la maladie. Plus tard, elle prend le nom d'**acné inversée**. Aujourd'hui, l'HS est définie comme une maladie auto-inflammatoire du follicule pileux. La prévalence est discutée, avec une moyenne globale récente de 0,2%, variant largement entre les régions géographiques, sexes, et ethnies. La difficulté du diagnostic et la consultation tardive des patients exacerbent ces biais.

L'HS est multifactorielle, avec une importante composante environnementale : c'est une maladie principalement liée au tabagisme. Certains ligands présents dans la cigarette, tel que la dioxine, peuvent activer le **récepteur à l'aryl-hydrocarbone** (AHR). L'AHR est fortement exprimé dans l'unité pilosébacée, ayant un rôle dans la prolifération épithéliale et la fonction immunitaire par l'induction de l'IL-22. L'obésité est aussi souvent liée à l'HS et la sévérité des lésions, où plus de 80% des patients sont en surpoids ou obèses. En effet, de manière générale les adipocytes ont une importante capacité pro-inflammatoire par la production de cytokines capables d'activer le système immunitaire : les **adipokines,** comme l'IL-6 et le TNFα. Le microbiote cutané a aussi son rôle dans l'initiation et surtout la progression de la maladie (Figure 9), avec la prolifération de certaines espèces opportunistes sur la peau, comme *Staphyloccocus aureus* et plusieurs bacilles Gram-négatif. L'intensité de cette dysbiose semble avoir un lien direct avec la sévérité des lésions.

L'autre composante de l'HS est génétique, avec 40% des cas ayant un antécédent familial avéré. Le gène le plus retrouvé dans les séquençages de patients étant celui de la **γ-secrétase**, une protéase membranaire organisée en quatre sous-unités, deux étant particulièrement atteintes par les mutations recensées : **nicastrine**, une glycoprotéine de structure, et **préséniline**, portant l'activité enzymatique. La γ-secrétase clive de nombreux substrats, notamment Notch et les métalloprotéases ADAM. La plupart des mutations trouvées chez les patients HS produisent une protéine tronquée, induisant sans doute son élimination par la voie de réponse aux protéines non repliées (UPR). Les effets exacts de ces mutations ne sont pas encore connus, ni la relation entre la γ-secrétase et l'HS.

Le sexe est un élément important dans la variabilité de l'induction du HS, avec en France trois femmes touchées pour un homme. Les femmes enceintes montrent un arrêt du développement de lésions, et inversement les lésions resurgissent au cours des règles. Les hormones sexuelles sont donc certainement impliquées dans l'initiation et la progression de la maladie, bien qu'aucun lien n'ai été clairement identifié pour le moment.

L'HS débute par une prolifération excessive des kératinocytes de la gaine racinaire externe, conduisant à l'obstruction du canal folliculaire et l'accumulation de produits microbiotiques et de débris cellulaires dans l'infundibulum. Un défaut dans l'efferocytose des kératinocytes ou des macrophages résidents pourrait être à l'origine de cette accumulation. La membrane basale s'affine, réduisant la séparation entre épiderme et derme et permettant probablement un passage plus important de cellules immunitaires près de la surface. La production d'alarmines par les kératinocytes stimule le système immunitaire, qui s'active et produit à son tour des cytokines pro-inflammatoires caractéristiques de l'HS : TNFα, IL-6 et IFN-γ. Ces cytokines vont avoir plusieurs effets : premièrement, recruter davantage de leucocytes près du follicule, notamment des neutrophiles qui sont retrouvés en quantités importantes dans la peau lésionnelle. Les neutrophiles entrent en premier dans le derme et produisent des NETs en réponse à la flore microbienne envahissant le tissu. Cette réaction normale des neutrophiles a des conséquences néfastes au long cours : les cellules présentatrices d'antigène phagocytant ces NETs favorisent la production d'auto-antigènes puis d'auto-anticorps, un mécanisme déjà retrouvé dans plusieurs maladies auto-immunes. Dans le HS, l'intervention des lymphocytes est encore peu documentée : L'équilibre entre Th17 et Treg serait perturbé en faveur des Th17, entretenant l'inflammation chronique autour des follicules. Les lymphocytes B sont des acteurs récemment étudiés dans la maladie, où l'on retrouve des auto-anticorps dont le titre est proportionnel à la sévérité des lésions cutanées.

Un certain nombre de traitements sont proposés pour endiguer l'inflammation et réduire les lésions, tout d'abord des antibiotiques à large spectre, comme les tétracyclines, afin de stopper la prolifération bactérienne. Bien souvent, des cocktails d'antibiotiques sont utilisés, afin de toucher un maximum d'espèces bactériennes ; les anticorps recombinants anti-TNFα (adalimumab, Infliximab) sont largement prescrits afin de réduire l'inflammation, de même que l'anakinra, un antagoniste du récepteur à l'IL-1 ; D'autres méthodes moins conventionnelles sont aussi utilisées, comme des thérapies hormonales visant à inhiber l'effet des androgènes : le spironolactone et la finastéride sont deux exemples souvent utilisés en clinique, étant des analogues compétitifs du DHT, ils inhibent son action et réduisent l'activité cellulaire du follicule. Enfin, des méthodes de chimiothérapie et radiothérapie ont été essayées, avec un certain succès dans l'arrêt de la prolifération folliculaire.

Aujourd'hui, la recherche sur l'HS souffre d'une absence de modèle d'étude : étant une maladie typiquement humaine, elle n'est pas observée chez l'animal. Les échantillons prélevés sur le patient restent donc le seul modèle d'étude *in vivo* à ce jour, entraînant des problèmes d'accès, d'échelle et de reproductibilité : il existe relativement peu de patients de HS, et tous ne sont pas prêts à donner de leur peau ou leurs follicules pour la recherche ; le peu d'échantillons obtenus ne suffisent pas à mener des études approfondies et souffrent d'une variabilité importante d'individu à individu. Il est donc vital de développer un modèle *in vivo* de l'HS afin de pouvoir l'étudier en laboratoire, ce que plusieurs équipes de recherches ont essayé d'accomplir (Figure 10).

Un premier modèle de xénogreffe a été tenté par Quartey et al. en 2020 : le principe étant de greffer de la peau de patient HS sur le dos d'une souris NSG-SGM3 immunocompromise et produisant des SCF, GM-CSF et IL-3 humaines. La greffe ayant prise, la peau HS a montré une perte de pigmentation et une certaine inflammation deux semaines après. Les modèles de souris xénogreffes ont été largement utilisés dans l'étude des maladies de la peau, avec des modèles efficaces pour le psoriasis et la pelade. Ce modèle requière des échantillons de patients, ne résolvant pas le problème de disponibilité. Les xénogreffes nécessitent des souris immunodéprimées, ce qui exclut les études immunitaires de l'HS. Les auteurs reconnaissent cette limitation et proposent de repeupler les souris immunodéficientes avec des cellules immunitaires humaines.

La même année, Yang et al. ont publié un modèle de Nicastrine-KO dans la couche basale de l'épiderme. Les auteurs ont constaté une diminution de l'expression de la protéine Notch, une perte de cheveux et une hyperkératose, montrant une relation entre la perte de Nicastrin et l'homéostasie du follicule pileux. IL-36a, IL-17A et RORγt ont été observés dans la peau KO. La destruction du follicule pileux produirait une réponse inflammatoire. Ce modèle est basé sur la découverte d'une mutation de la γ-sécrétase dans certaines familles touchées par l'HS, cependant seule une minorité de patients HS présentent ces mutations. Les mutations chez les patients ne sont pas toujours des délétions totales et le niveau de destruction tissulaire observé est extrême, car il affecte l'ensemble de la peau. Le modèle ne présente pas d'infiltrat important de neutrophiles dans la peau, l'un des signes révélateurs de l'HS, mais il produit une réponse Th17.

En 2021, Nakamizo et al. ont montré l'effet d'un régime riche en graisses, pendant huit semaines, chez la souris dans l'inflammation cutanée. Les follicules pileux ont été obstrués par des kératinocytes morts, un phénomène généralement observé en histologie de la peau HS lésionnelle. Une irritation au PMA a produit une infiltration de neutrophiles dans la peau pendant 24 heures chez les souris ayant un régime riche en graisses, ce qui était absent chez les souris témoins. Le choix d'un régime riche en graisses est pertinent, car HS est corrélée à l'obésité. Ce modèle produit des follicules obstrués et une infiltration immunitaire, mais il ne donne pas les lésions typiques de l'HS. Le régime riche en graisses ne suffit pas à provoquer une inflammation. Le modèle ne peut pas expliquer l'HS chez les patients sans antécédents de surpoids ou d'obésité. Un régime riche en graisses constituera un ajout prometteur à tout modèle murin de l'HS.

Des souris ont été conçues pour une suppression ciblée de l'ADAM10, une métalloprotéase responsable du clivage de Notch, dans le follicule pileux. On observe un profil pro-inflammatoire dans les cellules du follicule pileux affectées. 35 jours après la naissance, une profonde dysbiose exacerbe la folliculite initiale, conduisant à la destruction complète du follicule pileux. Bien que cela ne représente pas un modèle direct d'hidradénite suppurée, car il ne présente pas l'invasion tissulaire caractéristique ni les lésions ultérieures, il reste intéressant pour de multiples raisons : le dysfonctionnement de la signalisation Notch, en relation avec les mutations de la γ-sécrétase ; La dysbiose, bien étudié dans l'HS ; et la fonction des défensines altérée. Dans leur modèle, les auteurs corrigent la dysbiose via des antibiotiques, arrêtant la destruction de la peau. Bien qu'il n'ait pas été démontré que la

réponse Th2 soit impliquée dans l'HS, où une réponse Th17 semble prédominante, elle est observée dans ce modèle. La folliculite chez la souris est déclenchée par une injection de poly(I:C), imitant une réponse d'interféron de type 1. Dans l'HS, la maladie n'est pas liée à un déclencheur pathogène, mais d'autres déclencheurs inflammatoires pourraient être testés sur le modèle de souris Adam10.

Préface aux résultats

À travers cette introduction, j'ai montré que l'hidradénite suppurée n'est pas encore entièrement comprise et traitable, causant des dommages importants aux personnes touchées et représentant un fardeau économique dans le monde entier.

Pour élargir nos connaissances sur la maladie et favoriser l'innovation dans l'arsenal thérapeutique dont nous disposons, cette thèse a été intégrée dans un effort plus vaste, paneuropéen : Biomolecular Analysis for Tailored Medicine in Acne inversa, ou BATMAN.

BATMAN regroupe plusieurs équipes cliniques et de recherche dans sept pays différents, avec l'objectif commun d'appliquer leur expertise dans la lutte contre l'HS.

Mes objectifs dans cette entreprise étaient la production de modèles in vitro et in vivo d'HS, comblant potentiellement le déficit de la boîte à outils disponible contre la maladie ; et l'analyse des populations de lymphocytes sanguins des patients pour découvrir des marqueurs de la progression de la maladie. A ce titre, notre travail s'est divisé en trois axes :

1. Reconstruction de peau humaine sur un modèle de culture 3D, déjà éprouvé, utilisé dans notre équipe.

2. Mise en place d'un modèle in vivo soit sur des souris génétiquement modifiées, soit par stimulation externe.

3. Récupération, stockage et analyse cytométrique des PBMC du patient.

RESULTATS

L'hidradénite suppurée (HS) est une maladie auto-inflammatoire affectant l'unité pilo-sébacée située dans les zones humides des plis cutanés (aine, aisselles, sous les seins, fesses et scrotum), touchant jusqu'à présent environ 0,2 % de la population mondiale. Les événements responsables de l'inflammation pilo-sébacée restent flous et aucun modèle in vivo ne permet encore d'étudier l'initiation et la progression de la maladie. Plusieurs cas familiaux d'HS ont été associés à des mutations de la γ-sécrétase. L'édition génétique médiée par CRISPR/Cas9 a permis de répliquer des mutations non-sens dérivées du patient des gènes NCSTN et PSENEN, codant pour les sous-unités γ-sécrétase, dans la lignée cellulaire épithéliale HaCat in vitro. Les deux altérations de la γ-sécrétase ont conduit à une altération du flux autophagique (Figure 11 & 12). Cela nous a incité à étudier si et comment les follicules pileux pourraient être modifiés par ces voies in vivo. Nous avons effectué une inhibition systémique de la γ-sécrétase chez des souris C57BL/6 juste après une épilation permettant de relancer un cycle synchronisé du follicule pileux. En conséquence, nous avons

pu observer un retard de croissance des follicules, une dépigmentation des cheveux et une altération de l'autophagie. Cela nous a amené à émettre l'hypothèse que l'autophagie serait impliquée dans la croissance du cycle du follicule pileux et dans la régulation inflammatoire. Ainsi, les souches de souris Sox9creERT2, Atg5flox et Atg5+/- ont été combinées pour générer une ablation sélective d'ATG5, un élément clé de la machinerie de l'autophagie, à partir du follicule pileux. Par conséquent, une légère altération du flux d'autophagie dans les cellules des régions folliculaires supérieures a pu être détectée. Cependant, nos résultats préliminaires n'ont pas mis en évidence d'altérations évidentes de la croissance des cheveux, de la pigmentation ou de l'inflammation induite par l'épilation. Par conséquent, bien que l'inhibition de la γ-sécrétase ait eu des effets puissants à la fois sur le cycle du follicule pileux et sur l'autophagie, nous ne sommes pas encore en mesure de démontrer sans équivoque qu'une déficience de l'autophagie pourrait à elle seule entraîner des défauts importants dans la croissance des cheveux et dans la surveillance immunitaire du renouvellement folliculaire.

Un objectif important de ma thèse est la production de nouveaux modèles 3D HS humains. Plusieurs possibilités existent, que nous décrivons et discutons dans une revue de la littérature publiée avec les partenaires de notre consortium européen axé sur l'HS Ici, nous avons utilisé une stratégie de culture 3D qui a été présentée à l'équipe il y a quelques années pour créer des équivalents dermiques ou des modèles de peau pleine épaisseur (derme + épiderme). Dans cette méthode, les composants cellulaires d'intérêt (fibroblastes, DC dérivées de monocytes et kératinocytes) sont ensemencés séquentiellement dans des éponges de chitosane/collagène. Nous espérons ainsi obtenir un épiderme multicouche recouvrant les éponges, qui représentent un équivalent dermique abritant des fibroblastes et des DC. Notre collaborateur Michele Boniotto à l'Institut Henri-Mondor (Créteil) a démontré que la mutation de la sous-unité γ-sécrétase modifie le profil sécrétoire des kératinocytes cultivés en 2D. Par conséquent, un modèle de peau immunocompétente serait un atout majeur pour déterminer les indices environnementaux associés aux kératinocytes mutés cultivés en 3D et pour étudier comment ils exercent une influence sur les CD et, par la suite, sur les réponses immunitaires induites par les lymphocytes T.

L'hidradénite suppurée a suscité un intérêt croissant au cours de la dernière décennie, tant de la part des communautés de recherche que médicale, car elle représente une maladie difficile à combattre. Cette maladie touche environ 40 millions de personnes dans le monde avec peu de traitements actuellement disponibles, la plupart étant orientés vers le soulagement des symptômes plutôt que vers un remède permanent. Les symptômes de l'HS, la douleur, les nodules et les cicatrices à la surface de la peau, sont difficiles à distinguer des autres maladies cutanées jusqu'aux stades ultérieurs, où la progression de la maladie devient sévère et la qualité de vie des patients considérablement réduite. Bien que plusieurs modèles de souris soient de bons candidats pour explorer certains aspects de l'HS, il n'existe actuellement aucun modèle spécifique capable de reproduire les aspects physiopathologiques clés de la maladie.

Nous avons d'abord travaillé en utilisant l'expérience collective précédente acquise à partir de peau humaine reconstruite à l'aide d'échafaudages 3D. L'objectif était d'évaluer la faisabilité de modèles de peau utilisant du matériel de patient ou des conditions pertinentes

à l'HS, révélant des défauts dans la peau reconstruite à l'origine de l'apparition de la maladie. L'utilisation de la lignée cellulaire HaCaT s'est avérée plus facile à manipuler pour la culture que les kératinocytes humains normaux ou même les cellules de la gaine radiculaire externe, qui se sont révélées nettement plus fragiles en culture. Les cellules HaCaT se sont également révélées capables de coloniser et de croître dans nos échafaudages 3D.

Cependant, la nature hautement proliférative et sensible au calcium de HaCaT a créé certains défis dans le protocole de culture 3D. Des cas de cellules HaCaT en surprolifération et ne produisant aucun épithélium cohérent ont été observés. On ne sait pas si le protocole par défaut a un impact sur la différenciation HaCaT en culture 3D, où la différenciation devrait être induite par le contact avec l'air. Certaines variantes de matrices testées, avec un maillage de chitine plus fin ou plus épais, étaient également plus difficiles à coloniser par les cellules épithéliales, mais ce problème a été rapidement résolu en standardisant sur une seule épaisseur.

Nous nous sommes concentrés sur l'aspect inflammatoire de l'HS, représenté par un fort infiltrat neutrophile autour des follicules pileux. Les modèles de souris déjà disponibles ont permis de cibler spécifiquement le follicule pileux à l'aide d'un Sox9-creERT2 inductible par le tamoxifène, qui affectait spécifiquement la partie supérieure du follicule pileux. L'élimination de la voie de l'autophagie chez ces souris via notre modèle Sox9-Atg5 n'a pas produit d'altérations du follicule pileux ni de l'infiltrat immunitaire recruté après stimulation. L'utilisation d'un inhibiteur de la γ-sécrétase s'est avérée plus efficace pour perturber l'autophagie dans les sous-ensembles de follicules pileux mais pas dans les kératinocytes interfolliculaires, bien qu'elle ne cible pas spécifiquement le follicule pileux.

Enfin, nous avons utilisé la cytométrie en flux pour étudier les populations sanguines de lymphocytes des patients HS. Partant de la nouvelle découverte de lymphocytes B et d'anticorps chez les patients atteints d'HS, nous nous sommes concentrés sur la description des différents sous-ensembles sanguins de lymphocytes B et T. Nous n'avons d'abord observé aucune anomalie dans les proportions des sous-ensembles par rapport aux individus non affectés par l'HS. Cependant, en nous concentrant sur les cellules CLA+, exprimées sur plus de 90 % des lymphocytes T cutanés, nous avons repéré des tendances différentes entre les témoins et les patients. Pour explorer davantage la fonction des lymphocytes T CLA de patients HS, nous avons essayé plusieurs tests de stimulation PMA-Ionomycine à partir de PBMC non congelées et avons essayé d'évaluer les cytokines qu'elles exprimaient.

De plus, nous avons confirmé que les lymphocytes B expriment le CLA à leur surface et que les lymphocytes B cutanés expriment le CLA dans une proportion similaire à celle des lymphocytes T. Les cellules B produisaient également des proportions différentes dans les cas familiaux, alors que les cas sporadiques n'étaient pas affectés. La ségrégation des patients familiaux ou sporadiques est toujours sujette à prudence, car la seule différence réside dans la connaissance des antécédents familiaux d'HS. Comme on sait que la maladie est sous-diagnostiquée, la possibilité que des patients sporadiques aient des antécédents familiaux demeure, et seul un génotypage approprié du patient et des membres de sa famille pourrait résoudre ce problème. L'utilisation du marqueur CLA devrait être encouragée pour d'autres études sur le sang des patients atteints d'HS et peut être facilement étendue aux sous-

ensembles de lymphocytes B. Bien que nous ayons trouvé peu de différences entre les sous-ensembles de cellules B, nous n'avons pas étudié les anticorps qu'ils produisaient.

Premièrement, les développements futurs des modèles de culture cutanée 3D devraient ouvrir la porte à la compréhension des différences infimes caractéristiques de la progression de la maladie des patients. Bien que le modèle in vitro offre un modèle entièrement humain, aucune maladie complexe ne peut être bien comprise sans des approches in vivo, notamment parce que si elle est liée aux follicules pileux, une structure complexe qui, malgré les développements récents, reste difficile à imiter in vitro. Décrypter la complexité d'une maladie à partir d'un simple prélèvement sanguin aiderait considérablement les cliniciens à confirmer leur diagnostic et à orienter leur choix thérapeutique, un concept déjà mis en pratique dans diverses maladies auto-immunes. Dans l'ensemble, nous pensons que les recherches futures sur l'HS devraient s'appuyer sur toutes ces différentes approches, afin d'atteindre des résultats significatifs qui pourraient être transposables aux patients.

Wacym BOUFENGHOUR

3D Models of acne inversa

Résumé

L'hidradénite suppurée (HS) est une maladie chronique et récidivante touchant plus de 600 000 personnes en France, bien qu'elle soit sous-diagnostiquée, et découverte en 1839 par le chirurgien français Velpeau. Des lésions incapacitantes sont provoquées par des follicules pileux obstrués qui finissent par s'infecter, conduisant à une inflammation cutanée sévère et douloureuse. La progression de la maladie est propre à chaque individu, certains pouvant voir une rémission intermittente des symptômes ou au contraire une aggravation permanente. Les causes de l'HS sont donc complexes et multifactorielles, et encore aujourd'hui mal comprises. Le diagnostic de l'HS est rendu difficile par une ressemblance avec d'autres maladies cutanées, des praticiens inexpérimentés, et une consultation parfois tardive. De plus, la recherche biomédicale est limitée par une indisponibilité de modèle d'HS, seul le matériel humain, difficile d'accès, pouvant être utilisé. Au sein du consortium européen BATMAN, nous avions l'objectif de la mise en place de modèles pour l'HS, afin d'en faciliter l'étude en laboratoire et ainsi mieux comprendre et combattre la maladie. Utilisant des lignées épithéliales et du matériel primaire humain, nous avons étudié la mise au point de modèles *in vitro* de peau reconstruite. Nous avons également étudié des modèles murins ciblant l'autophagie dans le follicule, imitant des mutations connues chez certains patients. Enfin, l'analyse cellulaire du sang de patients de l'HS a permis d'identifier plusieurs potentiels marqueurs de la maladie et de sa progression.

Mots-clé : maladie de Verneuil, acne inversa, hidradénite suppurée, hidrosadénite, peau, follicule pileux, autoimmunitaire, inflammatoire, modèle murin, épithélium, sang, peau reconstruite, autophagie, BATMAN.

Résumé en anglais

Discovered in 1839 by French surgeon Velpeau, hidradenitis suppurativa (HS) is a chronic and relapsing disease affecting more than 40 million people worldwide, although it is an underdiagnosed condition. Debilitating lesions are caused by clogged hair follicles that eventually become infected, leading to severe and painful skin inflammation. The progression of the disease is specific to everyone, some may witness an intermittent remission of symptoms or, instead, experience worsening symptoms. HS causes are therefore complex and multifactorial, and still poorly understood today. HS diagnosis is hindered by a close resemblance to other skin diseases, inexperienced healthcare professionals, and sometimes late medical visits. Moreover, biomedical research is limited by the unavailability of HS models, and only hard-to-come-by human material can be used effectively. Within the European consortium BATMAN, we were tasked with creating HS models to facilitate its study in laboratories, thus better understand and fight the disease. Using epithelial cell lines and human primary material, we studied the generation of *in vitro* models of reconstructed skin. We also generated mouse models targeting autophagy in the hair follicle, mimicking known patient mutations. Finally, white blood cell analysis of HS patients allowed the identification of several potential markers of the disease and its progression.

Keywords: Verneuil's disease, acne inversa, hidradenitis suppurativa, skin, hair follicle, autoimmune, inflammatory, mouse model, epithelium, blood, reconstructed skin, autophagy, BATMAN.